CORROSION OF POST-TENSIONED TENDONS WITH DEFICIENT GROUT

FINAL REPORT
Project BDV29-977-04
(800002803)

Submitted To:

FDOT Research Center
605 Suwannee Street
Tallahassee, FL 32399

Project Manager:
Ivan Lasa
Florida Department of Transportation, State Materials Office
5007 NE 39th Avenue
Gainesville, FL 32609

Submitted By:

Kingsley Lau
Florida International University
10555 W. Flagler Street
Miami, FL 33174

October 2016

Prepared by:
Samanbar Permeh,
Krishna Vigneshwaran, K.K., and
Kingsley Lau

DISCLAIMER

The opinions, findings, and conclusions expressed in this publication are those of the authors and not necessarily those of the State of Florida Department of Transportation

Portions of the report have been published in conference proceedings:

S. Permeh, K.K. Krishna Vigneshwaran, K. Lau, and I. Lasa. “Corrosion of PT Tendons in Deficient Grout in Presence of Enhanced Sulfate and Chloride Concentration”. NACE Corrosion Risk Management Conference. May 23-25. Houston, TX. 2016. Paper No. 16-18751. 12pp.

S. Permeh, K.K. Krishna Vigneshwaran, K. Lau, and I. Lasa. “Anodic Behavior of Steel in Enhanced Sulfate Solutions.” NACE Corrosion/2016. Paper No. 7712. 13pp.

K.K. Krishna Vigneshwaran, S. Permeh, I. Lasa, and K. Lau. “Corrosion of Steel in Deficient Grout with Enhanced Sulfate Content.” NACE Concrete Service Life Extension Conference 2015. Paper No. CCC15-6942, 10pp.

S. Permeh, K.K. Krishna Vigneshwaran, K. Lau, I. Lasa, and M. Paredes. “Material and Corrosion Evaluation of Deficient PT Grout with Enhanced Sulfate Concentrations.” NACE Corrosion/2015. Paper No. 5828. 13pp.

K. Lau, I. Lasa and M. Paredes. “Update on Corrosion of Post-Tensioned Tendons with Deficient Grout”, NACE Corrosion/2014. No. 4225. 13pp. March 2014.

K.Lau, M. Paredes, I. Lasa. “Corrosion Failure of Post-Tensioned Tendons in Presence of Deficient Grout.” CORROSION/2013 NACE Int. Houston, TX, 2013. Paper No. 2600. 15pp.

K.Lau, J. Rafols*, M. Paredes, I. Lasa. “Laboratory Corrosion Assessment of Post-Tensioned Tendons Repaired with Dissimilar Grout.” CORROSION/2013 NACE Int. Houston, TX, 2013. Paper No. 2602. 15pp.

K.Lau, R. Powers, M. Paredes. “Corrosion Evaluation of Repair-Grouted Post-Tensioned Tendons n Presence of Bleed Water.” CORROSION/2013 NACE Int. Houston, TX, 2013. Paper No. 2604. 15pp.

K. Lau, I. Lasa, and M. Beljkerdid. “Assessment of SAW Corrosion Sensors in Concrete Environments,” CORROSION/2012. NACE Int., Houston, TX, 2012. C2012-0001737. 15pp.

K.Lau, M. Paredes, and J. Rafols*. “Corrosion Evaluation of Post-Tensioned Tendons with Dissimilar Grout,” CORROSION/2012. NACE Int., Houston, TX, 2012. C2012-0001738. 16pp.

APPROXIMATE CONVERSIONS TO SI UNITS

SYMBOL	WHEN YOU KNOW	MULTIPLY BY	TO FIND	SYMBOL
LENGTH				
in	inches	25.4	millimeters	mm
mils	mils	25.4	micrometers	µm
ft	feet	0.305	meters	m
yd	yards	0.914	meters	m
mi	miles	1.61	kilometers	km

SYMBOL	WHEN YOU KNOW	MULTIPLY BY	TO FIND	SYMBOL
AREA				
in^2	square inches	645.2	square millimeters	mm^2
ft^2	square feet	0.093	square meters	m^2
yd^2	square yard	0.836	square meters	m^2
ac	acres	0.405	hectares	ha
mi^2	square miles	2.59	square kilometers	km^2

SYMBOL	WHEN YOU KNOW	MULTIPLY BY	TO FIND	SYMBOL
VOLUME				
fl oz	fluid ounces	29.57	milliliters	mL
gal	gallons	3.785	liters	L
ft^3	cubic feet	0.028	cubic meters	m^3
yd^3	cubic yards	0.765	cubic meters	m^3
NOTE: volumes greater than 1000 L shall be shown in m^3				

SYMBOL	WHEN YOU KNOW	MULTIPLY BY	TO FIND	SYMBOL
MASS				
oz	ounces	28.35	grams	g
lb	pounds	0.454	kilograms	kg
T	short tons (2000 lb)	0.907	megagrams (or "metric ton")	Mg (or "t")

SYMBOL	WHEN YOU KNOW	MULTIPLY BY	TO FIND	SYMBOL
TEMPERATURE (exact degrees)				
°F	Fahrenheit	5 (F-32)/9 or (F-32)/1.8	Celsius	°C

SYMBOL	WHEN YOU KNOW	MULTIPLY BY	TO FIND	SYMBOL
ILLUMINATION				
fc	foot-candles	10.76	lux	lx
fl	foot-Lamberts	3.426	candela/m^2	cd/m^2

SYMBOL	WHEN YOU KNOW	MULTIPLY BY	TO FIND	SYMBOL
FORCE and PRESSURE or STRESS				
lbf	poundforce	4.45	newtons	N
lbf/in^2	poundforce per square inch	6.89	kilopascals	kPa

APPROXIMATE CONVERSIONS TO SI UNITS

SYMBOL	WHEN YOU KNOW	MULTIPLY BY	TO FIND	SYMBOL
LENGTH				
mm	millimeters	0.039	inches	in
µm	micrometers	0.039	mils	mils
m	meters	3.28	feet	ft
m	meters	1.09	yards	yd
km	kilometers	0.621	miles	mi

SYMBOL	WHEN YOU KNOW	MULTIPLY BY	TO FIND	SYMBOL
AREA				
mm^2	square millimeters	0.0016	square inches	in^2
m^2	square meters	10.764	square feet	ft^2
m^2	square meters	1.195	square yards	yd^2
ha	hectares	2.47	acres	ac
km^2	square kilometers	0.386	square miles	mi^2

SYMBOL	WHEN YOU KNOW	MULTIPLY BY	TO FIND	SYMBOL
VOLUME				
mL	milliliters	0.034	fluid ounces	fl oz
L	liters	0.264	gallons	gal
m^3	cubic meters	35.314	cubic feet	ft^3
m^3	cubic meters	1.307	cubic yards	yd^3

SYMBOL	WHEN YOU KNOW	MULTIPLY BY	TO FIND	SYMBOL
MASS				
g	grams	0.035	ounces	oz
kg	kilograms	2.202	pounds	lb
Mg (or "t")	megagrams (or "metric ton")	1.103	short tons (2000 lb)	T

SYMBOL	WHEN YOU KNOW	MULTIPLY BY	TO FIND	SYMBOL
TEMPERATURE (exact degrees)				
°C	Celsius	1.8C+32	Fahrenheit	°F

SYMBOL	WHEN YOU KNOW	MULTIPLY BY	TO FIND	SYMBOL
ILLUMINATION				
lx	lux	0.0929	foot-candles	fc
cd/m²	candela/m²	0.2919	foot-Lamberts	fl

SYMBOL	WHEN YOU KNOW	MULTIPLY BY	TO FIND	SYMBOL
FORCE and PRESSURE or STRESS				
N	newtons	0.225	poundforce	lbf
kPa	kilopascals	0.145	poundforce per square inch	lbf/in²

1. Report No.	2. Government Accession No.	3. Recipient's Catalog No.

4. Title and Subtitle	5. Report Date
CORROSION OF POST-TENSIONED TENDONS WITH DEFICIENT GROUT	October 20, 2016
	6. Performing Organization Code
7. Author(s)	8. Performing Organization Report No.
Samanbar Permeh, Krishna Vigneshwaran, K.K., and Kingsley Lau	
9. Performing Organization Name and Address Florida International University 10555 W. Flagler St. Miami, FL 33174	10. Work Unit No. (TRAIS)
	11. Contract or Grant No. BDV29-977-04
12. Sponsoring Agency Name and Address Florida Department of Transportation 605 Suwannee St. MS 30 Tallahassee, FL 32399	13. Type of Report and Period Covered Final Report March 11, 2013-October 20, 2016
	14. Sponsoring Agency Code

15. Supplementary Notes

16. Abstract

Recent corrosion failures of post-tensioned (PT) tendons in the Ringling Causeway Bridge (and corrosion development of PT tendons elsewhere in Florida) utilizing pre-packaged low-bleed specified grout products have spurred the need to evaluate what mechanisms were involved to cause the failure and to determine to what extent the problem is in PT tendons with similar materials. Severe corrosion was accommodated by segregated grout that was characterized as having high moisture content, low total chloride content, high free sulfate concentrations and high pore water pH. Accumulation of bleed water and grout void formation, considered sometimes as the cause of PT strand corrosion, were not consistently present with corrosion formation in the recent tendon failures. Furthermore, in addition to grout segregation with enhanced sulfate concentration, another separate issue of enhanced chloride content in PT grouts had garnered significant attention. Initial testing and chloride limit recommendations did not directly address the possible combined effect of enhanced chlorides in deficient grout. Elucidation of the role of the pore water chemistry of these deficient grouts in the corrosion mechanism is needed so that appropriate inspection and management decisions can be made.

The objective of the research is to identify criteria of deficient grout properties that may cause active corrosion of strand in post-tensioned tendons. Important material and corrosion parameters that may need to be more comprehensively studied as well as refinement in the proposed set of criteria is to be identified in this phase of research. The following approach was followed: 1). Identify the characteristics of deficient grout associated with steel corrosion including grout conditions formed when cast in presence of enhanced moisture presence, 2) Identify the role of sulfates in alkaline solutions and its possible adverse effects on steel corrosion activity, 3) Identify the behavior of steel in deficient grout with enhanced sulfate concentrations, and 4) Identify combined effect of enhanced chloride content and free sulfate content in deficient grout on corrosion initiation and identify practical threshold limits.

17. Key Word	18. Distribution Statement
Corrosion, Post-Tension, Tendons, Strand, Grout, Deficient, Sulfate	

19. Security Classif. (of this report)	20. Security Classif. (of this page)	21. No. of Pages	22. Price
unclassified	unclassified	202	

ACKNOWLEDGMENT

The contributions by Md. Ahsan Sabbir, Bin Li, and Roberto Rodriguez are acknowledged here as is the support and assistance from the FDOT State Materials Office and Dr. H.R. Hamilton.

EXECUTIVE SUMMARY

Recent corrosion failures of post-tensioned (PT) tendons in the Ringling Causeway Bridge (and corrosion development of PT tendons elsewhere in Florida) utilizing pre-packaged low-bleed specified grout products have spurred the need to evaluate what mechanisms were involved to cause the failure and to determine to what extent the problem is in PT tendons with similar materials. Severe corrosion was accommodated by segregated grout that was characterized as having high moisture content, low total chloride content, high free sulfate concentrations, and high pore water pH. Furthermore, research on a separate issue of enhanced chloride content in PT grouts did not directly address the possible combined effect of enhanced chlorides in deficient grout. Elucidation of the role of the pore water chemistry of these deficient grouts in the corrosion mechanism was needed so that appropriate inspection and management decisions can be made. The objective of the research was to identify criteria of deficient grout properties that may cause active corrosion of strand in post-tensioned tendons. The following approach was followed: (1) Identify the characteristics of deficient grout associated with steel corrosion including grout conditions formed when cast in presence of enhanced moisture presence, (2) Identify the role of sulfates in alkaline solutions and its possible adverse effects on steel corrosion activity, (3) Identify the behavior of steel in deficient grout with enhanced sulfate concentrations and (4) Identify combined effect of enhanced chloride content and free sulfate content in deficient grout on corrosion initiation and identify practical threshold limits.

Laboratory testing of pre-packaged PT grouts showed that formation of deficient grout can be promoted by enhanced moisture presence, and the effect of excess mix water was more significant than grout pre-hydration in high humidity. High sulfate concentrations can be accumulated in the deficient grout without external sulfate source, and even vestigial sulfate concentrations may locally aggregate due to segregation. Laboratory test such as the Modified Inclined Tube (MIT) test and an introduced Inverted Tee (INT) tests can be used to promote grout deficiencies and accumulation of sulfate ion. Corrosion testing in these samples showed that enhanced corrosion occurs in deficient grout.

It was proposed that significant early sulfate accumulation and availability of sufficient levels is necessary to hinder stable steel passive film formation, but depassivation of steel by sulfates is otherwise difficult. No corrosion developed for steel submerged in alkaline sulfate solutions with pH 13.3. In the open circuit potential condition for pH 12.6 solutions, additions of sodium sulfate with concentrations as high as 65,000 ppm after pre-conditioning in sulfate-free solution did not show ability to depassivate steel. However, in the open circuit potential condition for pH 12.6, destabilization of passive film growth resulting in severe corrosion occurred in pre-mixed >4,000 ppm sodium sulfate solution. Testing indicated instability of passive film resulting

in severe corrosion sometimes exhibiting pitting corrosion. As initial assessment, the possible role of sulfates in steel corrosion initiation were thought to be related to localized corrosion process by reaction such as $Fe^{2+} + 2H_2O + SO_4^{2-} \rightarrow Fe(OH)_2 + H_2SO_4^{2}$.

Additions of 0.08% and 0.2% chloride by cement in itself did not initiate corrosion of steel in segregated grout layers in INT tests, but corrosion developed in deficient grout materials with similar low-level additions of chlorides (0.03% to 0.18% of total grout mass) when combined with as low as 2,000-ppm sodium sulfate in its mix water. The enhanced sulfate addition apparently had the effect of initiating corrosion in the presence of low-level chlorides, indicating adverse effects of low level chlorides in the presence of sulfate. The finding would suggest that assessment of corrosion susceptibility of deficient grout by chloride content alone would not be sufficient.

Changes in pore water chemistry can affect the initiation of steel corrosion in the presence of sulfate ions, and it was evident that a propensity for corrosion initiation in solution can't be defined by sulfate content alone. However, practical limits accounting for expected grout pore water conditions may be proposed. Active corrosion conditions developed where sulfate levels exceeded ~0.0007 $g_{sulfate}/g_{Powder}$. Test results suggested an upper limit of $[SO_4^{2-}]/[OH^-] = 0.15$ for typical grout pH environments.

TABLE OF CONTENTS

LIST OF FIGURES

LIST OF TABLES

1. INTRODUCTION

Recent corrosion failures of post-tensioned (PT) tendons in the Ringling Causeway Bridge (and corrosion development of PT tendons elsewhere in Florida) utilizing pre-packaged low-bleed specified grout products have spurred the need to evaluate what mechanisms were involved to cause the failure and to determine to what extent the problem is in PT tendons with similar materials. Severe corrosion was accommodated by segregated grout that was characterized as having high moisture content, low total chloride content, high free sulfate concentrations, and high pore water pH. Accumulation of bleed water and grout void formation, considered sometimes as the cause of PT strand corrosion, were not consistently present with corrosion formation in the recent tendon failures. Furthermore, in addition to grout segregation with enhanced sulfate concentration, another separate issue of enhanced chloride content in PT grouts had garnered significant attention. Initial testing and chloride limit recommendations did not directly address the possible combined effect of enhanced chlorides in deficient grout. Elucidation of the role of the pore water chemistry of these deficient grouts in the corrosion mechanism is needed so that appropriate inspection and management decisions can be made.

The objective of the research was to identify criteria of deficient grout properties that may cause active corrosion of strand in post-tensioned tendons. Important material and corrosion parameters that may need to be more comprehensively studied as well as refinement in the proposed set of criteria were to be identified in this phase of research. The following approach was followed:

1. Identify the characteristics of deficient grout associated with steel corrosion, including grout conditions formed when cast in presence of enhanced moisture presence.

2. Identify the role of sulfates in alkaline solutions and its possible adverse effects on steel corrosion activity.

3. Identify the behavior of steel in deficient grout with enhanced sulfate concentrations.

4. Identify the combined effect of enhanced chloride content and free sulfate content in deficient grout on corrosion initiation and identify practical threshold limits.

The report is separated into eight major sections organizing the various research findings: (1) literature review, (2) assessment of deficient grout caused by enhanced moisture content, (3) electrochemical testing in alkaline sulfate solutions, (4) testing in laboratory cast grout samples, (5) modified inclined tube tests, (6) analysis of deficient grout, (7) analysis of corrosion development, and 8) development of practical sulfate limits.

2. LITERATURE REVIEW

2.1 BACKGROUND

Corrosion-related failures of post-tensioning, PT, strand have been documented in several Florida bridges in the late 1990's. The alkaline (chloride-free) cementitious environment in grout promote steel passivation that typically prevents any significant corrosion; however, the presence of voids in the grout of tendon ducts would provide conditions whereby corrosion development may occur. The early failures of several PT systems in Florida and Virginia (including the Niles Channel Bridge, Midbay Bridge, Sunshine Skyway Bridge, and Varina-Enon Bridge, after only 18, 7, 15,and 17 years service; respectively) were cases of severe corrosion associated in part with grout voids (Powers, 1999; Corven, 2001; FDOT, 2002; Sagüés, 2005; Trejo et al., 2009; Hansen, 2007). The causes of the voids have been attributed to development of bleed water during grouting and subsequent re-absorption or evaporation from the grout. Poor grouting during construction were of concern as well. After void formation moisture, oxygen, carbon dioxide and chloride ions may be introduced at joints, anchorages, and defects in the outer high density polyethylene (HDPE) duct. The strand at void locations can then be susceptible to deterioration by carbonation, accumulation of chloride ions, galvanic interaction with the metal ducts and anchorages and possible enhanced macrocell corrosion.

Consequent to field experiences of corrosion development associated with accumulated bleed water, new PT grout material specifications in the early 2000's have required low bleed water formation. Florida specifications for PT grout require 0% bleeding at 3 hours determined by a modified wick induced bleed test (ASTM C940) (FDOT, 2010). Recent field observations from a bridge construction project in Texas of a PT grout product conforming to low bleeding requirements have shown indication of grout segregation and stratification leaving part of the grout material in a wet plastic state (Merrill, 2010). The wet grout there contained large quantity of visible air voids and saturated with unbound water. Preliminary analysis of the grout showed high chloride, potassium, sodium, and sulfur content. The total chloride content was determined to be in some cases greater than 5% by weight and free chloride content greater than 2% by weight.

Corrosion failure of post-tensioned tendons in Europe has been identified to be related to grout segregation (Bertolini and Carsana, 2011). Deep localized corrosion of strand and tendon failure after only 2 years after construction was observed. The segregated grout was described as a whitish plastic paste which upon drying becomes incoherent. Laboratory analysis of the segregated grout there identified non-uniform material composition with enhanced concentrations of alkalis and sulfates and absence of chloride ions. Importantly, the grout pore water chemistry maintained an alkaline environment. Laboratory tests suggested localized corrosion due to enhanced macrocell interaction due to oxygen depletion in the interstitial spaces of the strand.

Recent corrosion failures of post-tensioned (PT) tendons in the Ringling Causeway Bridge (and corrosion development of PT tendons elsewhere in Florida) utilizing pre-packaged low-bleed specified grout products have spurred the need to evaluate what mechanisms were involved to cause failure and to determine to what extent is the problem in PT tendons with similar materials (Lau et al., 2013a; 2013b; 2013c). Severe corrosion was accommodated by segregated grout that was characterized as having high moisture content, low total chloride content, high free sulfate concentrations and high pore water pH. Accumulation of bleed water and grout void formation, as earlier described and considered sometimes as the cause of PT strand corrosion, were not consistently present with corrosion formation in the recent tendon failures. The most severe segregated grout had putty-like consistency. Less strongly manifested forms of segregated grout had grout characterized as friable and chalky. Elucidation of the role of the pore water chemistry of these deficient grouts in the corrosion mechanism is needed so that appropriate inspection and management decisions can be made.

There are several important issues that need to be addressed to resolve the failure mechanism. The first issue is not only to identify the cause of grout segregation but also possible resulting adverse changes to the grout solid matrix and pore water chemistry. It is important to consider that the physical manifestation of segregated grout alone may not necessarily cause corrosion development if the grout chemistry allows steel passivation to occur in the absence of bleed water and grout/air interfaces in void spaces. The grout chemistry in conjunction with grout consistency must be considered jointly to elucidate cause of corrosion. It is important to elucidate the extent of separation of cement and other grout components including fillers due to segregation. At this time, the role of enhanced concentrations of free sulfates is among important material parameters to be addressed. Additionally the cause of localized enhanced free sulfate concentrations has not been identified. Other important grout parameters in terms of corrosion development include adverse variation in grout porosity and electrical properties such as solution resistance.

To what extent prevention or loss of steel passivation occurs while embedded in the deficient grout needs to be addressed. Preliminary research (Lau et al., 2013a; 2013b; 2013c) has shown detrimental effects of sulfate ions in solution but understanding of what conditions with the presence of enhanced sulfate concentration causes active corrosion to begin has yet to be resolved. Specifically, initiation of corrosion in the presence of high levels of sulfate ions if the steel had already attained stable passivity has not been found. However, significant corrosion development was seen at moderate sulfate levels if sulfates were introduced very early to the system (Lau et al., 2013b; Gouda, 1970; Al-Tayyib et al., 1982). The combined role of pore water pH, free sulfate concentration, oxygen presence and crevice conditions should be considered when identifying the level of sulfates that may contribute to corrosion initiation.

The third issue should consider the role of chloride ions in corrosion development in the presence of segregated grout. In corrosion development in PT tendons observed in Florida, the total chloride content was low in terms of conditions commonly associated with normal

hydration of cementitious materials. This may not be valid in the presence of segregated grout when the amount of cement cannot be easily measured and is most likely less than what is anticipated for normal hydrated grout. Indeed, the content of the segregated grout still has yet to be completely identified in samples from PT tendon failures. To what extent will corrosion develop for the chance that enhanced chloride concentrations were present in the segregated grout also has not been addressed. The combined effect of chloride ion and enhanced sulfate concentrations and determination of what concentrations can be accepted as conservative threshold values for these cases with segregated grout should be addressed. Furthermore, since cement content cannot be easily measured, what appropriate unit of measure of chloride threshold concentrations should also be addressed.

2.2 DEFICIENT GROUT IN FLORIDA PT BRIDGES

2.2.1 Ringling Causeway Bridge

2.2.1.1 Background

Corrosion failure of longitudinal external post-tensioned (PT) tendons was identified in 2011 in the Ringling Causeway Bridge after being in service for ~8 years. The bridge was a PT segmental bridge with internal and external tendons. The location of corrosion on the two failed tendons was in the upper portion of the sloped region of the tendon immediately adjacent to the upper deviator. The external PT tendons were nominally 4 inch (~10.2 cm) internal diameter with 22 ~1.6 cm diameter seven-wire strands. Severe grout segregation with severe corrosion was observed in numerous other tendons. It was apparent that the corrosion condition was not isolated and major repair operations at several tendon locations besides those originally identified were in progress.

Work by Lau et al., 2013a was conducted to investigate possible material and corrosion issues. In that work, sections of the two failed tendons were examined but other tendons with significant corrosion were not readily available for testing at the time. General description of that work and its findings follow and details can be found in reference (Lau et al., 2013a). Visual examination for corrosion development, grout placement, grout consistency, duct condition, and presence of voids were made and grout samples from various locations from the failed tendons were sampled. Bulk and thin-film petrographic analysis was made for grout in the vicinity of and away from the corrosion failure to identify deficiencies in the grout material. Chloride content, free moisture, pore water pH, and chemical make-up were measured to characterize and determine variation in grout consistency. Corrosion assessment was made by visual observation of corrosion development of embedded strand during tendon autopsy, as well as electrochemical methods such as open circuit potential (OCP), and linear polarization resistance (LPR), electrochemical impedance spectroscopy (EIS), and galvanic macrocell current. Corrosion test cells were made by coupling short tendon segments recovered from failed tendons (Figure 2.1). The top coupled segment of the test cell contained

hardened grout away from corrosion sites and the bottom segment contained segregated grout and strand with corrosion. Activated titanium reference and auxiliary electrodes were placed within a ponding dam that was filled with a cement paste.

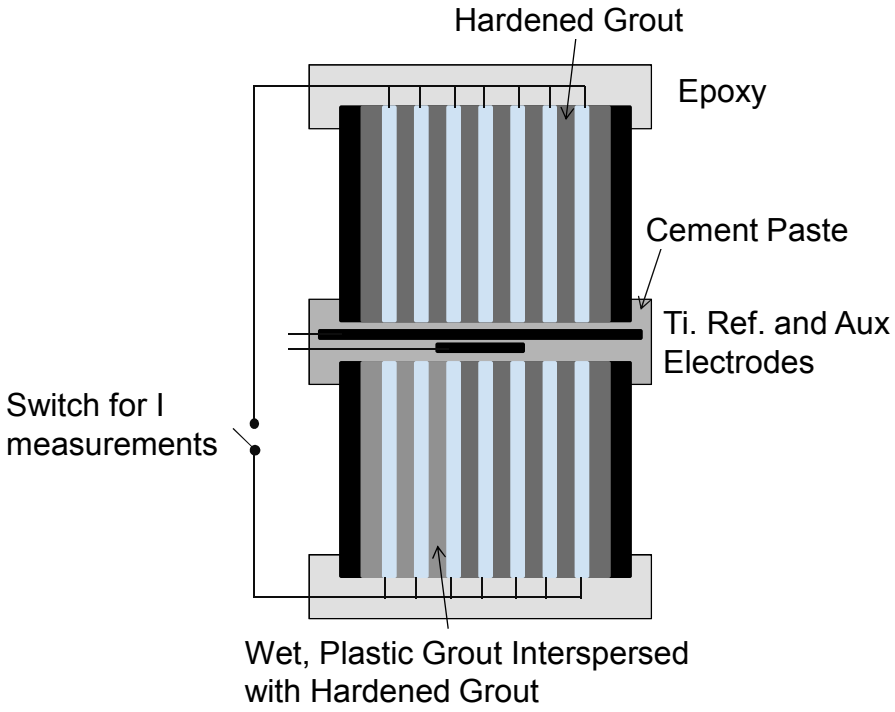

Figure 2.1. Schematic of corrosion macrocell test sample. (From Lau et al., 2013a)

2.2.1.2 Findings

2.2.1.2.1 Field Corrosion Assessment

Field Observation: Strand in the location of the tendon failure exhibited severe corrosion (Figure 2.2) mostly concentrated in the upper portion of the tendon cross-section. In addition, steel corrosion was also observed nearby in the upper portion of the galvanized pipe sleeve in the upper deviator. The galvanized pipe had minor impact in mitigating corrosion of the steel strand in immediate contact at the bottom of the tendon and thus subsequent tendon failure. Any possible hydrogen formation caused by active zinc corrosion and hydrogen embrittlement of the steel would have occurred very early (shortly after initial pour) when the galvanized pipe would develop highly cathodic potentials. Of note large amounts of wet segregated plastic grout was also sometimes observed at low points in the tendon drape such as at anchor caps. There, severe corrosion of the anchor plate and strand also occurred.

Figure 2.2. Strand corrosion at failure location. (Photo by author and courtesy of FDOT.)

It was readily apparent that wet segregated plastic grout was present at numerous other sites and could be present in very large regions within the tendon. It was also apparent that severe strand corrosion was associated with this form of poor grout material. The poor grout material had three distinct forms: the wet plastic grout had a clay-like consistency and often was associated with a strong ammonia-like odor, portions of the segregated grout had a white chalky consistency, and areas of the segregated grout had black striated layers that were attributed to sedimentation of silica fume.

Grout -Tendon Characterization: Grout fill deficiency was seen in the first failed tendon but the void space along the tendon length and elevation was not consistent with the grout fill deficiency being attributed to drainage of the grout when the mix was still fluid. Rather, the grout in the upper horizontal region appeared to have subsided possibly due to segregation of grout material in the sloped region. It was apparent by the presence of a groove or bleed trail and remnants of bubbles at the top portion of the duct that a large amount of entrapped air and water was transported along the length of the tendon. This movement of liquid and gases (particularly towards the unsealed vent opening near the upper deviator) and associated severe grout segregation may have contributed to the formation of the large voids.

Unlike the first failed tendon, large scale void spaces were not present in the second. Instead the tendon cross-section there was filled with grout material, albeit that significant portions of the tendon were filled with highly segregated and poor quality grout material. Stratification of a black layer with some indication of gas venting was observed at the top surface of the grout

Grout Consistency: Figures 2.3 and 2.4 show the typical appearance of the wet segregated plastic grout. Other manifestations of segregated grout were observed as well, including stratification of apparently silica fume and inter-mixing of the white chalky grout. The appearance of the grout segregation and stratification did not appear to be directly caused by gravimetric sedimentation as the various forms of segregated grout was typically interspersed within the tendon cross-section.

Bulk petrographic analysis of grout samples from apparent segregated grout and away from locations with major segregation showed significant differences in structure . The segregated grout had a white color contrasted to the dark grey color for non-segregated grout. It was apparent from the micrographs that the segregated grout material had a larger content of fine material (likely being in part crushed limestone) than the non-segregated grout.

However, the segregated grout material had appearance of fewer coarse fine-grained crushed limestone particles (~0.2 mm diameter). This observation is consistent with the contention that denser materials such as the coarse limestone grains as well as cement grains segregated away from these locations and moisture and finer particles accumulated in its place. The highly segregated grout had large pores that were filled with ettringite crystals, and as shown in Figure 2.5, the highly segregated grout was porous and appeared to consist of an agglomeration of grout particles without a consistent matrix of cementitious materials.

Figure 2.3. Wet, segregated plastic grout. Pink color show phenolphthalein indicator. Upper portion of picture shows screwdriver embedded in soft grout. Lower right picture shows surface condition prior to autopsy. (Photo by author and courtesy of FDOT.)

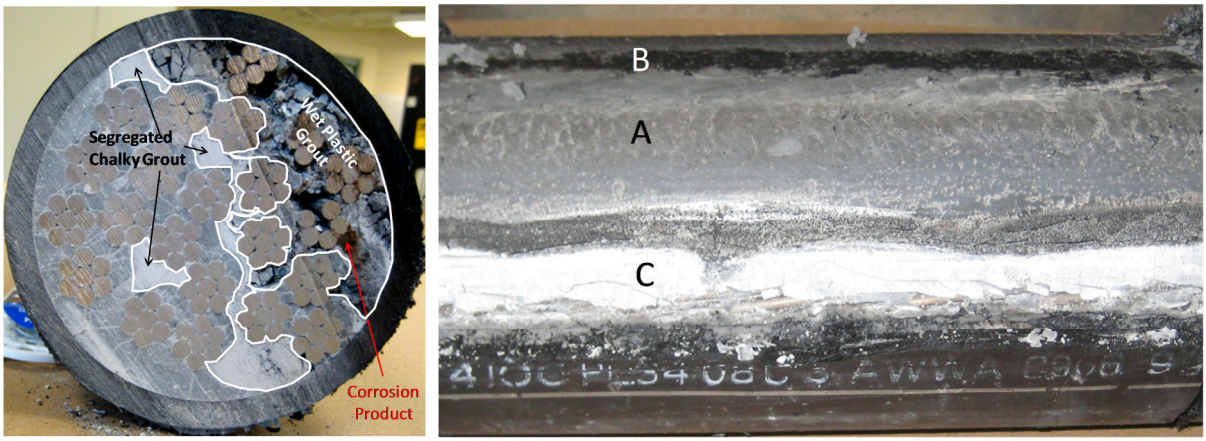

Figure 2.4. Grout segregation appearance. (A) Wet plastic grout. (B) Dark band of sedimented silica fume. (C) White chalky grout. (Photos by author and courtesy of FDOT.)

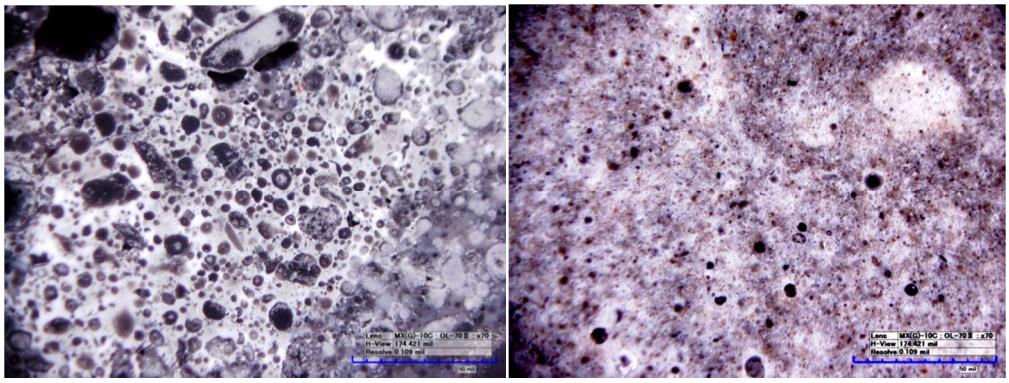

Figure 2.5. Micrographs contrasting wet, plastic grout to hardened grout.
Magnification 70x. Cross light. Left: Wet plastic grout. Right: Hardened grout. (Photo by author and courtesy of FDOT.)

2.2.1.2.2 Grout Laboratory Analysis

The water content of hardened grout was typically ~20% by mass. It was apparent that there was high water content in the segregated grout material that was in the upper portion of the tendon cross-section. The water content exceeded 60% by mass in grout characterized as having a wet and plastic consistency and was as high as 50% in grout characterized as soft and chalky. The total chloride content in the segregated grout was low to moderate but there was indication of enhanced chloride accumulation in the wet segregated grout (Figure 1.6). This may in part be due to accumulation of the dried-out segregated material in the sample preparation for the total chloride content analysis. Since the unit weight of a segregated grout is vastly different and could not be predetermined, the chloride content was represented as mass of chloride per mass of dry grout powder. Analysis of expressed pore water of grout from select locations generally gave similar indication of low but accumulated free chloride ions in the region of soft grout material in agreement with trends observed for total chloride concentrations noted above.

It is noted that the solution from the wet plastic grout tested by ion chromatography was obtained by an ex-situ leaching method. The results were treated qualitatively in the following discussion. Calcium, sulfate, and chloride concentrations of solution from wet plastic grout obtained by the ex-situ leaching were comparable to that obtained by pore water expression. The sodium and potassium concentrations of solutions obtained by ex-situ leaching were significantly lower than those obtained by pore water expression.

Significant detection of sulfur was observed in segregated grout in both tendons by XRF but the aqueous sulfate ion concentration was apparently generally high along the free-length portions of the tendon. As will be discussed later, the high concentration of sulfate ions is expected to facilitate the depassivation of steel strand. The sulfate ion concentrations here were significantly higher than compared to pore water analysis of silica fume cement paste by Page and Vennesland, 1983. Page and Vennesland measured as high as 3,800 ppm SO_4^{2-} in

cement paste solution whereas as much as 9,700 ppm SO_4^{2-} was measured in solution extracted from grout from the bridge. Pore solution obtained by the ex-situ leaching method from deficient grout showing localized sedimentation in an anchor cap provided useful comparison of the various grout deficiency modalities. As shown in Figure 2.7, the deficient grout had significantly greater sulfate content than the hardened grout and a new control batch of similar grout material. The mechanism of the accumulation of sulfate ions could not be determined, but speculation could be made that ionic transport of the ion in part due to grout segregation and moisture accumulation in localized regions and confined spaces. More generally, it may be speculated that sulfates were admixed into the grout.

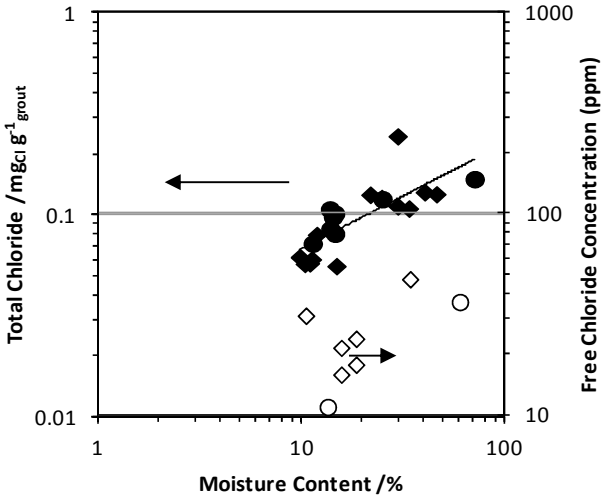

Figure 2.6. Chloride accumulation due to moisture. (From Lau et al., 2013a)

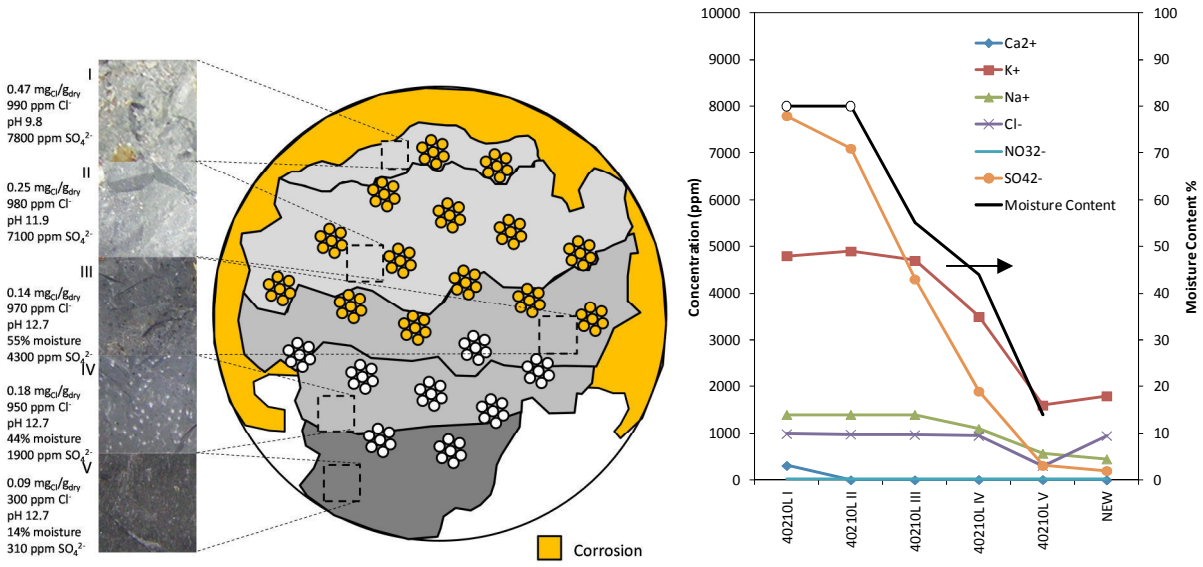

Figure 2.7. Chemical characteristics of segregated grout.
Geometry of anchor cap: total chloride, free chloride, pH, and sulfate content per layer shown (left). Chemical concentration and moisture content per layer shown (right).

Pore water pH for select locations from the tendons was generally greater than 13 and did not give any indication of possible mechanisms which may cause a decrease in pH, such as carbonation. The measured pH of solution obtained from one sample of wet plastic grout was as low as 11; however, measurements of the same wet plastic grout with phenolphthalein did not give any color indication of significant drop in pH. The presence of corrosion products and the segregation and accumulation of silica fume, may in part account for the consumption of hydroxyl ions ion and slight decrease in pH of the pore water.

X-ray diffraction of powder samples from the tendons did verify the presence of calcium carbonate compounds as a filler component in the grout material. The identification of carbonates especially in the white chalky grout was consistent with the morphology of fine material in the petrographic micrographs described earlier. Calcium hydroxide was commonly observed as expected. Gypsum was identified throughout both tendons as well. Consistent with the measurement of high sulfate contents in the grout pore water solution and observation of acicular crystalline material observed in grout macro-pores, ettringite was also identified. Corrosion products in the grout were identified as FeOOH and Fe_3O_4. It is noted that further oxidation upon exposure of the corrosion product to the laboratory air and during sample preparation may have occurred.

As was mentioned earlier, high sulfate concentration was measured in the grout pore water and was further supported by the identification of ettringite in the macro pores of segregated grout by bulk petrography and XRD. Compiled data from XRF and XRD relating to sulfur-containing compounds is shown in Figure 2.8. It was noted that the visual observations of macro pores filled with materials consistent with ettringite (as described earlier) was predominant in the segregated grout. Larger hit count rates by XRF for sulfur was detected for grout collected from the top portions of tendon cross-sections where segregated grout was typically more prominent than compared to grout from the bottom portion of the tendon cross-section. But, gypsum and ettringite presence did not show clear preferential orientation in the tendon cross-section.

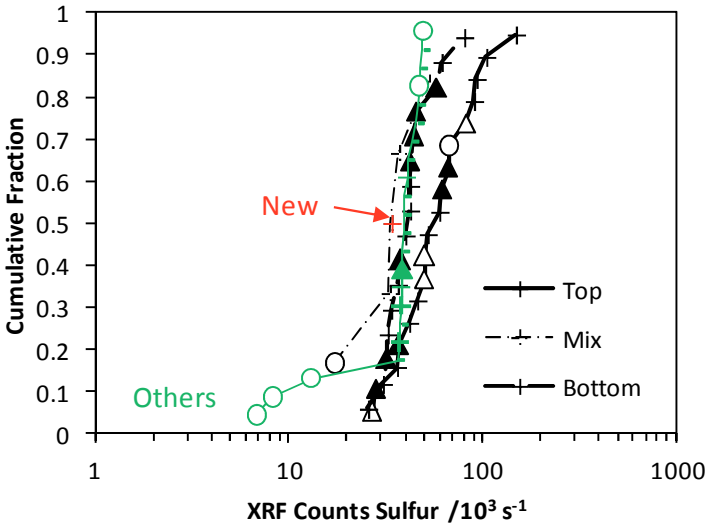

Figure 2.8. XRF detection of S compounds from grout extracted from tendon top and bottom.

'New' refers to a new batch of grout. 'Others' refers to other similar grout samples from other PT bridges. XRD Analysis: Plus-Gypsum; Open Triangle-Ettringite; Solid Triangle-Both; Circle-None; Dash-XRD not performed. This listing of compounds only includes gypsum and ettringite. (From Lau et al., 2013a)

2.2.1.2.3 Strand Corrosion

Open Circuit Potential (OCP): The cumulative fraction of open-circuit potentials (OCP) for individual strands within tendon sections is shown in Figure 2.9. Severe active corrosion was apparent in some tendon segments, and distinctly negative potentials were, as expected, measured there. In these sections with active corrosion, a wide range of potentials was measured for strand in the various forms of segregated grout, which signifies the differences in the corrosion activity even within a small area. The differences were attributed to the amount of moisture, concentration of chloride and sulfate ions, and oxygen present in the grout. As will be discussed later, these differences in potentials could lead to accelerated corrosion due to local and extended macrocell formation. The differences in potentials may be even greater if there is significant depletion of oxygen in the crevices of strand in wet grout. It was thought that local anodes formed within the porous wet plastic grout with greater moisture presence and greater sulfate concentrations. Cathodic reactions could occur everywhere but significantly in the hardened grout where there was less moisture and the steel strand remained in passive condition.

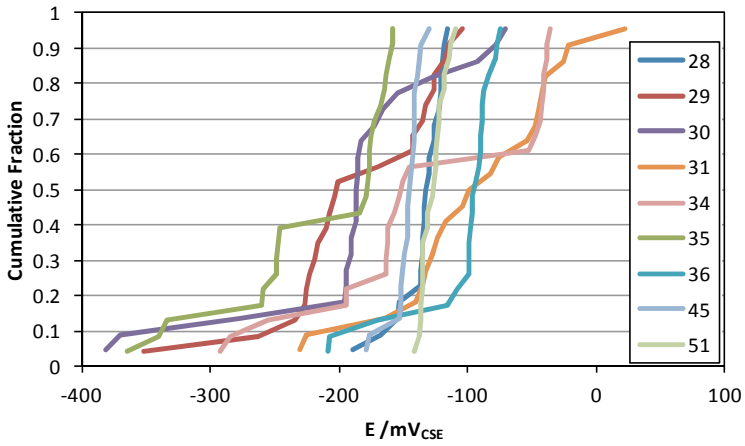

Figure 2.9. OCP of individual strands.
Legend lists tendon section numbers**.** (From Lau et al., 2013a)

Macrocell Corrosion: The tendency for corrosion macrocell activity in tendons with segregated grout was tested by coupling tendon sections with wet plastic grout and tendon sections with hardened grout. As presented earlier, the top tendon sections contained grout with apparently hardened grout and the bottom sections contained deficient grout (each segment having significant amounts of wet plastic grout). Electrochemical testing of these sections (prior to galvanic coupling or the sections) presented earlier showed that the deficient grout had a much lower electrical resistivity than the hardened grout, consistent with the high moisture and high porosity of the segregated grout. Importantly, the tests also showed that the steel in the segregated grout did have active corrosion.

After ~10 days, the sections were coupled, and the open-circuit potential, corrosion rate, and macrocell current were monitored. Results are shown in Figures 2.10-2.12. As expected, the galvanic coupling of the tendon sections created a mixed system potential intermediate to the OCP of the bottom and top sections. This mixed potential was consistent throughout the ~1 month test period. This provided anodic polarization of the bottom section that already had active corrosion and thus enhanced rate of steel dissolution. Two of the test samples showed large macrocell currents corresponding to the bottom section with segregated grout acting as the net anode. One of the samples unexpectedly showed the top tendon section acting as net anode. Testing of the sample prior to galvanic coupling did show that active corrosion was present in the bottom section with segregated grout, but corrosion activity was also present in the top tendon section.

The macrocell current after ~1 day was ~60-120 µA but decreased to ~40 µA after ~3 months. The decrease in macrocell was thought to be in part due to continual hydration of the introduced cement paste. It is noted that the surface of the cement paste used to provide ionic coupling of the two sections was not sealed and oxygen may be readily available. Differential oxygen availability to the anode and cathode, as may have been present in the field, would provide larger macrocell polarization and possibly greater degree of enhanced corrosion.

The apparent corrosion current (determined by LPR and EIS) increased after the top and bottom samples sections were coupled. The apparent corrosion rate presented below was not area normalized because differentiation between anodic and cathodic areas could not be quantified. As expected, the measured macrocell current was less than the apparent corrosion current as the macrocell current is a measure of the net behavior between local and extended anodic and cathodic regions in the top and bottom sample sections.

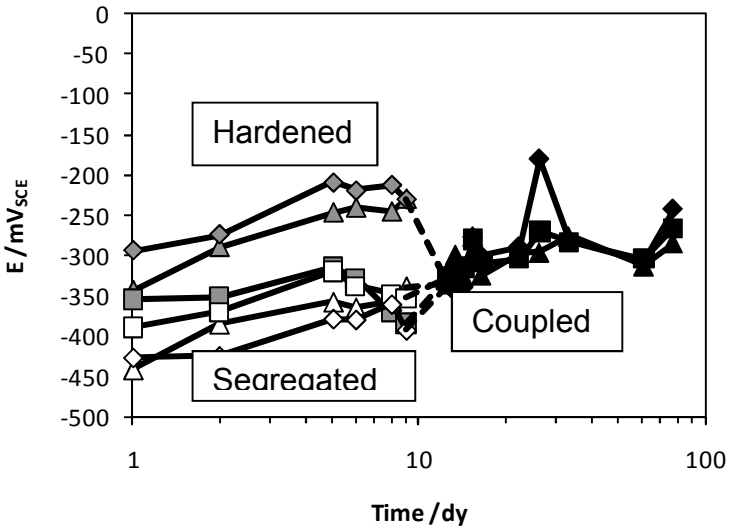

Figure 2.10. OCP development after galvanic coupling of strand in hardened and segregated grout. (From Lau et al., 2013a)

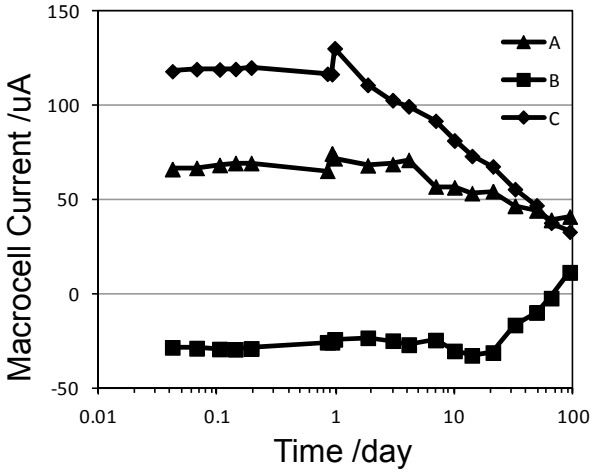

Figure 2.11. Macrocell current after galvanic coupling of strand in hardened and segregated grout.

Positive values represent the bottom sample section with steel in deficient grout acting as net anode. A,B,C replicate samples. (From Lau et al., 2013a)

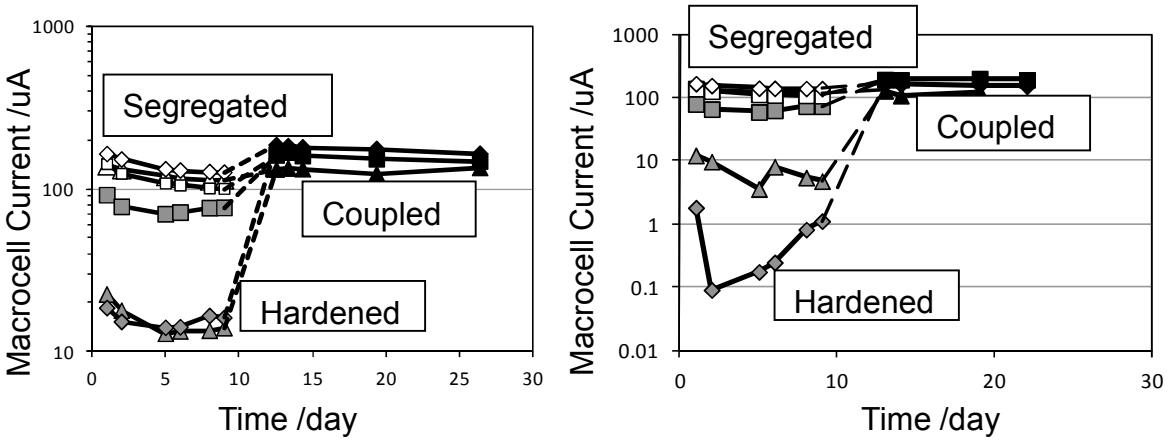

Figure 2.12. Corrosion rate development after galvanic coupling of strand in hardened and segregated grout.

Left: Measured by LPR. Right: Measured by EIS. (From Lau et al., 2013a)

2.2.1.3 Durability Implications

The large localized area of significantly segregated grout in the tendon at the failure locations is of utmost concern because of its detrimental impact on the tendon corrosion resistance. The area of significant grout segregation appeared to create a localized environment with large amount of free moisture. The severe and fast rate of corrosion to cause failure that occurred within 8 years was thought to occur due to local depassivation of steel strand in the segregated grout where the porous wet grout provided no protection. There a moderate amount of chloride ions may accumulate due to capillary transport as part of the grout segregation process and a significant amount of sulfate ions contributed to destabilizing the steel passive layer. Corrosion was accelerated due to macrocell formation between the steel in the segregated grout and elsewhere. Oxygen availability in the segregated grout especially in crevice regions with high moisture content was greatly limited. Oxygen availability in regions with hardened grout and regions with voids was replenished due to the poor seals at the vent caps.

Although relatively high alkalinity was maintained in the segregated grout, the corrosion mechanism proposed by Bertolini and Carsana and elsewhere (Bertolini and Carsana, 2011; Blactot et al., 2007), where active corrosion was maintained due to high pH and large cathodic polarization, may not have been the primary cause here. It was apparent that significant silica fume sedimentation and accumulation in the segregated grout may have slightly reduced the pH. Additionally, ettringite crystals (that may not be stable in very high pH) were prominent in segregated grout. As mentioned earlier, the exact cause for the grout segregation is not known but developing case studies with similar PT systems should be closely reviewed.

2.2.2 Other Bridges

Other PT bridges in Florida that utilized or may have utilized low-bleed water formation grouts have been inspected to identify the extent of possible grout deficiencies. At least five other bridges have been identified to have deficient grout analogous to the grout associated with corrosion failure, but the amount and level of severity of deficient grout varied significantly between those bridges. Four of those bridges had deficient grout associated with external tendons and one of those bridges had deficient grout associated with internal tendons. It is noted that one of those bridges with external tendons containing grout deficiencies was built in the time period with material specifications in transition from neat grouts to low bleed grout requirements and the grout material was not positively identified. Two additional bridges were noted to have hardened grout with small amounts of soft or chalky grout during inspections of internal tendons. One of the bridges where significant deficient grout was observed was in construction. After early observations of grout anomalies in external ducts, the grout product was changed and construction awareness of grout segregation was increased to mitigate possible material deficiencies. It was noted that deficient grout was observed at a high elevation anchor cap as well as along the low elevation free span length of a tendon as shown in Figure 2.13

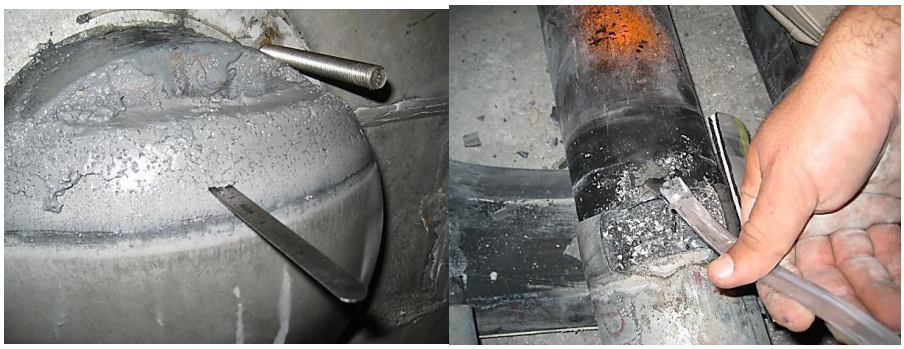

Figure 2.13. Deficient grout. (Photos courtesy of FDOT.)

Early grouting records from the construction project were reviewed to elucidate possible trends that may have part in the manifestation of segregated grout. Review of these documents was only meant to possibly identify what grouting parameters were present when segregated grout was identified.

The grouting records for 132 tendons were reviewed. 42% of those tendons used a particular commercially available PT grout and 58% were made of one of three other commercially available PT grouts. Soft or wet grout, here treated as segregated grout (but not necessarily to the extent shown in Figure 2.13), was observed on 14% of the 132 tendons (84% of those observations with one grout product). Graphical plots of grouting parameter

statistics are shown in Figure 2.14. It is noted that there were four different grouts used and thus the numbers presented likely represent variation due to multiple populations.

No major differences in the pump time between tendons with and without wet/soft grout was distinguishable although the median value for tendons with wet/soft grout was higher. The pumping pressure was similar for tendons with hard and wet/soft grout. No distinct differences in water ambient temperatures for grout batches with and without wet/soft grout was distinguishable although the median ambient temperature for tendons with observed wet/soft grout was higher. No distinct differences in efflux time for sampled grout (likely prior to pumping) corresponding to where wet/soft grout was distinguished. The cumulative curve for grout specific gravity showed multiple populations indicative of the different grouts used in construction. Interestingly, but likely circumstantially, wet/soft grout had mostly specific gravity associated with one of the populations. It is noted that that population consisted of more than one grout product.

The apparent batch time and elapsed pumping time were determined by processing data from the mixing records and any incongruities there may be translated into these metrics as well. The apparent batch time per bag was calculated by dividing the total cumulative time of mixing all the grout batches within a series of batches by the total number of bags in that series. This metric may show if possible delays in between batches had any significance in the observation of wet/soft grout. The metric does not directly indicate mixing time. The elapsed pumping time is the cumulative pumping start time from pumping of the first tendon in the sequence of tendons. This metric may show if possible delays in time of start of pumping had any significance in the observation of wet/soft grout.

No distinct differences in the elapsed pumping time between tendons with and without wet/soft grout. Interestingly, there was a difference in the apparent batch time. The median apparent batch time for grout where wet/soft grout was observed was faster (indicating greater time efficiency during batching); however, the range in time was not dissimilar for hard and wet/soft grout. It is noted that the mixing time for each batch (typically 10 bags) was typically 3 minutes or greater. Validation of any inferences made from these statistics will have to be made, but possible inconsistencies in the batching, mixing, and pumping times should be further addressed to determine its significance in the manifestation of segregated grout.

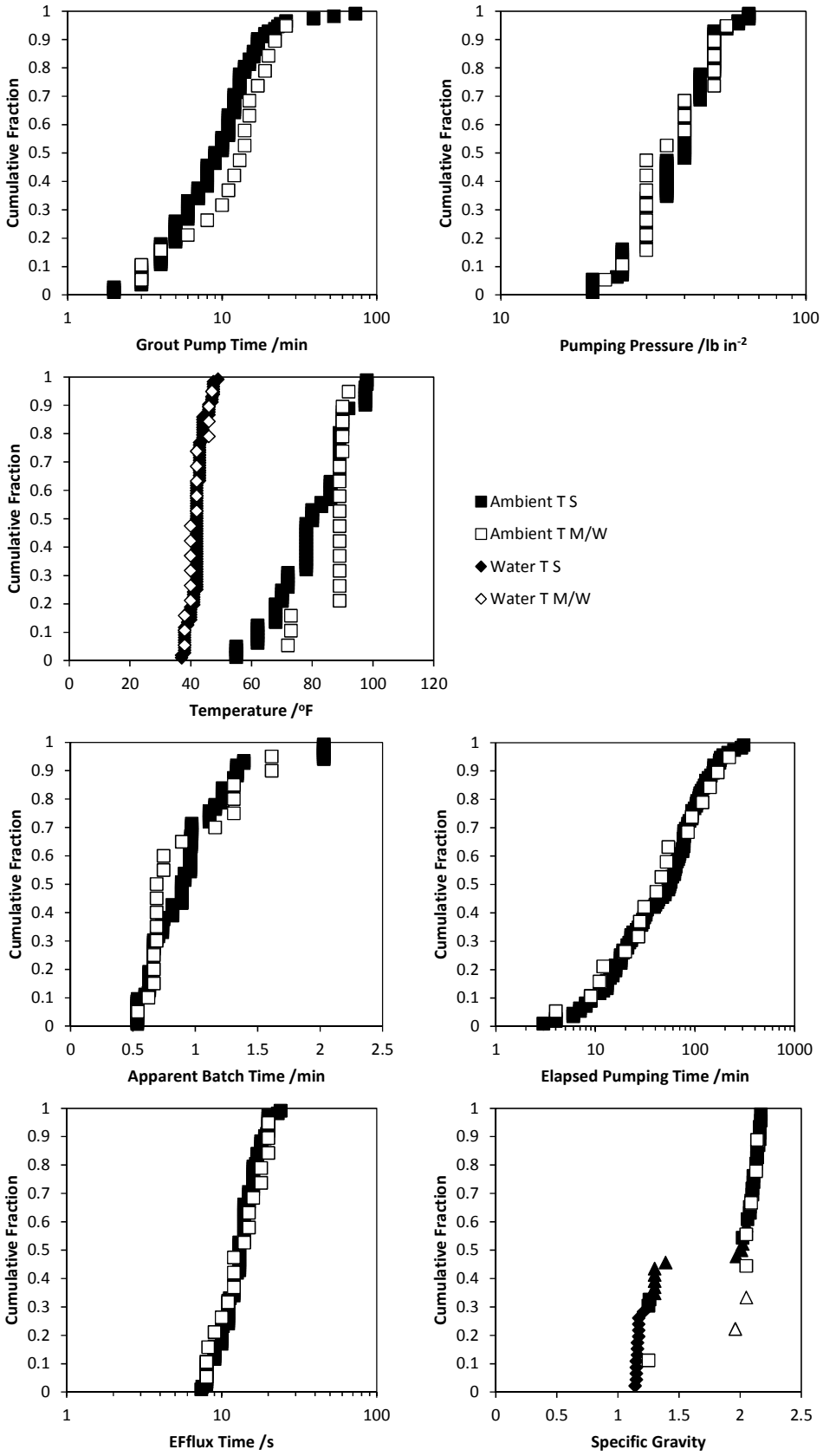

Figure 2.14. Grouting statistics for PT bridge construction case.
Black symbols: Hardened grout. White symbols: Wet or soft grout.

The four other bridges where significant deficient grout was observed have been in service from 3 to 14 years. Corrosion of steel tendon components associated with the deficient grout was present in two of those bridges. In one of those two bridges, significant surface rust and widespread wire surface pitting was observed on strand in external tendons with grout deficiency associated with void presence. As mentioned earlier, the grout material has not been positively identified and may possibly be a neat grout. Two grout samples from the vicinity of corrosion development were analyzed by powder X-ray diffraction. Of note, the two samples were different in composition particularly with the presence or absence of crystalline silica and absence or low relative peak intensity for calcium carbonate. Localized corrosion spots were observed in other external tendons with deficient grout in that bridge. The total chloride content, moisture content, and sulfate content were measured. The acid soluble chloride content analysis followed FDOT test protocols. The moisture content was determined by gravimetric comparison after heating the grout samples. The sulfate content was determined by ion chromatography of solution extracted by an ex-situ leaching method. Details on sample preparation and test methodology were not disclosed in the post-inspection report and differentiation in content compared to earlier studies has not been addressed. However, as shown in Figure 2.15, differentiation in moisture content did corroborate with visual description of the hardened and deficient grout. Similar to earlier observations, the deficient grout had moisture content greater than ~20%. There was enhanced sulfate content in the deficient grout as compared to the hardened grout from the same tendons but at levels significantly lower than that observed in the deficient grout in the Ringling Causeway Bridge. Furthermore, the most severe observed corrosion developed in strand in contact with the deficient grout. The chloride content (assuming a unit weight 3,105 lb/yd^3) was on the order of $0.09 < [Cl^-] < 0.45$ lb/yd^3 for both hardened and deficient grout and the pH of the extracted leachate was in the range of $12.7 < pH < 13.2$ for both hardened and deficient grout.

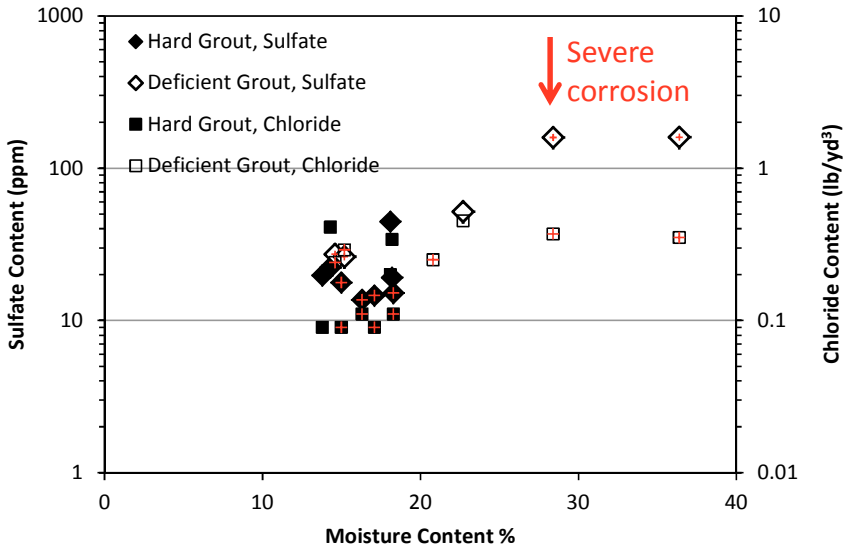

Figure 2.15. Chemical characteristics of deficient grout.
Symbols in red represent locations with localized corrosion spots.

The second bridge where significant corrosion of steel components in presence of deficient grout occurred in internal tendons of continuous PT beams. The tendons were accessed through cutouts on the outer concrete face of the beam exposing the metal duct. Severe corrosion occurred on the metal duct in the vicinity of deficient grout contained within the upper cross-section of the tendon. In some cases, the thickness of the duct had been penetrated by corrosion. Under the corroded duct was soft grout analogous to the grout consistency observed in the bridge where tendon corrosion failure occurred (Figure 2.16). In the tendons inspected, the deficient grout was contained within the upper tendon cross-section and due to the drape pattern and tensioning of the PT strand, the strand were completely embedded in hardened grout in the lower tendon cross-section and was not exposed to the deficient grout. No corrosion was observed on the strand during the limited inspection. Figure 2.17 shows XRD patterns for representative hardened grout from field-extracted samples as well as a control mix of similar grout product. Of note, ettringite was present in the material extracted from the bridge. As seen in Table 2.1, the moisture content of soft grout extracted from the bridge ranged from ~30-66% by mass. The moisture content of hardened grout extracted from the bridge ranged from ~12-18% by mass.

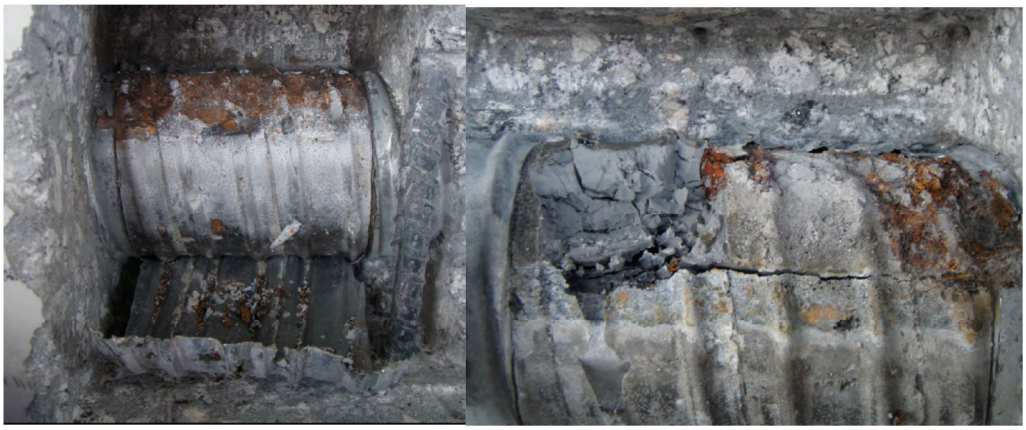

Figure 2.16. Corroded metal duct in vicinity of deficient grout. (Photos courtesy of FDOT.)

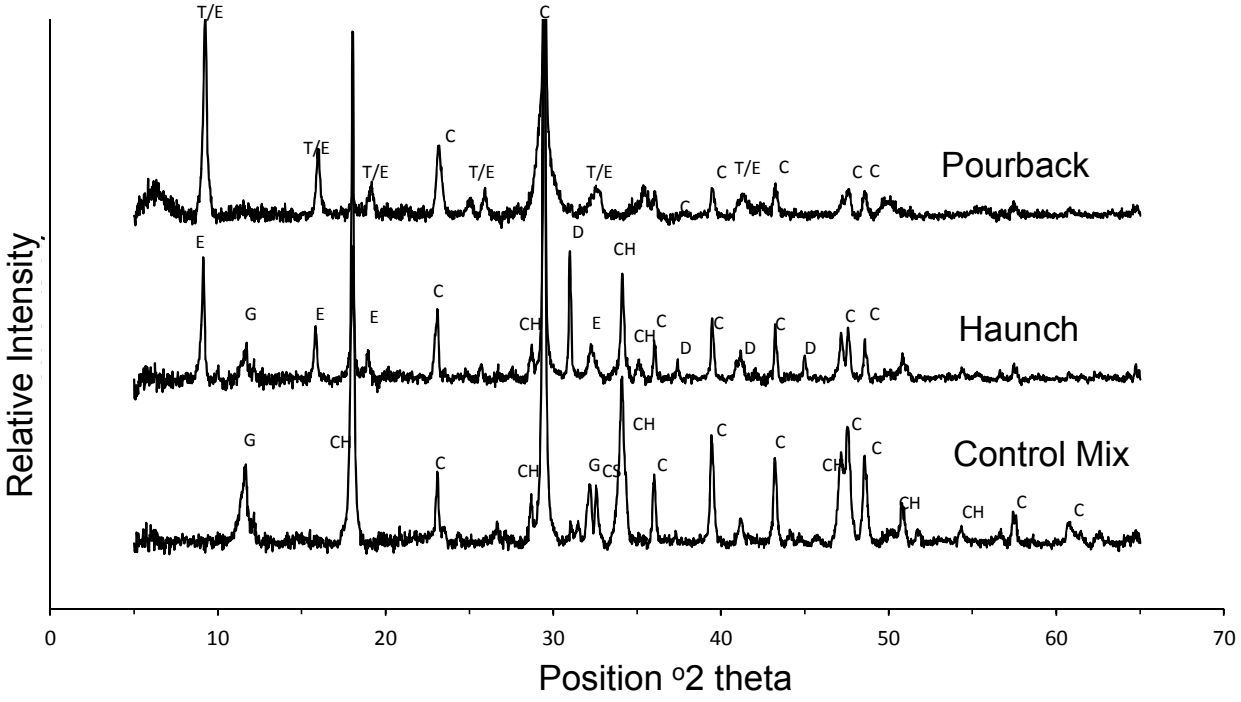

Figure 2.17. XRD patterns of hardened grout material.

C:Calcium Carbonate; CH:Calcium Hydroxide; E:Ettringite; G:Gypsum; T:Thaumasite.

Table 2.1. Characteristics of Grout in a Florida Bridge

	Sample Description		Moisture Content	Potassium (ppm)	Sodium (ppm)	Chloride (ppm)	Sulfate (ppm)
Sample 1	Haunch section of Girder 8 at Pier 10 4/23/12	Good grout from inside duct on Tendon 2	12%	2,500	1,100	13	28
Sample 2	Haunch section of Girder 8 at Pier 10 4/23/12	Soft chalky grout from inside duct in Tendon 2	32%	6,400	1,900	55	12,000
Sample 3	Haunch section of Girder 8 at Pier 10 4/23/12	Putty-like grout from inside duct in Tendon 2	61%	5,200	1,600	40	10,000
Sample 4	Location 9 s#35 7/30/12	Hard grout	14%	2,500	1,000	0.5	8.3
Sample 5	Location 9 s#34 7/30/12	Soft chalky black material	52%	5,700	1,900	410	7,100
Sample 6	Location 9 s#33 7/30/12	Putty-like grout	66%	4,300	1,400	33	6,800
Sample 7	Location 12 s#50 8/3/12	Hard grout	18%	4,600	1,600	10	210
Sample 8	Location 27 s#15 7/19/12	Good grout	12%	2,800	1,100	11	39
Sample 9	s#16 7/19/12	Soft chalky grout	30%	7,400	2,200	11	870

The concentrations of select ionic species in leachate from the grout samples are shown in Table 2.1 and Figure 2.18. Similar to the grout leachate from the Ringling Bridge, the deficient grout had greater moisture content (>20%), enhanced sulfate ion concentrations (as high as 12,000 ppm) and enhanced potassium and sodium ion concentrations. Somewhat enhanced concentration of chloride ions in the leachate was measured for one of the samples but was otherwise generally low regardless of grout quality.

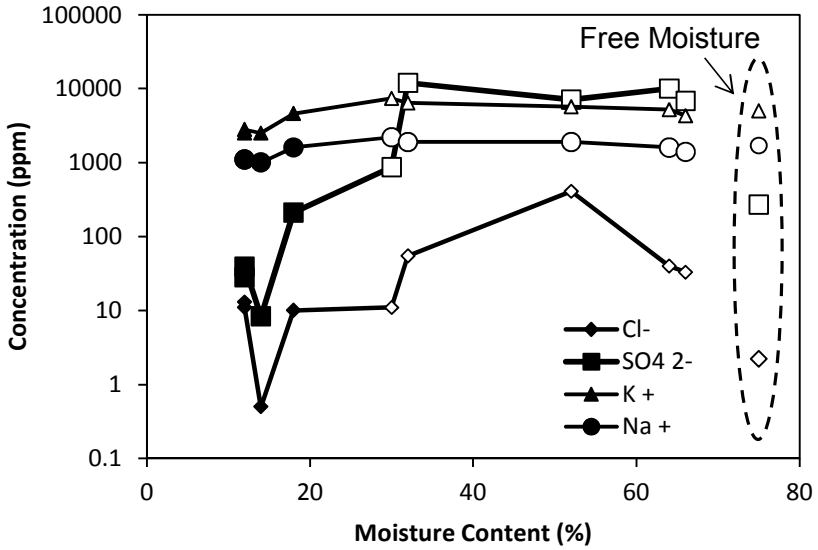

Figure 2.18. Ionic constituents in deficient grout.
Black: Hardened Grout. White: Deficient Grout

During field inspection of the internal tendons, it was discovered that free moisture was present in some of the tendons. Initial chemical analysis of the collected water indicated that the pH was 13.2 and had ~250 ppm sulfate ion concentration. Additional testing for the ionic species shown in Table 2.2 was conducted. The high pH and comparable potassium and sodium ion concentrations from leachate from other grout samples from the bridge would indicate that the water had been in the duct for some time in order for the ionic species to be leached into solution. It was not determined if steel corrosion was associated with the free moisture. If the system remained sealed and the strand were fully embedded or submerged in the grout and free moisture, respectively, passive conditions should remain since the pH remain high and low chloride and sulfate levels were present. If the strand were to be partially exposed to air, corrosion may develop similar to corrosion of strand due to bleed water.

Table 2.2. Free Moisture Chemical Analysis.

	Concentration (ppm)
Calcium	84
Iron	0.5
Potassium	5,000
Sodium	1,700
Zinc	13
Chloride	2.2
Sulfate	270

Grout material parameters (such as grout consistency, moisture content, chloride content, sulfate content and pH) for 40 of the PT structures in Florida that have been inspected were available at the time of writing and findings have been combined as shown in Figures 2.19 and 2.20. As earlier mentioned, the amount and severity of grout deficiencies varied from

bridge to bridge. Grout deficiencies characterized as soft, chalky, crumbly, and putty were grouped together as deficient grout. Data from Figures 3 and 6 was reproduced in the graphs.

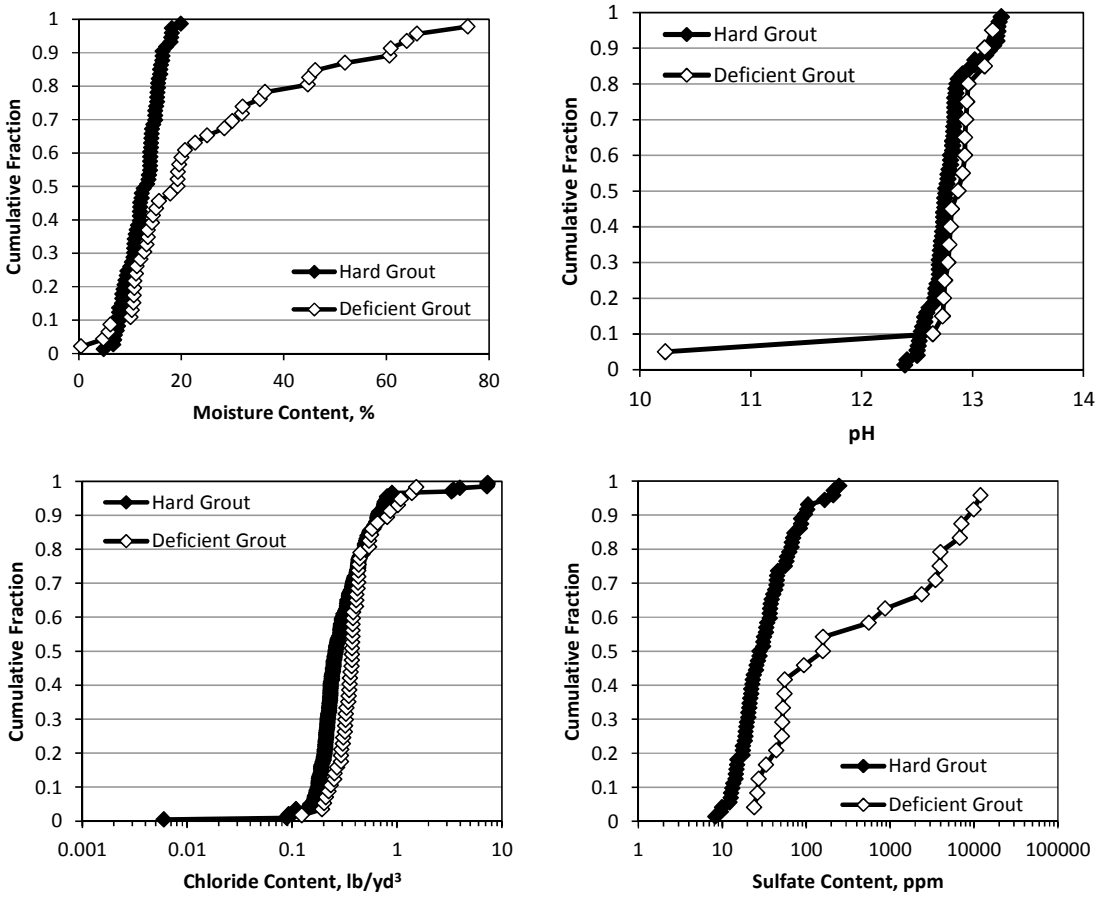

Figure 2.19. Moisture, pH, chloride, and sulfate content in hard and deficient grout.

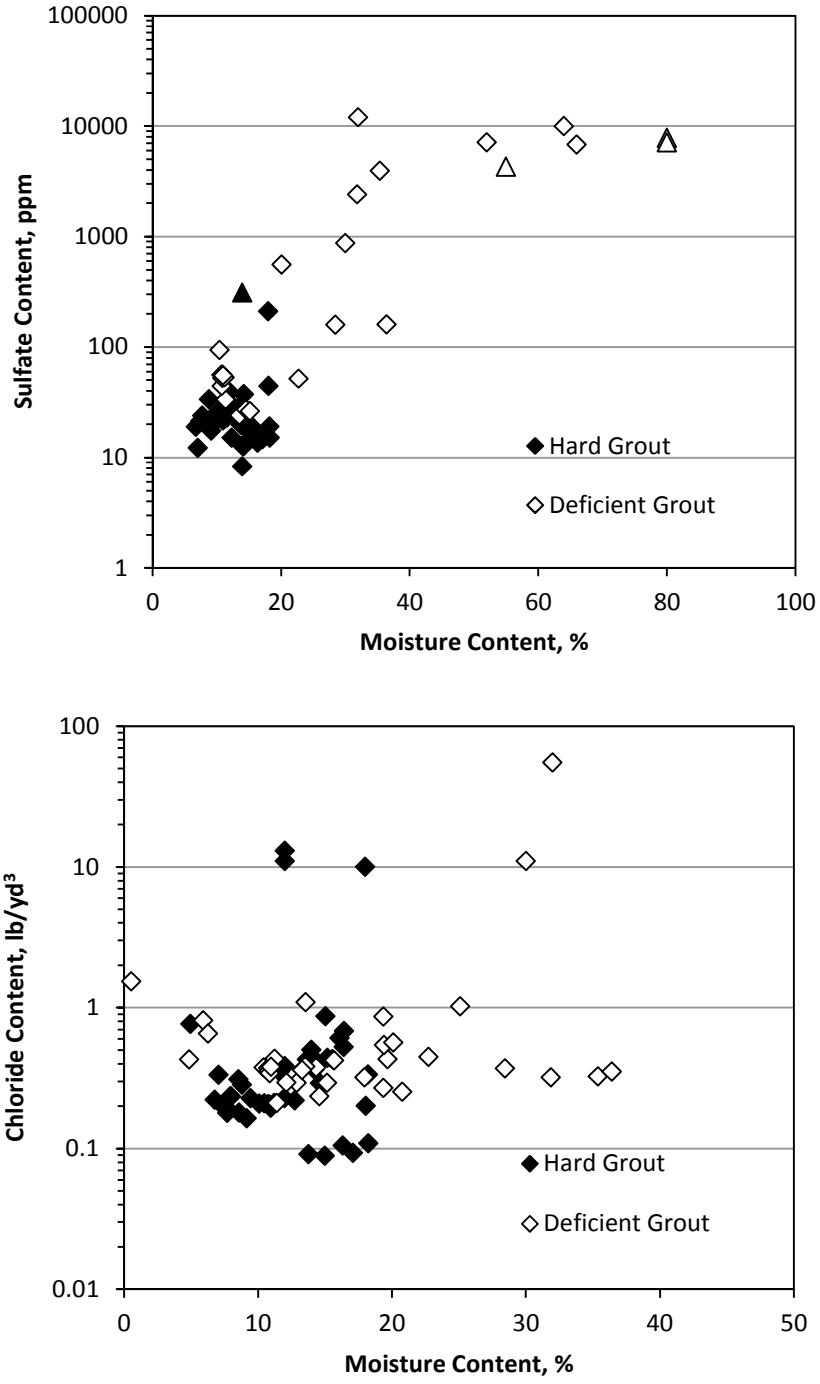

Figure 2.20. Sulfate and chloride content in deficient grout.

The moisture content of deficient grout can exceed 20% by mass and moisture in hardened grout as expected was lower. The triangular symbols in Figure 2.20 shows values from the bridge where corrosion failure occurred. The pH of leachate from extracted grout samples was alkaline, typical of cementitious materials. No significant differentiation in pH was observed between hardened and deficient grout.

The chloride content was expressed as lb/yd^3 of grout with the assumption of a grout unit weight of 3,105 lb/yd^3. The chloride content was not greatly different in the hard and deficient grout (with the exception of some instances of high chloride content), and the total chloride content did not correlate well with moisture content. The cases of high chloride content have been mostly attributed to already-identified chloride contamination in the raw material (FHWA, 2012). In the case of soft grout, the somewhat enhanced chloride content may in part be due to accumulation of oven-dried grout solids during sample preparation.

As expected, the deficient grout typically contained enhanced moisture and sulfate content and the enhanced sulfate content correlated well to the enhanced moisture content. Corrosion was observed in deficient grout with widely variable low-end limits of free sulfates values (in one case as low as 150 ppm and in other cases with low-end values in the order of one thousand ppm). Discrepancies are in part due to the combined influence of other grout material deficiencies and variability in sampling size and test methodologies.

2.3. ROLE OF CHLORIDES AND SULFATES

2.3.1 Chlorides in PT Grout

The discovery of elevated chloride content in pre-packaged PT grout in a construction project in Texas in 2010 led to inquiries by Texas DOT and the Federal Highway Administration. The chloride content in early testing was estimated to be as high as 5% by weight (Merrill, 2010), but others report chloride concentrations has high as 0.5% by weight (Lee, 2014). Nevertheless, these values exceed typical acceptance limits. Current FDOT specifications allow a maximum of 0.4 lb/yd^3 chloride content. Formerly, the specification allowed a maximum of 0.08% chloride by weight of cementitious material. Current PTI guidelines allow a maximum chloride of 0.08% by weight of mixed grout (PTI, 2012). A summary of allowable chloride limits defined by existing codes is available in a review by the Federal Highway Administration (FHWA, 2012).

A comprehensive literature review of chloride threshold concentrations was published by Angst, Elsener, Larsen, and Vennesland (Angst et al., 2009). Compilation of reported data and discussion of important testing parameters were presented. Literature review of chloride threshold concentrations particularly for PT tendons was published by the Federal Highway Administration (FHWA, 2012).

An investigation by Lee and Zielske examined chloride threshold concentrations for PT tendons (FHWA, 2012;Lee and Zielske, 2014). Steel strand was cast in mockup tendons using a pre-packaged grout product with enhanced concentrations of chlorides ranging from 0.08% to 2% by weight of cement. Enhanced corrosion environments were created whereby the tendons were exposed to cycles of temperature and relative humidity. Other testing placed single wire or single strand embedded in grout or immersed in simulated pore solutions. Testing in solution as expected showed greater corrosion susceptibility at lower pH and greater chloride concentration. In accelerated environmental conditioning, strand embedded in grout

showed greater corrosion susceptibility at higher temperatures. Results from large scale mockups showed corrosion development above 0.4% chloride concentration by cement weight for strand embedded in normally hydrated grout.

2.3.2 Sulfates

2.3.2.1 Sulfates in Alkaline Environments

Gouda examined the corrosion behavior of steel in alkaline solutions (Gouda, 1970). As part of that work, the effect of sulfate ions in saturated calcium hydroxide solution (pH 12.1) was investigated. The sodium sulfate concentrations ranged from 0 to 2%. Steel samples immersed in the solution were held at a constant anodic current density of $10uA/cm^2$. In those galvanostatic tests, a drop in potential (to terminal values ~-150 to -450 mV_{SCE}) in time was seen for samples immersed in solution with sodium sulfate concentrations greater than 0.20%, indicative of breakdown of passivity. The $[SO_4^{2-}]/[OH^-]$ ratio was greater than 1.1.

Acha, Alonso, and Andrade also examined the role of sulfates in aerated alkaline solutions (Acha et al., 1990). Steel samples were immersed in saturated calcium hydroxide solution with 0.2M potassium sulfate with a pH of 12.85. The $[SO_4^{2-}]/[OH^-]$ ratio was ~5. In potentiostatic testing, severe localized corrosion was observed at potentials ranging from -300 to +200 mV (reference scale was not reported). The discussion in their work proposed that local acidification in pits creates differential corrosion conditions and prevent metal repassivation. In alkaline environments with pH greater than 12.6, sulfate ions greater than 0.01M may inhibit passive layer formation in local areas. Differential aeration and surface potentials were also though important in the corrosion mechanism.

Al-Tayyib, Somuah, Boah, Leblanc, and Al-Mana examined the role of sulfates on steel corrosion in simulated concrete pore solution (Al-Tayyib et al., 1982). Steel samples were immersed in saturated calcium hydroxide solution with sodium sulfate concentrations ranging from 0.1 to 1% with a pH of 12.5. Linear polarization tests showed decrease in polarization resistance from 81.7k-ohm in sulfate-free solution to 4.3k-ohm with sulfate addition ranging from 0.1 to 0.5%. Electrochemical impedance spectroscopy showed similar corrosion trends with up to 1% sulfate solutions.

Gouda and Halaka furthermore investigated the role of sulfates in corrosion of steel in concrete (Gouda and Halaka, 1970). Concrete samples were made of Portland cement and blast furnace slag. The sodium sulfate content was as high as 8%. In concrete, no indication of breakdown of passivity was observed. However, in testing of steel immersed in concrete pore water leachate containing sodium sulfate, depassivation of steel occurred similar to that measured for testing in calcium hydroxide solution. It was evident that the corrosion behavior of steel in alkaline environments differed when in hardened cementitious materials than in solution. It was thought that alumina-containing cement phases react with the sulfate to form insoluble compounds.

Al-Tayyib and Khan examined the role of sulfates admixed into concrete using ASTM Type V Portland cement (Al-Tayyib and Khan, 1991). Sulfates were added 0.6 to 1.8 kg/m^3 by weight of concrete. Corrosion rate measurements by linear polarization tests showed modest increase in corrosion rate with sulfate additions increasing 1.3 to 1.5 times that of sulfate-free concrete samples after 670 days.

Dehwah, Maslehuddin and Austin examined the role of sulfates in chloride-induced corrosion of steel in concrete (Dehwah et al., 2002). Different cements including a sulfate-resisting cement were used for lab concrete test samples. Exposure solution incorporated 5% sodium chloride and sulfate ranging from 1% to 4% using either sodium sulfate or magnesium sulfate. The sulfates were not shown to affect time to corrosion initiation but the corrosion rate increased with sulfate content. The corrosion rate was up to 2.2 times greater in chloride/sulfate containing solution than in just chloride solution.

2.3.2.2 Sulfates in PT Grout

The cause of the lack of steel passivation (or loss thereof) that led to corrosion activity and macrocell corrosion in the corrosion failure of PT tendons in Florida was thought to be due to the enhanced presence of free sulfate concentrations in the segregated grout that contained high moisture content. Severe corrosion was seen in the presence of segregated grout consistently characterized by high moisture content, high pH, low chloride concentrations, and enhanced sulfate concentrations as high as ~10,000 ppm (Lau et al. 2103a). In laboratory testing in solution, significant corrosion activity was identified in samples initially exposed to pore solution with high concentrations of sulfates in very short periods of time after exposure (approximately 1 day) (Lau et al., 2013b). In other laboratory testing, samples initially exposed to alkaline pore solution free of chlorides and sulfates for up to 60 days did not show significant corrosion activity despite subsequent addition of sodium chloride and sodium sulfate up to 2,000 and 20,000 ppm, respectively. It was thought that if steel was allowed to develop a stable passive layer, later exposure to sulfates at levels tested may not be sufficient in the high pH environment to cause local depassivation of the steel and corrosion development. The results suggested that early exposure to sulfates in the deficient grout is among conditions where development of a stable passive layer may be impaired.

The pH of the pore water solution greatly affects the corrosion behavior of steel in alkaline environments. Generally, higher pH levels were thought to help create stable passivation of the steel. It was noted however that greater corrosion current densities were observed at higher pore water pH (Bertolini and Carsana, 2011; Blactot et al., 2007; Lau et al.,2013d). The near passive current density was as much as an order of magnitude greater in pH 13.3 than pH 12.6 albeit at moderate to low currents (Lau et al., 2013d). Corrosion activity, although in the form of crevice corrosion, was seen in steel samples exposed to pH 13.3 and 20,000 ppm sodium sulfate. However, severe corrosion development also occurred in laboratory samples with pH 12.6 and 2,000 ppm sodium sulfate (Figure 2.21).

A plot of the corrosion potential and corrosion rate developed at the various test conditions of sulfate to hydroxyl ion concentration ratio is shown in Figure 2.22. In the Florida bridge, corrosion was observed in grout environments with sulfate to hydroxyl ion concentration as low as 0.1. The upper bound for the minimum ratio for corrosion development can be considered with the value of 0.35 where corrosion initiation may occur at ratios above that value. It was assumed in those cases where corrosion was active that the passivity was prevented from initially forming. When the steel was allowed to passivate, it is seen that $[SO_4^{2-}]/[OH^-]$ as low as 0.7 did not cause depassivation during the time of the experiment (~100 days for the last dosage regime) even when up to 0.12% chloride was added.

The source of enhanced concentrations of free sulfate ions in the deficient grout from the Florida bridge was not identified, but was thought to be associated with dissolution of phases associated with cement. Regardless of cause, high moisture content was associated with the deficient grout and may in part have contributed to the leaching of sulfates into solution. It was noteworthy that there was strong presence of ettringite crystals in the deficient grout yet the pore solution retained enhanced sulfate concentrations (up to 10,000 ppm SO_4^{2-}) after several years, indicative of an abundance of free sulfates.

The role of accumulated bleed water in corrosion development in repaired tendons was addressed in research by Lau et al., 2013c. Pore water leachate and bleed water from grout samples were analyzed for sulfate content when possible. Negligible sulfate concentrations were reported in the materials (cast in the lab or extracted from a bridge tendon segment) used as a base grout for simulated tendon repair scenarios. Significant amounts of bleed water formed after vibration of a base neat-grout with 0.5 w/cm; and there, the water soluble sulfate concentration was >3,000 ppm. Repair grout materials were placed and allowed to intermingle with that bleed water augmented with additional collected bleed water, DI water, or simulated bleed water with enhanced sulfate additions (>6,000 ppm). After testing, the pore water leachate from hardened repair grout material was analyzed and the water soluble sulfate content was typically <50 ppm even in the test conditions where enhanced sulfate concentrations were present in the intermixed bleed water. It was not known how the sulfate content in the bleed water interacted with freshly cast repair grout, but the sulfates may have in part participated in the hydration process of the repair grout and become associated with solid phases. Furthermore, some of the sulfate content from the bleed water may have diffused back into the base grout accompanying the reabsorption of the bleed water into the grout. It was noted that no significant adverse effects on grout setting occurred in the small laboratory samples with the excess amount of bleed water and repair grout content present. Moisture content for all cases was <20%.

Introduction of the simulated sulfate solution, as well as introduction of DI water, to the exposed portion of strand embedded in base neat and gypsum-based grout prior to placement of repair grout did lead to enhanced corrosion rates. Notably, the enhanced corrosion rates were mostly sustained after the sulfate solution was added whereas some decrease in the enhanced corrosion rate was observed when DI water was introduced. After repair grout was

introduced there, more negative potentials, greater corrosion rates, and larger macrocell currents were consistently observed when the sulfate solution was added in comparison to the samples with DI water augmented bleed water. Furthermore, visual comparison of the strand segment that was initially exposed to the bleed water in simulated void space showed more significant rust formation when exposed to sulfate solution than compared to samples exposed to DI water augmented bleed water.

The enhanced corrosion activity observed in the work by Lau et al., 2013b,c would indicate that complete passivation of the steel strand could be impaired by the early presence of sulfates. However, the amount of sulfates in solution that can be considered to be detrimental in terms of corrosion development has not been well established in the literature. Work by Gouda and Halaka, 1970 showed that passivity of steel in concrete containing up to 8% sodium sulfate was not affected but corrosion occurred in steel immersed in alkaline solution with as little as 0.2% sulfate. The corrosion behavior in concrete was interpreted as being due to reaction of most of the sulfates with cement phases. Low sulfate content in the leachate of repair material despite of intermixing of sulfate in intermixed bleed water in lab samples by Lau et al, 2013c may be explained by this as well. This explanation does not necessarily disagree with observations of the deficient grout considered here as the deficient grout associated with corrosion was associated with water contents as high as 80% by mass and there was indication that the deficient grout did not contain high cement content. In such a condition, the sulfate ions would mostly be in the aqueous phase and indeed concentrations as high as 0.9-1% sulfate were measured.

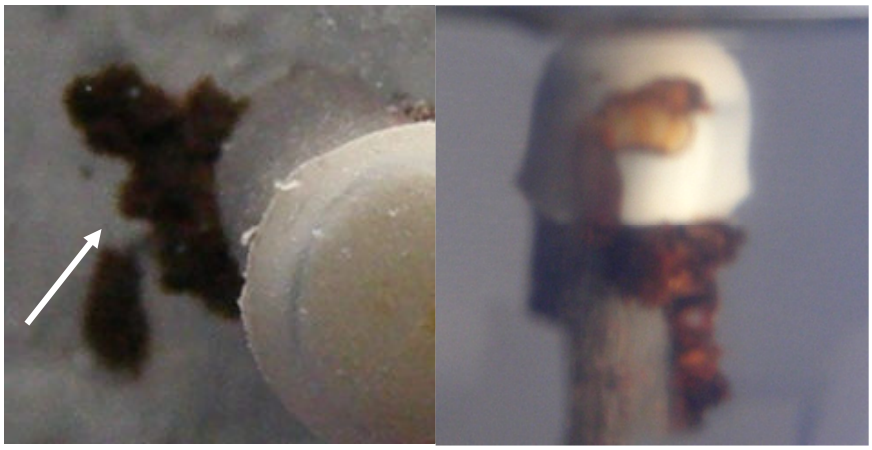

Figure 2.21. Solid corrosion product on steel in 0.13% sulfate solution, pH 12.6. Photos of samples submerged in solution. (From Lau et al., 2013b.)

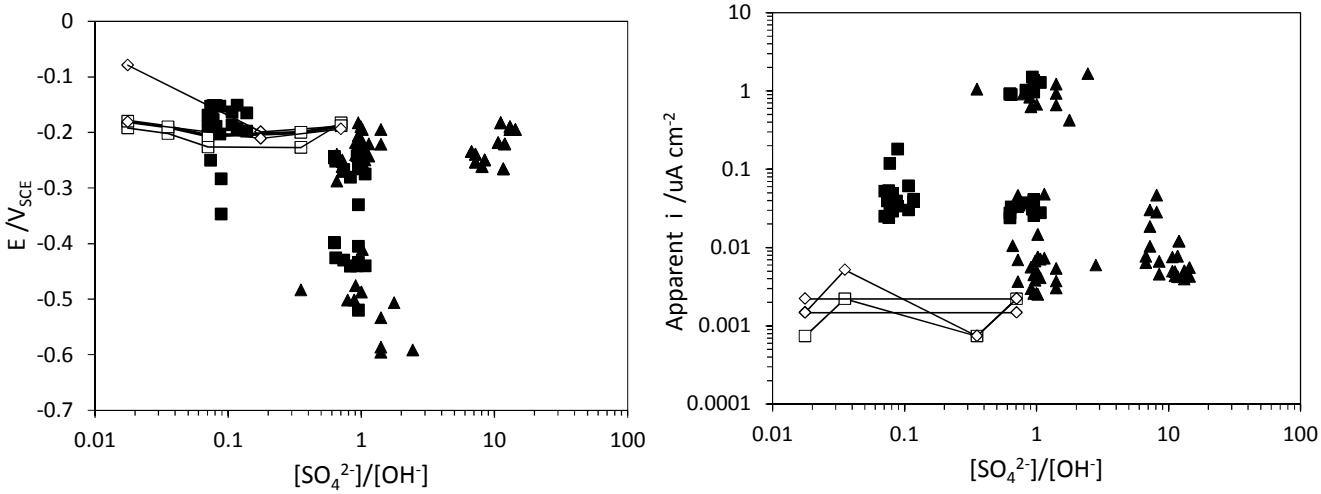

Figure 2.22. Corrosion of steel in alkaline sulfate solution.
(Sodium sulfate solution immediately introduced- Black Triangle: pH 12.6. Black Square: pH 13.3.) (Sulfate-free solution initially introduced- White Square: pH 13.3, sodium sulfate incrementally added. White Diamond: pH 13.3, sodium sulfate and sodium chloride incrementally added.) Some data points represent macrocell current where the net anodic current was measured and presented as a nominal corrosion current density. (From Lau et al., 2013b.)

Corrosion of PT strand in segregated grout characterized by having alkaline pH, high sulfate ion content and low chloride content has also been reported in Europe (Bertolini and Carsana, 2011). Laboratory tests with steel in de-aerated sodium hydroxide alkaline solution and reconstituted segregated grout were conducted to address possible corrosion mechanisms.

The mechanism proposed had basis on the electrochemical activity of steel in highly alkaline solution and large cathodic polarization as shown in the Pourbaix diagram for iron. The accelerated localized corrosion was thought to be caused by depassivation of steel in very alkaline environments (pH>14) within crevice regions depleted of oxygen where large cathodic polarization ($-1V_{SCE}$) can occur and then enhanced corrosion rates caused by macrocell coupling of those active regions with larger extended passive regions.

In lab testing of steel in alkaline solution, corrosion occurred when in the presence of large cathodic polarization ($-1V_{SCE}$); however, the morphology of that corrosion was not consistent with the localized corrosion observed in the field. It was also noted that potentials more negative than -800 mV_{SCE} was difficult in laboratory settings by bubbling nitrogen or helium. It was posed that characteristic localized corrosion occurs in crevices. In preliminary testing, modest corrosion was reproduced in lab tests placing steel in the presence of the reconstituted segregated grout but characteristic localized corrosion was only observed in crevice regions of the test cell.

Modest increase in the anodic current exchange density for steel in pH>14 solution was observed with the addition of 74g/L Na_2SO_4 solution (5%); however, greater increase in anodic current exchange density was observed with the increase in pH from 14 to 14.3. The role of sulfates in the corrosion mechanism was not further addressed.

Work by Blactot et al., 2007 also addressed the stress corrosion cracking behavior of steel in high pH sulfate solution characteristic of segregated grout. As much as 150g/L Na_2SO_4 was added to sodium hydroxide test solution at pH ~13.6. Anodic polarization curves created at fast scan rates (~83.3 mV/s) showed somewhat greater current densities in solution with presence of sulfates. Interestingly, two anodic peaks (at -750 and -1,000 mV_{SCE}) that may be analogous to a critical passivation current density were observed with greater anodic current densities in the presence of sulfates. Similar to results by Bertolini and Carsana (2011), a strong influence of solution pH on increasing current densities was also observed. As described above, anodic peaks with large anodic current densities were observed for the solution with pH 13.6. In solution with pH 12.9, the anodic peak was seen at -500 mV_{SCE} with significantly lower anodic current density.

In test samples incorporating segregated cement described as containing ettringite and portlandite (at pH 13.7), the strong anodic peaks were also observed. However, a so-called diluted sample obtained from cement and described to contain sulfate and hydroxyl ions (pH 13.2), the anodic peak was seen at -500 mV_{SCE} with much lower current densities and comparable to the polarization curves for steel in pH 12.9 solution described earlier.

In the work by Lee and Zielske (Lee and Zielske, 2014), significant corrosion occurred at the steel interface between void space and some form of deficient grout with enhanced sulfate concentration. In that test subset, no chlorides were present and the deficient grout characterized and black and porous had sulfate content as high as 1.5% of the grout weight. Samples without the deficient material had sulfate content that ranged from 0 to 0.5% of the grout weight.

2.4. CONSIDERATIONS FOR REPAIR OF TENDONS WITH DEFICIENT GROUT

The deficient grout with varying extent of segregation and characterized as having different properties and chemistry was seen to support corrosion activity. Although early repair procedures have been implemented in Florida bridges to remove the most severe segregated grout from some locations of the deficient tendons, some concerns on future corrosion progression after initial repairs have been completed were raised. Furthermore, the corrosion failure of a tendon in the Varina Enon Bridge in Virginia in 2007 occurred in a vacuum-grout repair section where the steel strand was in contact with deficient grout and repair grout (Sprinkel, 2010; Sprinkel and Napier, 2008).

Laboratory work to address some of these concerns is detailed elsewhere (Lau et al., 2013b and c; O'Reilly et al., 2012) and is summarized in the following.

O'Reilly, Darwin, and Browning, 2012 (O'Reilly et al., 2012)

Research was conducted to address possible corrosion mitigation or corrosion progression due to the presence of dissimilar grout materials in PT tendons after repair of grout voids. Several grout materials were tested including prepackaged low bleed grouts. Corrosion behavior was evaluated by rapid macrocell tests along with other conventional d.c. electrochemical techniques.

As expected, the pH of pore solution extract (obtained by pore water expression technique) was alkaline (pH>13) with low chloride concentrations. The sulfate concentrations were in the order of 100 ppm or less except for a gypsum tile grout and one commercial grout where the sulfate content was in the order of ~1,000 ppm. It is noted that the products with enhanced sulfate content were not products specified by FDOT at the time of this report.

As expected, significant corrosion of test samples occurred when exposed to 3% chloride simulated grout pore solutions or when partially exposed to neutral pH solution. Less corrosion was observed in samples exposed to chloride-free simulated grout pore solution. The authors also provide cursory discussion to the possible role of pore solution pH (in the range from pH 13-13.98) in corrosion development but without elaboration on mechanisms. Some comments refer to galvanic interaction between steel sections embedded in differential pH environments. Recommendation of similar pH of repair and existing grout pore solution was made.

Greater corrosion rates were measured for steel strand embedded in gypsum grout than in other grouts. Also, enhanced corrosion (relative to performance of simulated pore solution for low-bleed grouts) was observed for steel embedded in simulated solution of the gypsum grout was noted. The cause has not been fully elucidated but may be related to elevated sulfate concentration in the pore solution. Some correlation to greater corrosion activity with enhanced sulfate concentrations in solution was reported and recommendations to address sulfate concentrations were made.

Lau, Rafols, Lasa and Paredes, 2013 (Lau et al., 2013b)

There was no evidence of significant corrosion development in laboratory tendon mockups with voids repaired with dissimilar grout when the base and repair grouts were properly cast and conditions were free of tendon material deficiencies. In the experiments with steel embedded in a base neat grout and coupled with steel embedded in commercially available repair grouts, no indication of corrosion development was observed. The laboratory tests incorporating field-extracted tendon segments with pre-existing voids and repaired with commercially available repair grouts also typically showed passive corrosion behavior. Some minor corrosion did develop at a localized region of deficient grout possibly due to moisture from the repair grout but corrosion activity diminished after approximately 1 month. The laboratory tests incorporating base neat grout and field-extracted tendon segments cast with commercially-available repair grouts showed indication of corrosion mitigation; however, there

was some marked differentiation of corrosion behavior of the samples between the two repair grouts possibly being attributed to the marginal difference in the developed solution resistance of the repair grouts.

Surface rust formed on steel wire partially cast in grout and subsequently exposed to 100% humidity. Corrosion also developed on the wire at the interface of the base grout where bleed water and moisture condensation accumulated. However, it was observed that that corrosion was significantly reduced after introduction of the repair material. If the accumulated moisture does not contain aggressive chemical species such as chloride ions, the moisture may likely combine with the repair grout without significant detrimental long-term effects. Significant corrosion activity was observed in field-extracted samples with deficient grout characterized as white/chalky and/or wet plastic. As described in earlier sections, analysis of deficient grout obtained from bridge tendons revealed high pH level, low chloride content, and enhanced concentrations of sulfates. When steel embedded in these deficient grout materials was coupled to steel in good hardened grout, it was apparent that enhanced corrosion can occur by macrocell coupling. The steel in the deficient grout acts as the local anode and the rest of the strand assembly acts as an extended cathode.

In absence of abnormal grout and other tendon deficiencies, repair of void space with dissimilar repair grout materials can be expected to be completed without corrosion development. Both grout materials should yield high pH environments and the steel should maintain passive corrosion behavior. Moderate levels of polarization in the anodic region due to coupling of steel in the dissimilar grout materials is not expected to cause significant enhanced corrosion rates if the repair is made to prevent moisture accumulation and exposure from aggressive chemical species.

Extra consideration for repair should be made for tendons with deficient grout. Generally from the information garnered from field observations and laboratory testing, deficient grout that would provide environment for severe corrosion would have excessive moisture content, low cement content, and enhanced sulfate ion concentrations. If grout segregation in the form of wet soft grout was observed to any degree, it may be posed that the hardened grout in the near vicinity of the poor grout material may also have defiencies, and a decision will have to be made to determine if that material is acceptable. Complete removal of deficient grout should be considered if no other remediation methods are implemented. It is also important to have assurance that the complete void space is repaired. Partial/incomplete repairs that result in part of the strand remaining exposed could be susceptible for corrosion development.

The effect of accumulated bleed water was not fully addressed in the research, but limited laboratory testing did show corrosion mitigation after placement of repair material. The higher electrical resistance of the commercially available low bleed grouts in comparison to a 0.45 w/cm neat grout is a benefit to reduce macrocell corrosion development in some cases.

Lau, Powers, and Paredes, 2013 (Lau et al., 2013c)

Results of research described here focuses on determining the extent to which corrosion may continue after detection and repair of deficient PT ducts with presence of unmitigated moisture accumulation and the subsequent variation of grout pore water chemistry of the original grout and newly placed repair grout. Small lab specimens were cast in replicate to simulate tendon repair conditions (with dissimilar grout) representing grout in dry conditions, bleed water conditions, and bleed water conditions with enhanced sulfate ion presence. Repair grout was introduced to additional samples prepared from a bridge tendon containing hardened non-homogenous grout.

As expected, negligible corrosion activity was observed for the tendon repair condition where the pre-existing grout was relatively homogenous, hardened and in relatively dry condition. Marked indication of relatively greater corrosion activity was observed in conditions where moisture was introduced into the tendon and allowed to intermix with the repair grout material. There, somewhat greater corrosion currents were measured when the excess moisture contained enhanced sulfate concentrations. Correspondingly in those cases, a greater presence and severity of surface rust was observed on strand exposed to the moisture prior to introduction of the repair grout material. Forecasting of corrosion severity to full scale tendon scenarios from the measured and observed corrosion was not intended in the limited scope of the experiments; rather the experiments were in part made to identify if there was gross susceptibility for corrosion development for repaired tendons with unmitigated moisture accumulation. Indeed, the data from the experiments did indicate that tendon conditions with greater moisture contents repaired with dissimilar grout could be conducive for comparatively enhanced corrosion activity. The increased corrosion activity could in part be attributed to the lower cement content of the grouts mixed with enhanced water volume and the associated reduction of grout electrical properties and greater permeability; however, the development of bleed water in the base grout may be associated with those conditions and are as such considered to be relevant test conditions.

Indication of maintained corrosion activity in strand from sections from a post-tensioned tendon (with unmitigated hardened non-homogenous grout) after introduction of repair grout material was observed; however, there was differentiation in behavior for experiment subsets utilizing different repair grout materials. The cause of the differences in behavior between the two grout products was not elucidated and was further complicated by the conditions of the as-received grout sections. Two possible scenarios were posed to explain the differentiation in behavior. In the first scenario, the corrosiveness of the grout environment in the base grout tendon section repaired with one of the repair grout products may have been less than that of the samples repaired with the other repair material (in part due to sample aging in the lab prior to sample fabrication). In the second scenario, the material conditions and properties of the different repair grouts may have influenced the corrosion activity of the strand in the base tendon section by either mitigating or enhancing corrosion after placement of the respective repair grout. In prior research, rewetting of deficient grout through the strand interstitial spaces

and porous grout matrix was shown to lead to corrosion activity. It was not in the scope of research to evaluate the efficacy of repair grouts for these scenarios and the differentiation in behavior was not further evaluated.

Corrosion behavior of strand in tendons repaired with dissimilar grout did not appear to be related to reduced grout pore water pH. In all tested cases, the pH of the pore water leachate was high with values typical for cementitious material (pH>13) and no significant differentiation in pH was measured for portions of the grout that were characterized as partly chalky or when augmented or simulated pore solution was introduced to the mix. Samples with enhanced presence of sulfate ions in bleed water intermingled with the repair grout showed indication of somewhat greater corrosion even though the sulfate content in the grout pore water leachate after grout hydration were not significant. Even in test conditions where the sulfate concentration in the bleed water was high either developed during vibration or augmented, the pore water leachate from hardened grout materials was typically <50 ppm. It was not elucidated how the sulfate content in the bleed water interacted with freshly cast repair grout, but the sulfates may have in part participated in the hydration process of the repair grout and become associated with solid phases. Furthermore, some of the sulfate content from the bleed water may have diffused back into the base grout accompanying the reabsorption of the bleed water into the grout. Larger test sample geometries may provide further insight on the adverse effects of excess water presence on grout segregation and hydration where high moisture content and the presence of water-soluble sulfates may become of greater significance. Quantification of a critical concentration of sulfates was beyond the scope of this work.

The negligible corrosion activity found for non-deficient grout with low moisture content would indicate that tendons with similar grout conditions with voids may be repaired with dissimilar grout materials without major corrosion development. However, grout conditions with accumulated moisture may continue to support enhanced corrosion activity after repair. Unmitigated deficient grout may support corrosion activity with possibility of enhanced corrosion due to macrocell formation between local anodic locations and strand in the repair grout. Further assessment of the pore water chemistry and the role of sulfate ions on corrosion initiation was recommended. Evaluation of the effectiveness of available repair grouts to mitigate corrosion of strand was recommended as well.

3. DEFICIENT GROUT

As field evidence has shown that steel corrosion in thixotropic grouts occur where both deficient grout with high bulk moisture content and enhanced sulfate ion concentrations were observed, it is of importance to differentiate and characterize that grout deficiency. The work in part was aimed to consider the role of moisture in the formation of deficient grout and accumulation of sulfate ions, to differentiate physical and chemical grout properties by grout deficiency, and to differentiate corrosion behavior of steel by degree of grout deficiency and sulfate presence. The testing to identify deficient grout that may form in presence of enhanced moisture content is referred throughout the report as Grout Cylinder test.

3.1 METHODOLOGY

Testing of grout materials utilized two commercial pre-packaged PT grout products that were labeled here as Product A and B. Except for the variance noted below, the mixing procedures for small grout quantities followed manufacturers recommendation. Initial testing (referred to here as 'Pre-Exposed Grout') was made to evaluate the severity of grout degradation due to pre-exposure in high humidity and excess moisture content. Grout was removed from its original packaging and was placed in containers within a 100%RH chamber for 3 or 7 days. Some grout material was exposed for up to 28 days. A control set of grout was not exposed in high humidity. In addition to possible absorbed moisture, the grouts were mixed with an additional 20% water (by mass of grout after exposure for treated samples) above the manufacturer recommended mix water content to enhance material deficiency. Additional test samples (referred to here as 'expired grout') considered grout mixing conditions that were reported to produce deficient grout with enhanced bulk moisture content. For those experiments, expired-grout of Product A was mixed with 15% additional water. Furthermore, subsets of those samples (used for corrosion evaluation) contained sodium chloride and sodium sulfate. The test subsets included grout mixed with 0.08% Cl^- and 0.2% Cl^- by mass cement; and 2,000, 20,000, and 150,000 ppm sodium sulfate concentrations in the mix water. The grout was cast in standard 3-inch diameter cylinder molds.

Relevant grout material parameters (that were thought possibly higher in deficient grout) included bulk conductivity, void content, and moisture content. The inverse of electrical conductivity was calculated as wet resistivity using a four-point resistance test setup. The void content was determined per ASTM C642-13. The moisture content of the grout samples was determined by gravimetric methods. The pre-exposed Grout and expired grout samples had different curing conditions. The pre-exposed Grouts (demolded 4 days after casting) were placed in 100%RH for 40 days. The expired grout samples (cast as part of Modified Inclined Tube test sample preparation) were cured in ambient conditions for ~200 days and then de-molded and placed in 100%RH for 60 days. Mass change and wet resistance measurements were made during the conditioning period in high humidity. After conditioning, the samples were subjected to drying as part of ASTM C642 and also to measure moisture content.

The free sulfate concentrations in leachate from the expired grouts with zero amended sodium sulfate and with 20,000 and 150,000 ppm sodium sulfate were measured by ion chromatography. The expired grout samples all showed varying layers along its 6 inch height. Although none of the layers had the degree of deficiency as observed in the field, the textures of the layers (especially at the top) were synonymous with grout segregation. Representative samples of those layers were collected and crushed to pass a No. 100 sieve. Three leaching procedures were used to elucidate the availability of sulfate ions in the pore water of deficient grout. The procedures following modified ASTM method for determination of sulfates in soils as well as methodology used in earlier phases of research on deficient grout. Important leaching conditions included sample drying, leaching volume, leaching time, and leaching temperature. Method 1 included procedures to dry the powder samples at 55^{o}C for 24 hours, combine 1g of the dried powder with 1:10 leaching volume at 66^{o}C for 15-18 hours, and filter and dilute the leachate into 100mL solution. Method 2 included procedures to use 1g powder as received with 1:10 leaching volume at room temperature for 1 week, and filter and dilute the leachate into 100mL. Method 3 included procedures to use ~12 g of powder as received, use 1:1 leaching volume at room temperature for 7 days, filter, and collect leachate. The results were reported as gram of sulfate per gram of powder (dry powder mass used for calculation for Method 1).

3.2 RESULTS AND DISCUSSION

3.2.1 Physical Grout Properties

As indicated in the Methodology section, two grout sample preparation methodologies were followed. In the test setup to consider the impact of early moisture availability to the grout as pre-exposure before casting (pre-exposed Grout), the grout powder was placed in high humidity conditions. As shown in Figure 3.1, Grout product A and B had less than 1% moisture in the as-received condition. Sampling of the powder after exposure showed increase in moisture content in the raw grout material. As much as 5% moisture content was measured. The grout was stored in several uncovered plastic bins that were kept in 100%RH chambers. Although the moisture content of the exposed grout initially at the top portion of the containers could have had the most moisture uptake, the sampling of the raw grout was made after mixing of the material to determine the overall grout quality. The mixing of the grout powder was subjective and indeed, variability in the measurements was shown where the sampling of grout exposed for 3-days yielded higher moisture content than the 7 day and 28 day exposure. Nevertheless, all exposure conditions created physical changes such as clumping in the raw grout. The grout in the as-received condition and exposed to high humidity for 3 and 7 days were mixed with 20% excess mix water content and cast into 3-inch diameter cylinder molds. After initial curing, some portions of the grout separated due to segregation (as described later). Each segment was treated as individual samples except for some samples that were made from non-pre-exposed Grout B (used for resistivity measurements) where the

segregated grout was well-adhered to hardened grout portion. Each segment was placed into 100%RH chambers.

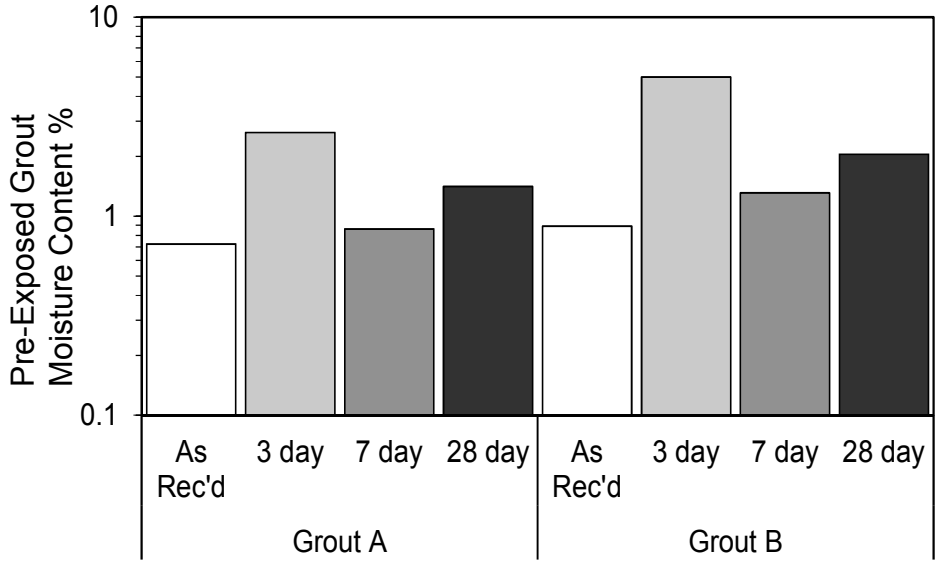

Figure 3.1. Moisture content of grout powder after exposure.

Similar grout cylinder samples had been cast ~200 days earlier (expired grout) as part of large scale operations to create large mock-up tendons containing expired grout with excess 15% mix water for corrosion testing that will be described later. Those mature grout samples were likewise placed in 100%RH chambers.

3.2.1.1 Grout Segregation

In the pre-exposed grout, exposure of the raw grout material to 100%RH for 3, 7, and 28 days as well as application of excess mix water was thought to create grout material deficiencies. As shown in Figure 3.2, Grout Product A generally formed uniform well-hardened samples (with minor material stratification) regardless of the pre-exposure conditions and the extra introduced water but Grout Product B after exposure and casting with excess water formed two segments where the bottom portion was generally uniform and well hardened and the top portion consisted of a light and friable material. As shown in Figure 3.3, the relative percent volume of the top segregated material in Grout Product B was 10-20%. The top portion is referred to as being segregated, but it is noted that the modality of physical deficiency of the created segregated grout was not overtly representative of the soft grout observed in the Florida bridges. The cast expired grout (Grout Product A) samples were made from the outflow material during pumping operations for the large scale tendon mockups. The severity of grout segregation in those large scale samples was identified after termination of corrosion testing and detailed in Chapter 6. The outflow material nevertheless did show stratification of material along the height of the cast cylinders and the material at the top did appear less cohesive than the bulk material.

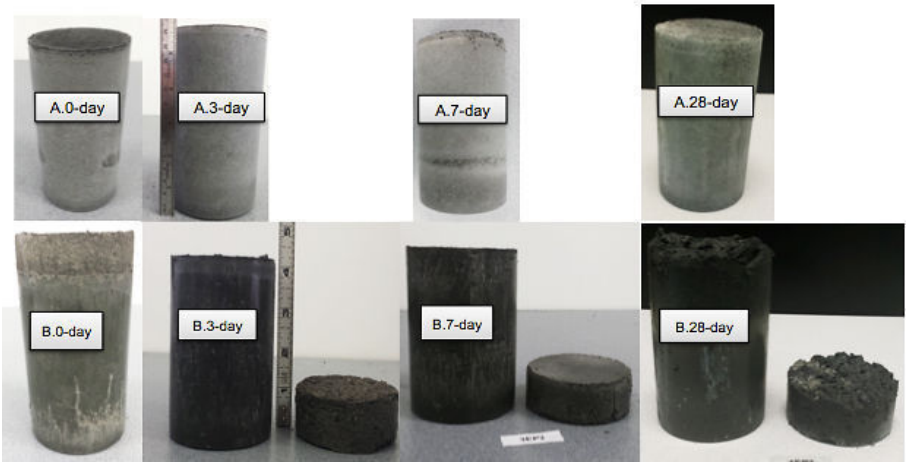

Figure 3.2. Pre-exposed grout products A and B cylinder samples.

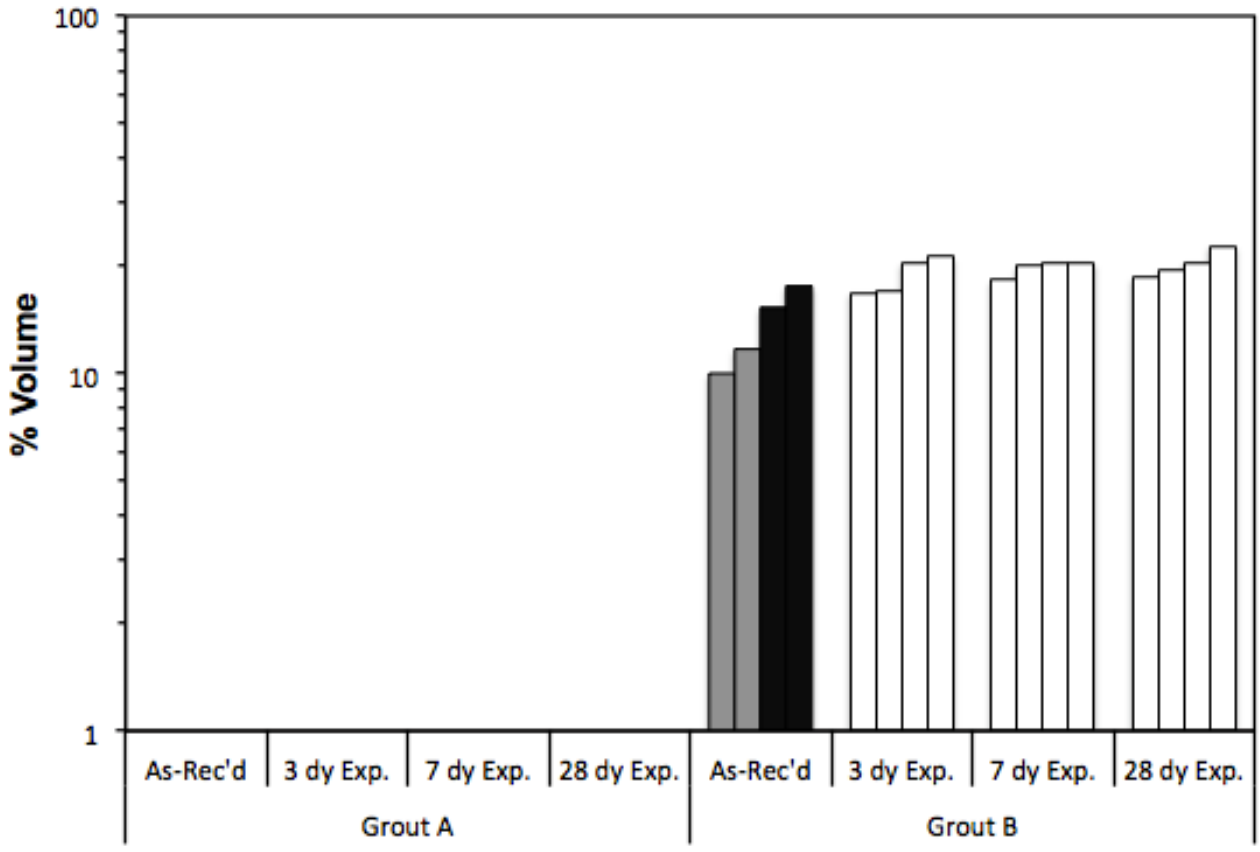

Figure 3.3. Percent volume of segregated grout.
(White bars: Segregated grout layer separated after de-molding. Gray bars: Segregated grout layer separated during testing. Black bars: Segregated grout layer adhered.)

3.2.1.2 Moisture and Void Content

In agreement with visual observation of severe grout segregation, the cast pre-exposed Grout B samples with excess mix water had higher bulk moisture and void content than cast

samples made with Grout A (Figure 3.4). At first look, the enhanced moisture presence in Grout B would allow for a high water-to-cement ratio grout mix that can be characterized by enhanced moisture presence within the porous material. The excess mix water there evidently had more significant contribution to material segregation than its pre-exposure to high humidity. The segregated top portion of cast samples from Grout B showed higher moisture content and void content. In earlier work, Grout A was shown to contain significant amounts of crushed limestone and thus was thought to have high porosity. However, even with the enhanced moisture allowances in mixing, Grout A did not show significant differentiation in bulk moisture content and void space and overall had lower bulk moisture and void content than Grout B. Matured grout samples cast from expired Grout A with relatively less excess mix water generally showed similar bulk moisture and void content. In those expired grout samples, the grout cast with enhanced sulfate concentrations in its mix water did tend towards lower moisture and void content. This was thought to be due to the comparatively lower water availability for cement hydration in those samples mixed with sodium sulfate solution rather than plain water.

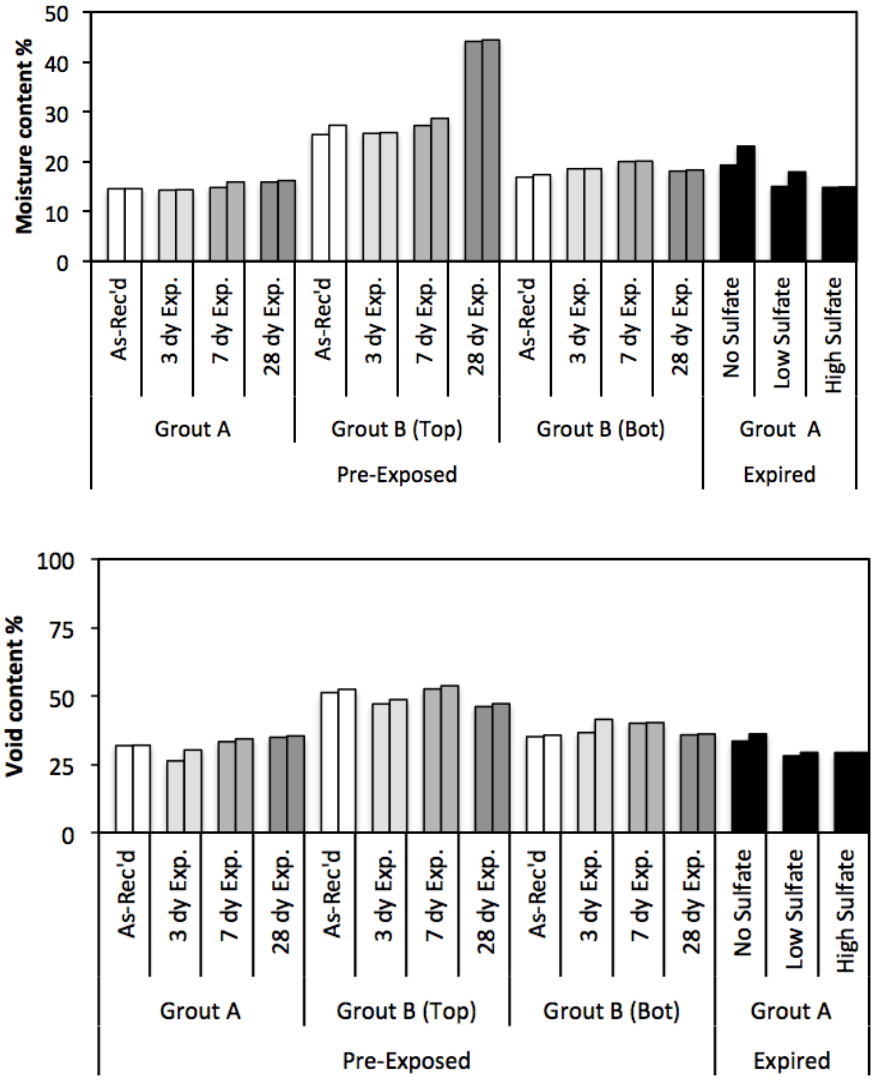

Figure 3.4. Grout bulk moisture and void content.

3.2.1.3 Wet Resistivity

Wet resistivity and mass trends are shown in Figure 3.5. For clarity, the data shown in Figure 3.5 were averages from duplicate samples. Also the initial grout resistivity prior to conditioning in 100%RH is shown as separate points arbitrarily placed at day 0.1 on the logarithmic time scale. For the pre-exposed grouts, the mass uptake as shown as cumulative mass fraction increase generally showed continued mass increase even after ~40 days in 100%RH. Moisture uptake trends were inconclusive for the separated segregated grouts, namely Grout B samples, due to minor crumbling of the friable material. The wet resistivity also continued to increase with prolonged conditioning likely reflective of the continued hydration of the relatively young grout material. Contrastingly, the older expired grout samples showed terminal wet resistivity values, but unexpectedly showed continued mass increase presumably due to water uptake.

Grout Product B used in the pre-exposure test samples (as described earlier) showed propensity for material segregation. The friable segregated material that had higher bulk moisture content and greater void presence than its hardened grout counterpart was shown to have relatively high wet resistivity (about an order of magnitude higher than the hardened portion of the same material). The resistivity of the segregated grout from the as-received (non-pre-exposed) condition could not be measured individually due to the initial cohesion of the segregated grout portion to the hardened grout portion. Thus, the measurements of the Grout B samples from the as-received condition (non-pre-exposed raw material) showed higher resistivity than the separated hardened grout samples from the pre-exposed materials.

The segregated grout samples from material pre-exposed to high humidity for 7 days showed greater resistivity values than those pre-exposed for only 3 days. Grout A and B used in the pre-exposure grout samples did not show consistent differentiation of mass increase and resistivity due to pre-exposure times. This would indicate minor influence of pre hydration by exposure in high humidity. The resistivity of samples made from Grout A in the pre-exposure conditions was in the order of those in the expired condition. The grout samples in the expired condition made with varying sulfate additions did show differentiation in resistivity and those trends in resistivity values correlated well with the moisture uptake as well as the bulk moisture and void content described earlier (i.e. higher resistivity for grouts with lower moisture presence).

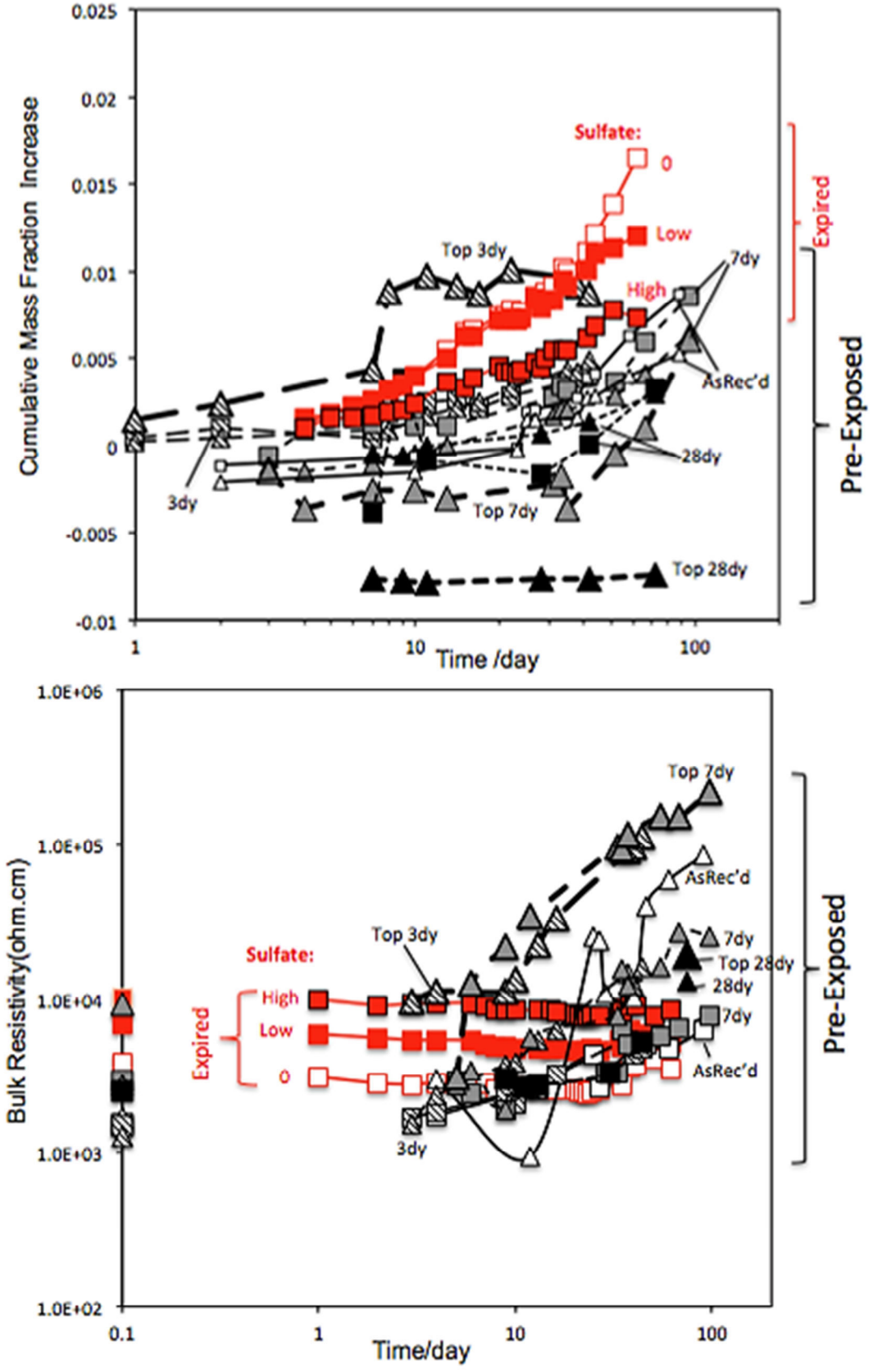

Figure 3.5. Moisture uptake and grout wet resistivity.
(Square: Grout product A. Triangle: Grout product B)

3.2.2 Sulfate Content

It was documented earlier that tendon locations with deficient grout that had severe strand corrosion typically also contained high sulfate ion concentration. As part of the current work, identifying sulfate ion accumulation in laboratory created (and defined) deficient grout was of importance. Grout samples collected from the outflow of pumped grout in large scale tendon mockups were collected and analyzed for sulfate ions. As the source and form of sulfur-bearing ions in field-extracted grout materials (and its relation to corrosion initiation) has not been completely verified, lab samples incorporated intentional sodium sulfate contamination and lab testing incorporated heating of samples to promote dissolution of sulfate ions in the leachate. Other leaching parameters as presented in the Methodology section were considered as well. Procedure to heat and to use greater leaching volumes was described in standardized methodologies to determine sulfate ion concentrations. However, the initial sulfate content in the grout pore water was thought to be important. Greater leaching volumes and temperatures (although facilitating dissolution) were thought to inflate the level of sulfate ions in the grout pore water.

Sulfate levels were initially measured as concentration of sulfate ions in leachate, but units of $g_{sulfate}/g_{powder}$ were reported instead in order to normalize for leachate volume and powder sample mass. One discrepancy that remains in the reported values is the non-standardization of the powder sample mass in terms of drying by the methodologies employed. This discrepancy also remains in field sample testing. The moisture content of grout samples (especially in powder form) may rapidly change due to environmental exposure and time of exposure. However, drying of the powder may lead to aggregation of sulfate due to the need to maintain consistency in samples mass per leaching method.

Results of initial testing of sulfate ion content in expired grout samples are shown in Figure 3.6. Leaching Method 3 (that required larger grout powder mass) was only conducted in the central portion of test samples for the expired grout samples. Similar leaching methods were used in earlier work on a Florida bridge that had tendon failure due to deficient grout (Bridge I). Grout samples from a second Florida bridge (Bridge II) that had steel corrosion in the presence of deficient grout were similarly test. Results from both bridges were shown for comparison.

It was apparent that the reported sulfate content for the expired grout samples had variability by leaching methods. Generally, it was observed that for replicate powder samples, higher sulfate content was resolved by leaching Method 1 that employed methodologies to dry the powder sample and to use higher leachate temperature and greater volume. Lower sulfate concentrations were resolved by Methods 2 and 3. This was not unexpected per caveats described above. Leaching Method 3 did yield higher sulfate concentration for expired grout with 20,000 ppm sodium sulfate in the mix water solution. Some rational on this observation is provided later but additional testing is needed for verification. The test results indicated that

material separation possibly due to enhanced moisture content at the top of the sample can affect the pore water chemistry. It was apparent that there was enhanced sulfate content in the top portions (albeit at relatively thin segments) of the test samples. Electrical measurements indicated permeable grout (that may be associated with grout deficiency) in high elevation portions of the large tendon mockups that used the same expired grout materials. Those results are described later. Samples that had added sodium sulfate contamination showed greater availability of sulfate ions in the leachate. In comparison to the resolved sulfate content measured in grout from Bridge I and II, it is seen that separation of grout material cast in lab conditions can allow for accumulation of sulfate ions without external sulfate sources.

Enhanced sulfate content measured in expired grout mixed with intermediate added sulfate content (20,000 ppm sodium sulfate mix water) by leaching Method 3 in comparison to the other leaching methods of the same material may provide insight on the role of moisture, sulfate content, and grout deficiency. It was assumed (based on the high levels of sulfates measured in the top layers of expired grout where no externally added sulfate contamination was introduced and also the high levels of sulfates measured in deficient grout in Florida bridges) that internal sulfate content may accumulate due to capillary action and changes in pore water chemistry due to grout segregation in presence of high moisture content. Factors such as pore water pH, pore water constituency, and solubility of hydrated cement phases can affect the availability of free sulfates. The expired grout without added sulfate had greater moisture content than expired grout with added sulfates as discussed earlier. The greater moisture content in the former evidently caused a greater level of grout deficiency in upper portions of the grout sample where there was indeed enhanced sulfate content than the rest of the sample. The mobile internal sulfate ions in the pore water would seem to be transported with free moisture towards the upper region of the sample. In the case of expired grout with high levels of added sulfate content, the lower moisture content would presumable cause less grout segregation and thus minimize accumulation of internal sources of sulfate ions. The measured sulfate levels there would then presumably be due to the dissolution of the added sodium sulfate. In the case of expired grout with intermediate level of added sulfate content, the greater excess moisture presence would lead to a greater degree of grout segregation, which would then allow accumulation of free internal sulfate ions in addition to that added by dissolution of sodium sulfate. Indeed, the trends in possible inflation of sulfate ion content in pore water due to higher leaching temperatures and greater leachate volumes in leaching Methods 1 and 2 do not contradict the scenarios proposed above. In the expired grout that contained high levels of added sulfate and had lower moisture content, the enhanced leaching procedures caused a significant increase in the sulfate ion content (presumably due to enhanced dissolution of sulfates that were maintained in cement solid phases or crystalline form such as ettringite). In the expired grout that contained no added sulfates but had higher moisture content, the effect of enhanced leaching procedures was less pronounced (presumably due to the already incurred dissolution of sulfate caused by the excess moisture content and grout degradation). The preceding requires further testing for validation; however, it serves to provide insight on possible grout material degradation as well as corrosion

behavior in deficient grout. Further research to address the importance of cement chemistry on the availability of soluble sulfates is needed.

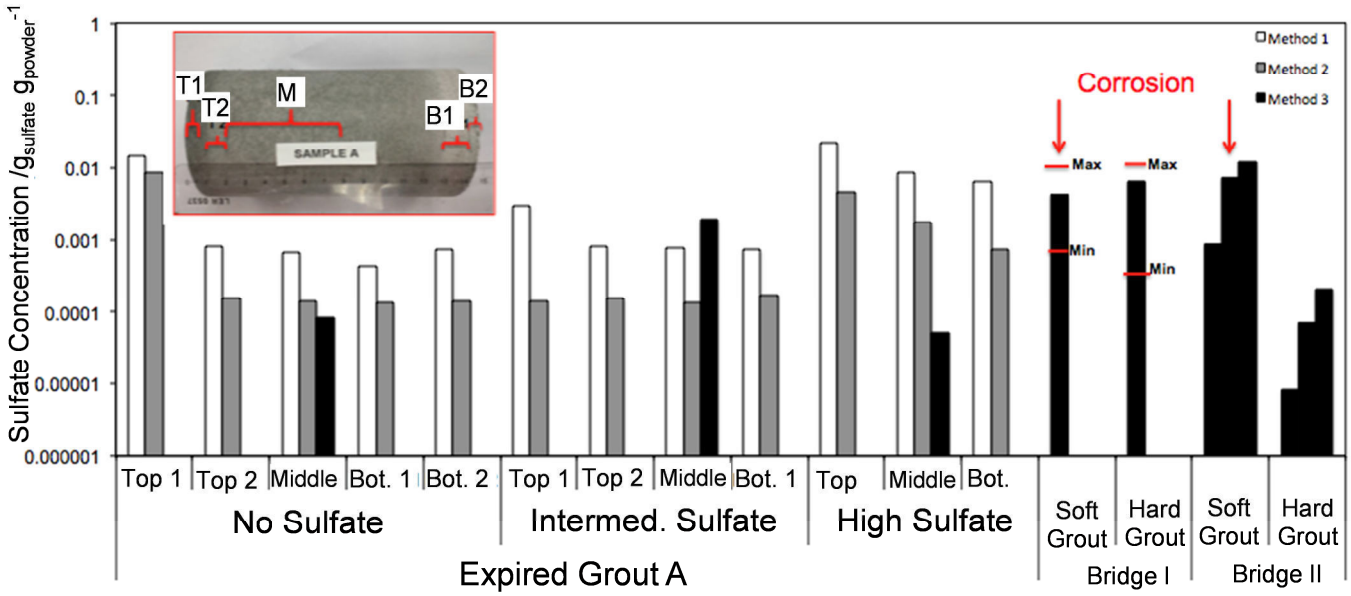

Figure 3.6. Sulfate content for expired grout and field samples.

3.3. SUMMARY OF FINDINGS

- Grout leachate from deficient grout contained enhanced sulfate concentrations. Deficient grout associated with steel corrosion found in a second bridge was similar to that found in deficient grout from the Ringling Bridge.

- High moisture content promotes grout deficiency. Excess mix water appears more significant than up to 7 day of grout powder pre-exposure in 100% relative humidity.

- The level of grout deficiency caused by excess mix water and pre-exposure in 100% relative humidity can vary by grout product.

- High sulfate concentrations can be accumulated in deficient grouts without external sulfate sources.

4. ELECTROCHEMICAL BEHAVIOR OF STEEL IN SULFATE SOLUTION

4.1. INTRODUCTION

Documentation of steel corrosion development in alkaline sulfate environments and its cause was not consistent in the literature. One of the objectives of the work was to identify the role of sulfate ions and corrosion characteristics of steel in alkaline sulfate solution and other environmental conditions that may be involved in corrosion development. The work was also to identify sulfate concentration limits where steel corrosion may develop.

4.2. EXPERIMENTAL SETUP

The test setup described here was made to determine if sulfates in alkaline solutions can depassivate steel or if early presence of sulfates in alkaline solution may provide conditions that would adversely affect stable passive film formation. As the role of sulfates in alkaline solutions in initiating corrosion has not been widely disseminated, only general electrochemical methods and visual analysis was conducted to gauge the issue. The tests were in two general groups but the general test setup of both groups was similar. The steel test samples were 1.5 inch long, 1/4 inch diameter steel rods that were drilled and tapped to attach to encased threaded rod sample holders. Activated titanium rods and saturated calomel (SCE) electrodes were used as reference electrodes. Activated titanium rods were used as counter electrodes. Test solutions as described later were mixed with deionized water. Unless described otherwise, the tests were made in ambient laboratory environments with natural solution aeration. All tests were conducted in duplicate. An example of the test cell is shown in Figure 4.1.

Table 4.1. Base Solution Constituents. Gram per 1L H_2O

	NaOH	KOH	$Ca(OH)_2$	pH
Solution 1	-	-	2.1	12.6
Solution 2	3.7	10.5	2.1	13.3

In the first set of testing, the steel samples were maintained at its steady-state open circuit potential condition in two different alkaline solutions yielding different pH conditions (Table 4.1) (Li and Sagüés, 2001). The steel samples were immersed in those solutions in a sulfate-free base case as well as solutions with admixed sulfate solutions containing 2,000 ppm or 20,000 ppm sodium sulfate. In these tests, the steel was directly immersed in the admixed sulfate solution. In additional samples, testing included incrementally adding sodium sulfate into the solution after allowing the steel sample to be immersed in the sulfate-free solution (ideally promoting steel passivation) to identify if and at what levels sulfates may cause steel depassivation. Sodium sulfate was added every week at 5,000 ppm increments for approximately a month but in some cases the length of the tests was extended and the doping level of sodium sulfate was increased. Additional tests parameters included adding a Teflon gasket around to the steel sample to promote crevice conditions as well as heating the solution

to 37.5^{o}C. Electrochemical testing included monitoring of corrosion potentials with a saturated calomel reference electrode (SCE) and linear polarization resistance measurements.

Figure 4.1. Test setup.

In the second set of testing, short term tests were made to determine the anodic behavior of steel in alkaline sulfate solution. As in the first set of testing, base sulfate-free solutions as well as solutions with admixed sulfate solutions containing 2,000 ppm or 20,000 ppm sodium sulfate in Solutions 1 and 2 per Table 4.1 were used. Also similar to the first set of testing, parameters such as temperature and crevice conditions were assessed. Anodic polarization measurements were made initially from -1 V_{SCE} to +500 mV_{SCE} with a slow scan rate 0.05 mV/s. Comparative testing of samples pre-conditioned at the open-circuit potential and at -1V_{SCE} for 1 day were made. The intent to pre-condition the sample at OCP was to initially allow any possible passive film growth to occur and then measure the anodic behavior of the steel to assess any adverse role of sulfate ions and the other test parameters to initiate corrosion. The intent to cathodically pre-condition the steel sample at -1V_{SCE} was to maintain the steel at a low corrosion rate but remaining at active corrosion condition prior to the slow polarization scan to identify any adverse role of sulfate ions and the other test parameters to impede stable passive film formation. The samples pre-conditioned at OCP conditions were temporarily held at -1V_{SCE} for 30 minutes prior to testing to minimize transient behavior when the scan started at the large -1V_{SCE} cathodic polarization condition.

4.3. RESULTS AND DISCUSSION

Figures 4.2-4.3 shows the corrosion potential and corrosion current densities for steel samples immersed in sodium sulfate solutions with pH level 13.3 or 12.6. The graphs in the figures also show comparative results for steel pre-conditioned in sulfate-free alkaline solution for 1 week prior to the incremental additions of sodium sulfate.

Figure 4.2 shows the results of tests in pH 13.3 sulfate solutions including the additional elevated temperature and crevice environmental test parameters. Sulfates showed no effect on initiating or enhancing corrosion in any of the test conditions. At room temperature, the

effect of the crevice was nominal. The corrosion potential for all sulfate levels with or without crevice conditions was $-260 < E_{corr} < -220$ mV_{SCE} and corrosion current densities were ~0.01uA/cm^2. The corrosion potential for the elevated temperature condition was more negative $-300 < E_{corr} < -240$ mV_{SCE} but corrosion current densities were similar to those measured at room temperature. The results of the incremental sulfate additions up to 20,000 ppm sodium sulfate were similar to the pre-exposed sulfate as well as the base sulfate-free solutions. It was apparent that stable passive film can develop for steel immersed in pH 13.3 solution with little adverse effect from sulfate ion presence and sulfate ions cannot destabilize already developed passive film.

Figure 4.3 shows the results of testing in pH 12.6 sulfate solutions. Pictures of corrosion development are shown in Figure 4.4. Corrosion developed in the cases where the steel was immersed in greater than 4,000 ppm sodium sulfate solution. Severe corrosion particularly at sodium sulfate concentrations >8,000 ppm was observed. The corrosion potential quickly dropped more negative than -500 mV_{SCE} and the corrosion current density was >0.5 uA/cm^2. No visual corrosion was observed for the sulfate-free and up to 2,000ppm sodium sulfate solutions. The corrosion potential there was ~-250 mV_{SCE} and the corrosion current density was $0.005 < i_{corr} < 0.09$uA/cm^2. Notably, no corrosion was observed for the steel samples where incremental sulfates were added even when the test was extended for over 60 days and with sulfate levels as high as 65,000 ppm sodium sulfate (much greater sodium sulfate level than where severe corrosion occurred for the steel directly immersed in sulfate solution). The results would indicate that in pH 12.6 solutions, sulfates may not be able to depassivate steel, but the early presence of sulfates can destabilize passive film growth.

pH 13.3, T~27.5°C

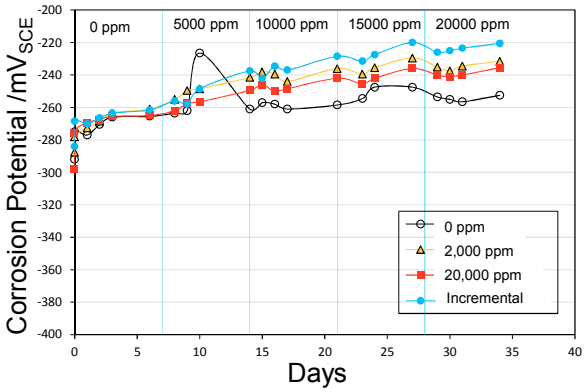

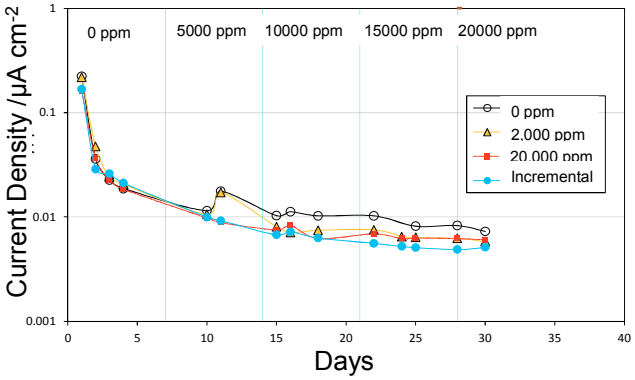

pH 13.3, T~37.5°C

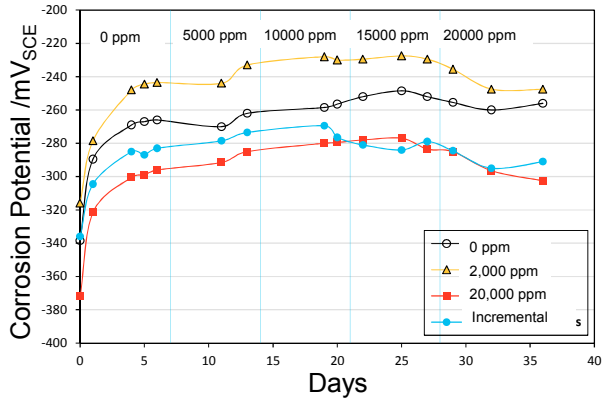

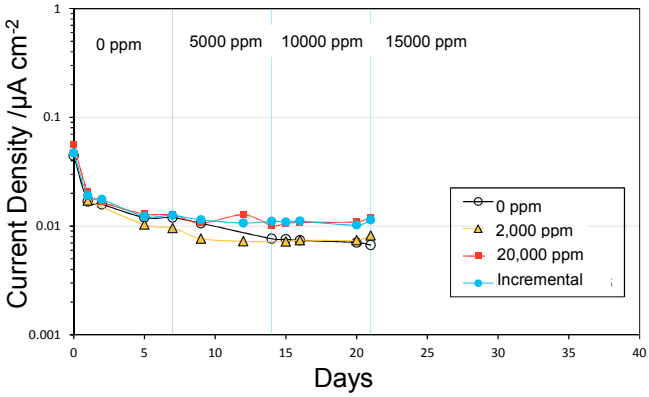

pH 13.3, T~27.5°C Crevice

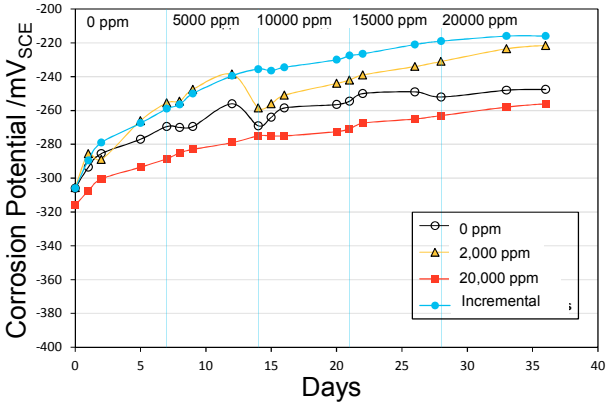

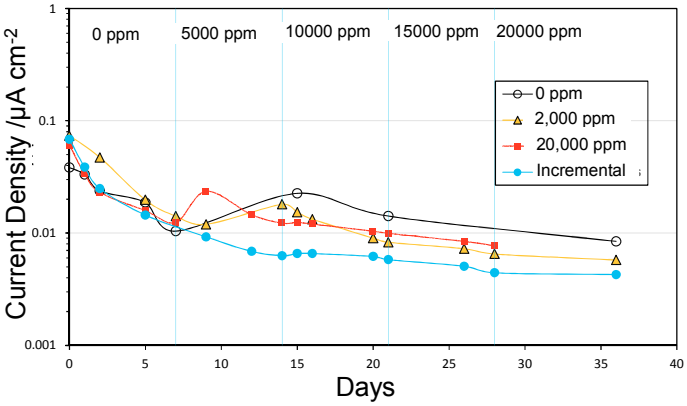

Figure 4.2. Corrosion potential and corrosion current density for steel in alkaline sulfate solution at pH 13.

pH 12.5, T~27.5°C

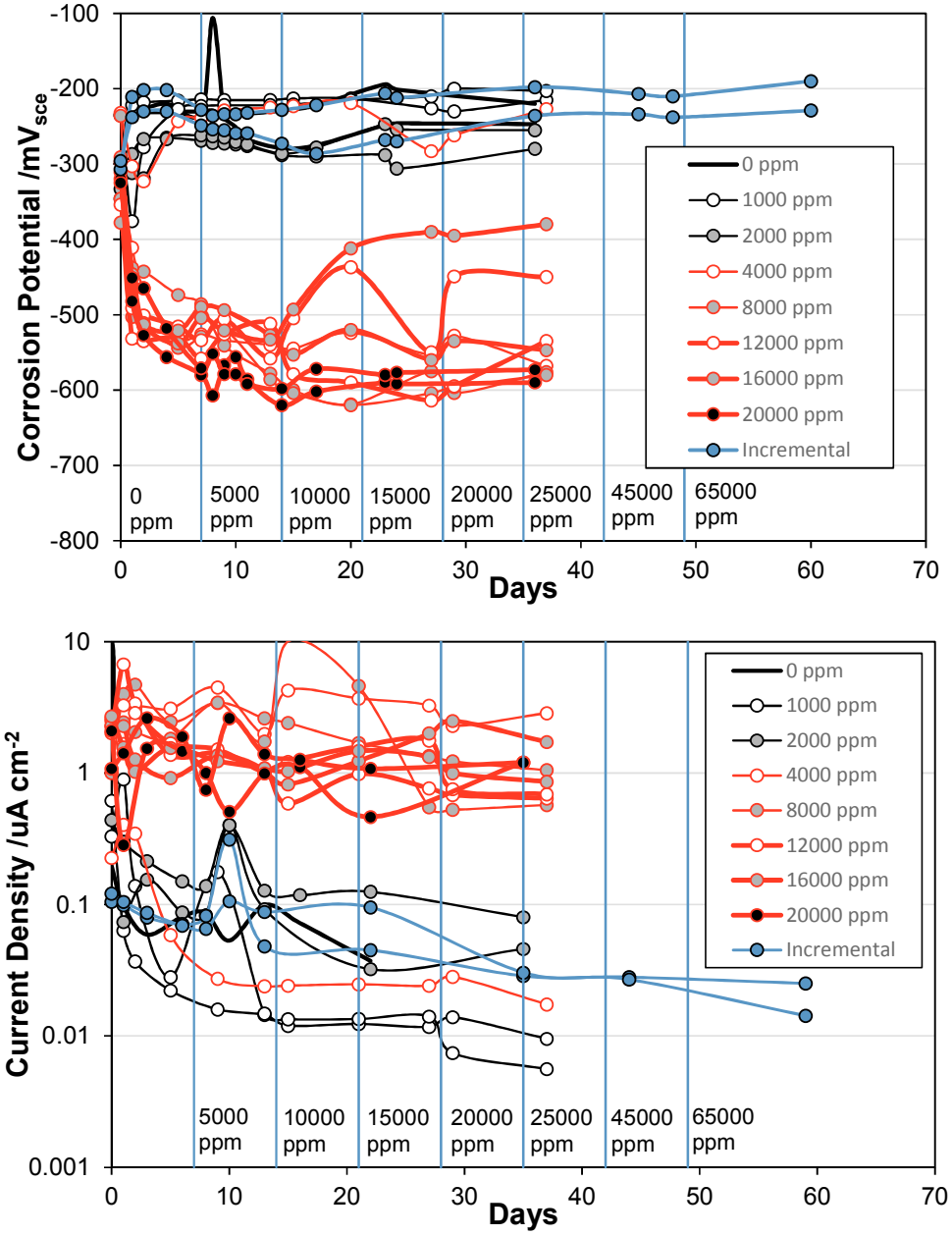

Figure 4.3. Corrosion potential and corrosion current density for steel in alkaline sulfate solution at pH 12.6.

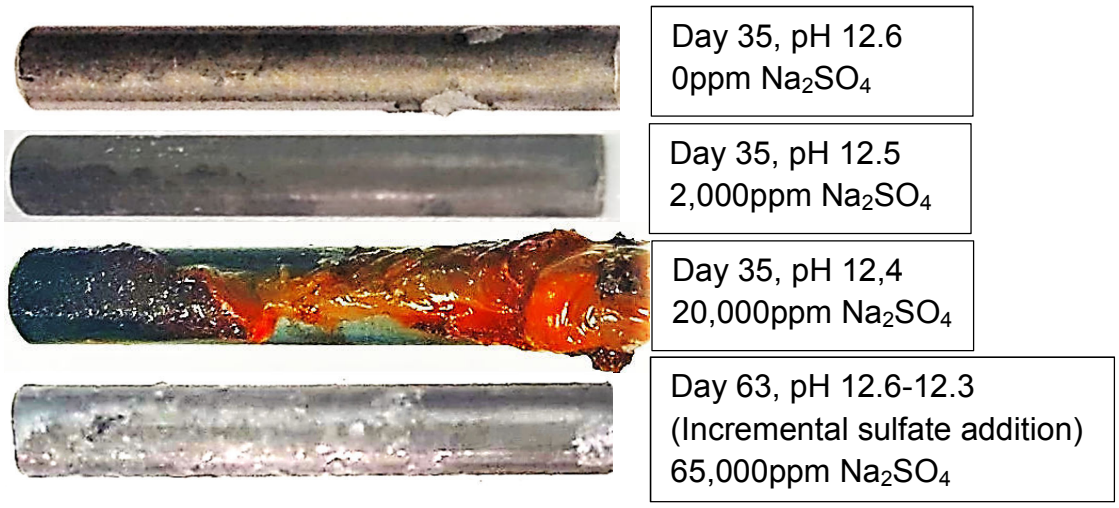

Figure 4.4. Corrosion development on steel in pH 12.6 sulfate solution.
(Open Circuit Potential Condition)

Figure 4.5 shows the result of tests for steel pre-conditioned to -1V_{SCE} for 1 day upon immersion in pH 13.3 solution with up to 20,000 ppm sodium sulfate and for steel that were left in OCP condition for 1 day in similar solutions and then subjected to -1V_{SCE} for 30 minutes prior to testing. It was thought that, as a low scan rate of 0.05 mV/s was used, passive film formation could develop during course of the test for any possible disruption that may be caused by the large cathodic polarization and that any possible detrimental effect caused by sulfate ion presence may be discriminated. However, the anodic polarization curves were not well differentiated by sulfate ion presence at pH 13.3 solution. In these tests, the cathodic reactions were attributed to hydrogen formation near -1V_{SCE} and oxygen reduction. Limiting cathodic current density (i_L ~1x10^{-5} A/cm^2) due to oxygen diffusion was observed in all tests. In most of the 1-day cathodically pre-conditioned samples at ambient temperatures (regardless of sulfate content), an active open circuit potential ~-650 mV_{SCE} was observed. Also, a passive open circuit potential ~-200 mV_{SCE} developed for testing in both 1 day and 30 minute cathodically pre-conditioned cases.

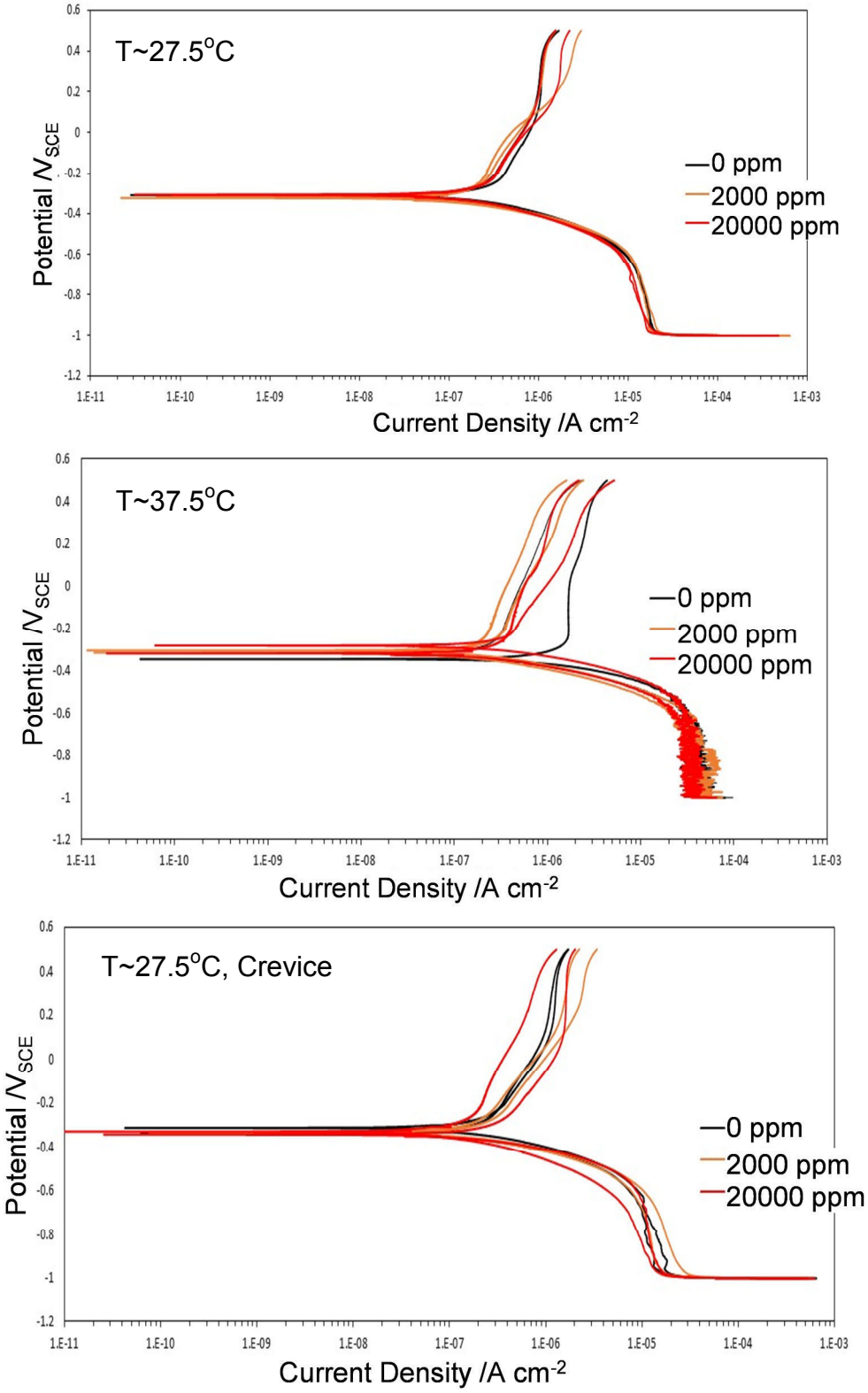

Figure 4.5a. Anodic polarization graphs at pH 13.3. 30-min cathodic polarization.

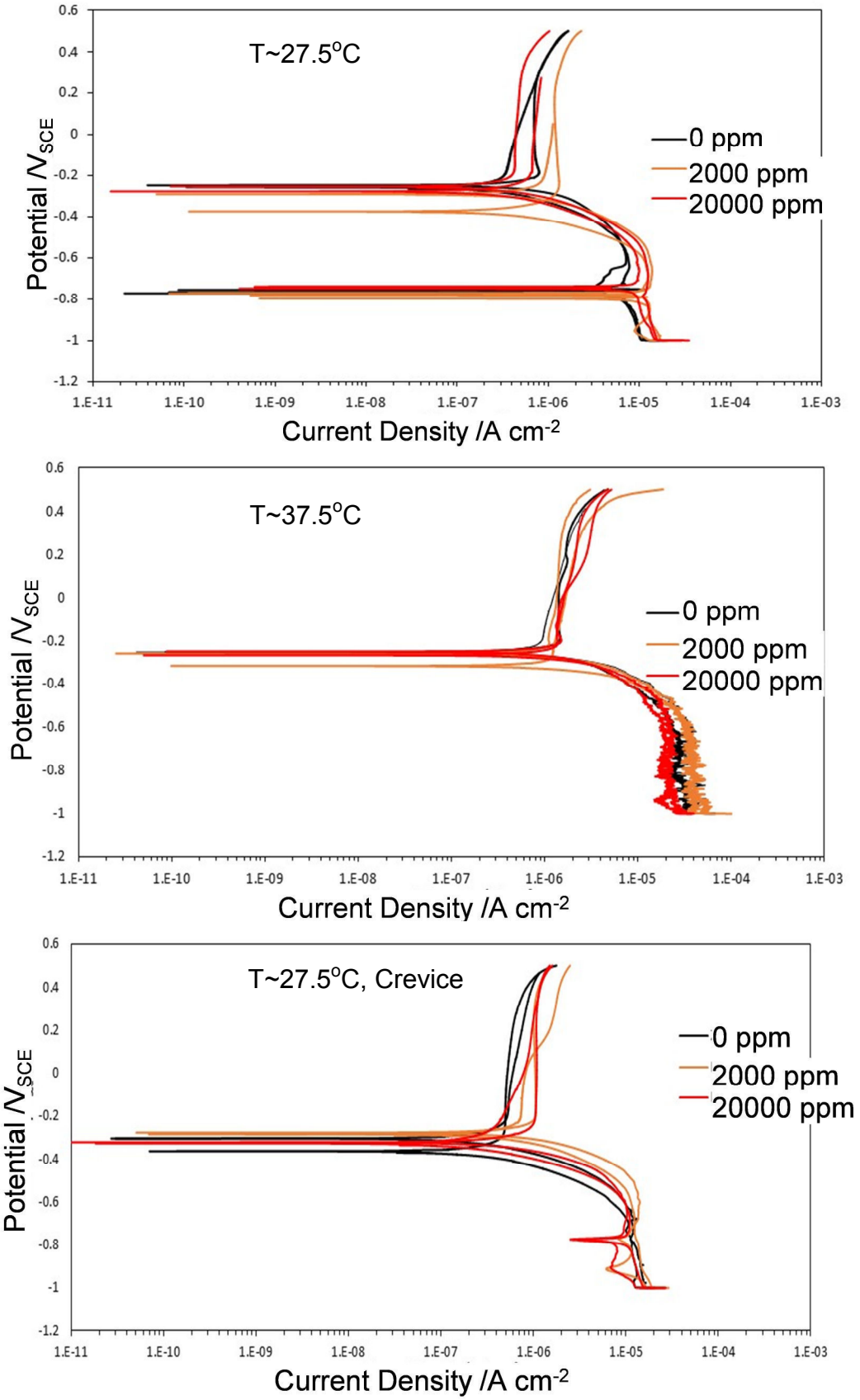

Figure 4.5b. Anodic polarization graphs at pH 13.3.
1-day cathodic polarization

The initial OCP at ~-650 mV_{SCE} in the 1-day cathodically pre-conditioned samples were thought to be indicative of active conditions of the steel surface during the early stages of the tests due to the prolonged large cathodic polarization and is indicative of a higher critical passivation current density for samples subjected to the pre-conditioning. This behavior was not observed in the 30-minute cathodically pre-conditioned case due to the passive film apparently already developed prior to the test and evidently little degradation to the passive layer. In the 1-day cathodically pre-conditioned cases, the passive current density was generally stable in the anodic potential regime from OCP to ~+400 mV_{SCE}. In the 30 minute cathodically pre-conditioned cases, there was a shift in apparent passive current at ~+200 mV_{SCE} from lower to higher current densities. The increase in passive current (for the steel in 2,000 and 20,000 ppm sodium sulfate solution additions) was greater than the similarly observed change in the control solution case, which may indicate some adverse role of sulfate. In both pre-conditioning cases, there was general tendency of greater passive current for steel in the sodium sulfate solutions than in the control solution. The enhanced passive current in sulfate solutions may indicate increase in the anodic current exchange density. Similar results were observed for samples containing crevice environments. At elevated solution temperatures, the only differentiating characteristics included generally the overall greater anodic and cathodic current densities, greater cathodic limiting current, and significant fluctuations in current in the net cathodic regime.

Generally, these initial tests in the pH 13.3 conditions did not indicate strong potential for sulfates to disrupt passive film formation. Somewhat enhanced corrosion can occur if there are conditions to significantly increase the anodic current exchange density or to increase the passive current density. Sulfate ions have shown minor indication to increase the anodic current exchange density. Crevice and enhanced temperature did not seem to aggravate corrosion conditions.

The pH of deficient grout extracted from corroded bridge tendons was typically ~13, but lower pore water pH (>12.6) in the deficient grout material have been measured and can be adverse especially within the crevices and interstitial spaces of the strand braided wire. Similar anodic polarization tests of steel in sulfate solutions at pH ~12.6 were conducted. Unlike in the pH 13.3 solution, striking differentiation in anodic behavior was observed with the presence of sulfate ions. As shown in Figure 4.6, corrosion potentials of the steel samples in the 30-minute cathodically pre-conditioned case in the presence of sulfate ions could be more negative (<-400 mV_{SCE}) than that of steel in sulfate-free solution (~-200 mV_{SCE}) and the apparent corrosion current density was significantly larger for steel in the presence of sulfate ions. Also, development of OCP at ~-650 mV_{SCE} in solution with 20,000 ppm sodium sulfate (similar to that observed for steel in pH ~13 subjected to 1-day cathodic pre-conditioning) shows initial instability of the passive layer. With the admixed presence of sodium sulfate, the passive current density showed up to an approximate threefold increase. In some cases, anodic current excursions are indicative of localized depassivation. Indeed, some samples showed indications of pit development. This can be in part explained by the mechanism presented by

Gavele (1976) where repassivation of pits can occur in the presence of increased sulfate concentrations within pits but may subsequently diffuse out leading to activation/passivation events. This change of a critical passivation sulfate concentration may result in the observed quick shifts in anodic current. More prominently however, the polarization graphs show transition from passive to active corrosion behavior of steel in solution with the admixed presence of 12,000 to 20,000 ppm sodium sulfate with anodic Tafel slope on the order of ~100 mV/dec.

pH 12.5, T~27.5°C

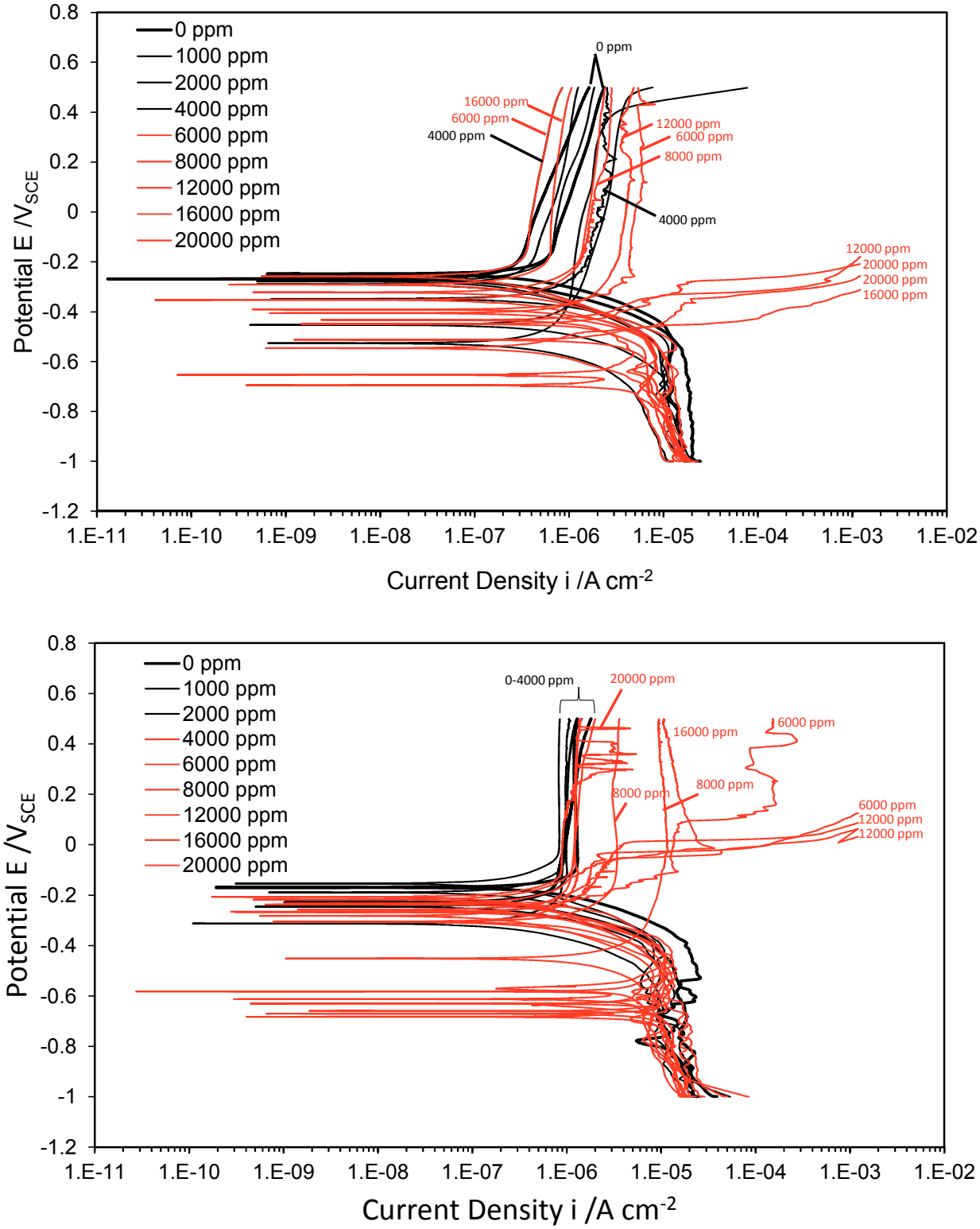

Figure 4.6. Anodic polarization graphs at pH 12.5.
Top: 30-min cathodic polarization. Bottom: 1-day cathodic polarization

The anodic polarization graphs for steel with 20,000 ppm sodium sulfate cathodically pre-conditioned for 1 day did not show the same dramatic activation controlled corrosion conditions seen at lower sulfate concentrations (Figure 4.6). The corrosion was characterized by apparent temporal anodic current excursions that can be explained by local passive film instability as mentioned earlier. Indeed those steel samples after testing showed severe pitting corrosion throughout the steel sample and is contrasted to the heavy surface corrosion observed in other cases (Figures 4.7 and 4.8). It is pondered, alluding to Gavele (1976), what effect the extended pre-cathodic polarization (and then removal of that polarization) can have if early pits had initiated and if electrical migration of ionic species such as sulfates in the pit would change the corrosion behavior of sulfates and electrical potential within the pit may not be uniform. It is noted that in the field case studies, corrosion of strand in deficient grout often were often near galvanized PT components. For samples immersed in sodium sulfate solutions 6,000-16,000 ppm, large anodic currents with characteristics of passive film breakdown and onset of pitting were observed at ~-50 mV_{SCE}. Localized instability of passive film throughout the steel sample was apparent in the case with extended large cathodic polarization of steel in pH 12.5 sulfate solution. These findings indicate ramifications of early sulfate presence on the formation of a stable passive film development.

Figure 4.7. Corrosion development of steel in pH 12.6 sulfate solution (20,000 ppm Na_2SO_4, 30-Min Cathodic Pre-Conditioning).

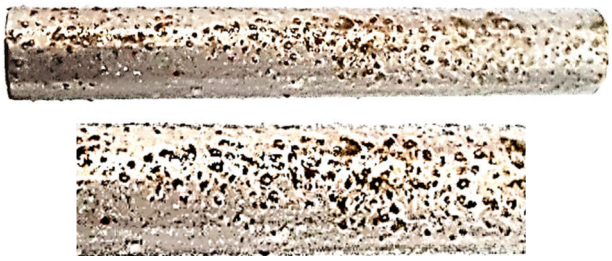

Figure 4.8. Corrosion sevelopment of steel in pH 12.6 sulfate solution (20,000 ppm Na_2SO_4, 1-Day Cathodic Pre-Conditioning).

Figures 4.9-4.10 shows comparative anodic current densities at 50 mV_{SCE} and 250 mV_{SCE} for the steel in the various test conditions. These potential values were chosen anecdotally based on observed changes in the anodic curves shown in Figure 4.4. As described earlier, anodic current densities were slightly higher in the presence of sulfate ions for steel immersed in pH 13.3 solutions, but large anodic current densities were observed for steel immersed in pH 12.5 sulfate solution. The large anodic current for the steel samples

placed in high sulfate solutions was capped in Figure 9 to 5μA/cm^2 due to termination of the polarization tests at 1mA/cm^2, well before anodic polarization to the potentials of comparison. The anodic current density for the samples with developed pitting corrosion was lower due to the nominal steel sample surface area rather than the area of the pits being used for calculation.

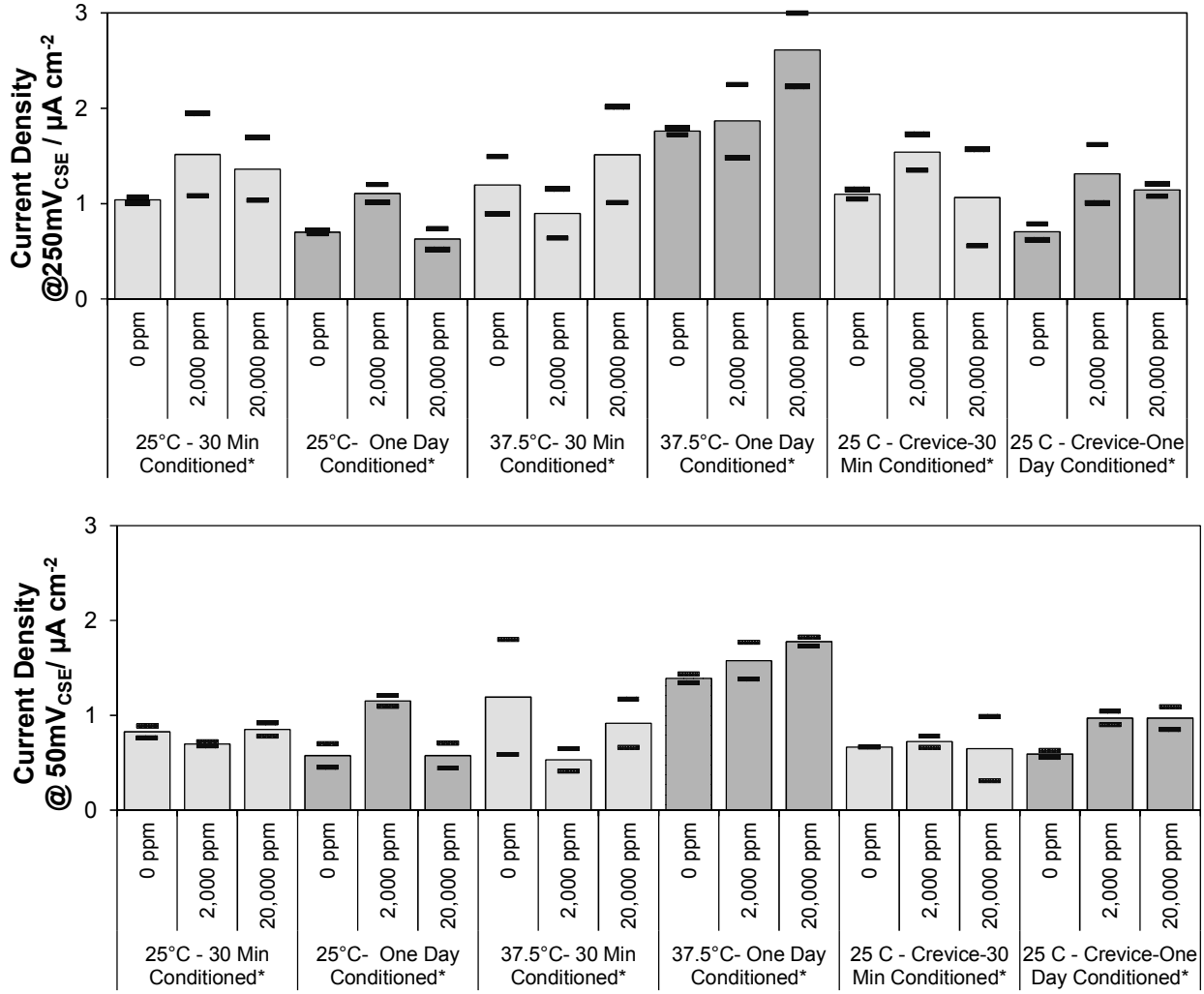

Figure 4.9. Anodic current densities for steel in pH 13.3 sulfate solutions.
Top: Current Density at 50 mVsce; Bottom: Current Density at 250 mVsce
*Cathodic precondition to -1VSCE

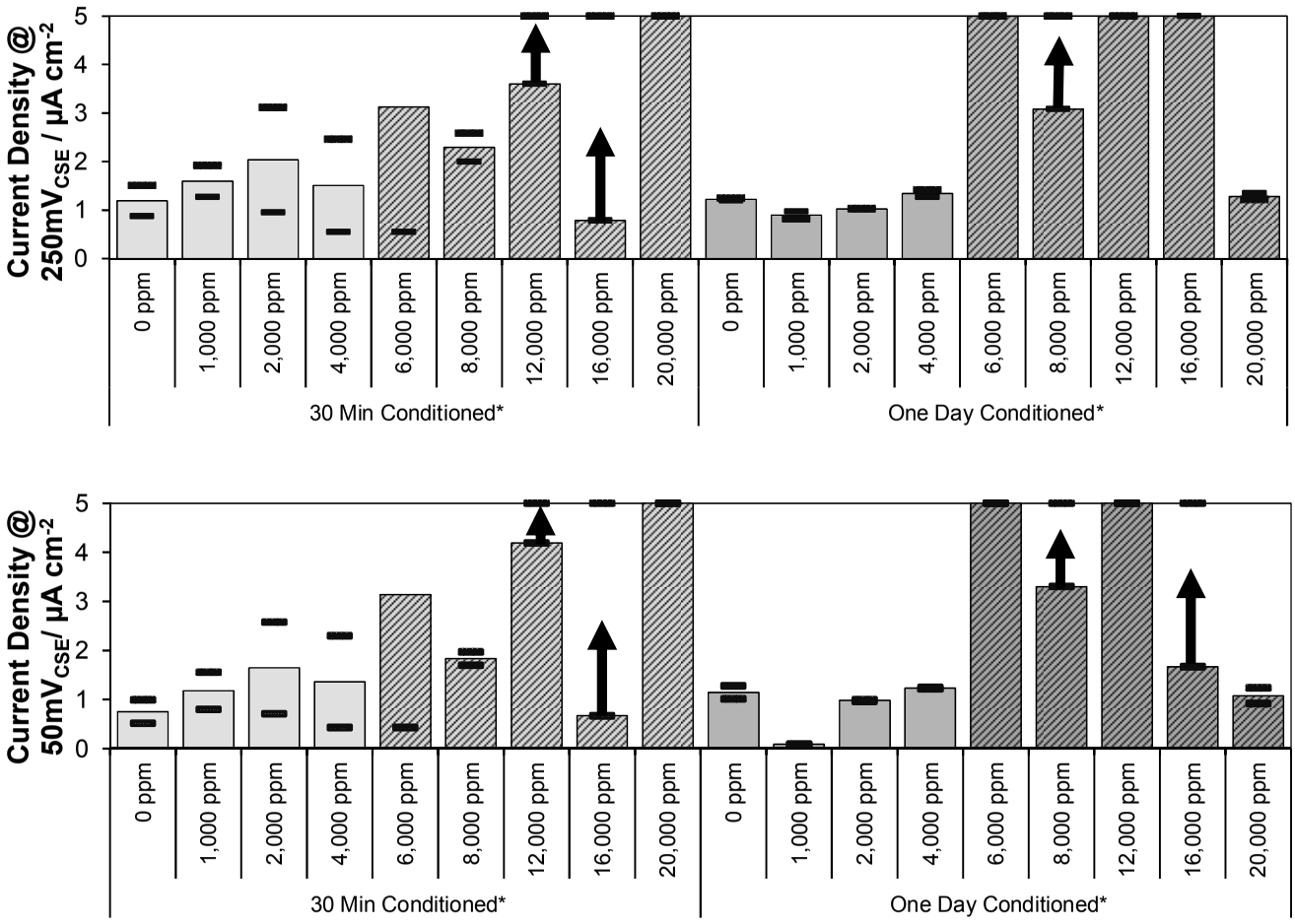

Figure 4.10. Anodic current densities for steel in pH 12.6 sulfate solutions.
Top: Current Density at 50 mVsce; Bottom: Current Density at 250 mVsce
Hash marks denote where visual corrosion developed.

4.4. SUMMARY OF FINDINGS

- In the open circuit potential condition for pH 13 solutions, additions of sodium sulfate with concentrations as high as 65,000 ppm after pre-conditioning in sulfate-free solution did not show ability to depassivate steel. Admixed sodium sulfate concentrations as high as 20,000 ppm did not show indication to destabilize passive film growth.

- In the open circuit potential condition for pH 12.6 solutions, additions of sodium sulfate with concentrations as high as 65,000 ppm after pre-conditioning in sulfate-free solution did not show ability to depassivate steel.

- In the open circuit potential condition for pH 12.6, destabilization of passive film growth resulting in severe corrosion occurred in the admixed presence of >4,000 ppm sodium sulfate.

- Results from anodic polarization tests of steel in pH 13 solution with up to admixed 20,000 ppm sodium sulfate did do not indicate strong tendency of sulfates to disrupt passive film formation.

- Results from anodic polarization tests in pH 12.6 and admixed >4,000 ppm sulfate solution indicated instability of passive film resulting in pitting corrosion.

5. STEEL CORROSION IN DEFICIENT GROUT

5.1. INTRODUCTION

The work was to assess the role of deficient grout on strand corrosion development. Testing described in Chapter 5 was to expound upon test conditions used for the large scale testing described in Chapter 6 including testing different pre-packaged grout products and evaluating the effect of chlorides in the corrosion development of steel in deficient grout. An economical and easy-to-fabricate test protocol described as the Inverted Tee (INT) is introduced. These small laboratory samples were made to identify grout robustness and corrosion initiation due to sulfate content, chloride content and combine sulfate/chloride with varying grout exposure condition and varying grout products.

5.2 TEST SETUP AND METHODOLOGY

Small laboratory sample were cast with grout products (Grout A and B) pre-exposed in high humidity conditions for 32 days. These samples were cast in (2×2×1½ " ø, 4 ¾ "length) PVC tees and mixed with 20% excess water with varying sodium sulfate (2000 ppm, 20,000 ppm , 100,000 ppm) and sodium chloride additions (0.08% and 0.2% chlorides by cement mass). Table 5.1 lists the test cases and Tables 5.2-5.3 show the mix conditions. The samples contained embedded high strength carbon steel wire within the tee header as well as within the tee body (Figures 5.1-5.2). An activated titanium reference electrode that was routinely calibrated with a copper/copper-sulfate reference electrode was used and a stainless steel rod was used as the counter electrode. Duplicate samples were made and tested for each test case.

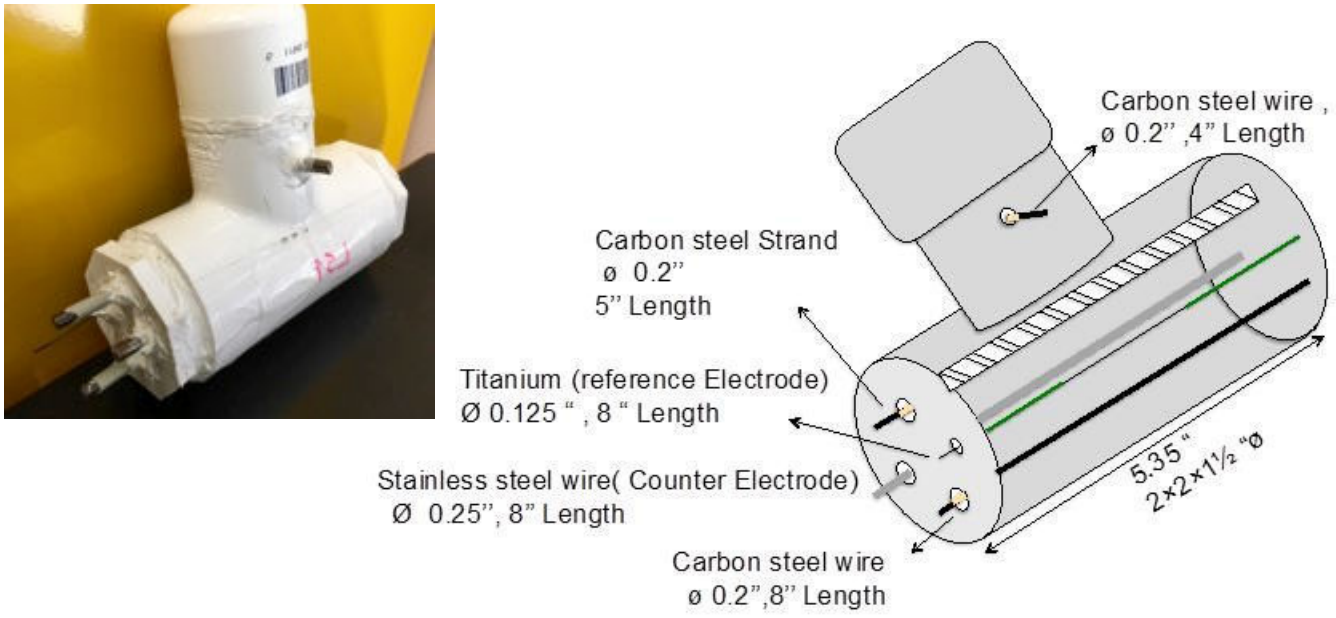

Figure 5.1. Schematic of INT test samples.

Figure 5.2. INT test samples after casting.

Table 5.1. INT Test Case Conditions

Test Case	Grout Product	Grout Condition	Sulfate Amount (ppm)	Chloride Amount (% by Cement)
BA1	B	As-Rec'd	0	0
BA2	B	As-Rec'd	2,000	0
BA3	B	As-Rec'd	20,000	0
BP1	B	Pre-Exposed	0	0
BP2	B	Pre-Exposed	2,000	0
BP3	B	Pre-Exposed	20,000	0
BP4	B	Pre-Exposed	100,000	0
AA1	A	As-Rec'd	0	0
AA2	A	As-Rec'd	2,000	0
AA3	A	As-Rec'd	20,000	0
AP1	A	Pre-Exposed	0	0
AP2	A	Pre-Exposed	2,000	0
AP3	A	Pre-Exposed	20,000	0
AP4	A	Pre-Exposed	100,000	0
AP5	A	Pre-Exposed	0	0.08
AP6	A	Pre-Exposed	0	0.2
AP7	A	Pre-Exposed	2,000	0.08
AP8	A	Pre-Exposed	2,000	0.2
AP9	A	Pre-Exposed	20,000	0.08
AP10	A	Pre-Exposed	20,000	0.2
AP11	A	Pre-Exposed	100,000	0.08
AP12	A	Pre-Exposed	100,000	0.2

The PVC tee was expected to facilitate volume displacement of the deficient grout material to the tee header and allow discrete testing and sampling of the deficient grout materials. The control set of the samples were cast with Grout A and B in the as-received

condition following the manufacturer recommended mix water content but contained different sodium sulfate concentrations (0 ppm, 2000 ppm, 20,000 ppm). After 1-2 days from casting, the samples were sealed either with Sikadur epoxy or a permanent PVC cap. The picture below show one set of the INT test samples after casting.

The corrosion potential (OCP) was measured with a copper/copper-sulfate reference electrode through an access port through the tee body. The polarization resistance of embedded steel probes was measured by linear polarization resistance method, and solution resistance was measured with a soil resistivity meter. After electrochemical testing, chemical analysis of the grout was made to quantify the levels of sulfates and chloride in the stratified grout layers. A modified test procedure adapted from TX-620-J was followed for sulfate analysis, and the total chloride content was measured following FM 5-516. The samples were also subjected to drying as part of ASTM C566-13 to measure moisture content. Grout pore water pH was measured using a pH spray indicator or an ex-situ leaching method.

Table 5.2. Detailed Mix Conditions for Grout B

Grout Product	Grout Condition	Test Cases	Date of Casting	Mix Water	Grout
B	Pre-Exposed for 32 days in 100% RH. + %20 Excess mix water	1	02/18/15	0.74 Liter Tap water	4.8lbs
		2	02/18/15	0.74 Liter Tap water: 1.48g Na_2SO_4/ L H_2O	
		3	02/18/15	0.74 Liter Tap water: 14.8g Na_2SO_4/ L H_2O	
		4	02/18/15	0.74 Liter Tap water: 74g Na_2SO_4/ L H_2O	
B	As-Received	1	02/17/15	0.61 Liter Tap water	4.8lbs
		2	02/17/15	0.61 Liter Tap water: 1.48g Na_2SO_4/ L H_2O	
		3	02/17/15	0.61Liter Tap water: 14.8g Na_2SO_4/ L H_2O	

(Each batch mixed for 3 min at 600 RPM)

Table 5.3. Detailed Mix Conditions for Grout A

Grout Product	Grout Condition	Test Cases	Date of Casting	Mix Water	Grout
A	Pre-Exposed for 32 days in 100% RH. + %20 Excess mix water	1	04/07/15	0.77 Liter Tap water	5.2 lbs
		2	04/07/15	0.77 Liter Tap water: 1.5g Na_2SO_4/ L H_2O	
		3	04/07/15	0.77 Liter Tap water: 15.4g Na_2SO_4/ L H_2O	
		4	05/27/15	0.77 Liter Tap water: 77g Na_2SO_4/ L H_2O	
		5	05/27/15	0.77 Liter Tap water: 2.083g NaCl/L H_2O	
		6	05/27/15	0.77 Liter Tap water: 5.2065g NaCl/L H_2O	
		7	05/28/15	0.77 Liter Tap water (Miami): 1.5g Na_2SO_4 & 2.083g NaCl/L H_2O	
		8	05/28/15	0.77 Liter Tap water: 15.4g Na_2SO_4 & 2.083g NaCl/L H_2O	
		9	05/28/15	0.77 Liter Tap water (Miami): 77g Na_2SO_4 & 2.083g NaCl/L H_2O	
		10	05/28/15	0.77 Liter Tap water: 1.5g Na_2SO_4 & 5.2065g NaCl/L H_2O	
		11	05/28/15	0.77 Liter Tap water: 15.4g Na_2SO_4 & 5.2065g NaCl/L H_2O	
		12	05/28/15	0.77 Liter Tap water: 77g Na_2SO_4 & 5.2065g NaCl/L H_2O	
A	As-Received	1	04/07/15	0.64 Liter Tap water	5.2 lbs
		2	04/07/15	0.64 Liter Tap water: 1.5g Na_2SO_4/ L H_2O	
		3	04/07/15	0.64 Liter Tap water: 15.4g Na_2SO_4/ L H_2O	

(Each batch mixed for 6 min at 600 RPM)

5.3. GROUT CONDITION

The grout was placed into the PVC tee gravimetrically without a pump and rodding was minimal due to the congestion of the test electrodes. Most test samples were fully grouted after casting except for Test Case B.P.4. Whereas, most of the grout mixes were flowable (especially with the excess mix water) the grout in Test Case B.P.4 had poor workability due to the enhanced level of solids attributed to the excess sodium sulfate. The grout was consolidated into the PVC tee with external vibration for several minutes; however, void spaces were found in one of these samples (Figure 5.3). High sulfate concentration (~100,000 ppm) weren't used for other test cases (particularly with grout in the as-received condition) due to the poor workability.

Figure 5.3. Case B.P.4.1 after ~300 days from casting.
(Corrosion product appear after exposure to the ambient lab air)

5.4 RESULTS AND DISCUSSION

5.4.1 Electrical Properties

Solution resistance and bulk resistivity are shown in Figure 5.4-5.5 for samples from the INT test. As shown in Figure 5.4, Grout A from the tee-header and tee-body have lower solution resistance and bulk resistivity than Grout B in both as received and pre-exposed conditioned. Consequently, the electrical properties of Grout A would apparently provide poorer corrosion resistance.

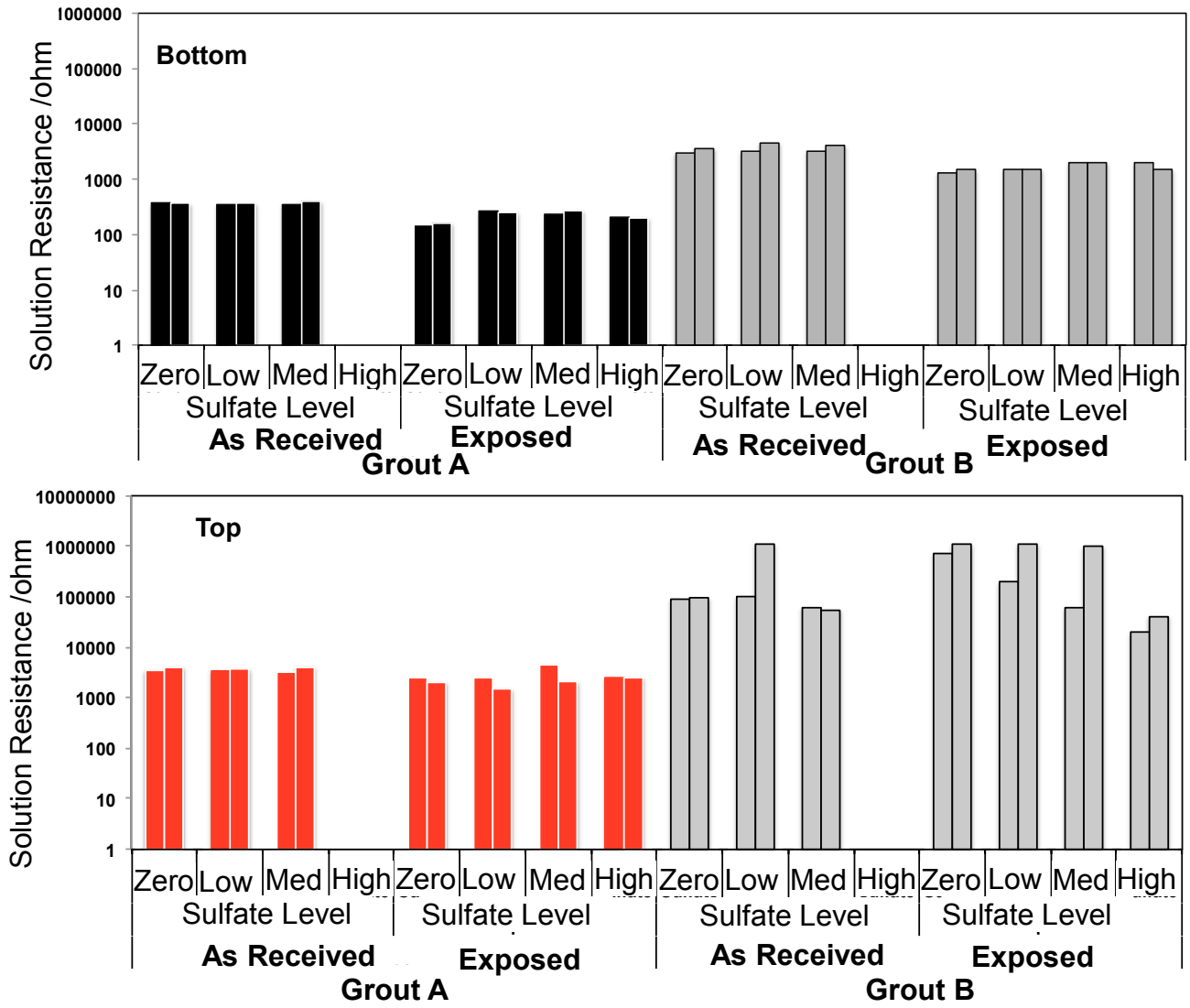

Figure 5.4. Solution resistance for INT test samples.
(Cases B.A.1-3, B.P.1-4, A.A.1-3 and A.P.1-4)

In these INT test samples, the working electrode in the tee header had a short length (3 cm) and had a greater distance from the reference electrode. This would result in larger resolved solution resistance for the tee-header section than the tee-body. In order to compare grout resistivity between the tee-header and tee-body, 2-point resistance measurements were made using two local electrodes in the tee header as well as the two local electrodes in the tee body. The apparent grout resistivity was approximated by application of Ohm's Law. The distance between each pair of local electrodes was 3 cm. The surface area of each of the tee-header electrodes was 4.9 cm^2. For the electrode pair in the tee-body, the surface area of each electrode was similar (21 cm^2 and 25.9 cm^2). A surface area of 21 cm^2 was assumed for calculation.

As shown in Figure 5.5, the bulk resistivity of pre-exposed Grout A in the tee-header was not significantly different from the tee-body. This was in part attributed to the water loss before capping the samples. Furthermore, there wasn't consistent differentiation of bulk resistivity as function of sulfate content at either the tee-header or tee-body. In pre-exposed Grout B, the top friable material had higher bulk resistivity than the bottom due to the existence of large and relatively dry voids (as described in Chapter 2). As shown in Figure 5.5 in pre-exposed Grout B, there was indication of bulk resistivity in the order of 1Mohm-cm for grout in the tee-header.

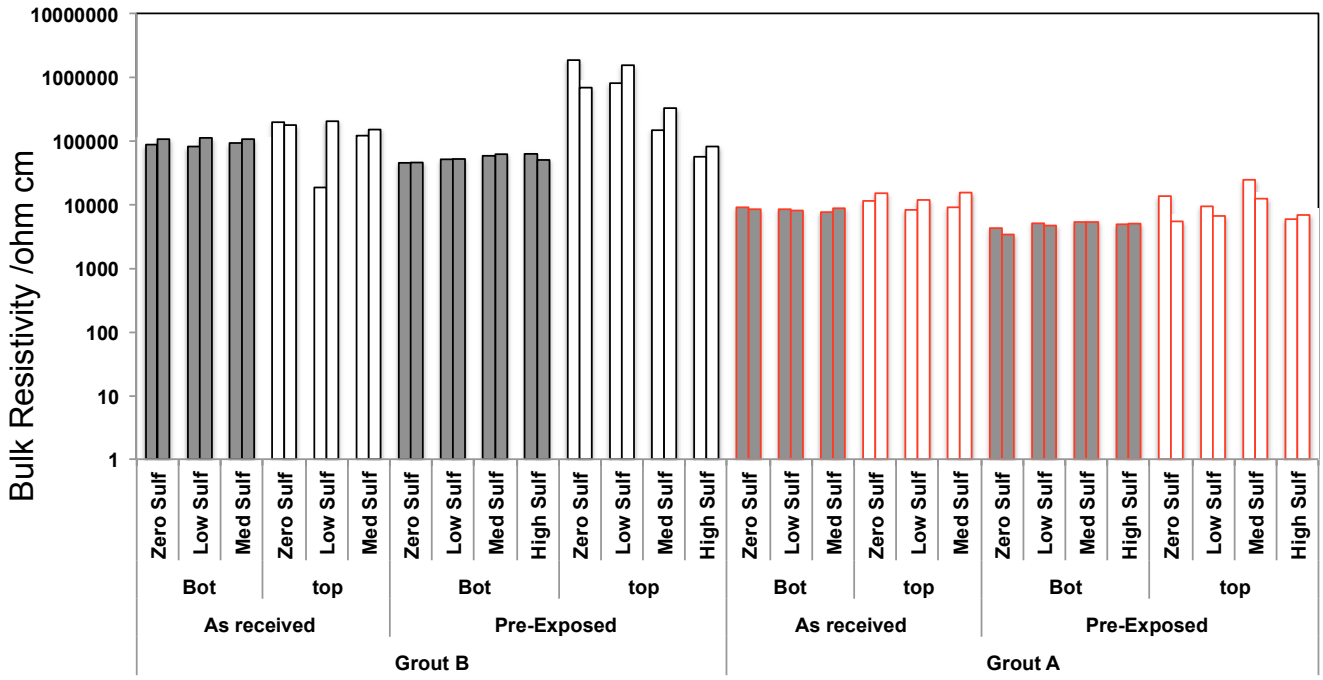

Figure 5.5. Bulk resistivity for INT test samples.
(Cases B.A.1-3, B.P.1-4, A.A.1-3 and A.P.1-4)

It was evident in earlier observations that moisture availability could affect the resistance measurements. For Grout A, the segregated grout is expected to have lower resistivity due to the expected enhanced moisture content. This was observed in Grout Cylinder test (Chapter 2) where sampled specimens were conditioned in 100%RH. However, in the INT tests, the initial high moisture content in the deficient grout quickly evaporated prior to capping of the samples. Nevertheless, in the moisture content analysis (detailed in Chapter 6), the deficient grout in the tee header had moisture content greater than 20%, and the hardened grout in tee body had moisture content less than 20%. Although the bulk moisture content of deficient grout was higher in the tee-header, resistance associated with large unsaturated pores in the grout may account for the apparent incongruity in resolved resistivity. For Grout B, a similar situation arises. The segregated grout in B had large pores that were not saturated even in the case in Grout Cylinder tests where the samples were held at 100% RH. This may be due to the self-desiccation of the hydrating grout. In the Grout Cylinder and INT tests, bulk resistivity of the segregated Grout B was high. The effect of sulfate presence could

not be elucidated for Grout A and B. Differentiation in moisture availability, ionic activity, hydration of cement and precipitation of salts in grout segregation can be important.

5.4.2 Corrosion Behavior

In the INT test setup, grout segregation was expected to occur when the grout was subjected to the aggravated mix conditions. The deficient grout was expected to accumulate in the tee header due to volume displacement. As steel electrodes were placed within the tee header and tee body, corrosion conditions due to grout segregation may be assessed. It is noted that the extent of grout segregation in these INT test samples were not as severe as in the MIT test or as that observed in the field.

As shown in Figure 5.6, Grout B had passive like corrosion behavior for all of the grout test conditions. The corrosion potential was in the range of $-200>E_{corr}>-100$ mV_{cse} and current density was 0.001-0.01µA/cm^2 for the as-received and pre-exposed conditions. There was no indication of active corrosion even in the top portion of the samples with segregated grout.

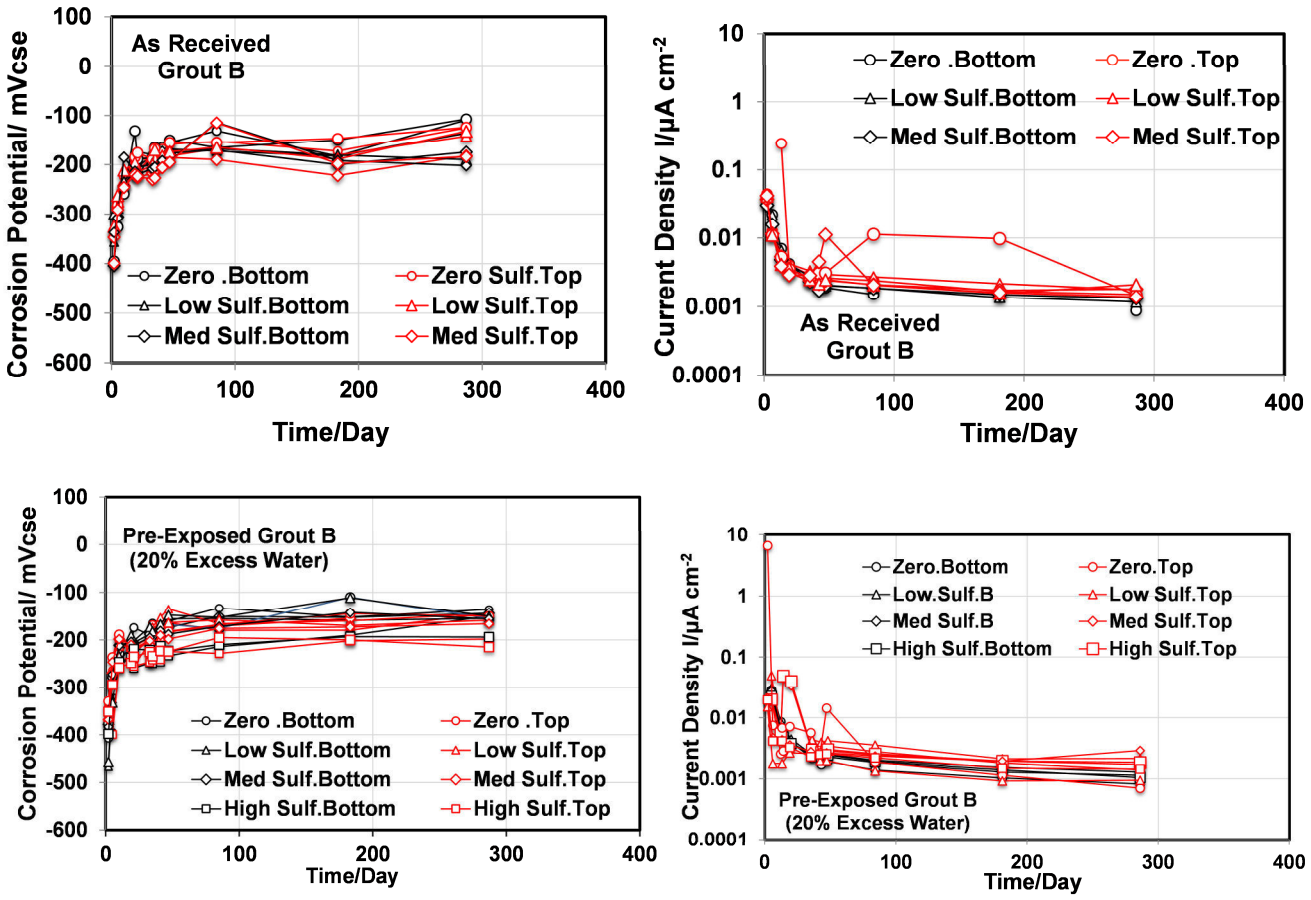

Figure 5.6. Corrosion potential and current density for INT testcases: B.A.1-3, B.P.1-4.
(Low Sulf: 2,000ppm. Med Sulf: 20,000ppm. High Sulf: 100,000 ppm)

As shown in Figure 5.7, INT test samples made with Grout A in the as-received condition (A.A.1-3) did not show active corrosion behavior for both tee header and tee body section regardless of the amount of admixed sodium sulfate. However for cases where sodium sulfate was admixed to the pre-exposed Grout A (cases A.P.1-4), there was differentiation in OCP and i_{corr} for steel embedded in the tee header and tee body. The general trend of enhanced corrosion activity in deficient grout was consistent with observations in the MIT test samples and in the field. However the conditions here appeared less adverse. The corrosion potential of steel in the tee body and tee header was ~-150 mV_{CSE} and -250 mV_{CSE}, respectively. In comparison corrosion potentials in deficient and hardened grout in the MIT test and in the field were less than -350 mV_{CSE} and greater than -200 mV_{CSE}, respectively. In the INT tests here, one sample with 20,000 ppm sodium sulfate addition (A.P.3) exhibited severe active corrosion conditions where i_{corr} exceeded 1 $\mu A/cm^2$.

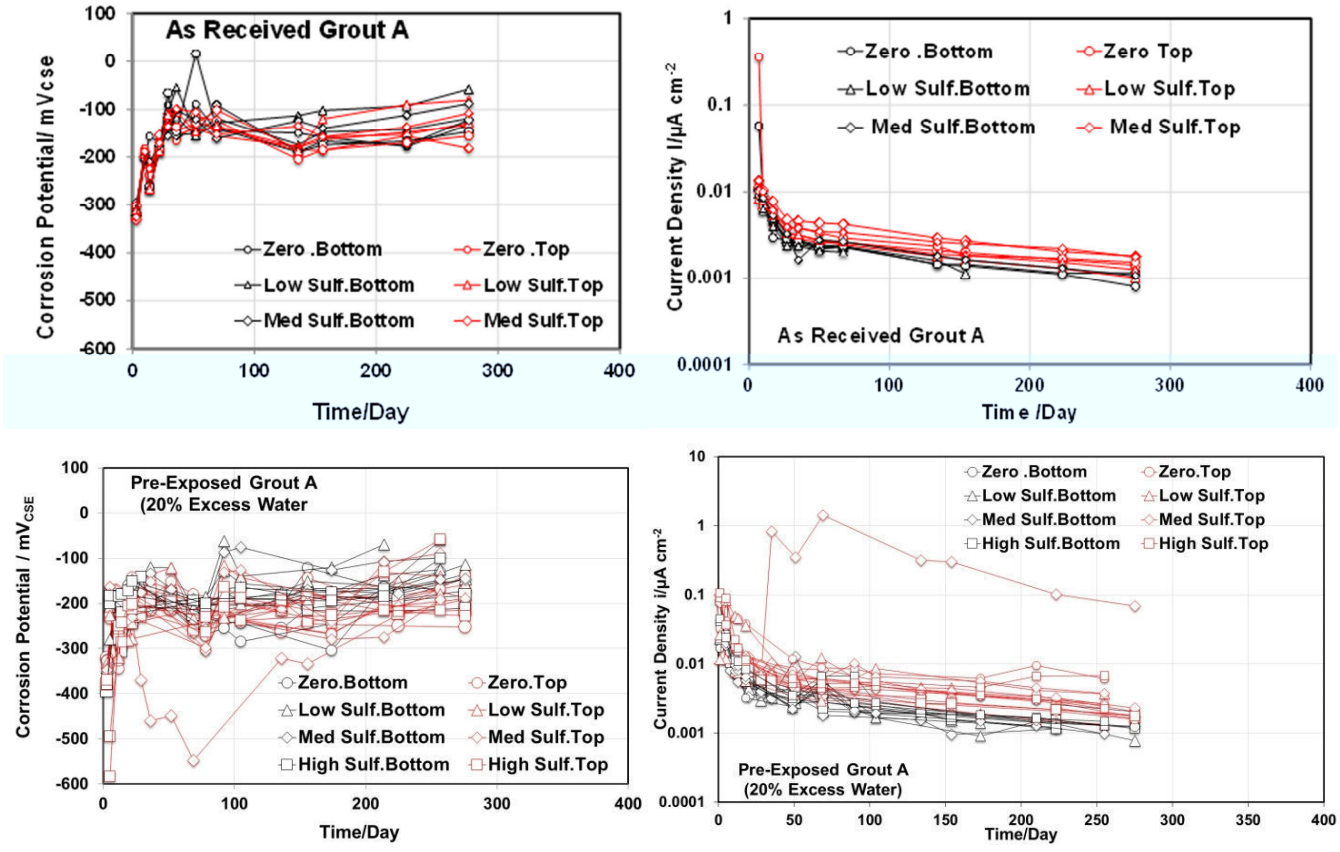

Figure 5.7. Corrosion potential and current density for INT test cases A.A.1-3 and A.P.1-4.
(Low Sulf: 2,000ppm. Med Sulf: 20,000ppm. High Sulf: 100,000 ppm)

Additions of sodium chloride (cases A.P.5-6) were made to levels associated with minimum chloride limits in cementitious materials (0.08% and 0.2% chloride by cement content). Vestigial chloride content was assumed to be negligible. As detailed in Chapter 6,

total chloride levels in as-received Grout A was less than 0.6 lb/yd^3. The total chloride content was measured but the effect of grout segregation on cement content was directly assessed here. The physical consistency of the grout in the tee header for these samples was not the wet and highly friable material characteristic of corrosive deficient grout observed elsewhere. With that in mind, the electrochemical characteristics were indicative of low corrosion conditions (Figure 5.8). Like other cases, the corrosion current density, albeit at relative low values, were differentiated by the segregated layers. The OCP for steel in both the tee header and body was ~-200 mV_{CSE}. Corrosion current densities for steel in the tee header and body were less than 0.01µA/cm^2. It was apparent that the levels of chloride located within the grout layers in these samples did initiate corrosion development.

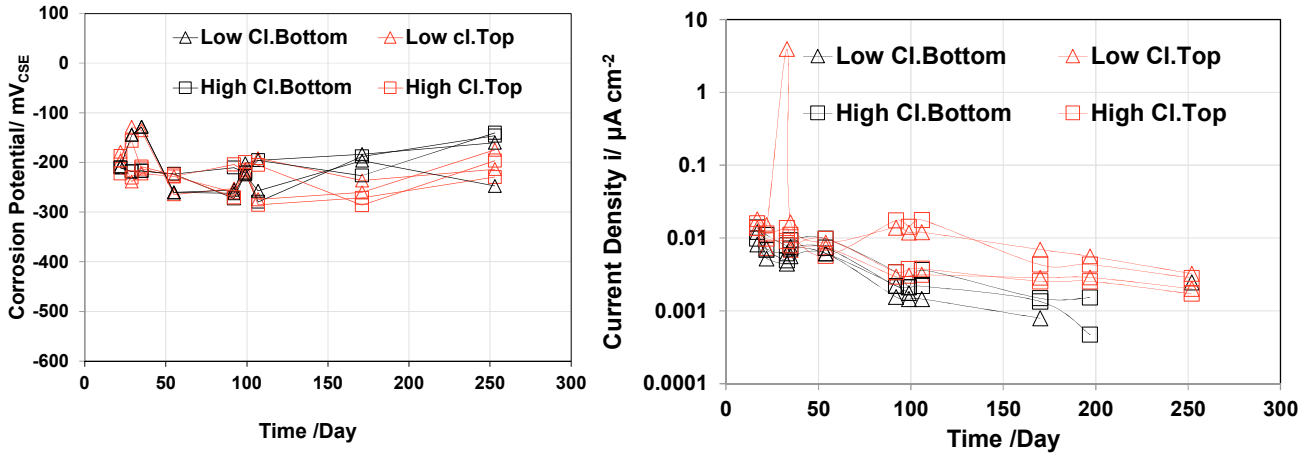

Figure 5.8. Corrosion potential and current density for INT test cases A.P.5-6.
(Low Cl:0. 08% and High Cl:0. 2% by Cement)

It was reported in the literature that the combined presence of sulfate and chloride ions in solution could enhance the corrosion rate of steel (Pradhan, 2014; Maslehuddin and Paget,1997; Dehwah et al., 2002, 2003; Saleem et al., 1996; Al-Amoudi et al., 1993, 1995; Holden et al., 1983; Yonezawa, 1989; Zuquan et al., 2007). In the testing here (cases A.P.7-8 and A.P.10-11), samples with chloride levels where corrosion is not expected to develop (and indeed were not observed in cases A.P.5-6), also incorporated sodium sulfate additions to examine the combined effect. Severe corrosion developed in the deficient grout within the tee header for cases with as low as 2,000 ppm sodium sulfate addition in combination with chloride additions as low as 0.08%. As shown in Figure 5.9, the steel in deficient grout with combined presence of sulfates with low level chlorides had active corrosion potentials <-400 mV_{SCE} and current densities as high as 6 µA/cm^2.

5.4.3 Chloride and Sulfate Content

The total chloride in the segregated grout layers was measured (Figure 5.10). On first inspection, it would appear that there was enrichment of total chloride content in the grout from the tee header which would indicate ionic transport due to the grout segregation. Although this

cannot be ruled out, the total chloride test preparation methods may over-sample the segregated grout due to uniform sample mass requirements and the inevitable moisture loss from initial conditions during sample preparation and therefore result in higher reported chloride concentrations. For chloride analysis a grout unit density of 3,105 lb/yd^3 was assumed (Lau et al., 2014), but this value is likely to be variable by the severity of grout segregation. With these uncertainties understood, the reported results should be considered qualitatively (values are given for comparison). The results show that in test cases AP5-6, the grout in the tee header and body had enhanced chloride (0.06 to 0.12% by total grout mass in header and 0.03 to 0.1% by total grout mass in body) but corrosion did not develop. However in test cases AP7-10, where similar chloride levels were present (0.03 to 0.18% by total grout mass in header), severe corrosion developed in the deficient grout. It is noted that corrosion did not develop in the tee body even though there was relatively enhanced chloride content there as well (0.03 to 0.09% by total grout mass in body). The enhanced sulfate additions apparently had effect in the corrosion development. It was reported in the literature that the presence of sulfate ion may reduce the chloride binding capacity of cement and release the chloride ion into pore solution (Dehwah et al., 2002, 2003).

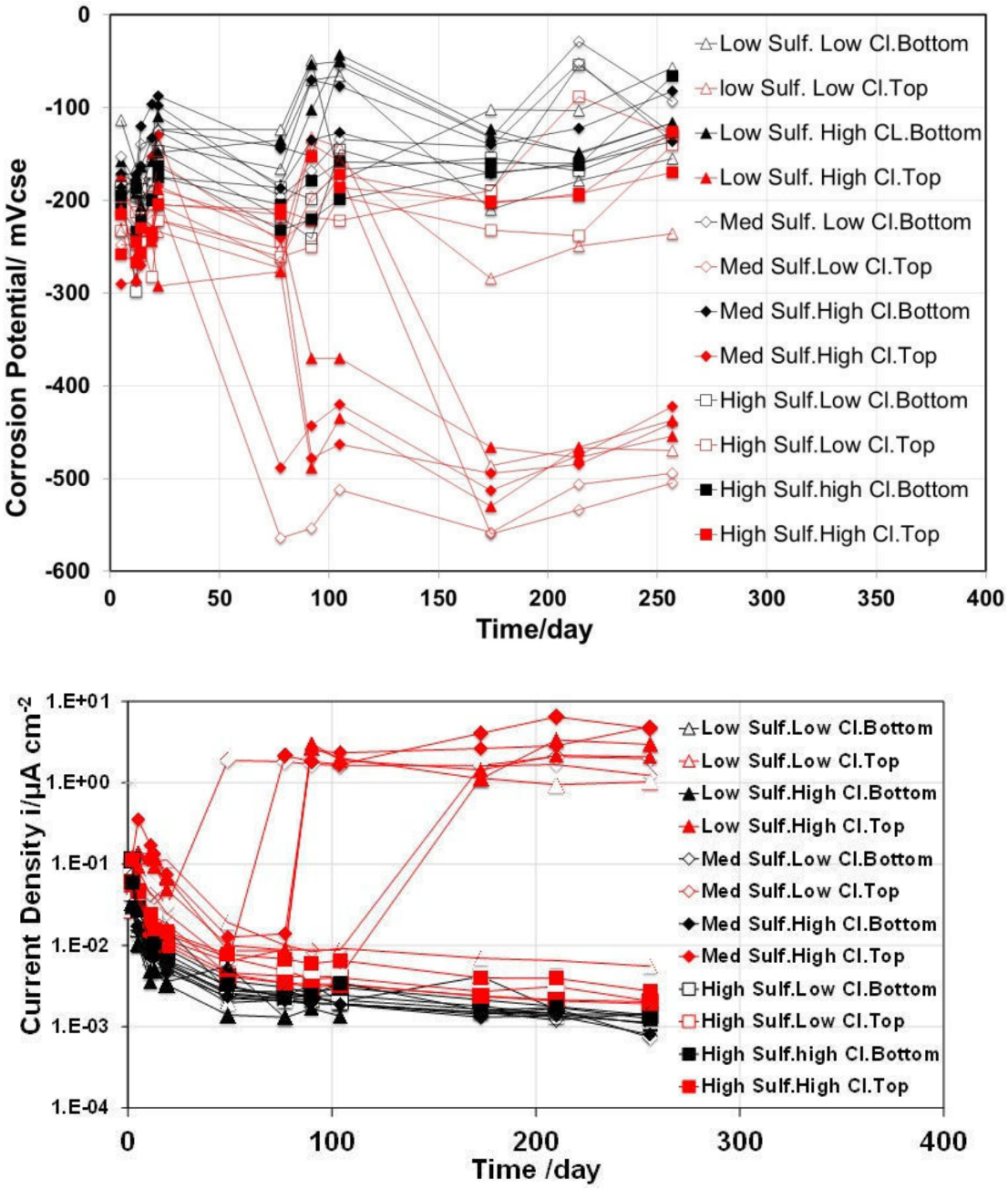

Figure 5.9. Corrosion potential and current density for INT test cases A.P.7-12.
(Low Sulf: 2,000ppm./Med Sulf: 20,000ppm. High Sulf: 100,000 ppm. Low Cl:0. 08% and High Cl:0. 2% by Cement)

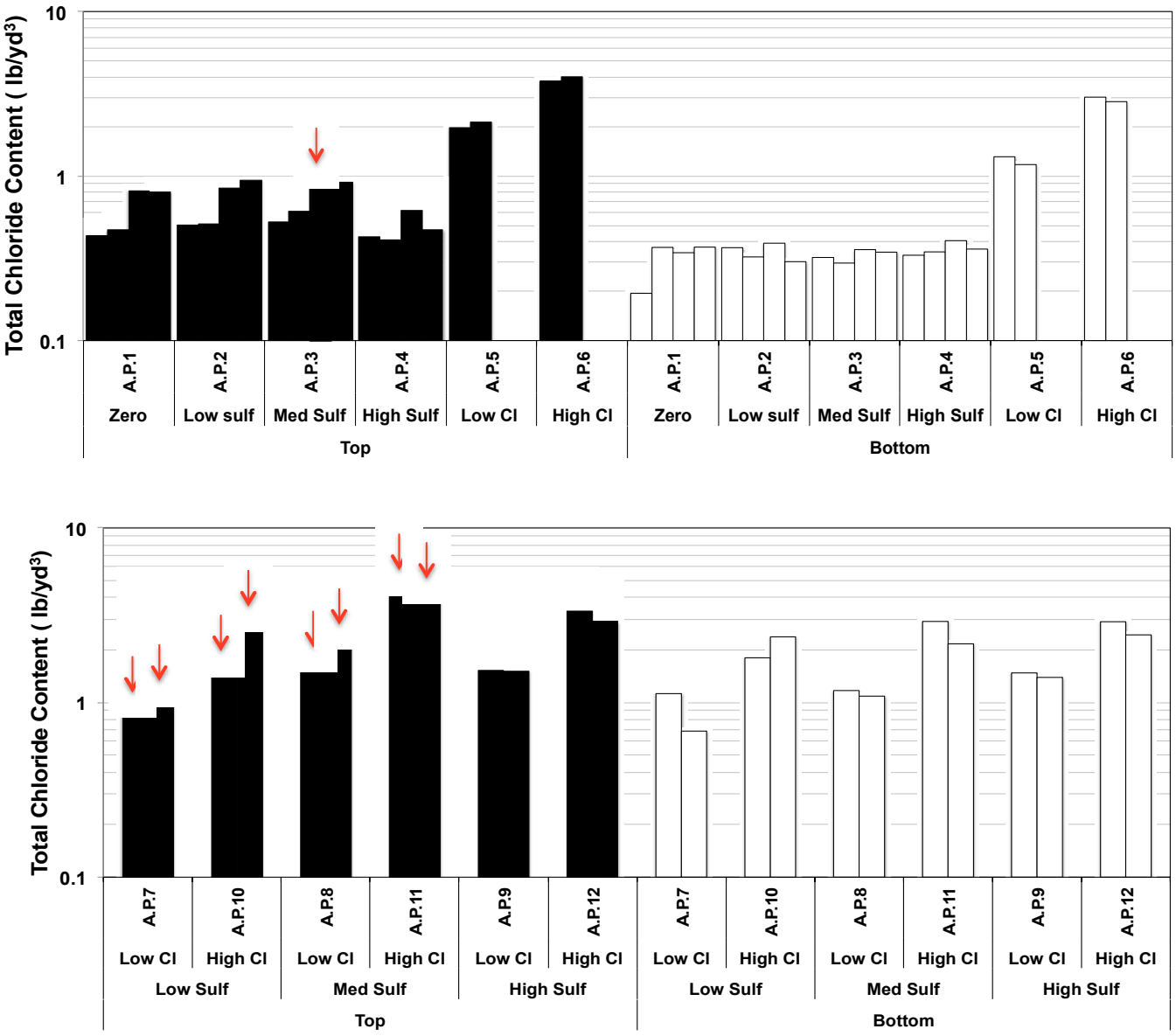

Figure 5.10. Total chloride content for INT tests with pre-exposed Grout A.
(Corroded samples marked with Red Arrow)

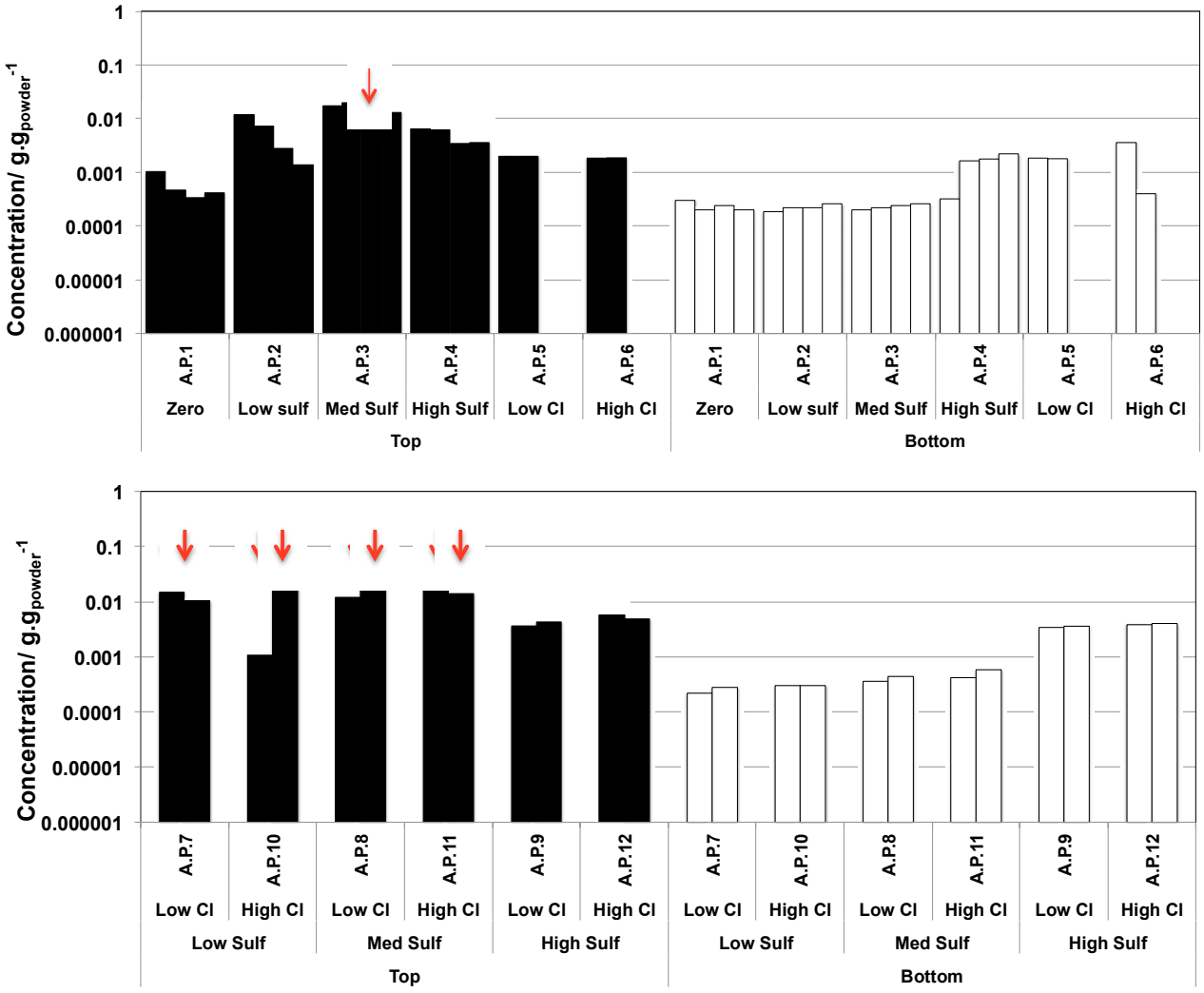

Figure 5.11. Sulfate content for INT tests with pre-exposed Grout A.
(Corroded samples marked with Red Arrow)

It is posed that sulfate can have differential roles in the corrosion development of steel in deficient grout. In test case AP3, severe corrosion developed in the presence of 20,000 ppm sodium sulfate additions. Furthermore field evidence and laboratory testing in sulfate solutions (Permeh et al, 2015; Lau et al, 2014; Gouda, 1970; Gouda and Halaka, 1970; Acha et al, 1990; Bertolini and Carsana, 2011; and Blactot et al, 2007) indicate corrosion conditions in the presence of sulfates. It is shown in Figure 5.11 that corrosion consistently developed in deficient grout that had enhanced sulfate content such as in cases AP3, AP7-10 where the sulfate ion content was generally >~0.01 $g_{Sulfate}/g_{Powder}$. Testing in Modified Inclined Tube tests showed similar values (Permeh et al, 2015; Krishna Vigneshwaran et al, 2015). In the combined presence of sulfates and chlorides, there is congruent effect to enhance corrosion development. This may cause enhanced corrosion rates or may be associated with changes in cement chemistry (Dehwah et al 2003; Zuquan et al, 2007). As initial assessment, the possible role of sulfates in steel corrosion initiation were thought to be related to localized corrosion process by reaction such as $Fe^{2+} + 2H_2O + SO_4 \rightarrow Fe(OH)_2 + H_2SO_4^2$ (Jones, 1996).

5.5. SUMMARY OF IMPORTANT FINDINGS

- INT test method can promote grout segregation and differentiate grout robustness to adverse mix conditions and identify corrosion activity.
- Corrosion developed in deficient grout with 20,000-ppm addition of sodium sulfate to its mix water. Corrosion was also observed in deficient grout with as low as 2,000-ppm sodium sulfate when combined with chloride. In these cases, corrosion occurred when the sulfate ion concentration was ~0.01 $g_{Sulfate}/g_{Powder.}$
- Additions of 0.08 and 0.2% chloride by cement in itself did not initiate corrosion in the stratified grout layers of INT samples. Corrosion developed in deficient grout materials with similar low-level additions of chlorides (0.03 to 0.18% of total grout mass) when combined with as low as 2,000-ppm sodium sulfate in its mix water. The enhanced sulfate addition apparently had effect to initiate corrosion in presence of low-level chlorides.

6. IDENTIFICATION OF DEFICIENT GROUT AND STEEL CORROSION IN TENDONS

6.1 TEST SETUP

The work was to verify corrosion activity of steel stand embedded in deficient grout cast in large scale test assemblies that would better represent geometry and material conditions found in Florida bridges where PT strand corrosion occurred. An objective was to identify steel corrosion in deficient grout such as that found in the Florida bridges, but the causes of that grout segregation was not yet fully identified and the mechanism of the formation of grout segregation in relevant materials continues to be controversial now. Based on trial testing at the State Materials Office and findings from other research, it was assumed that large scale samples would be required to promote adequate levels of grout segregation. The modified inclined tube test was adopted here. Other grout mixing variables included the use of excess mix water and the use of expired grout materials. Enhancement of chloride and sulfate ion content was included to help elucidate the roles of those chemicals in corrosion development. Furthermore, crevice conditions were examined.

The modified inclined tube test incorporated 15-foot-long 3-inch diameter PVC pipe inclined at 15 degrees with the horizon. Clear PVC was used so that grout anomalies could be viewed. The length of the tendon was made of two pieces of pipe (10 feet and 5 feet), joined by a coupler. The mockup tendon contained inlet and outlet regulators for grout flow. The materials used for the duct and fittings for the pumping process included 3-inch diameter Schedule 40 clear PVC, ¾ inch Schedule 40 spigot plug, ¾-inch Schedule 40 PVC cap, 3-inch diameter Schedule 40 PVC couplings, as well as a PVC tee section and a series of bushing, reducers, and valves for the inlet and outlet (Figures 6.1-6.2). The test sample setup for the grout injection is shown in Figure 6.3.

Figure 6.1. Assembled PVC inlet and outlet fittings.
Left: Inlet. Right: Outlet.

Figure 6.2. Assembled MIT test samples.

Figure 6.3. Assembled MIT test samples supported at incline for grout injection.

Two 7-wire strands were placed within the duct held in place only by its weight. Corrosion probes were placed at 5 points along the length of tendon located at 7.5”, 1’3”, 2’6”, 3’9” and 7’6” from the top of the tendon (Figure 6.4). The probes were inserted in 1” diameter holes drilled into the pipe and sealed with solvent cement and silicone gel.

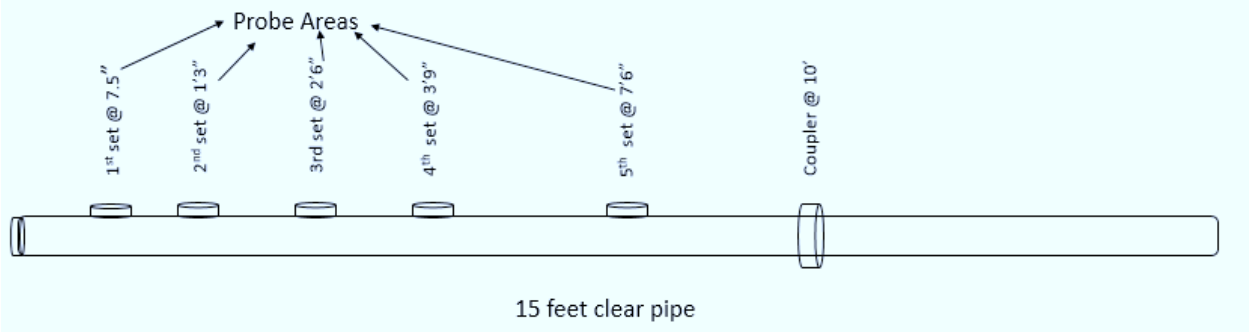

Figure 6.4. Placement of corrosion probes.

Three different styles of corrosion probes were used. The standard style basically comprised of one 1/8 inch diameter steel rod sensor and one 1/8 inch diameter activated titanium (ATR) rod. One standard style probe was placed in the top quarter of the tendon and another at tendon midspan. The second probe style (Figure 6.5) was similar to the standard style and contained a plain steel sensor but a second steel sensor contained a #60 rubber gasket to create a crevice between the gasket and the rod. The third probe style was similar to the standard type (including a plain steel probe) but included an additional 3/16 inch diameter galvanized steel rod probe for future work.

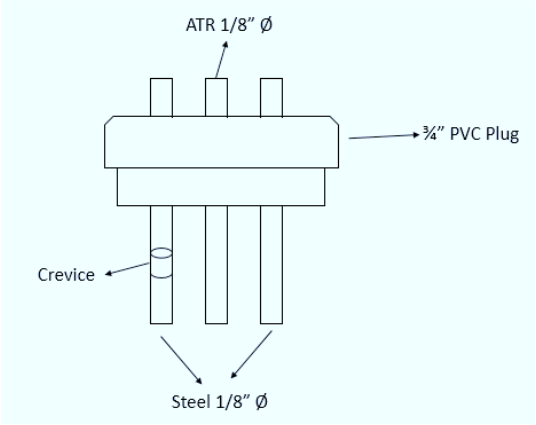

Figure 6.5. Schematic of corrosion probe.

Only the bottom 2 cm of the probes was exposed to the grout. The top of the probe allowed access for electrical connections and the rest of the probe was sealed with a two part epoxy. The steel probes were used as the working electrode for electrochemical testing, acting as proxy sensor for steel embedded in the grout. The ATR rod was used as a reference electrode that was periodically calibrated with a copper/copper-sulfate reference electrode (CSE) placed at access points drilled through the PVC pipe. The counter electrode was an embedded ATR mesh placed along the length of the tendon. The extended counter electrode mesh was tied down to a plastic grid sheet cut to fit within the duct to prevent contact of the electrode to the two strand pieces. The plastic grid can be seen in the ungrouted samples in Figure 6.3.

All large scale test samples were cast with degraded grout materials in non-ideal conditions in order to promote grout deficiencies. Only one grout product was utilized in these experiments. All grout materials used were past marked expiration dates and at least excess 15% mix water over manufacturers recommended high end limit was added. Due to the distress placed on the materials, the results of testing were not meant to be indicative of the grout product performance when appropriately used but rather to help elucidate causes for severe corrosion development.

As shown in Table 6.1, three main groups of test conditions were made for the large scale test samples. One set of samples was considered a base case of deficient grout with no external additions of aggressive chemical ions. A second set of samples contained ~0.09%, 0.9%, and ~5.5% sulfates by cement mass. The third set of samples contained ~0.08% and ~0.2% chlorides by cement mass. The actual mix proportions are shown in the Table. All test samples were created in duplicates for testing.

Table 6.1. Grout Mix Condition

Condition	Sample Label	Date of Casting	Grout Expiration	Mix Water/Solution Weight	Grout Weight
Base	A	11/25/13	11/4/13	88.4 lb Tap water (Gainesville, FL)	297.1 lb
Chloride	B	1/14/14	5/24/12	90.3 lb Tap water (Miami, FL): 2.8 g NaCl/L H_2O	301.9 lb
	C	1/14/14	5/24/12	89.9 lb Tap water (Miami,FL): 7.0 g NaCl/L H_2O	300.5 lb
Sulfate	D	1/14/14	5/24/12	88.5 lb Tap water (Miami, FL): 2 g Na_2SO_4/ L H_2O	296.1 lb
	E	11/25/13	11/4/13	86.54 lb Tap water (Miami, FL): 20 g Na_2SO_4/ L H_2O	289.4 lb
	F	11/25/13	8/2/12	107.0 lb* Tap water (Miami, FL): 150 g Na_2SO_4/ L H_2O	296.7 lb

* Plasticizer (200 mL) was added as well to aid in pumping.

Batching and mixing was conducted at the State Materials Office (SMO) using a high shear grout plant (Figure 6.6) with the assistance of Dr. Trey Hamilton and SMO staff. It is noted that for the batching and mixing of grout, the weight of pre-mixed solutions with sodium chloride or sodium sulfate was made. As shown in Table 6.1, mixing of grout for condition F with high sulfate additions utilized further additional water than the intended 15% excess. This

was due to the insufficient amount of water (despite the large solution volume) and subsequent poor pumping and flow characteristics.

Evidently that weight of the solution incorporated significant amount of contaminant solute and less water was available for cement hydration and other grout material chemical reactions. This was also evident in the sometimes higher resistance measured in the grout with contamination than compared to the base case. Other than the need to need to increase workability for the case with high admixed sulfates, the distressed grout generally maintained its thixotropic flow characteristic (Figure 6.6). Figure 6.7 shows some of the samples after casting.

Figure 6.6. Grout batching, mixing, and pumping sequence.

Figure 6.7. Modified inclined tube test.

Subjectively, the visual appearance and texture of the grout seen through the clear PVC was not greatly different at the top of tendon after casting than compared to the bottom low elevation sections for the samples with the exception of formation of voids and small amount of apparent deficient grout at the top of some of the samples. The tendon samples appeared to be fully grouted immediately after casting. The pumping procedure also called for closing of the top valve prior to the bottom valve in attempt to prevent air void development. However, void spaces subsequently developed by the next day typically at the top valve. The worst case of visual grout aberration was observed in test condition F where high levels of sulfates were admixed. In one of the duplicate samples there, a large void space developed near the center of the tendon span. As seen in Figure 6.8, unusual grout subsidence occurred creating a void space filled with solution. Color differentiation was observed in the tendons with high admixed sulfate content but that differentiation is likely in part associated with the high moisture content and plasticizer addition. Precipitation of sulfates after mixing the solution with the grout also occurred. The solubility of sodium sulfate was evidently smaller in alkaline grout pore water solution than in neutral solution used for mixing.

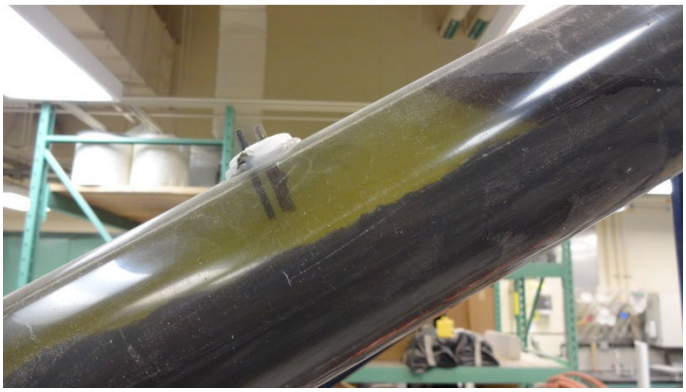

Figure 6.8. Grout subsidence observed 1 day after pumping.
Corrosion probe observed through clear PVC.

As will be described later, the solution resistance of the grout was found to be lower at the top elevation of the tendon samples than the lower elevations, indicating poorer grout quality at high elevations. Detailed physical examination of the grout analyzing its chemical constituency is reported in Chapter 6.

The corrosion potential (OCP) was measured with a copper/copper-sulfate reference electrode (CSE) via access points along the length of the tendon. Corrosion current density of embedded steel probes was calculated from linear polarization resistance method following Equation 1,

$$i_{corr} = \frac{B}{Rp \times A} \qquad 1)$$

where B was assumed to be 26 mV, Rp is the resolved measured polarization resistance, and A is the area of the probe exposed to the grout. Solution resistance was measured with a soil resistivity meter using a three-electrode configuration where the steel probe was the working electrode, the ATR rod was the reference electrode, and the ATR mesh was the counter electrode. The distance between the working and reference electrode was fixed at 1cm. Anodic polarization tests were conducted on select steel probes embedded in the large scale mockup tendons using similar three-electrode configuration. The electrode was cathodically conditioned to $-1V_{SCE}$ for 30 minutes prior to being subjected to polarization from $-1V_{SCE}$ to $+500\ mV_{SCE}$ at a slow scan rate of 0.05 mV/s. The anodic polarization tests were intended to identify if the anodic behavior of steel in deficient grout or with enhanced sulfate levels and determine if more adverse corrosion conditions exist in deficient grout. The data is also compared with tests conducted in aqueous solution to identify discrepant corrosion behavior between experiments in solution and in grout environments.

Steel corrosion probes were embedded along the length of the large mockup tendon samples. The different probe styles are not further differentiated in the results and discussion. Only results of the sensor type are discussed. Two corrosion probes were located within 1 ft.

of the top of the inclined tendon. Three corrosion probes were located at lengths 1 < l < 5 ft. from the top of the tendon. Averages for measurements for the two top corrosion probes on each tendon and its replicate tendon and averages for the bottom three probes on each tendon and its replicate tendon were reported for the plain steel sensors.

6.2 RESULTS AND DISCUSSION

Figure 6.9 shows the OCP and corrosion current density trends for the corrosion probes with time since tendon casting. Of note more active average potentials and greater average current densities were seen for probes located in the upper 1 ft. region of the tendons regardless of the level of external sulfate and chloride augmentation. Active corrosion current densities may not necessarily be unexpected for the tendons containing chloride augmentation even though relatively low chloride content was admixed (less than 0.2% by cement mass). Testing by Lee et al indicated 0.2% chloride content by cement content may be considered as an upper threshold bound for PT grouts (Lee et al, 2014, FHWA, 2012), but the cement content in the deficient grout is expected to be lower and there may be accumulation of chlorides as well in segregated portions of the cast grout.

The measured enhanced corrosion of steel in the top portions of the tendon samples without enhanced chloride concentrations may be analogous to the observed corrosion of steel in deficient grout observed in field conditions. As described earlier, the deficient grout created in the lab samples had analogous enhanced moisture and sulfate content as well as lower permeability. Further testing for direct validation of the extent of grout deficiency and sulfate content of the grout within the large mockup tendons is detailed in Chapter 6.

Generally similar results from OCP and LPR tests were obtained for the steel sensors with crevice conditions as compared to the plain steel sensors (Figures 6.10-6.11). As with the plain steel sensors, there was differentiation between upper and lower tendon elevation which was interpreted as differentiation between deficient and non-deficient grout. Sensors embedded in the upper tendon elevation had potentials generally more negative than ~-300 mV_{CSE}. Nominal corrosion current densities were >0.05 $\mu A/cm^2$ although the size of the anodic regions of the sensor cannot be quantified.

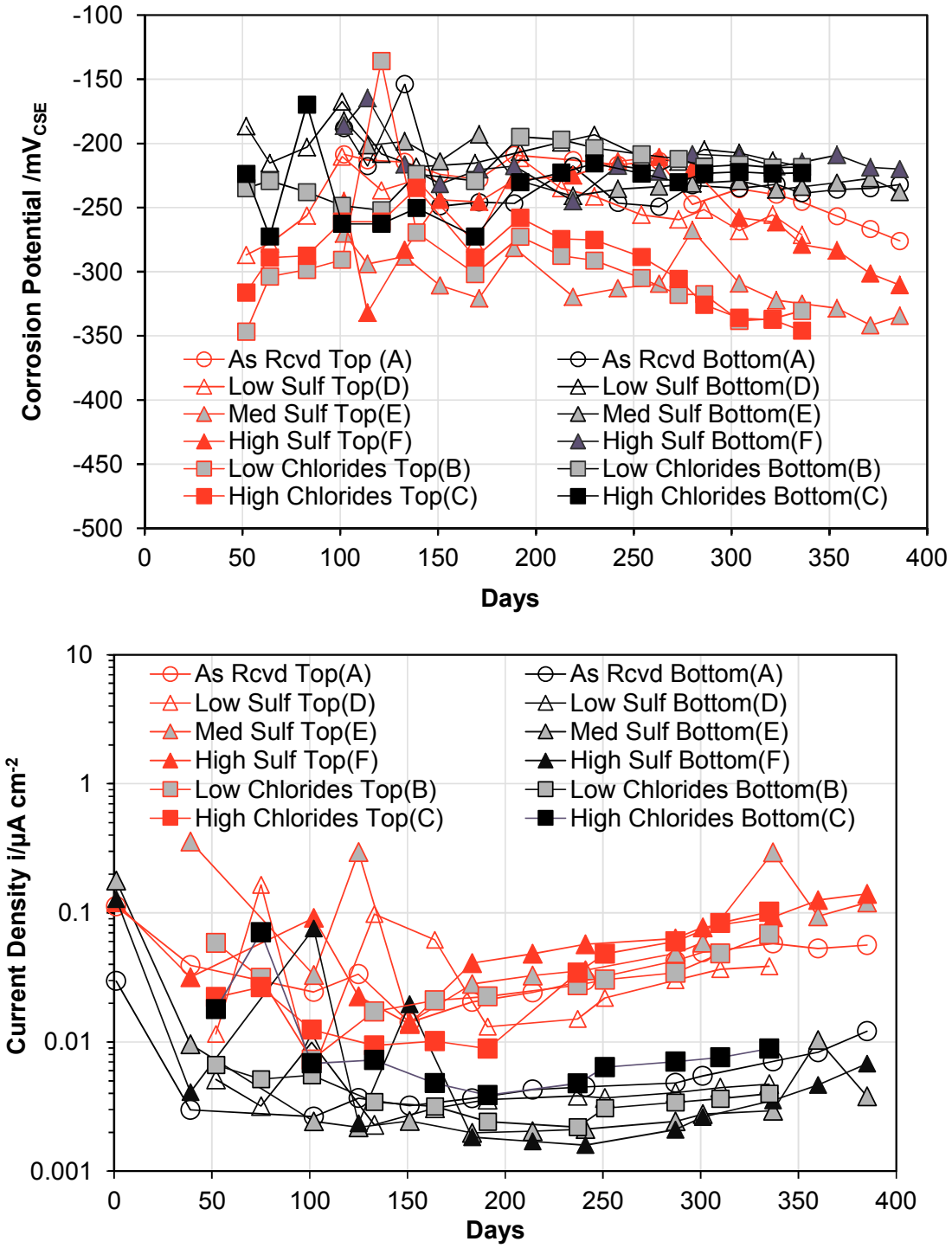

Figure 6.9. Corrosion potential and corrosion current density of steel MIT test samples.

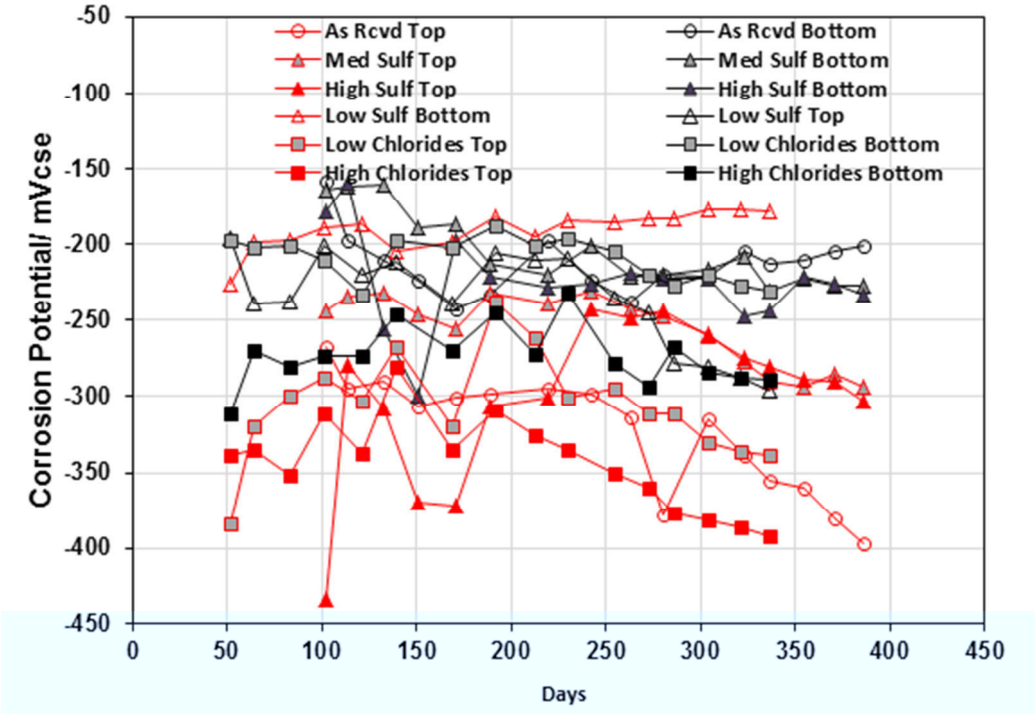

Figure 6.10. Corrosion potentials of steel sensors with crevice condition.

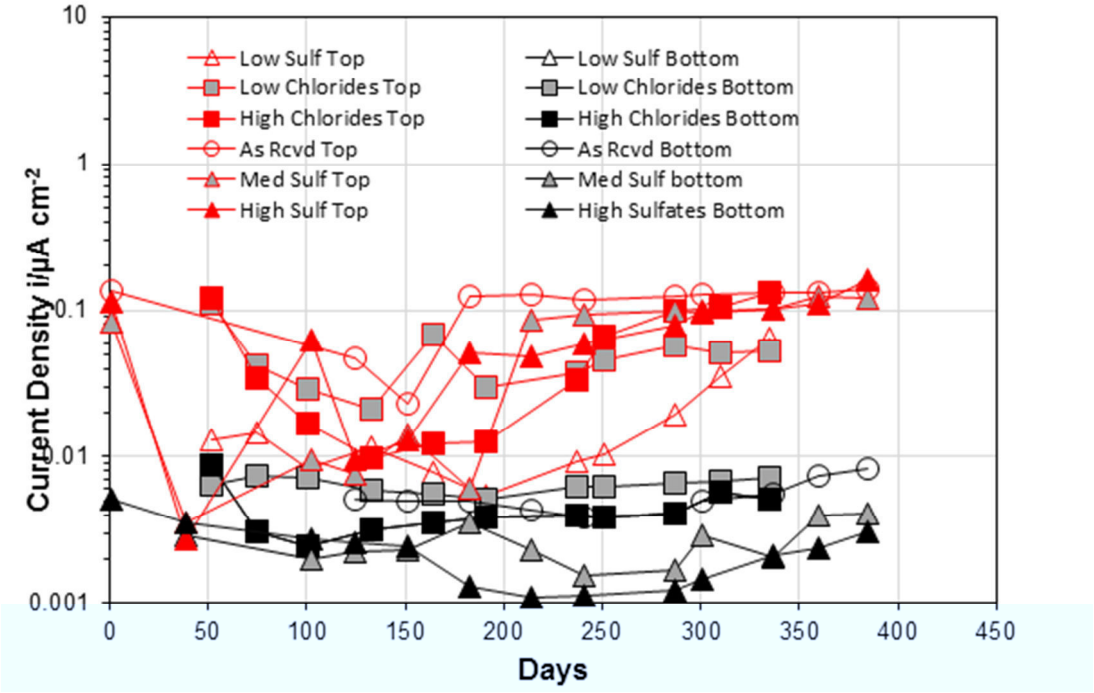

Figure 6.11. Corrosion current density of steel sensors with crevice condition.

After ~500 days, anodic polarization tests were conducted on duplicate plain steel sensors (Figure 6.12). The steel samples were preconditioned for 30 minutes at-1V_{SCE} prior to anodic polarization. The effect of short term large cathodic polarization on passive film stability was not directly addressed. The results of the anodic polarization scans were generally consistent

with earlier testing shown above where more active potentials and larger corrosion current densities were generally observed for probes placed at higher elevation locations. There was indication of passive film development as observed by relatively small change in anodic current after initial anodic potentiodynamic polarization. Apparent passive current densities were larger for the sensors placed at the higher elevation locations. A striking feature of the polarization graphs showed indication of abrupt increase in anodic current at ~+200 mV_{SCE} for steel in the upper portions of tendon sample cast with grout with high admixed sulfate conditions, which may give further implications on the role of sulfates in steel corrosion initiation. If conditions were able to cause significant anodic polarization, the steel may be near this range for breakdown of passive-like behavior and result in enhanced anodic currents. The low solution resistance of the deficient grout at upper elevations may be conducive for more efficient macrocell coupling.

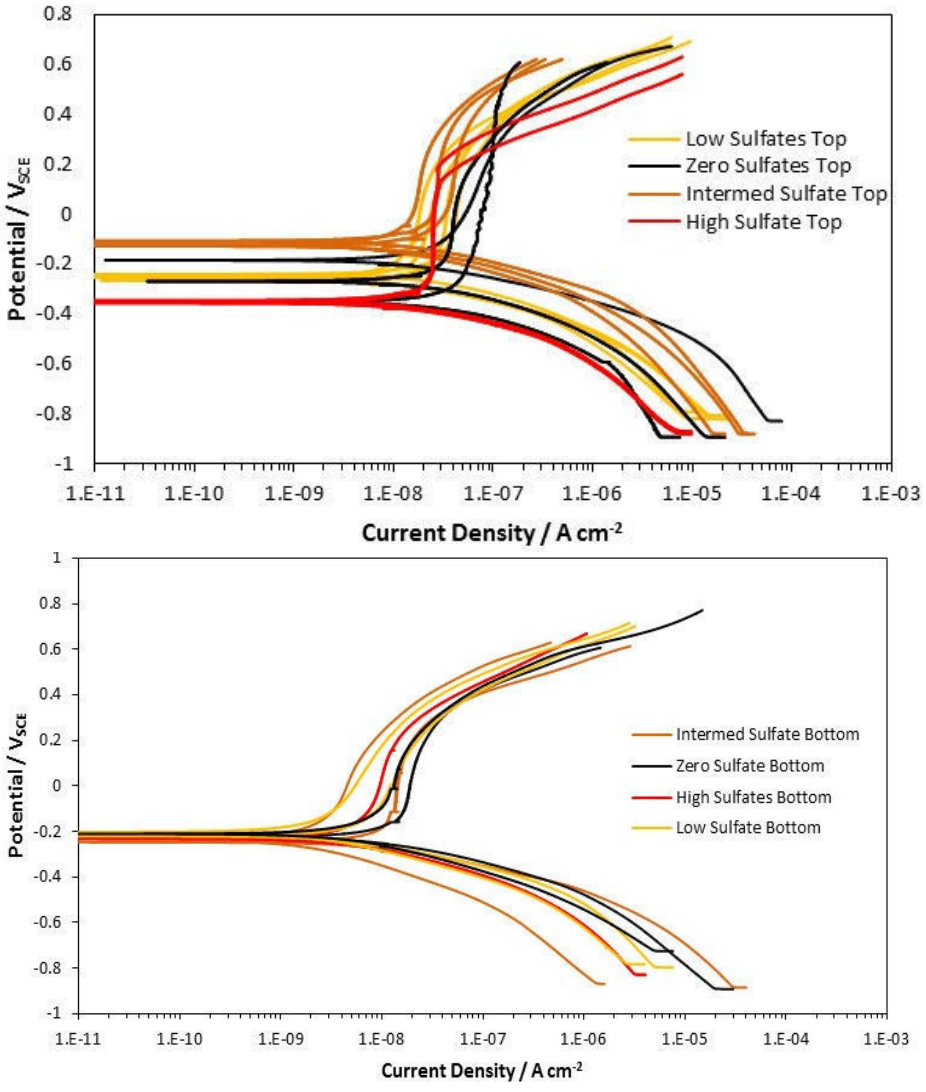

Figure 6.12. Anodic polarization of steel in MIT samples.
Top: Sensors embedded in grout at high elevation sections of tendon.
Bottom: Sensors embedded in grout at low elevation sections of tendon.

As shown in Figure 6.13-6.14, electrical solution resistance was lower for the grout from the upper elevations of the large mockup tendons than lower elevations indicating more permeable grout associated with grout deficiency at the former. The lower resistance at the top of the samples is consistent with the higher corrosion current density measured for the plain steel sensors. Until the extent of grout deficiency that occurred after grout mixing is quantified (Task 6), correlation between grout deficiency and tendon location is for now only qualitative. Nevertheless, it is striking that poorer grout quality (by comparison of solution resistance,Rs) was consistently observed in the upper elevation of the tendon. Interestingly, the solution resistance did not increase with time. For the grout in at the lower elevations, it was thought the grout would be of lower permeability and solution resistance would increase as the cement component of the grout hydrates. For the grout in the upper elevations, the solution resistance decreased with time. The drop in solution resistance in the suspected deficient grout would promote adverse galvanic interaction as described earlier and enhance macrocell corrosion development. The enhanced external addition of chloride and sulfates did not appear to be a major factor in the solution resistance in the top or bottom of the tendons.

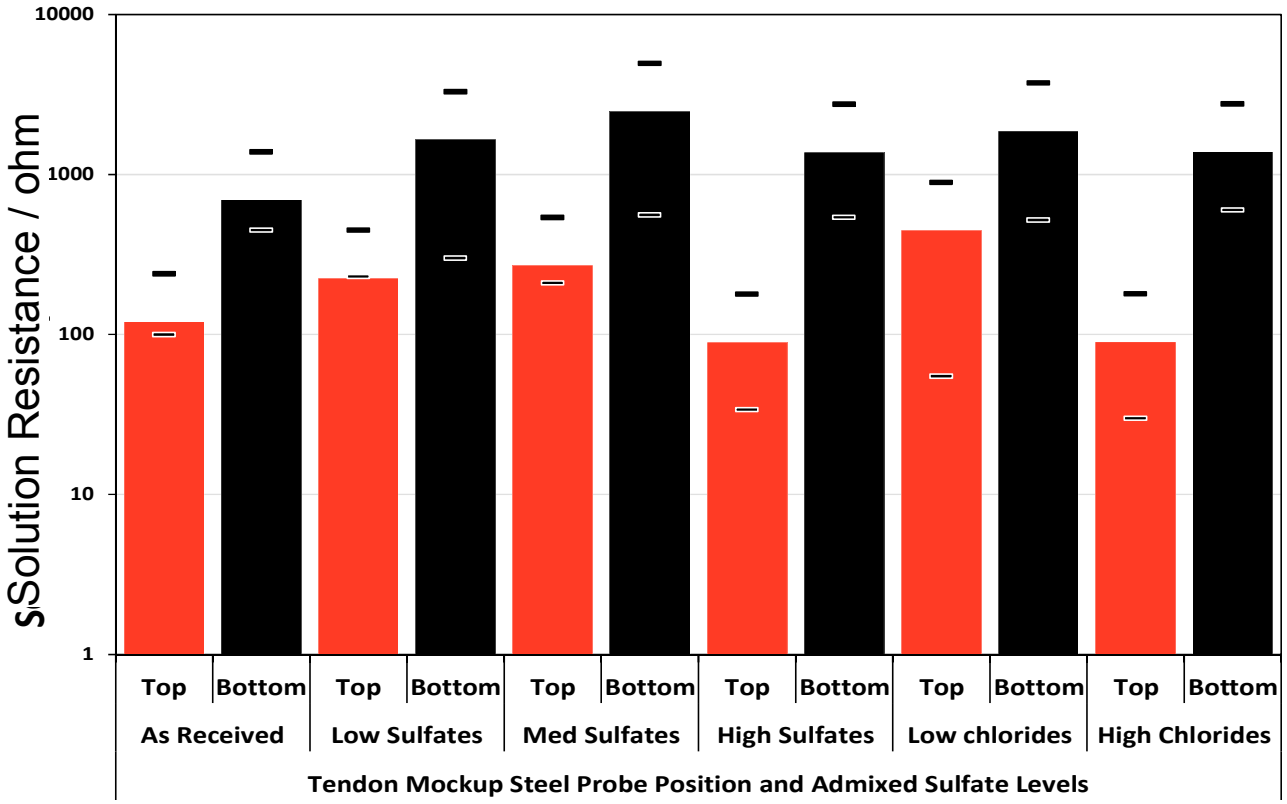

Figure 6.13. Solution resistance of grout in MIT samples.

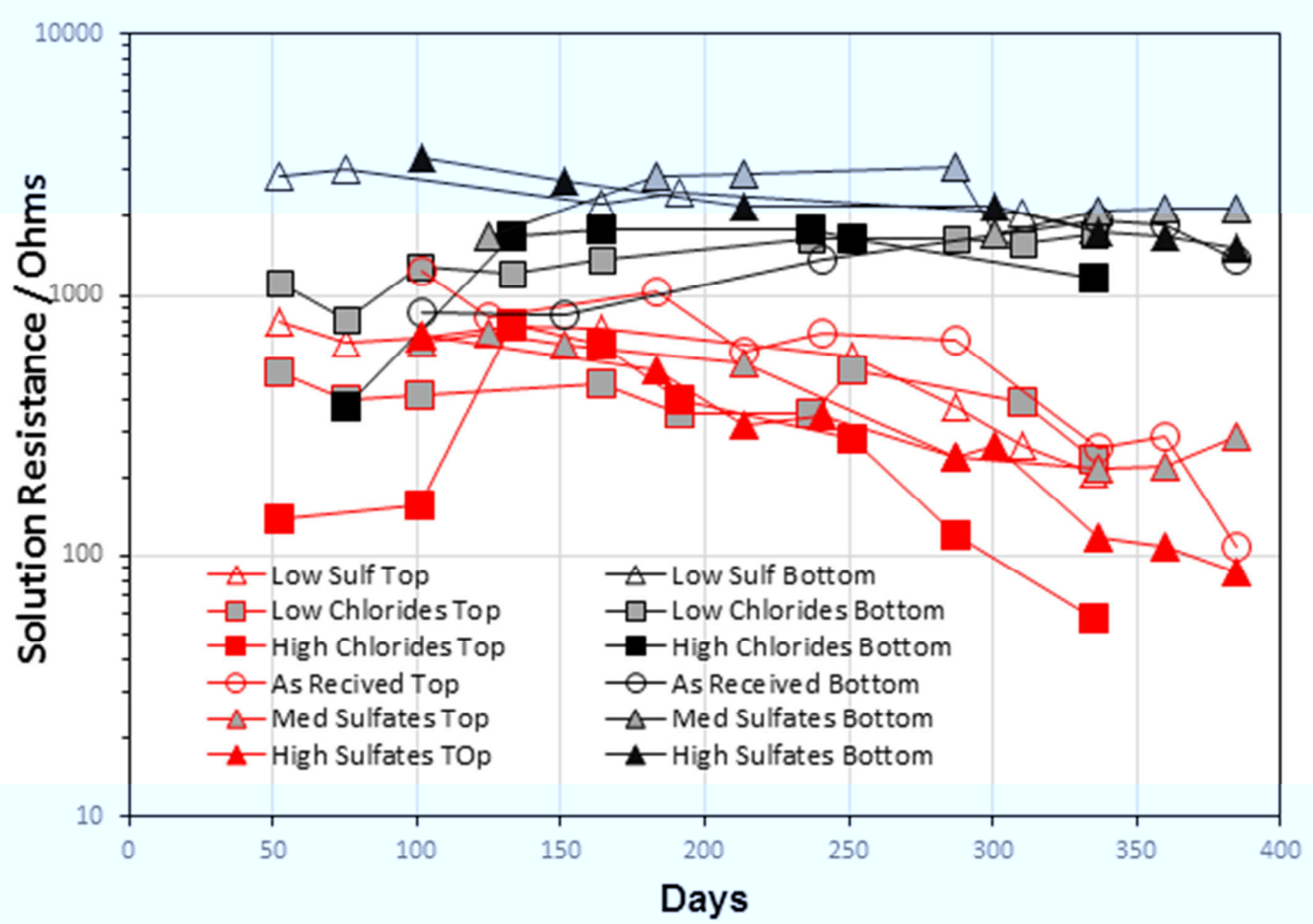

Figure 6.14. Solution resistance.

Free sulfate and free chloride concentrations from grout leachate from sections of the MIT samples as well as comparative values from two field sites are shown in Figure 6.15. In the MIT samples, corrosion only occurred in presence of deficient grout located in the upper elevations of the tendon. Free sulfate levels where corrosion developed typically exceeded 0.1% of the grout mass.

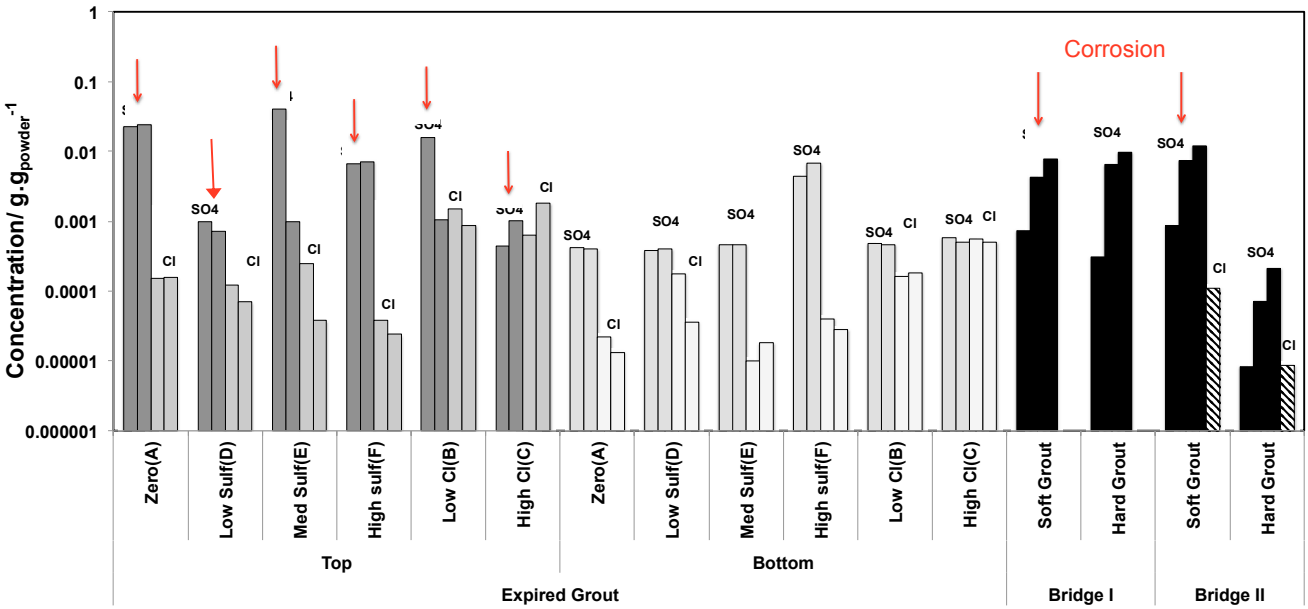

Figure 6.15. Sulfate and chloride content in MIT grout samples.

The measured enhanced corrosion of steel in the top portions of the tendon samples without enhanced chloride concentrations may be analogous to the observed corrosion of steel in deficient grout observed in field conditions. As described by testing of effluent grout materials from the same grout mix in The Grout Cylinder test, the deficient grout created in the lab samples had analogous enhanced moisture and sulfate content as well as lower permeability. Corrosion on the steel probes are detailed in Chapter 7.

6.3 SUMMARY OF IMPORTANT FINDINGS

- Enhanced corrosion can occur in deficient grout created with expired grout and excessive mix water. The enhanced corrosion occurred at elevated portions of the tendon.

- Steel in deficient grout with sulfates may have reduced range of oxidizing conditions where passive behavior is maintained.

- The disparate developed corrosion potential of steel in different grout conditions, apparent condition of maintained active corrosion, and apparent adverse electrical grout characteristics may lead to adverse macrocell development causing enhanced corrosion rates.

7. DEFICIENT GROUT CHARACTERIZATION

7.1. INTRODUCTION

The work was to provide physical and chemical assessment of deficient grout and corrosion from INT and MIT test samples described in Chapters 4 and 5. The grout material was assessed by physical, chemical and petrographic analysis. The materials were assessed for parameters such as moisture, sulfate content, total chloride content, and grout composition. Grout samples from the INT and MIT tests were compared with grout from the Ringling Causeway Bridge to identify grout characteristics where corrosion developed. The corrosion product that developed on the steel wires was evaluated by visual evaluation, X-Ray diffraction, scanning electron microscopy and energy dispersive spectroscopy to identify the role of sulfates. The identification of MIT and INT test samples are listed in Tables 7.1 and 7.2.

Table 7.1. Test Cases for Modified Incline Tube Test (MIT)

Grout Product	Grout Condition	Test Cases	Sulfate amount (ppm)	Chloride amount (%by cement)
A	**E**	A	0	0
		B	0	0.08
		C	0	0.2
		D	2000	0
		E	20,000	0
		F	150,000	0

(Grout Condition: E=Expired)

Table 7.2. Test Cases for Inverted Tee Test (INT) Test

Grout Product	Grout Condition	Test Cases	Sulfate amount (ppm)	Chloride amount (%by cement)
A	**P**	1	0	0
		2	2000	0
		3	20,000	0
		4	100,000	0
		5	0	0.08
		6	0	0.2
		7	2000	0.08
		8	20,000	0.08
		9	100,000	0.08
		10	2000	0.2
		11	20,000	0.2
		12	100,000	0.2
B	**P**	1	0	0
		2	2000	0
		3	20,000	0
		4	100,000	0
A	**A**	1	0	0
		2	2000	0
		3	20,000	0
B	**A**	1	0	0
		2	2000	0
		3	20,000	0

(Grout Condition: P=Pre-exposed, A=As-received)

7.2. GROUT SEGREGATION VISUAL APPEARANCE

7.2.1 MIT Test Samples

Grout segregation in the Modified Inclined Tube (MIT) test was severe at the top sections of the tube especially in Cases A and E with zero and medium sulfate concentration, respectively (Figures 7.1 and 7.2a). Grout at lower sections for all test cases was hardened. As expected and detailed later, the segregated grout had higher moisture content.

Figure 7.1. Photos of deficient grout from MIT test.
(Location was adjacent to a probe location at ~0.3 ft. from the top of sample A)

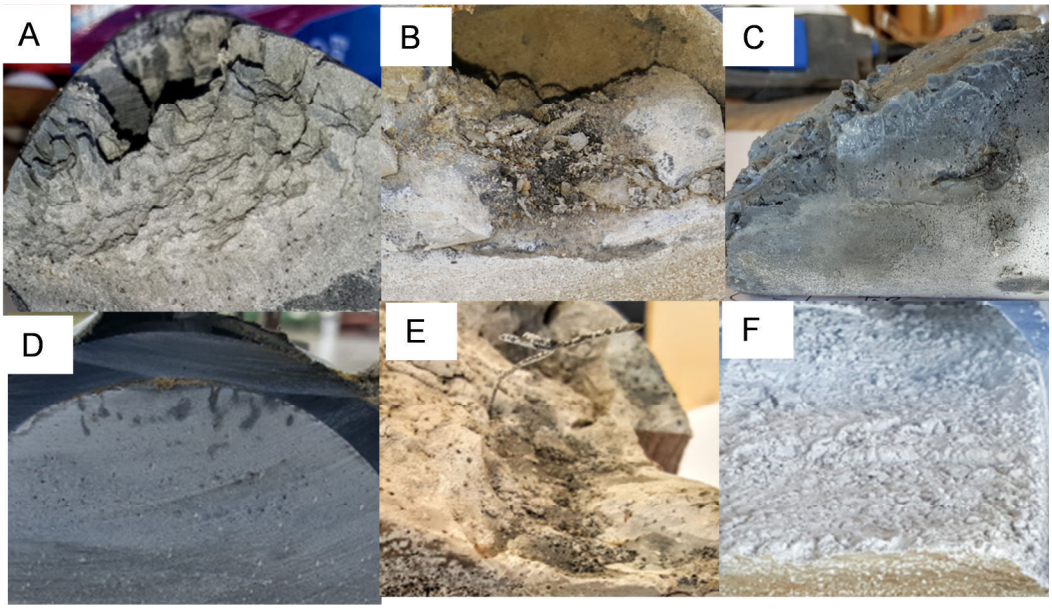

Figure 7.2a. Photos of deficient grout from elevated sections of MIT test samples.
(~0.3 feet from top of tendon)

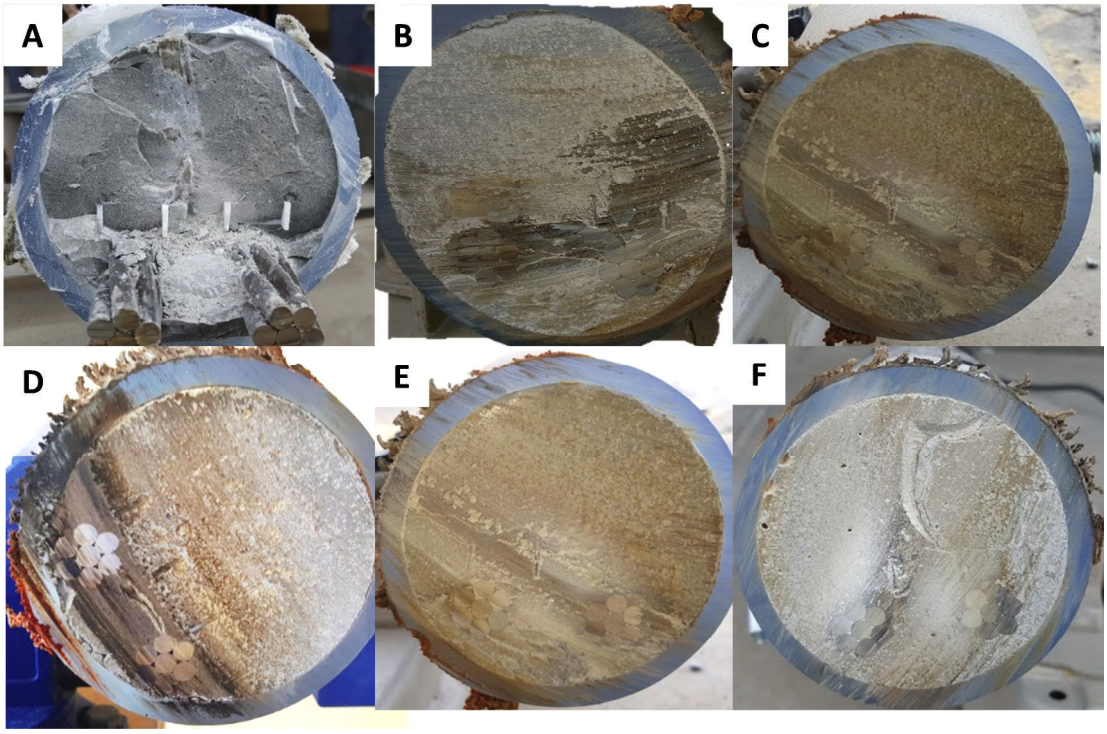

Figure 7.2b. Photos of grout from lower sections of MIT test samples.
(~7 feet from top of tendon)

The severe grout segregation in the MIT test was similar to that observed in the Florida bridges. Petrographic analysis was carried out for 4 samples from Case A and, for comparison, grout from the Ringling Bridge. The petrographic reports are also in the appendix. The results showed that the deficient grout from the MIT tests and field samples consisted of silica fume admixture, some carbonate flour and scant amount of hydrated Portland cement. The polished section of a segregated grout sample exhibited a clear cold joint (severe segregation) between a paste-rich cementitious zone and a darker silica fume-rich paste (Figure 7.3). Portions of the segregated grout showed darker silica fume-rich paste and soft porous portlandite and fine carbonate-rich paste. The water-to-cement (w/cm) ratios was estimated to range from 0.40 to 0.70.

The hardened grout section consisted of Portland cement and less abundance of silica-fume (Figure 7.4). The hardened grout material showed well to fully hydrated alite Portland cement clinker particles and moderately hydrated belite Portland cement clinker particles (Figure 7.4). The grout was more uniform and consistent in composition and had water to cement (w/cm) ratios estimated at 0.40 to 0.45.

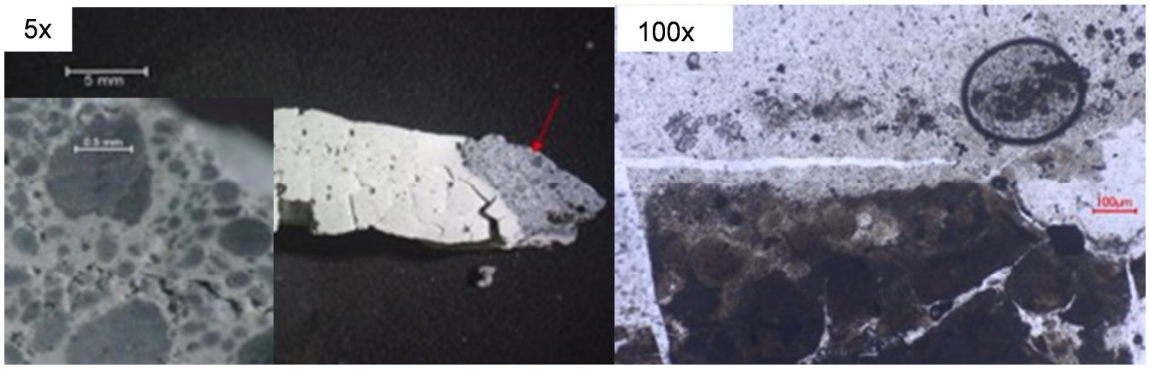

Figure 7.3. Micrographs of segregated grout from MIT test (Case A) samples.

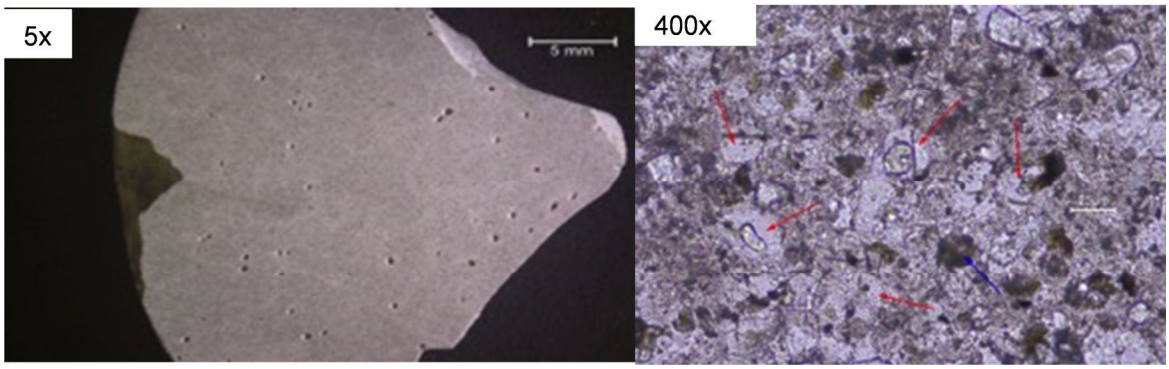

Figure 7.4. Micrographs of hardened grout from MIT test (Case A) samples.

Similar conditions were observed for the field samples from the Ringling Bridge. Figure 7.5 shows a polished section of segregated grout showing abundant shrinkage micro cracking. It was reported by the petrographer that the material was very soft (Mohs < 2). The bottom section of the field sample showed a gradation of darker to lighter-colored paste with presence of entrained-sized air voids that are partially filled with ettringite and portlandite.

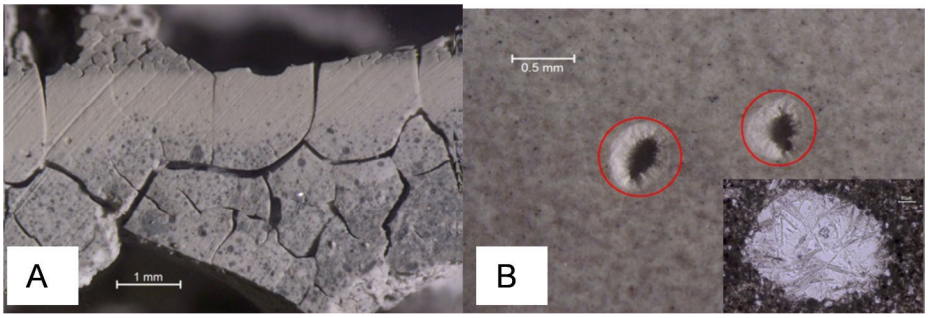

Figure 7.5. Micrographs of grout from field sample.
A. Segregated Grout. B Hardened Grout.

7.2.2 INT Test Samples

Samples from the INT test which were cast with two commercial grouts in either the as-received condition or pre-exposed raw material (32 days high humidity exposure) and 20% extra mix water. The as-received grouts (BA and AA) did not show significant grout

segregation in the samples. Figures 7.6 and 7.7 show pictures of material BA. Pictures of AA samples after demolding were unrecovered but pictures of grout fragments are shown later in the report. Pre-exposed grouts A and B showed differential grout consistency at the tee header and body for two commercial pre-packaged grout products (Figures.7.8-7.13)

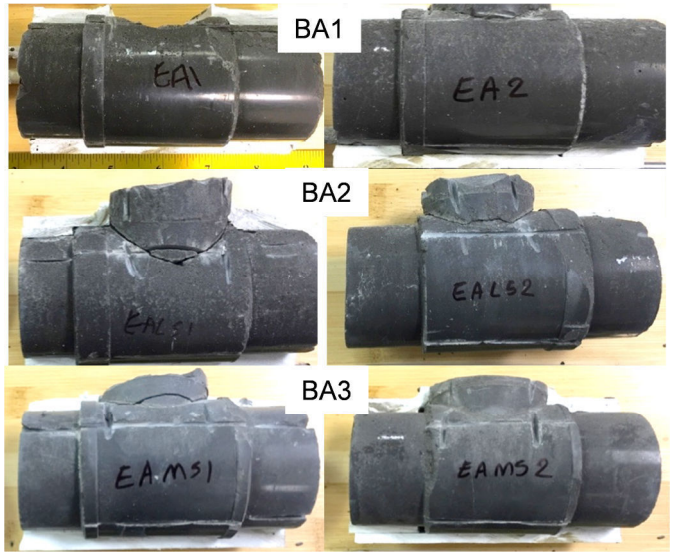

Figure 7.6. Photos of grout in tee body from INT test samples cast with as-received Grout B. (Cases BA1-3)

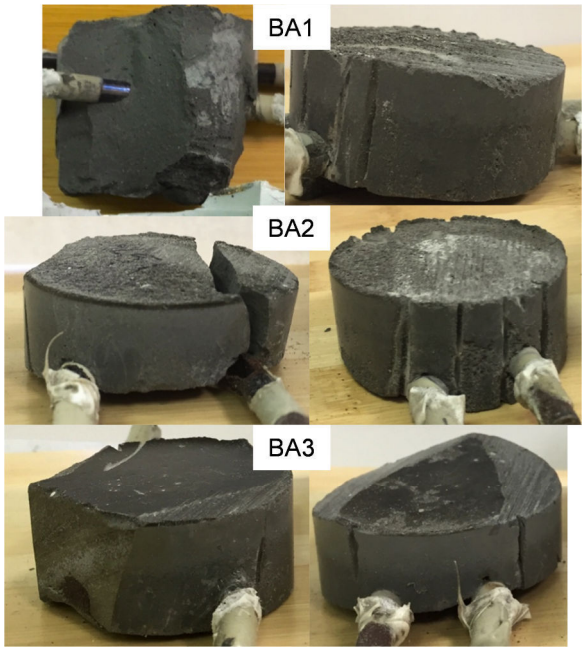

Figure 7.7. Photos of grout in tee header from INT test samples cast with as-received Grout B. (Cases BA1-3)

Figure 7.8. Photos of grout in tee body from INT test samples cast with pre-exposed Grout B. (Cases BP1-4)

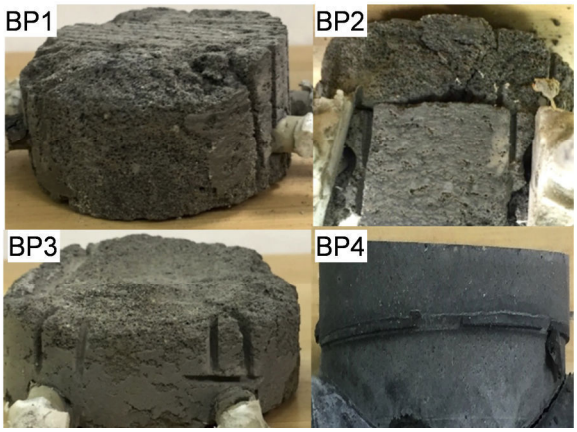

Figure 7.9. Photos of segregated grout in tee header from INT test samples cast with pre-exposed Grout B. (Cases B.P.1-4)

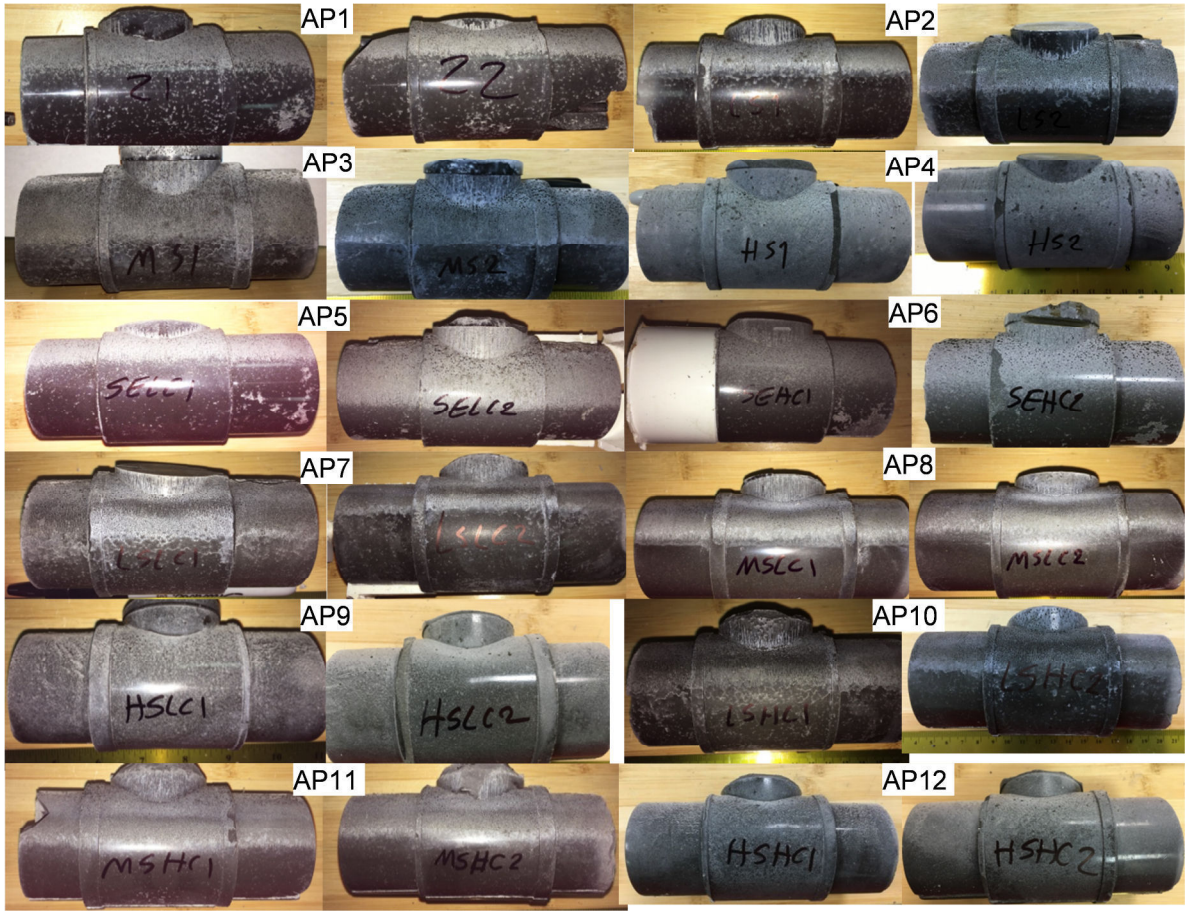

Figure 7.10. Photos of grout in tee body from INT with pre-exposed Grout A.
(Cases AP1-12)

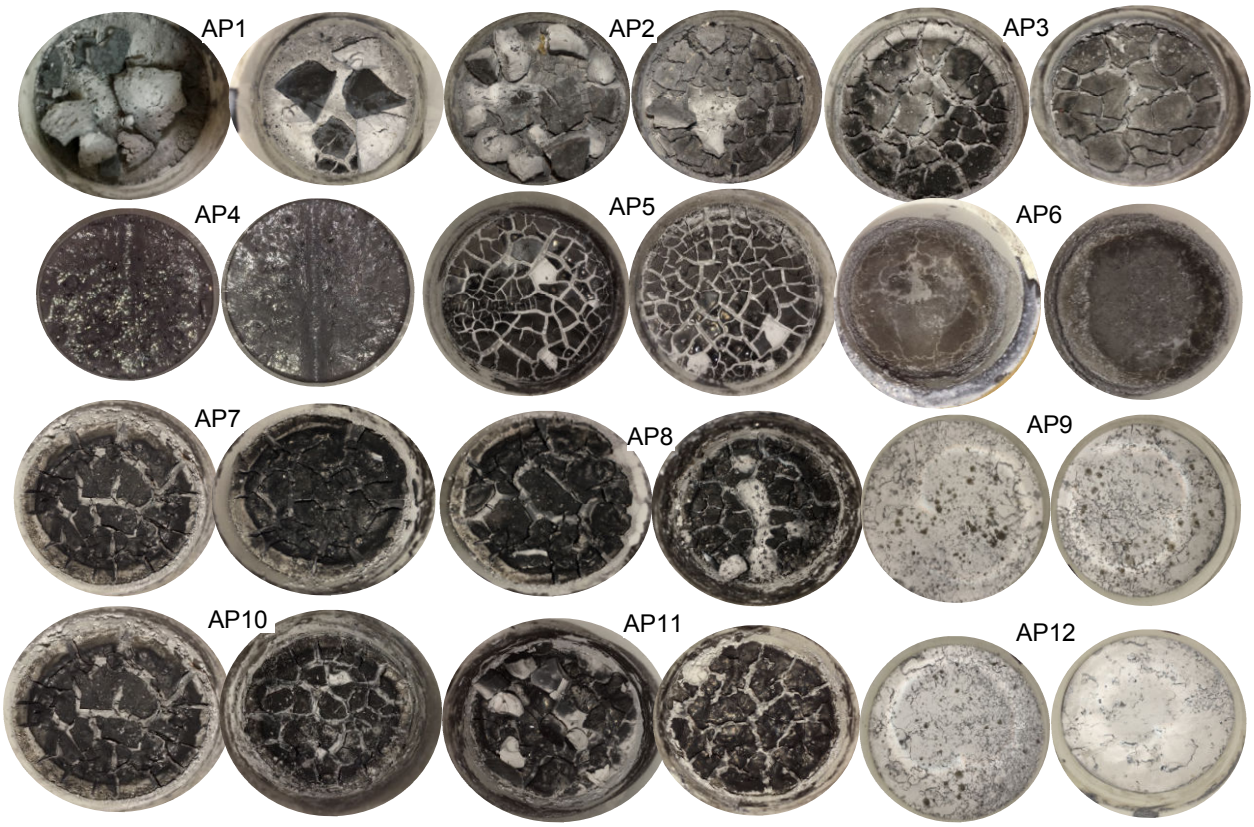

Figure 7.11. Photos of deficient grout surface from INT tee Headers 300 days after casting. (Cases A.P.1-12)

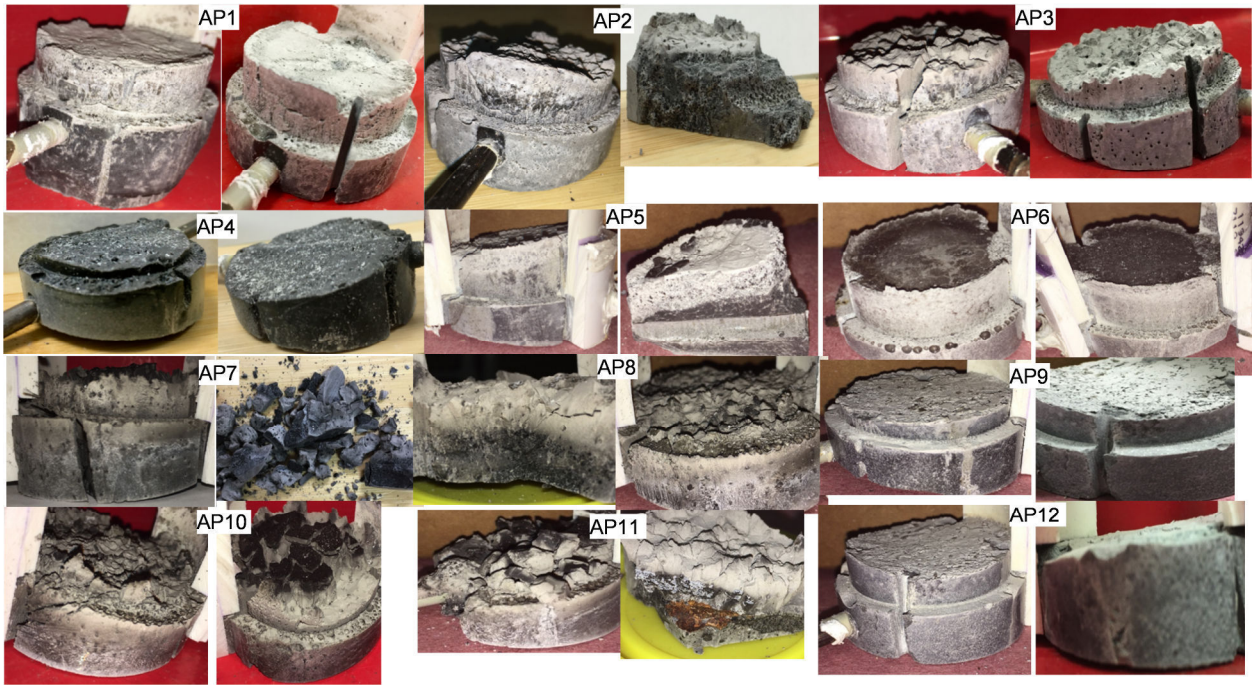

Figure 7.12. Photos of segregated grout in tee header from INT test cast with pre-exposed Grout A. (Cases AP1-12)

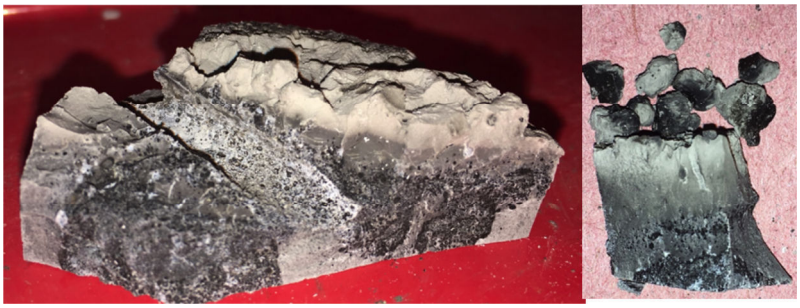

Figure 7.13. Close-up of segregation from INT test sample with pre-exposed Grout A. (Cases AP8)

The bottom section of both pre-exposed Grout A and B formed a hard material with dark color (Figure 7.8 and 7.10), but segregated grout typically formed in the PVC tee header for Grout A and B (Figures 7.9,7.11-713). Pre-exposed Grout B formed friable weak material in the tee header. The grout in the tee header of pre-exposed Grout A showed variation in the visual appearance of the grout but in the worst cases, stratification of grout was apparent with the grout showing the putty or chalky material similar to that observed in the Ringling Bridge.

Eight samples from the INT test representing hardened and segregated Grouts A and B in the as-received and pre-exposed grout condition were analyzed by thin film petrography: Sample AA1, AP1, AP8, BA1, BP1. Select figures from the petrographic report are shown in Figures 7.14-7.16. No unusual observations were made for Grouts A and B in the as-received conditioned. The estimated water to cement ratio (w/cm) for both materials was 0.35-0.45. The segregated Grout B material from the tee header of the pre-exposed grout did not show enhanced moisture content (est. w/cm ~ 0.43-0.48) relative to the hardened material formed in the tee body and in the as-received grout material (est. w/cm ~0.40-0.45). The segregated grout was characterized as having enhanced total air content compared to the non-deficient hardened grout. The composition was otherwise similar to the hardened grout: Portland cement, fly ash, silica fume, and hydrated lime.

Similar findings were made in the petrographic analysis of the segregated Grout A in the INT samples as for the MIT and field samples. The deficient Grout A material from the tee header from sample AP1 showed a cold joint between stratified layers (Figure 7.15). One side of the cold joint contained graded laminations of alternating paste coloration (darker gray to lighter gray), likely representing segregation of the mixture. The makeup was Portland cement, carbonate flour, and small amount of silica fume. The other side of the cold joint was mostly agglomerations of silica fume and Portland cement. The w/cm of the sample was highly variable due to the presence of the cold joint and observed segregation and was estimated to range between 0.40 and 0. 60. The w/cm for the segregated grout in sample AP8 was estimated to be over 0.70.

Figure 7.14. Hardened Grout A from sample AA1 (As-received grout).

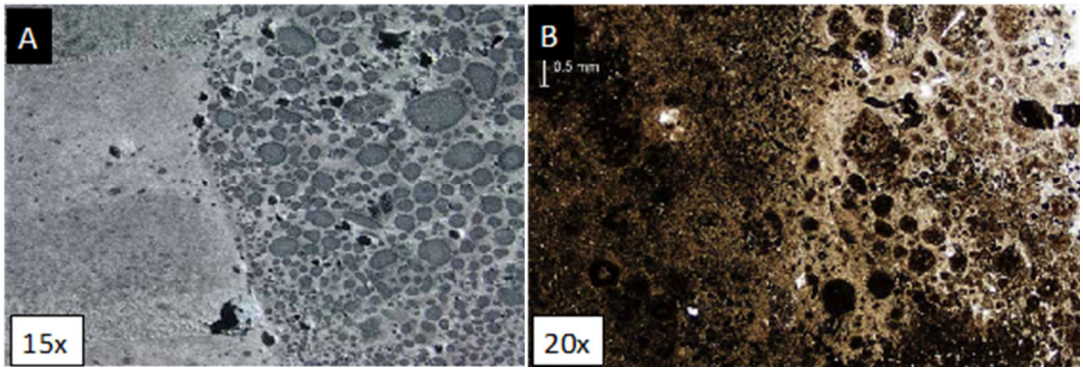

Figure 7.15. Segregated Grout A in tee header of sample AP1 (Pre-exposed grout).

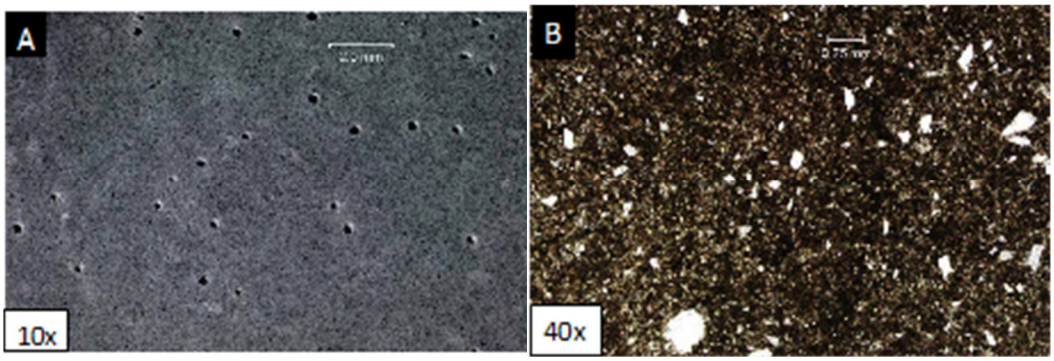

Figure 7.16. Grout A in tee body of sample AP1 (Pre-exposed grout).

7.3. MOISTURE CONTENT

7.3.1 MIT Test Samples

The grout segregation that was observed in the MIT test was thought to be related to available water content after mixing. Severe segregation in MIT test was correlated with high moisture content as much as 60-70% in samples A and E (Figure 7.17). When additions of sodium chloride or sodium sulfate were added, the ratio of solid to water content increased and the amount of available moisture for cement hydration can be lower. Even though very low

levels of chloride concentration was added to the mix condition in Cases B and C, the moisture content was half of that for samples with no additives in Case A (i.e. ~70 % for Case A and ~35 % for Cases B and C). Similar results were observed with the addition of sodium sulfate with the exception of one of the samples with sulfate concentration (20,000 ppm) (Case E) where high moisture content was measured. As detailed in Chapter 5, this sample also had high current density and low corrosion potential, which was related to the accumulation of sulfate ion as shown later.

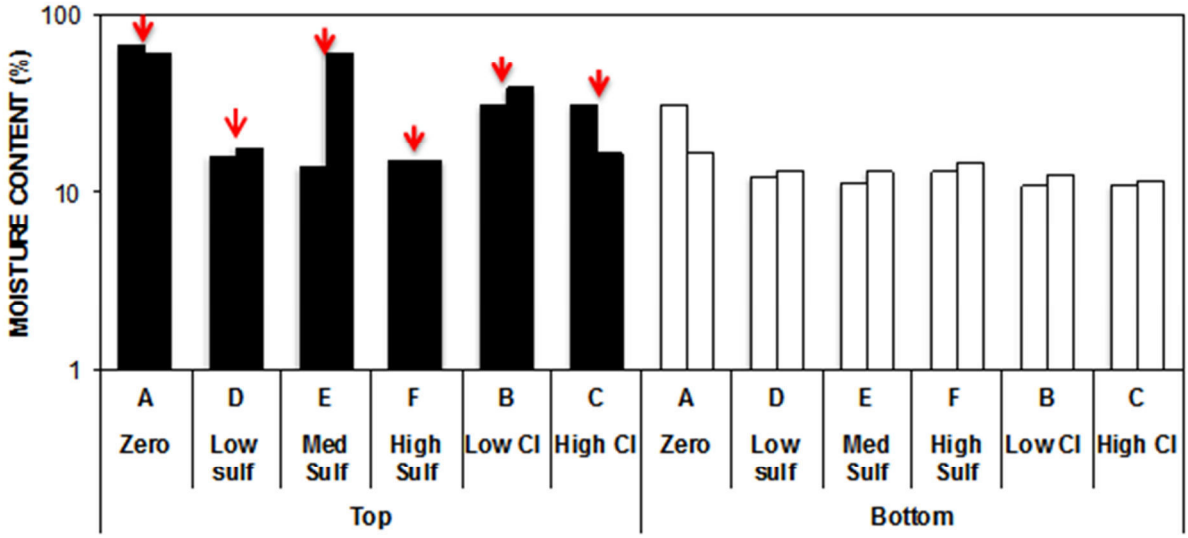

Figure 7.17. Moisture content of grout from MIT test samples.
(Red arrows show case where corrosion occurred)

7.3.2 INT Test Samples

As shown in Figure 7.18, moisture content results for INT test samples cast with as-received and pre-exposed Grout B was measured to be similar (test cases BA1-3 and BP1-4 (<20%)); however, the results were thought to have testing error due to the early water loss(1 day) immediately after casting and prior to capping the samples. It is recalled that the segregated grout from Grout B had high porosity and test results from the conditioned grout cylinders indicated retained moisture within the pores when maintained in 100% RH environments.

Significant differences in moisture content was observed for the as-received and pre-exposed Grout A samples (Figure 7.19). As expected, there was differentiation in the moisture content of the grout from the tee header and body, although with varying levels of severity for the different cases. The moisture content for grout from the tee body was 8-20% for all test cases consistent with values measured for hardened as received grouts and indicative of low propensity for corrosion development. The moisture content for the grout from the tee header was 16-60% for all test cases and corrosion developed in grout with moisture content in the range of 38-60% (Figure 7.19). Interestingly no corrosion developed on steel embedded in the

tee header for samples in test cases AP4, AP9 and AP12, where additions of 100,000 ppm sodium sulfate and up to 0.2% chlorides, but can be in explained in part due to the relatively low moisture content (less than 20%) and therefore greater electrical resistivity. It is noted again that corrosion did develop in grouts that had chloride additions (test case AP7-8 and AP10-11) at levels that were not expected to facilitate corrosion initiation (0.08-0.2% Cl^-). As mentioned earlier, the effect of grout segregation on cement content was not directly considered here and furthermore ion transport in grout segregation might be important. The high level of moisture content correlated well with enhanced sulfate concentration and corrosion development of samples cast with combined low to medium sulfate levels and chloride content (Cases AP7-8 and AP9-10).

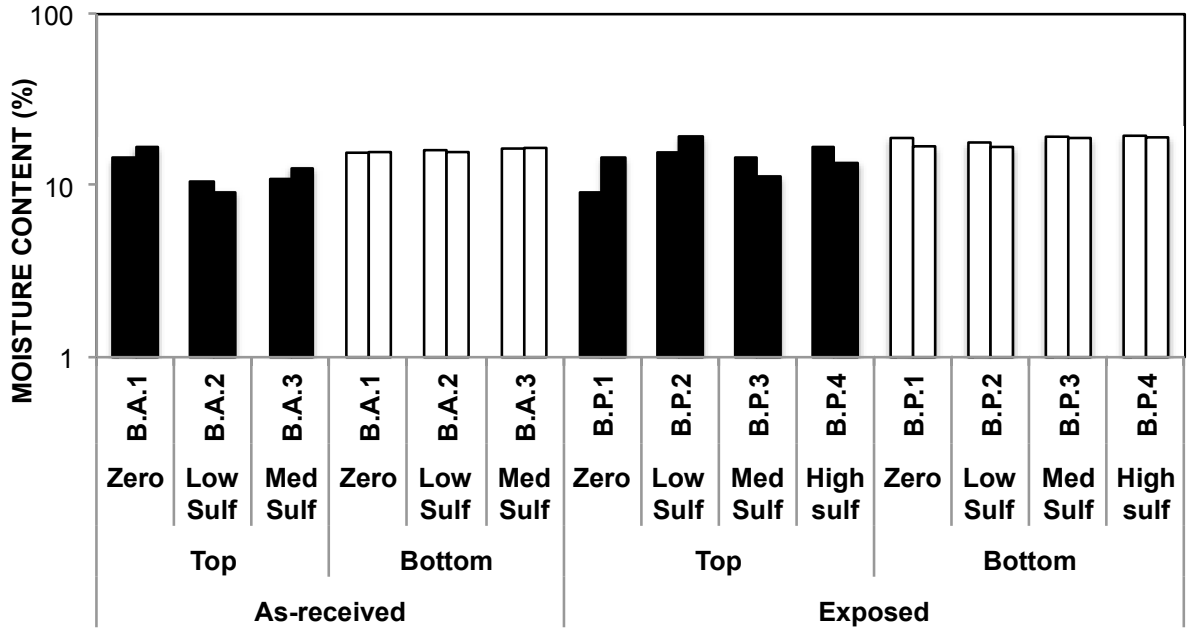

Figure 7.18. Moisture content of grout from INT test samples cast with Grout B. (Cases BA1-3, BP1-4)

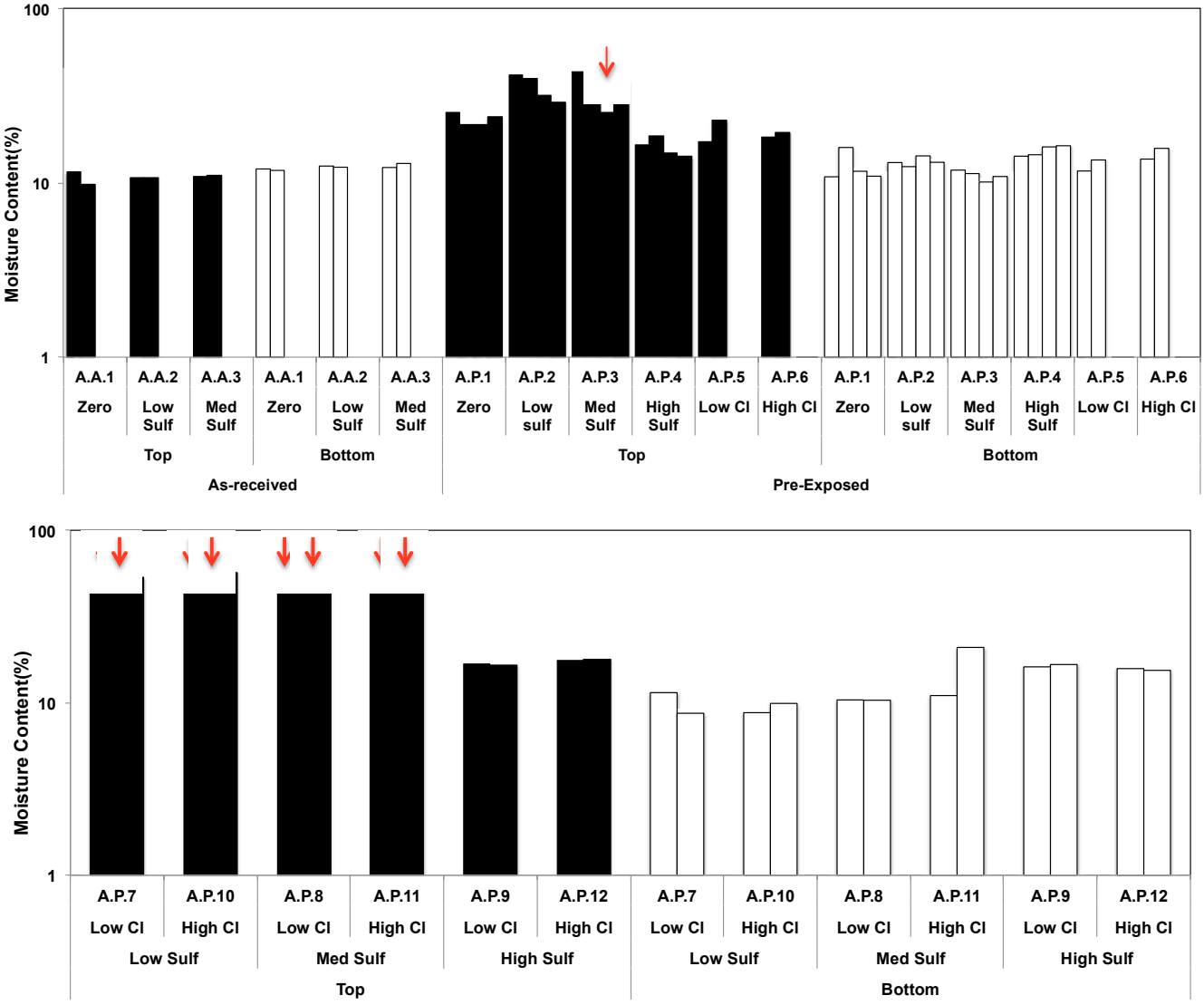

Figure 7.19. Moisture content of grout from INT test samples cast with Grout A. (Cases AA1-3, AP1-12) (Red arrows show where corrosion occurred)

7.4. CHEMICAL ANALYSIS

7.4.1 MIT Test Samples

Sulfate presence have been emphasized in much of the work; however, other ionic species were also tested for grout collected from the base Case A MIT test samples; calcium, potassium, sodium, nitrate, nitrite, phosphorus, sulfide, sulfate, and chloride (Figure 7.20). Grout samples were collected along the length of the test tendon from near the middle of the pipe where the grout was hardened to near to high elevation pipe cap where grout segregation was prominent. Similar to findings from the Ringling Bridge, only enhancement of potassium, sodium, sulfate, and chloride was observed in the upper portion of the test sample where grout segregation was prominent. The chloride content, although enhanced, was low. The enhanced

alkali content may be important in the development of high pore water pH. The sulfate content for Test Cases D-F is also shown in Figure 7.20 for comparison. Test Case D showed slight sulfate enhancement (<0.1%) and Test Case E showed significant sulfate enhancement (>1%). Test Case F where high levels of sodium sulfate was pre-mixed indeed showed high levels of sulfates throughout the sample. Importantly, the sulfate level in the segregated grout in the non-doped base condition (Case A) showed even higher sulfate levels which show that vestigial sulfate content in the grout can have significant accumulation in the segregated grout.

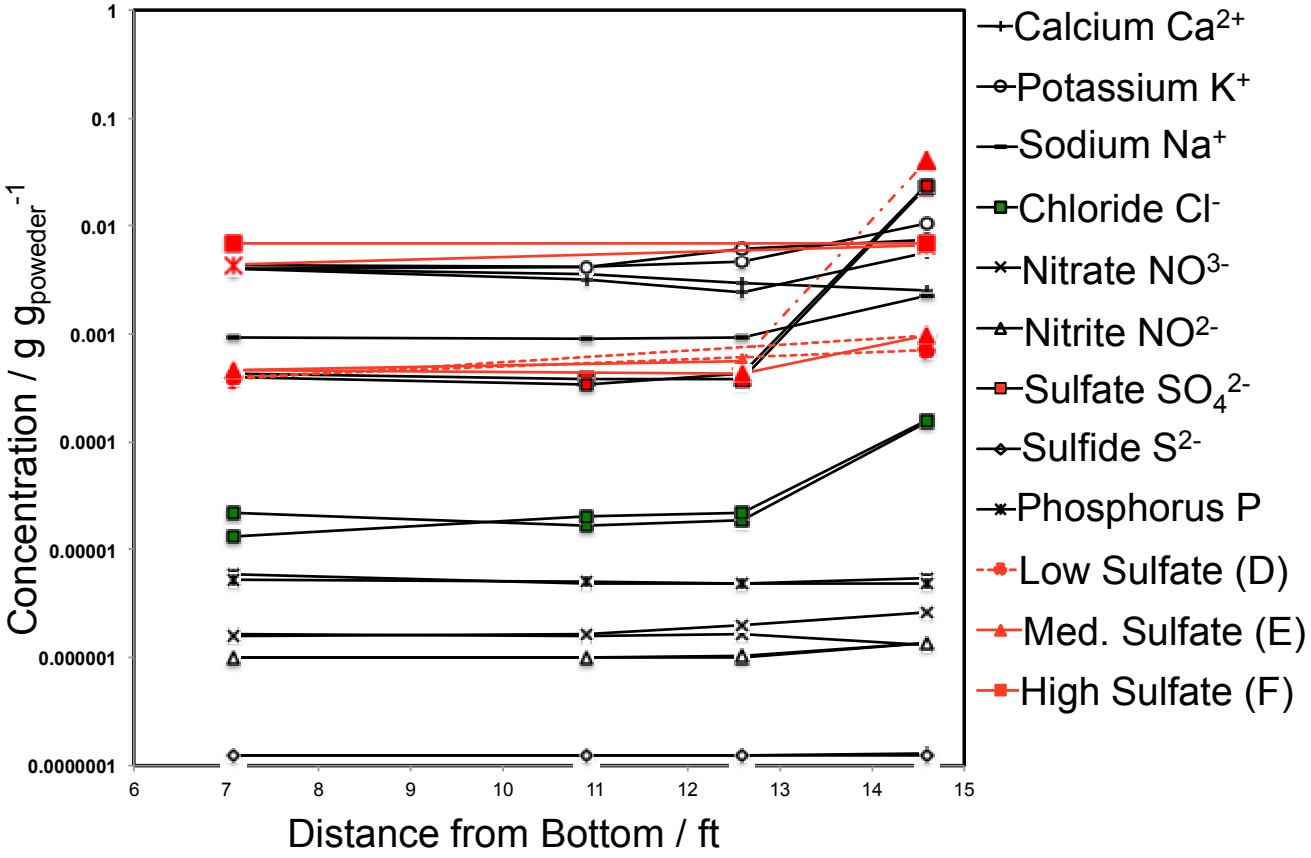

Figure 7.20. Chemical characteristic profiles along 15 ft. of MIT test case A.
Sulfate levels for Test Cases D-F shown for comparison.

7.4.2 INT Test Samples

Similar chemical analysis was made for INT test samples (Test Cases AA1, AP1, BA1, and BP1) (Figures 7.21-7.22). Grout materials A and B mixed in the as-received condition did not show any differentiation in chemical constituency in the tee header and tee body. In the pre-exposed condition, sulfate and chloride accumulation was evident in the tee header. Accumulation of sodium was also evident in the tee header.

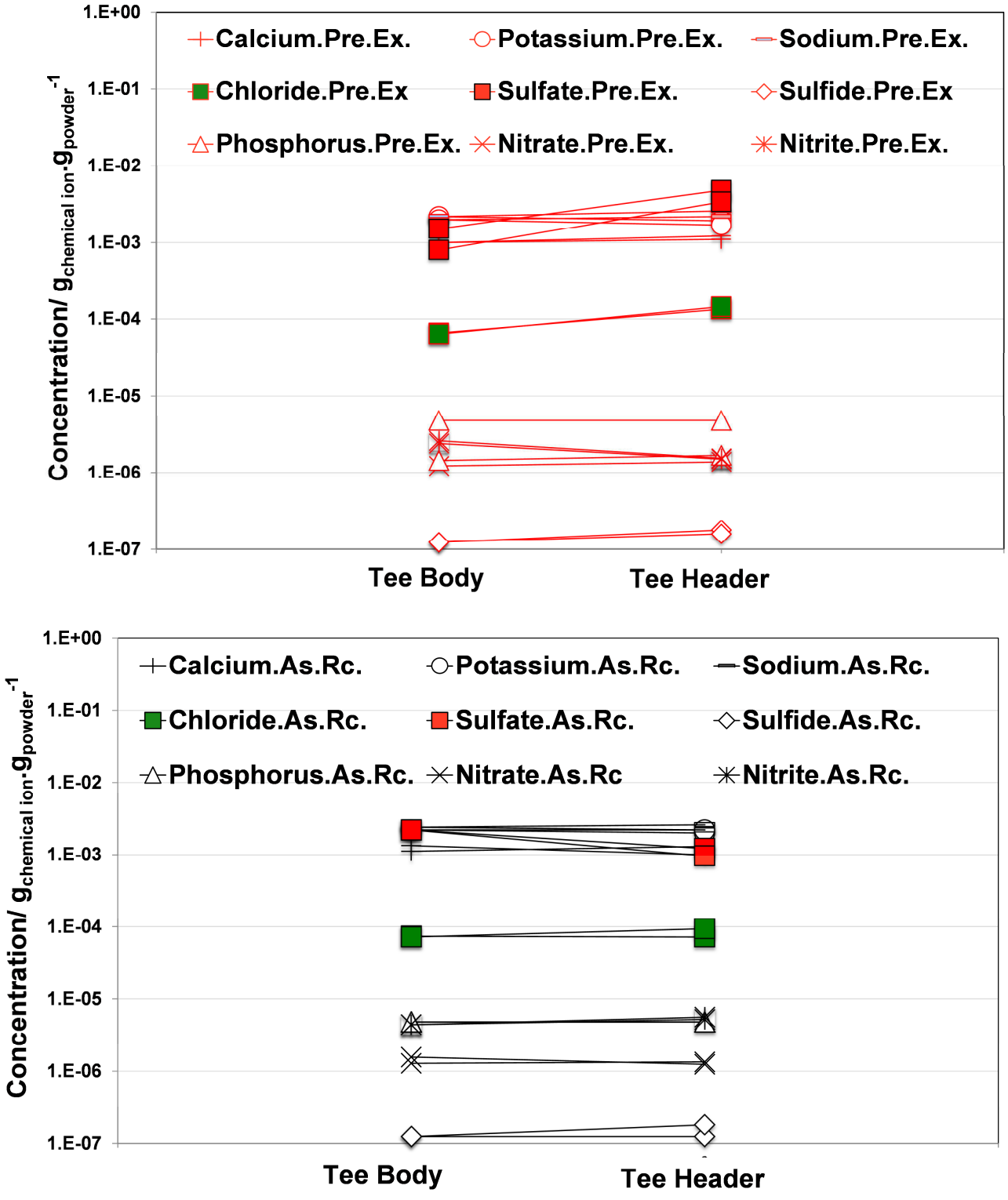

Figure 7.21. Chemical characteristic profiles of INT tests cast with Grout B.
(Cases BP1 and BA1)

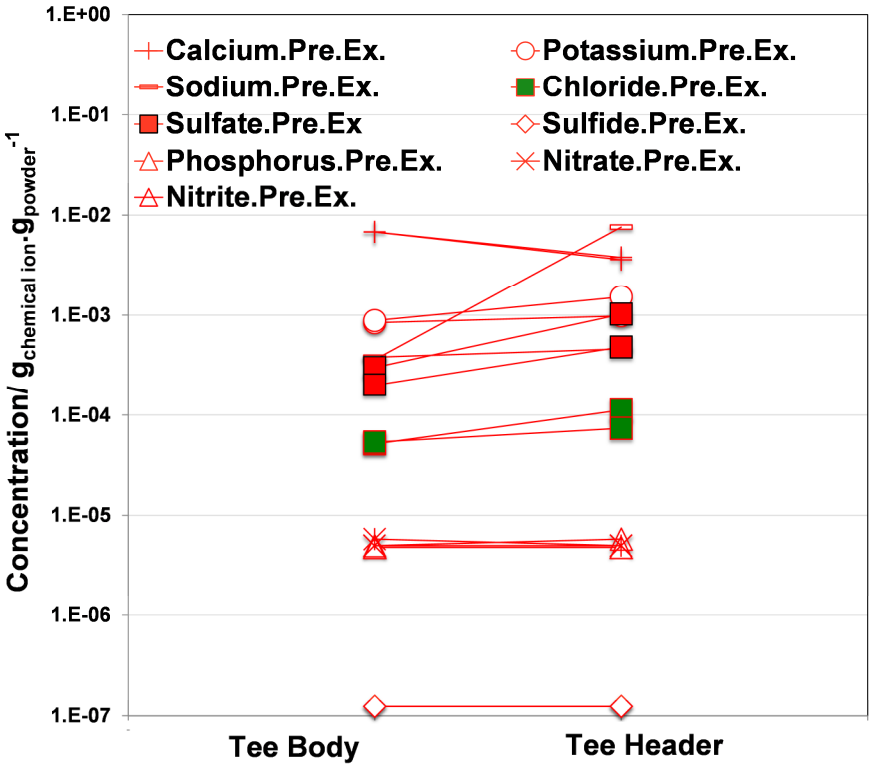

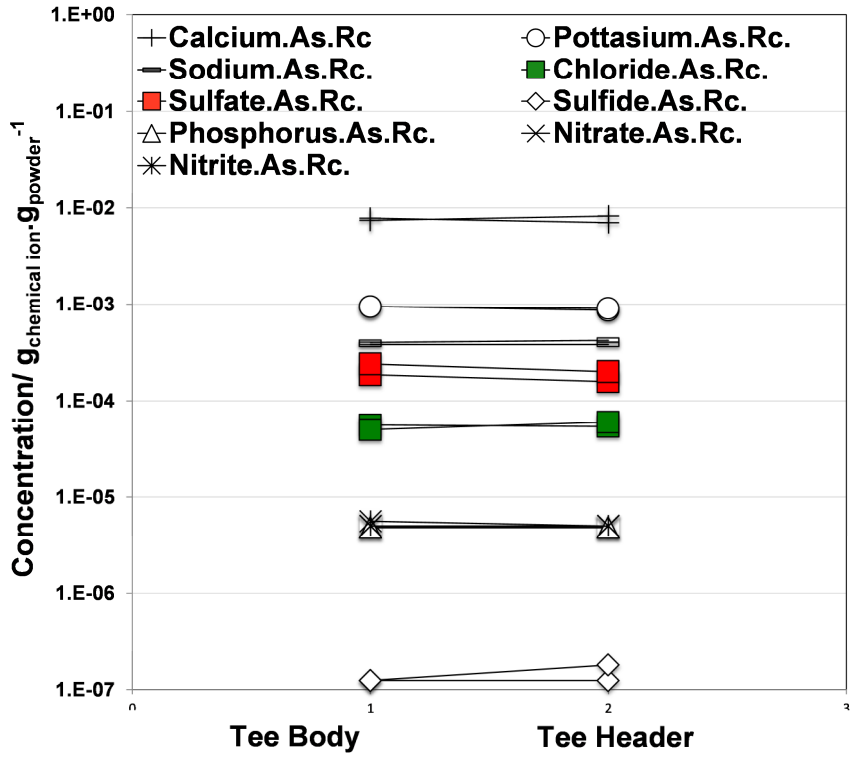

Figure 7.22. Chemical characteristic profiles of INT tests cast with Grout A.
(Cases AP1 and AA1)

7.5. SULFATE CONTENT

7.5.1 MIT Test Samples

Expired grout in the MIT test showed differentiation of sulfate by location in the tendon. High sulfate concentrations were found at the top section (upper elevation) of MIT test samples (Figure 7.23). It was noted that the highest sulfate concentration (>0.01 $g_{Sulfate}/g_{Powder}$) was found in samples without extra sulfate source (Case A). In comparison to the resolved sulfate content measured in grout from two Florida bridges with segregated grout, it is seen that separation of grout material can allow for accumulation of sulfate ions without external sulfate sources.

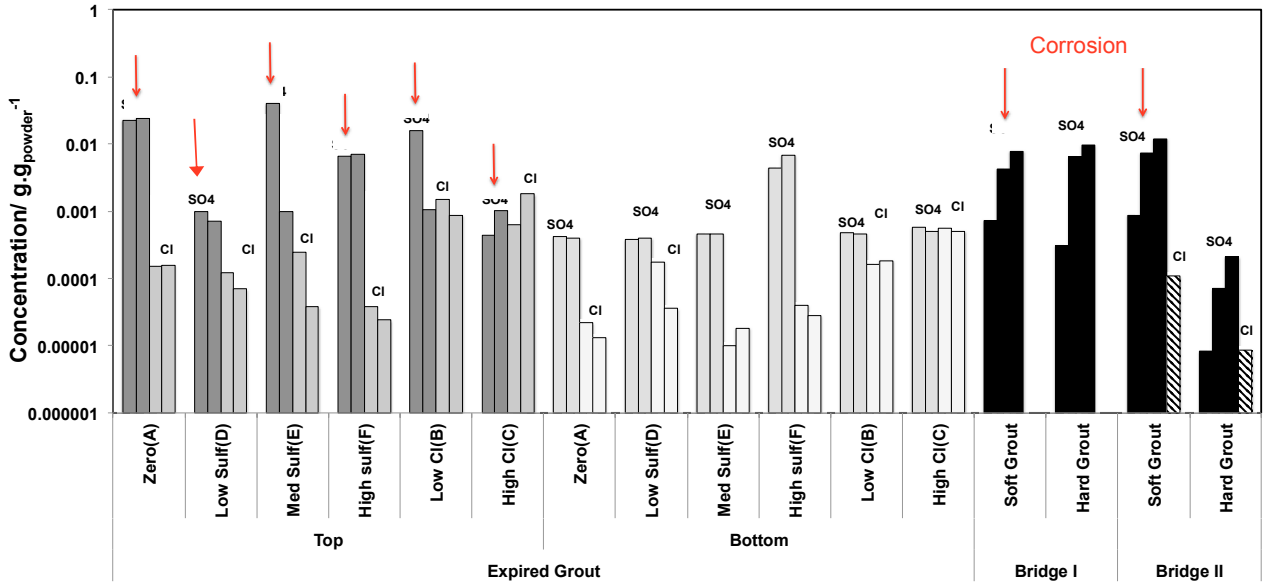

Figure 7.23. Sulfate and free chloride concentration in grout from MIT test samples. (Red arrows show where corrosion occurred)

7.5.2 INT Test Samples

For Grout B in the INT tests, there was no significant differentiation in sulfate content in the tee body and header when the grout was cast in the as-received condition but enhancement of sulfate in the tee header when cast with pre-exposed grout (Figure 7.24). Similar to MIT and field samples, sulfate accumulation in segregated grout occurred even with vestigial sulfate content. Despite the somewhat enhanced sulfate content in the deficient grout (up to 0.01 $g_{Sulfate}/g_{Powder}$), no corrosion was observed. Overall the low moisture content and dry macrovoids in these samples did not promote corrosion initiation.

Similarly, sulfate accumulation was low in the INT test samples with as-received Grout A (Figure 7.25a). However, in the pre-exposed condition, enhanced sulfate content was measured in the tee header. In test case AP3 (20,000 ppm sodium sulfate addition), severe corrosion developed in the presence of deficient grout material. As described earlier, corrosion

consistently developed in deficient grout that had enhanced sulfate content such as in cases AP3, AP7-8 and AP10-11 where the sulfate ion content was typically >0.01 $g_{Sulfate}/g_{Powder}$ (Figure 7.25). Testing in the MIT test showed similar values. In the combined presence of sulfates and chlorides, there is congruent effect to enhance corrosion development. This may cause enhanced corrosion rates or may be associated with changes in cement chemistry as described elsewhere (Pradhan, 2014; Maslehuddin and Paget.1997; Dehwah et al., 2002, 2003; Saleem et al., 1996; Al-Amoudi et al., 1993,1995;Holden et al., 1983; Yonezawa, 1989; Zuquan, et al 2007).

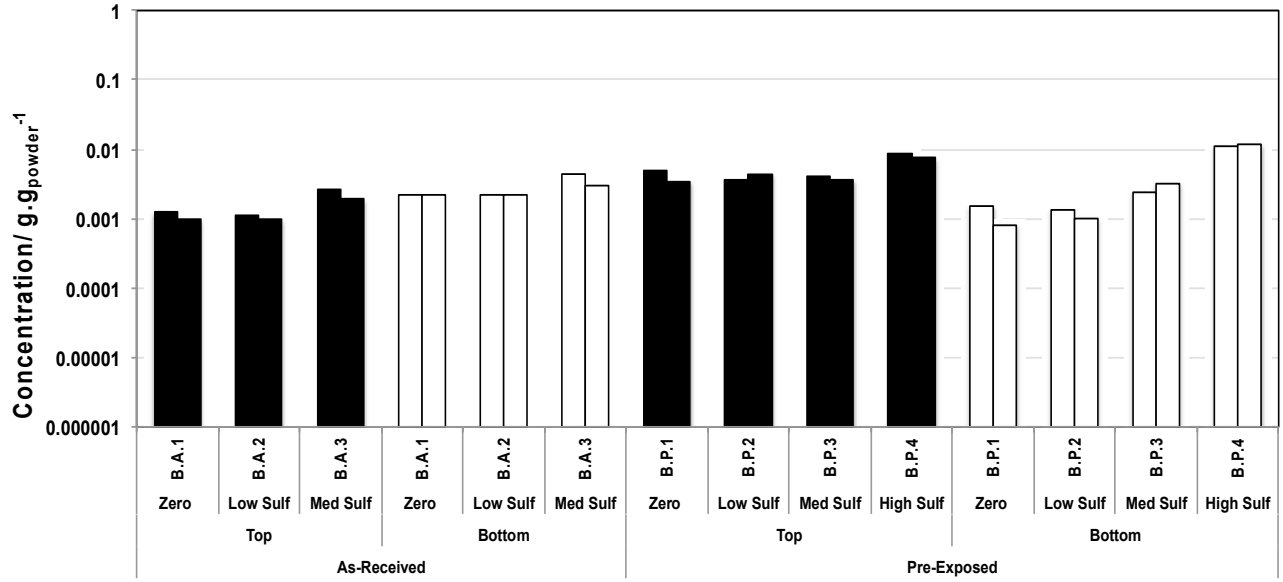

Figure 7.24. Sulfate concentration of grout from INT test samples cast with Grout B (Cases BA1-3, BP1-4).

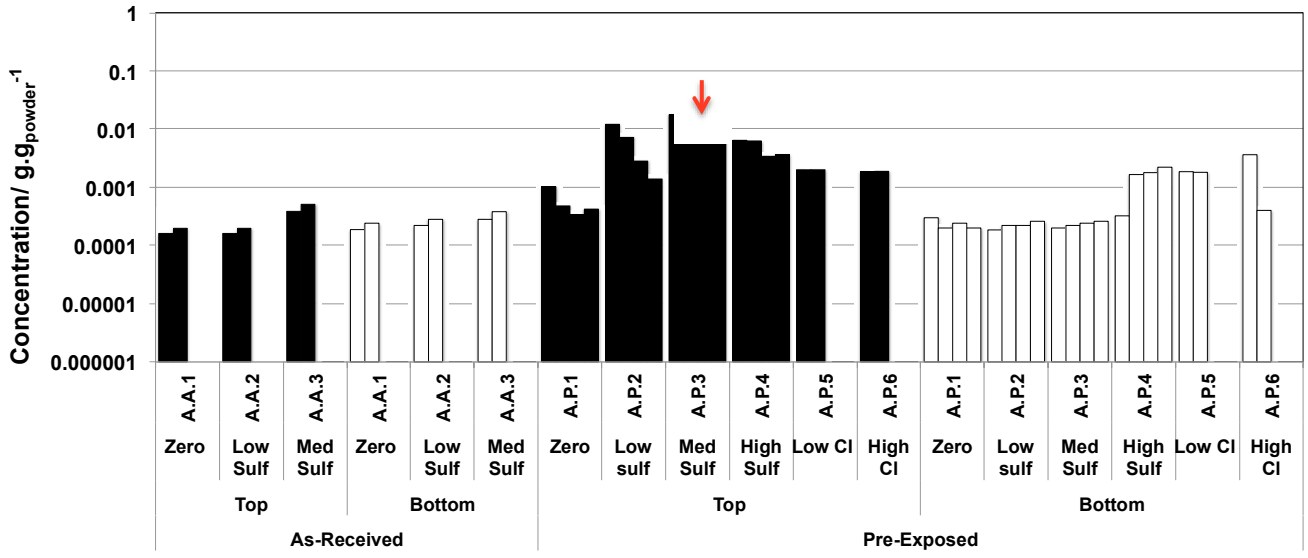

Figure 7.25a. Sulfate concentration of grout from INT test samples cast with Grout A (Cases AA1-3 and AP1-6). (Red arrow show where corrosion occurred)

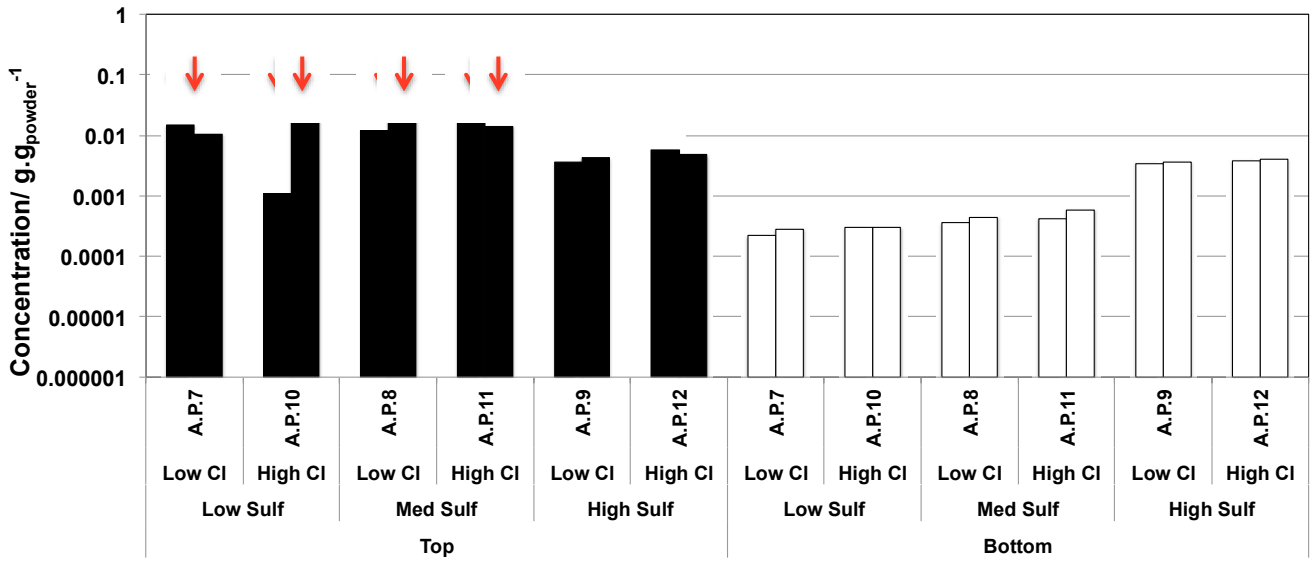

Figure 7.25b. Sulfate concentration of grout from INT test samples cast with Grout A. (Cases AP7-12). (Red arrows show where corrosion occurred)

7.6. CHLORIDE CONTENT

In order to assess the role of deficient grout on strand corrosion development, laboratory samples were created with excess water to enhance deficient grout materials and included enhanced sulfate (2000, 20,000, and 100,000 ppm) and enhanced chloride (low 0.08% and high 0.2% by mass cement) content. The segregated grout water chemistry including combinations of enhanced sulfate and chloride ion presence was thought to provide aggressive corrosion conditions. Generally as the chemical analysis showed, the chloride content in grout leachate was low in MIT and INT test samples where extra chlorides were not added to the grout mix (Figure 7.20-7.22). Of note, corrosion developed in MIT test samples initially cast with as little as 0.08% (by cement content) extra chlorides when in the presence of deficient grout that had accumulated by grout segregations. Additional chloride testing was made to elucidate the combined effect of chloride and sulfate ions in segregated grout.

The total chloride in the segregated grout layers was measured (Figures 7.26-7.29). On first inspection, it would appear that there was enrichment of total chloride content in the grout from pipe top section or the tee header, which would indicate ionic transport due to the grout segregation. Although this cannot be ruled out, the total chloride test preparation methods may over-sample the segregated grout due to uniform sample mass requirements and the inevitable moisture loss from initial conditions during sample preparation and therefore result in higher reported chloride concentrations. For chloride analysis a grout unit density of 3,105 lb/yd^3 was assumed (Lau et al., 2014), but this value is likely to be variable by the severity of grout segregation. With these uncertainties understood, the reported results should be considered qualitatively (values are given for comparison).

7.6.1 MIT Test Samples

Given the caveat described above, the results of total chloride content for MIT samples are shown in Figure 7.26. It is shown that even at relatively similar total chloride content in the pipe upper and lower elevations, corrosion developed only in the upper region where grout segregation was prevalent. As described earlier, these sections had higher sulfate content. It is not to be remised that the role of pH and cement content (described later) are also important for corrosion initiation process.

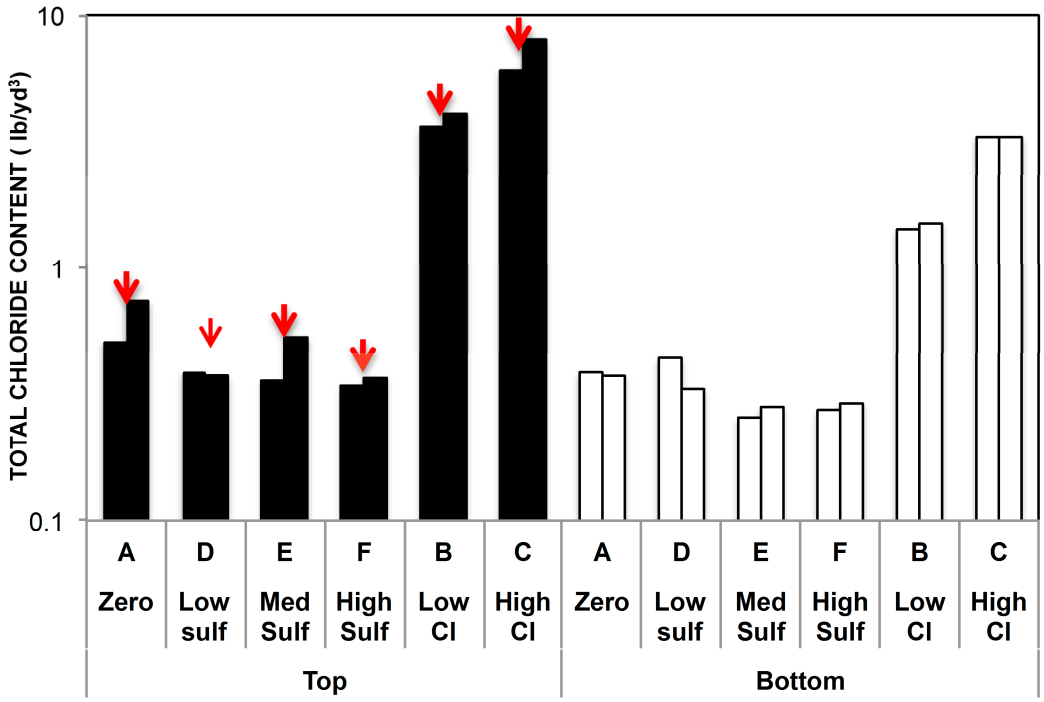

Figure 7.26. Total chloride content in grout from MIT test samples
(Red arrows show case where corrosion occurred)

7.6.2 INT Test Samples

With the earlier caveat in mind, there was differentiation in chloride content in the tee body and header for grouts A and B cast in the as-received and pre-exposed condition (Figures 7.27-7.29). At the total vestigial chloride levels present, no corrosion was observed in any of the Grout B samples or the tested Grout A samples in the as-received condition. No corrosion developed in pre-exposed Grout A with chloride additions up to 0.2% (Cases AP5-6) even though the total chloride content in the tee header may have been enhanced. In test cases AP5-6, the grout in the tee header and body had enhanced chloride (0.06 to 0.12% by total grout mass in header and 0.03 to 0.1% by total grout mass in body). However, severe corrosion condition was observed for pre-exposed Grout A in presence of the chloride additions for the cases with 2,000 and 20,000 ppm sodium sulfate additions (Cases AP7-8 and AP10-11). In test cases AP7-8 and AP10-11, similar chloride levels were present (0.03 to 0.18% by total grout mass in header). It is noted that corrosion did not develop in the tee body

even though there was enhanced chloride content there as well (0.03 to 0.09% by total grout mass in body). The enhanced sulfate additions apparently had effect in the corrosion development and would indicate adverse effects of combined low level chlorides and sulfate presence. It was reported in the literature that the presence of sulfate ion may reduce the chloride binding capacity of cement and release the chloride ion into pore solution(Dehwah et al., 2002,2003).The finding would also suggest that assessment of corrosion susceptibility of deficient grout by chloride content alone would not be sufficient.

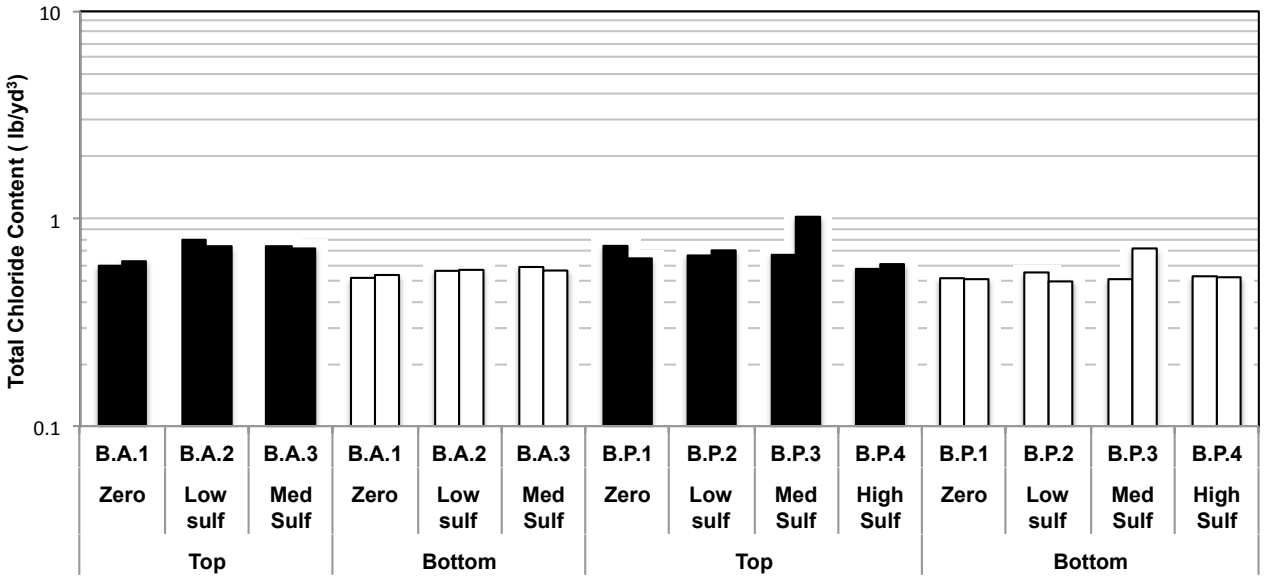

Figure 7.27. Total chloride content of grout from INT test samples cast with Grout B (Cases BA1-3, BP1-4).

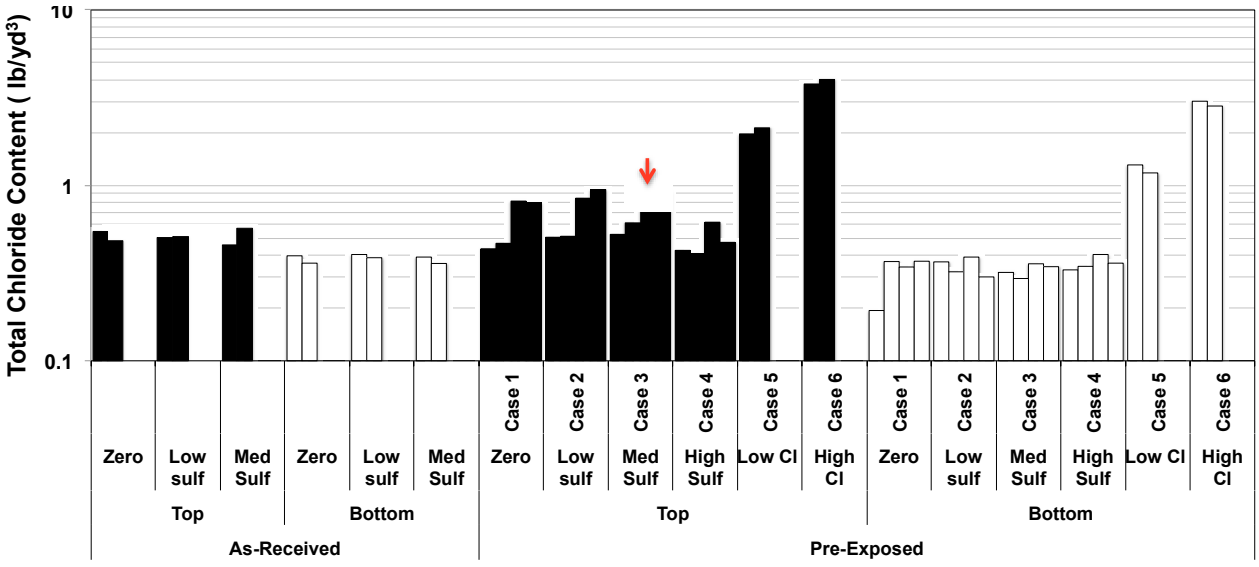

Figure 7.28. Total chloride content of grout from INT test samples cast with Grout A (Cases AA1-3 and AP1-6). (Red arrow show where corrosion occurred)

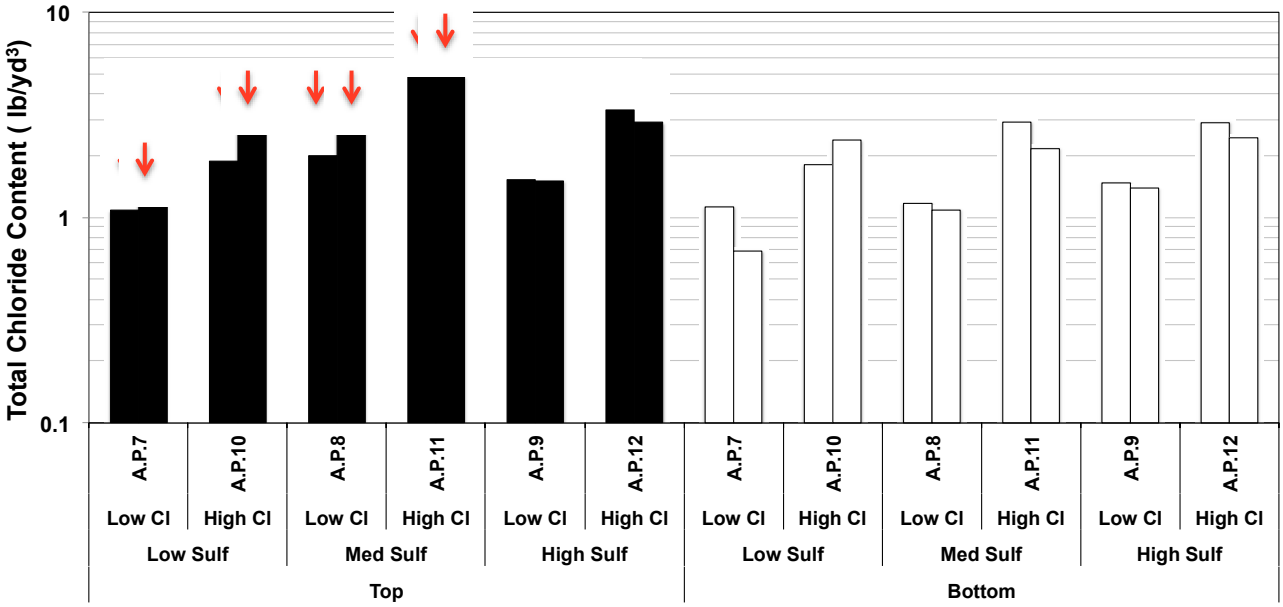

Figure 7.29. Total chloride content in grout from INT test cast with Grout A. (Cases AP7-12).
(Red arrows show where corrosion occurred)

7.7. PH RESULTS

7.7.1 MIT Test Samples

The results of pH measurements on extracted gout fragments using a pH color indicator and well as pH measurements from grout leachate are shown in Figures 7.30-7.31. The pH indicator showed a purple color indicative of pH 12 for all MIT test cases. The leachate typically had values between 12 and 13 for all samples except for segregated grout from Case A where the pH was low (pH<11).

7.7.2 INT Test Samples

The results of pH measurements on extracted grout fragments from the INT test tee body and header are shown in Figures 7.32-7.35. The freshly fractured surface of all samples showed a purple color after application of the pH indicator indicating pH12. The deficient grout typically had a lighter color tone whereas the purple coloration was dark for the hardened grout samples. Figures 7.36-7.38 shows the pH of the grout leachate. For Grout B, the pH was typically 12-13 for all test conditions. For Grout A, the leachate pH from samples cast with as-received grout was greater than 12 for all conditions. The leachate pH from hardened gout samples cast from pre-exposed grout also was greater than 12. The leachate from segregated grout cast with pre-exposed grout sometimes showed pH<12, notably samples AP3, AP7-8, and AP10-11. As detailed later, these samples all had severe steel corrosion. It could not be determined if the pH caused the observed corrosion but the measured pH may in part be due

to local acidification from the corrosion. Furthermore, segregated grout had shown to have aggregation of silica fume and its hydration may in part contribute to the consumption of hydroxyl ions. It is recalled that the freshly fractured surfaces of these samples showed pH 12 with the pH color indicator. Close-up pictures of the segregated grout fragments are shown in Figures 7.35. Also other segregated pre-exposed grout leachates where the steel did not corrode showed pH>12 (AP1-2,4-6,9,12). Mindess, 2003 stated that If the pH drop below 11.5, the passive iron oxide layer is destroyed and causing the normal, porous oxide layer (rust) to form during corrosion. This critical drop in pH by carbonation occurs when first the alkalis and the calcium hydroxide are converted to carbonate. Broomfield, 2000 and S.K. Lee, 2014 reported that the extent of carbonation may not be critical if the pH of the grout was above 10.0. All leachate pH values were above 11.5. Nevertheless, the sometimes depressed pH values in the INT samples with segregated grout in conjunction with enhanced chloride and sulfate levels, and lower cement content would exacerbate corrosion development.

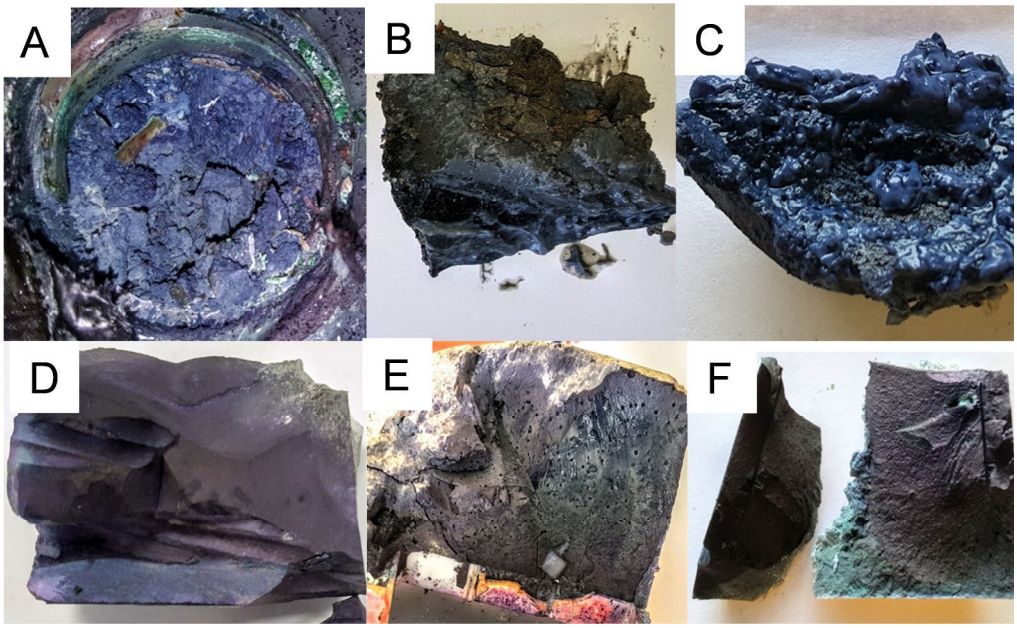

Figure 7.30. Photos of pH results for MIT test (Case A,B,C, D,E,F).

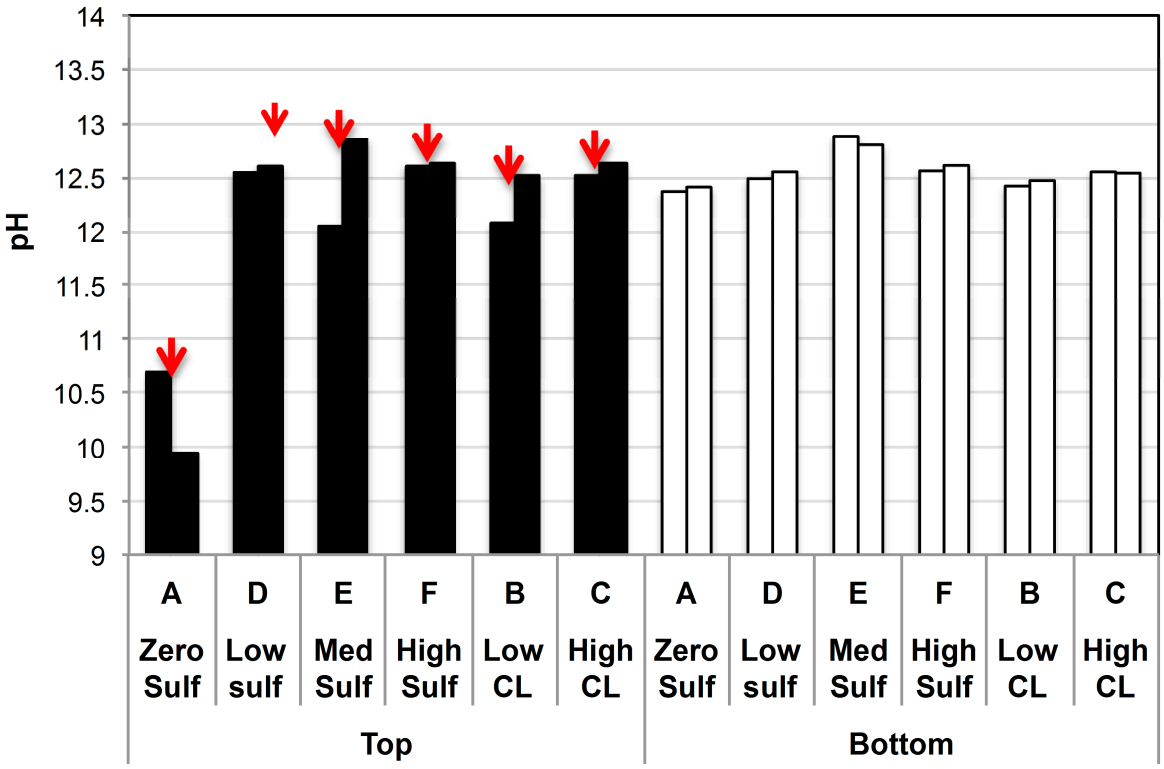

Figure 7.31. MIT test grout leachate pH.
(Red arrows show case where corrosion occurred)

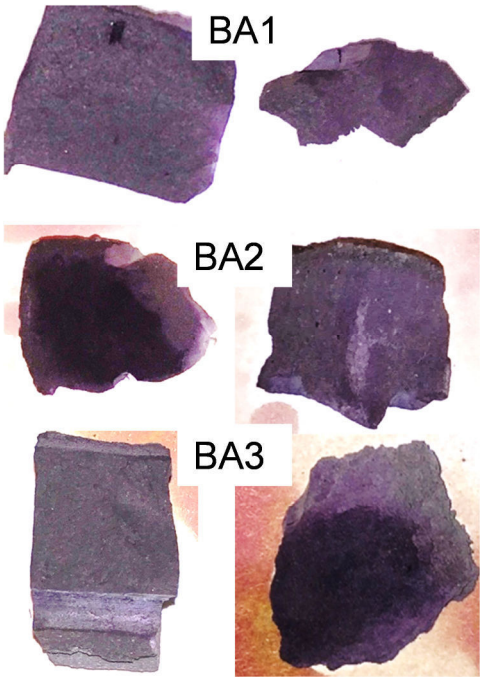

Figure 7.32. pH color indicator on fractured INT test grout surface
(Case BA1-3) Left (Tee Body). Right (Tee Header).

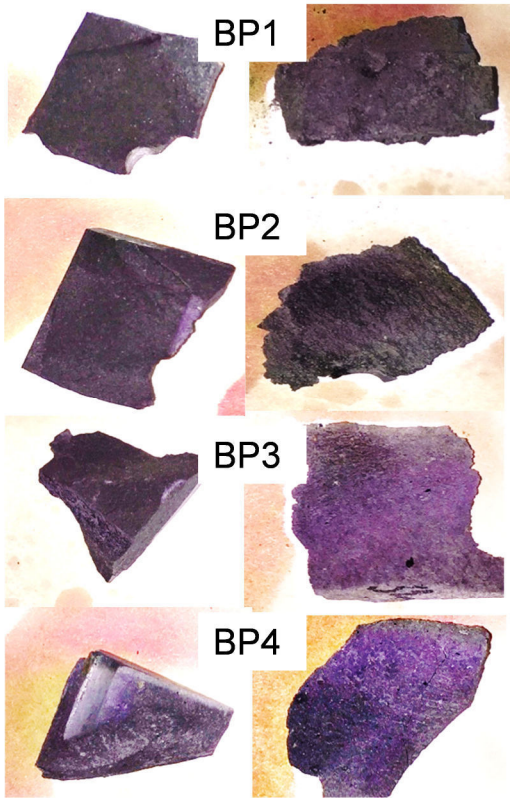

Figure 7.33. pH color indicator on fractured INT test grout surface (Case B.P.1-4)
Left (Tee Body). Right (Tee Header).

Figure 7.34. pH Color indicator on fractured INT test grout surface (Case A.A.1-3).
Left (Tee Body). Right (Tee Header).

Figure 7.35. pH color indicator on fractured INT test grout surface. (Case A.P.1-6).
Left (Tee Body). Right (Tee Header).

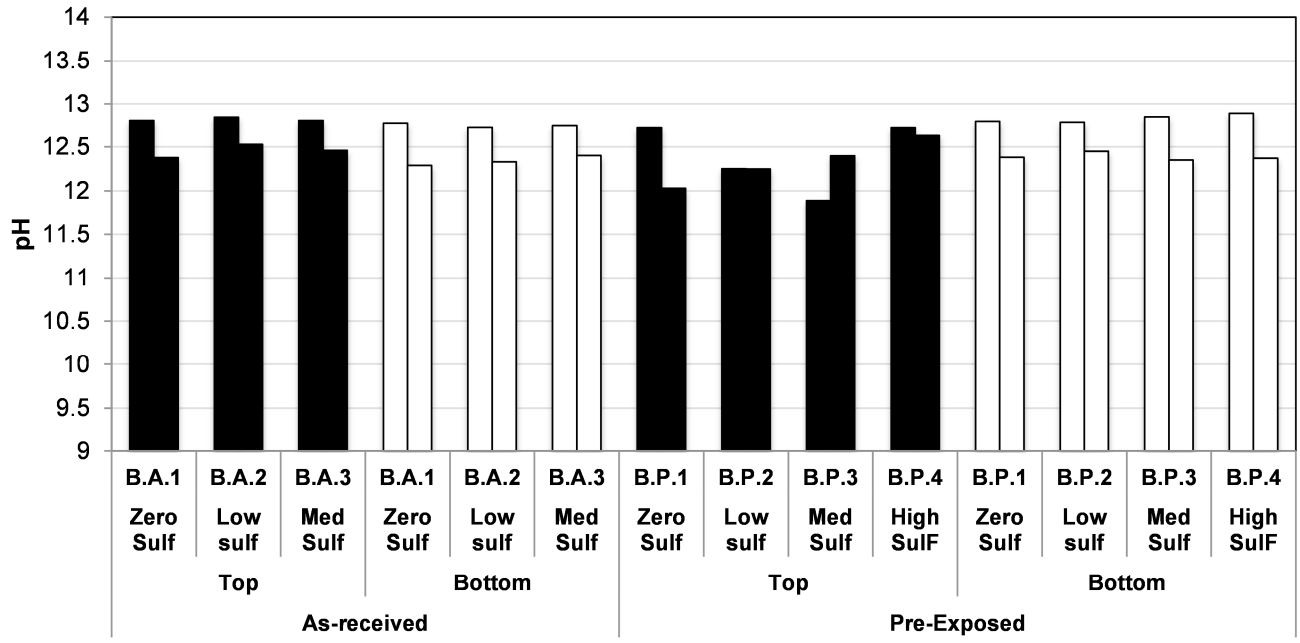

Figure 7.36. INT test Grout B leachate pH.
(Cases BA1-3, BP1-4)

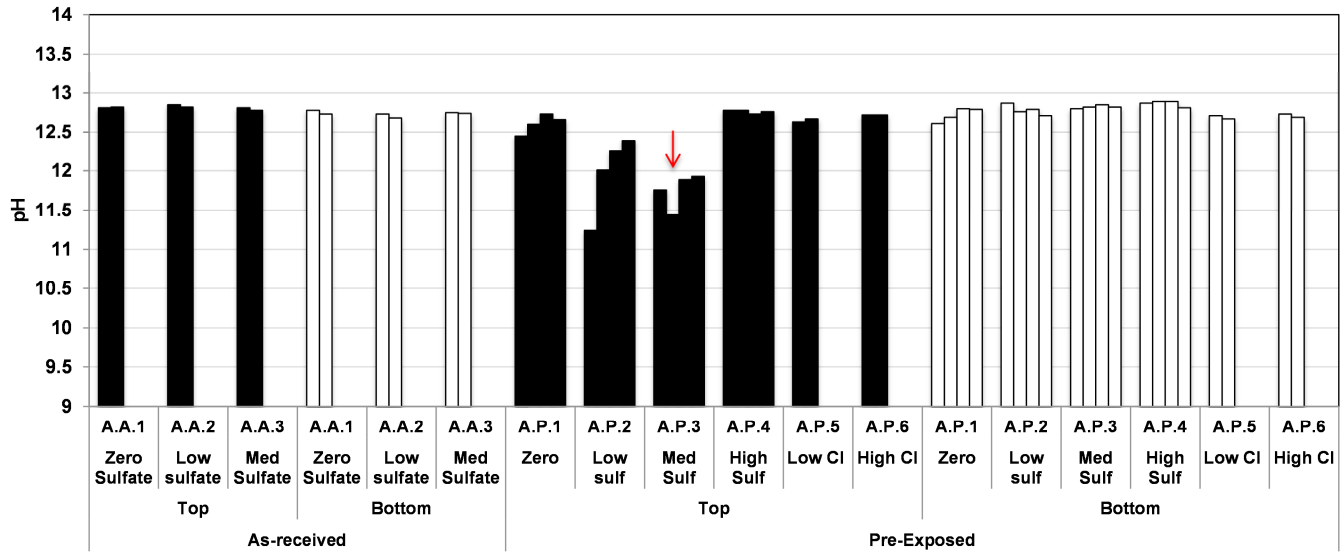

Figure 7.37. INT test Grout A leachate pH.
(Cases AA1-3 and AP1-6).
(Red arrow show where corrosion occurred)

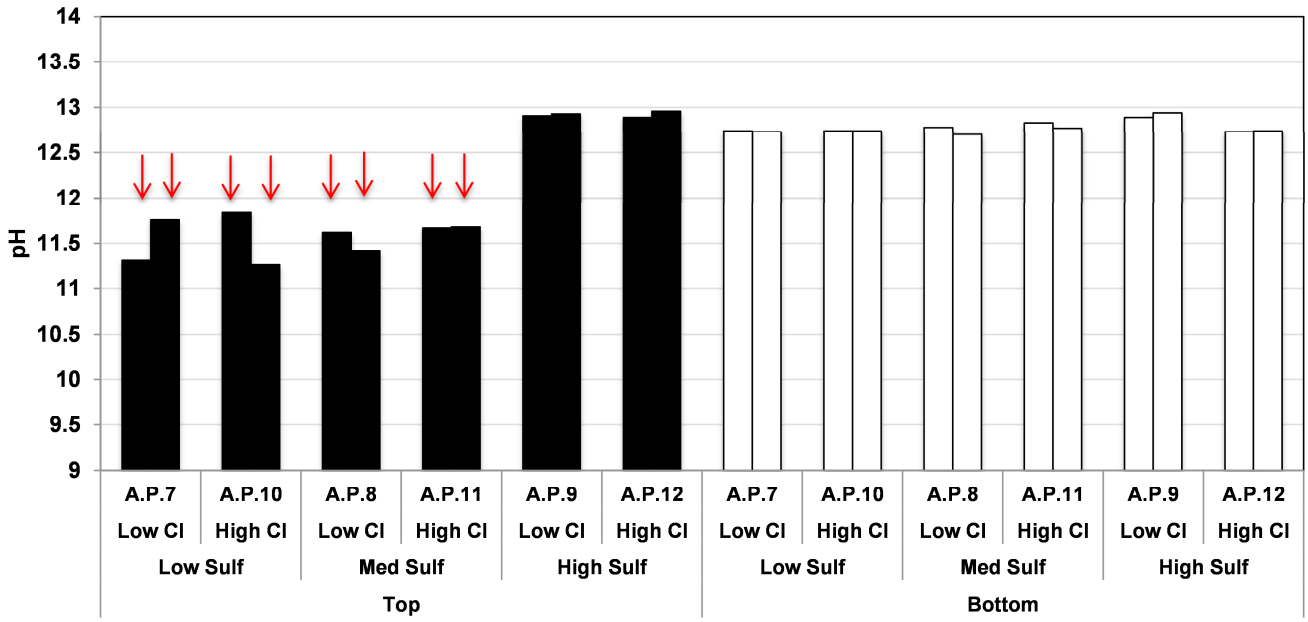

Figure 7.38. INT test Grout A leachate pH
(Cases AP7-12).
(Red arrows show where corrosion occurred)

8. CORROSION CHARACTERISTICS

8.1 MIT TEST SAMPLES

Figure 8.1 shows photos of the embedded 7-wire strand placed along the length of each MIT sample. Severe corrosion was typically observed on the section of strand in contact with segregated grout at the upper elevations of the pipe. The same strand in each sample did not exhibit corrosion development when embedded in hardened grout. The corrosion probes placed along the length of each sample are shown in Figures 8.2-8.3. The right hand side of each probe had been extended outside of the sample. The discoloration of the steel there was due to exposure to ambient lab atmosphere. The left hand portion of each probe was embedded in the grouted tendon. The corrosion product observed there was consistent to the measured corrosion where the active corrosion mostly occurred on sensors embedded in the upper elevations of the tendon where grout segregation was prevalent. For the steel probes simulating crevice conditions, localized discoloration under where the rubber gasket was placed was evident for all samples.

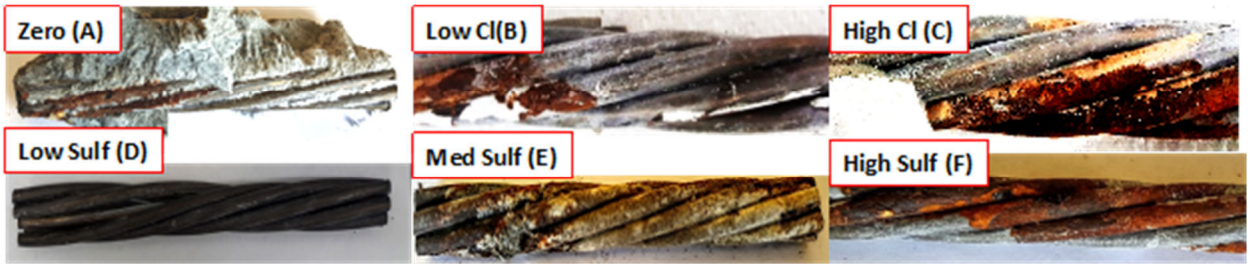

Figure 8.1a. Photos of embedded strands in MIT samples (Upper Elevation).

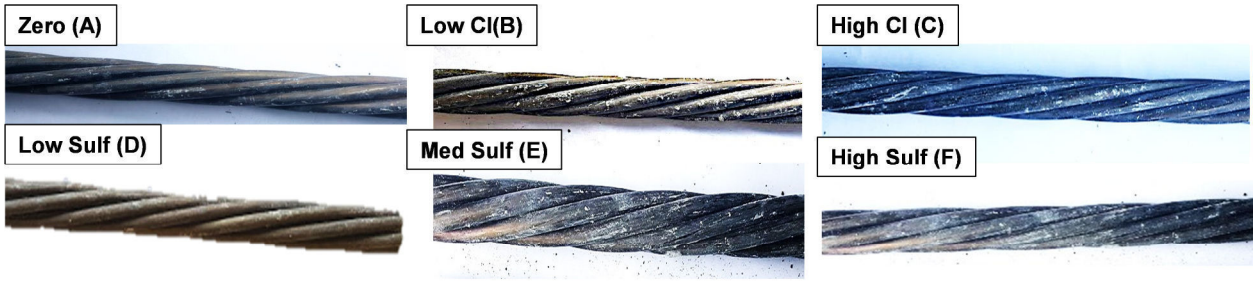

Figure 8.1b. Photos of embedded strands in MIT samples (Lower Elevation).

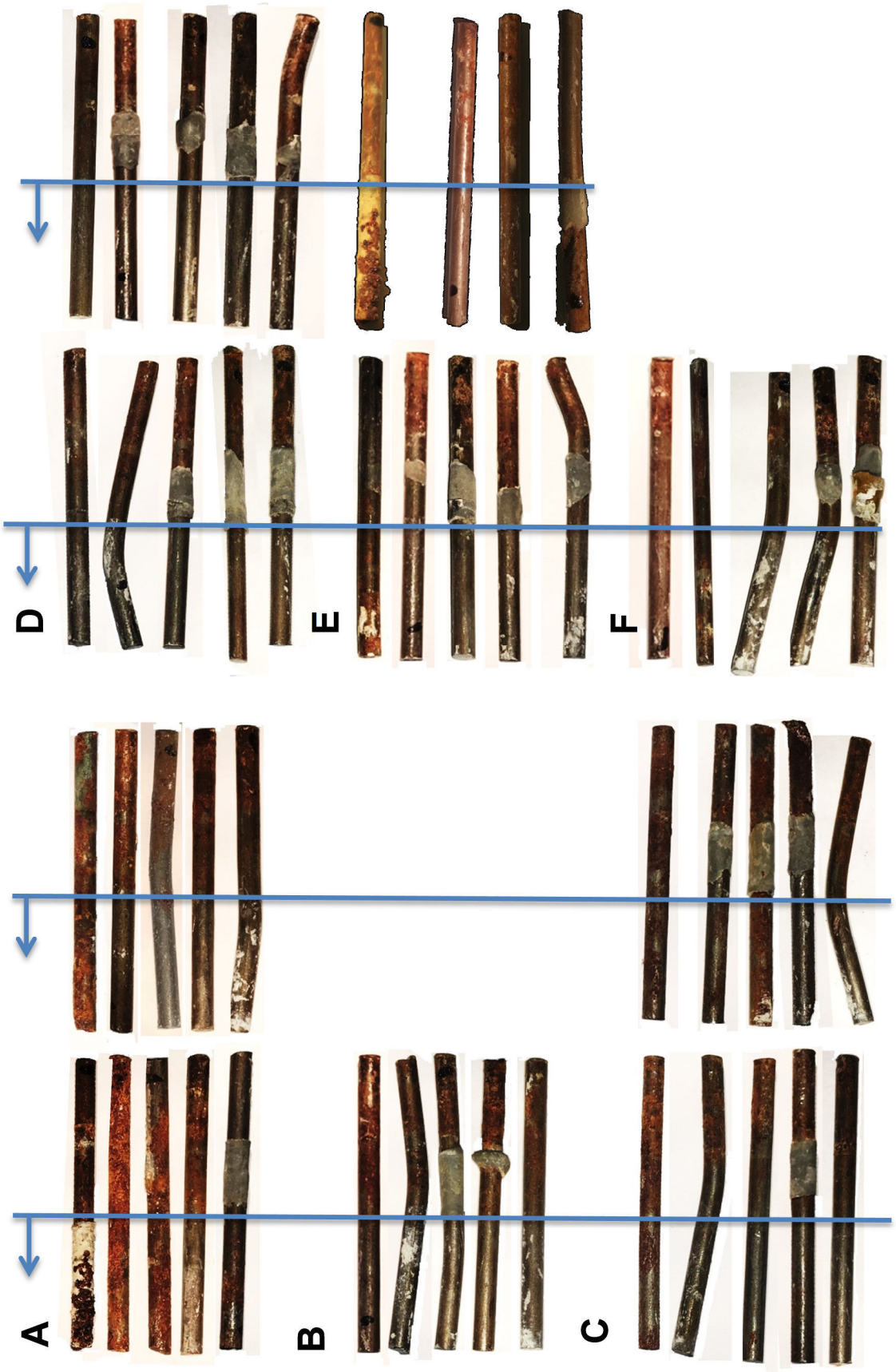

Figure 8.2. Photos of corrosion steel probes in MIT test.

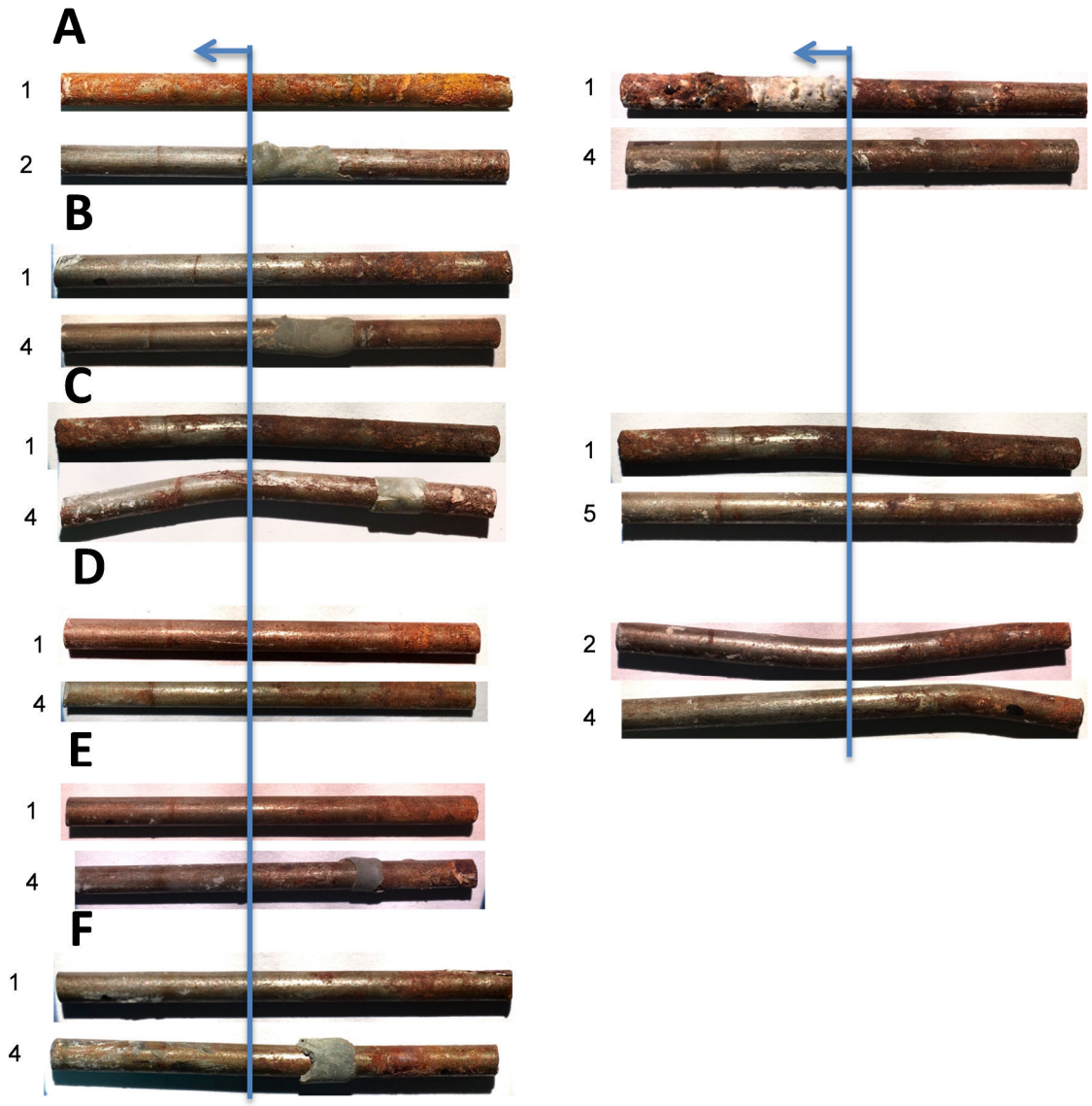

Figure 8.3. Photos of corrosion steel probes in MIT test (crevice condition).

X-Ray Diffraction was conducted on corrosion product removed from the embedded strand from test case A and E. Insufficient material was available from the test probes. Corrosion product from strand from the Ringling Bridge and from the electrodes from the solution testing was also testing for comparison.

The testing was conducted by using Diffraktometer D5000 along with data acquisition Diffrac Plus software. The rust product was collected by scribing from the tested samples in the form of powder. Approximately 3 grams of samples were sprinkled on an adhesive tape that was staged on a plastic holder to reduce the background noise. The testing procedure included diffraction scan with 2θ from 10 to 60 degrees with a 2 deg/minute scan rate. Peak normalization, subtraction of the background and integration was performed with Origin Lab 7.5 software. The data base PDF 4 was used for crystalline material identification.

The test results did not show strongly-defined diffraction peaks and the relative intensity of the peaks did not scale significantly above background noise. Nevertheless, the rust product was identified as goethite. Calcium carbonate, presumably from grout residue, was detected for the three grout test samples. There were indications that sulfur-bearing iron corrosion products were present but its presence did not appear to be very strong.

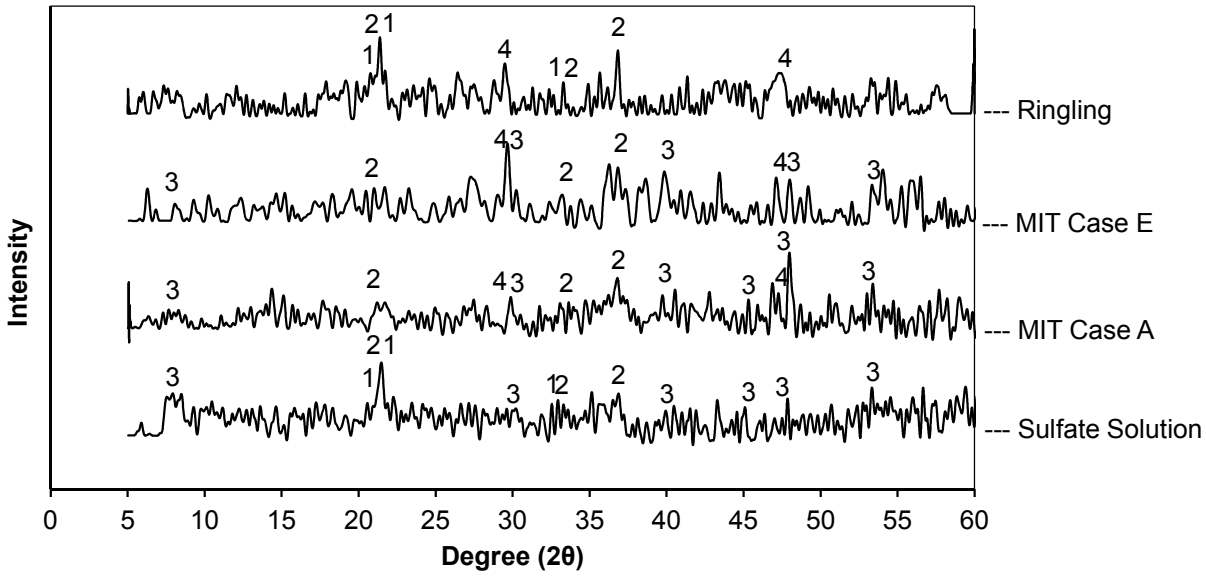

1 $Fe_2(SO_3)_2(H_2O)_5$ Iron Sulfite Hydrate
2 FeO(OH) Iron Oxide Hydroxide Goethite
3 Fe_9S_{11} Iron Sulfide
4 $Ca(CO_3)$ Calcium Carbonate

Figure 8.4. XRD diffractograms of corrosion product.

8.2 INT TEST SAMPLES

Figures 8.5-8.6 show the steel probes placed in INT samples cast with Grout B in the as-received and pre-exposed condition. No corrosion was observed on any of the tested samples. Likewise, no corrosion was observed on the steel probes in INT samples cast with as-received Grout A (Figure 8.7). As mentioned before and shown in Figure 8.8, significant corrosion developed on some of the pre-exposed Grout A samples: AP3, 7-8, and 10-11. A magnified picture of the corrosion on sample AP3 in Figure 8.9 and close-up pictures of the corrosion on samples AP7-8,10-11 in Figure 8.10 show that local corrosion pits developed on the wire surface.

XRD analysis was not conducted for INT tests due to insufficient quantity of recovered corrosion products. SEM images and EDS elemental maps for sample AP3 and AP11 are shown in Figures 8.11-8.16. Figures 8.12-8.13 show an area with mixed rust and residual grout material. Figures 8.14-8.15 show a corrosion spot with much of the grout removed. Analysis showed the corrosion product contained iron and oxygen without clear association with sulfur-bearing species or chloride in its composition. For the two locations on AP11 where analysis was made, the EDS analysis made on spots on rust (point 1 for both locations), the atomic and

weight percentages of iron and oxygen was not inconsistent with goethite as identified for MIT samples by XRD.

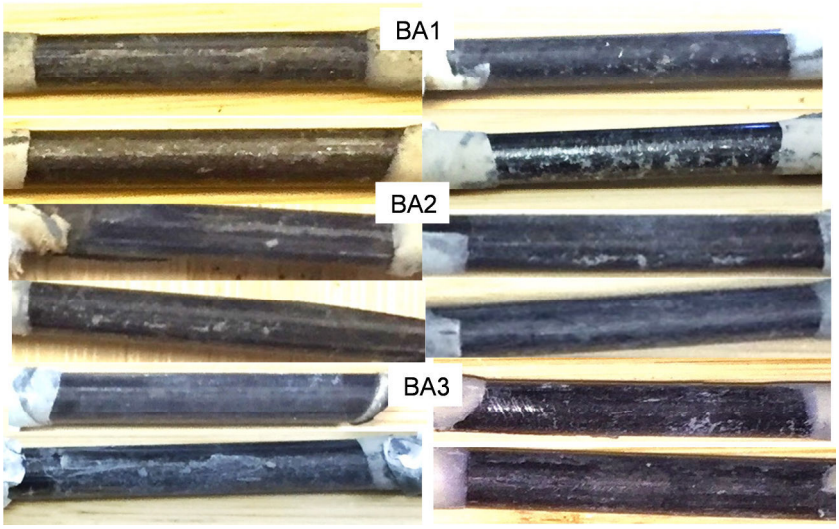

Figure 8.5. Photos of steel wire from INT samples (Cases BA1-3).

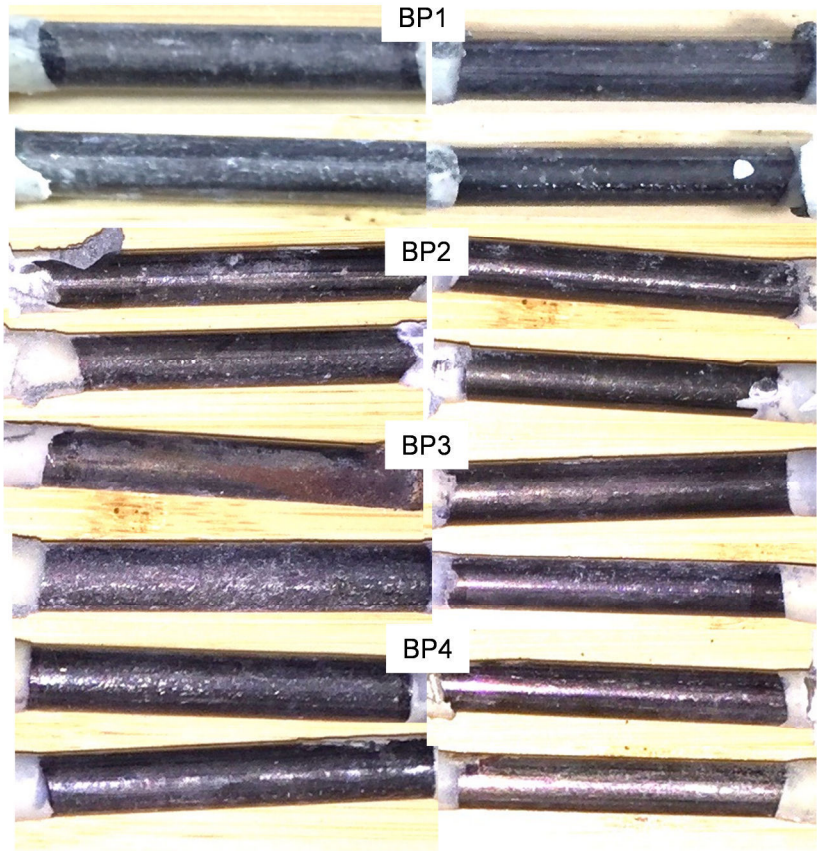

Figure 8.6. Photos of steel wire from INT samples (Cases BP1-4).

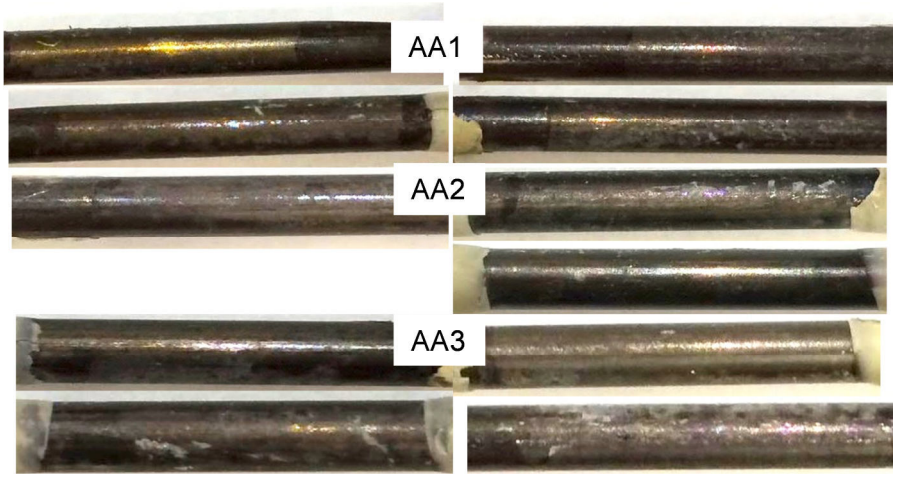

Figure 8.7. Photos of steel wire from INT samples (Cases AA1-3).

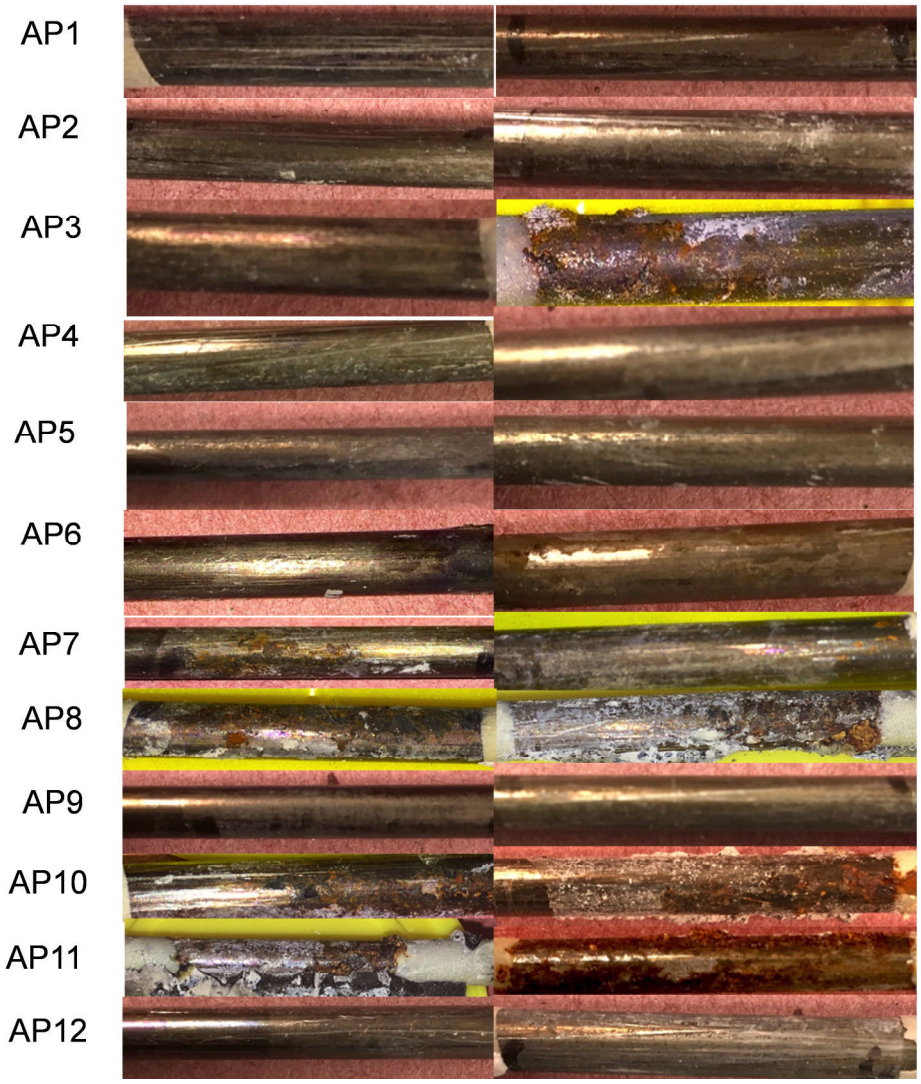

Figure 8.8. Photos of steel wire from INT samples (Cases AP1-12).

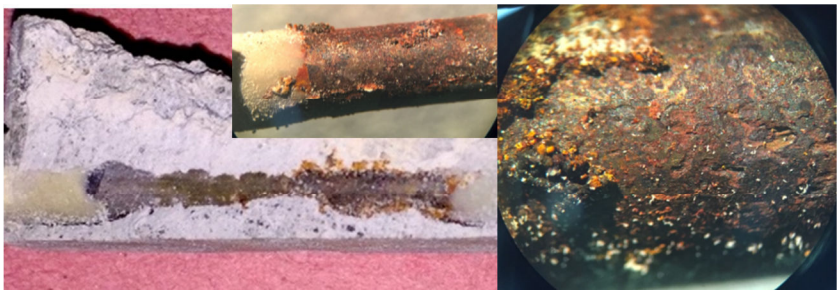

Figure 8.9. Close-up photos of corroded wire in segregated part of INT test samples (Case AP3).

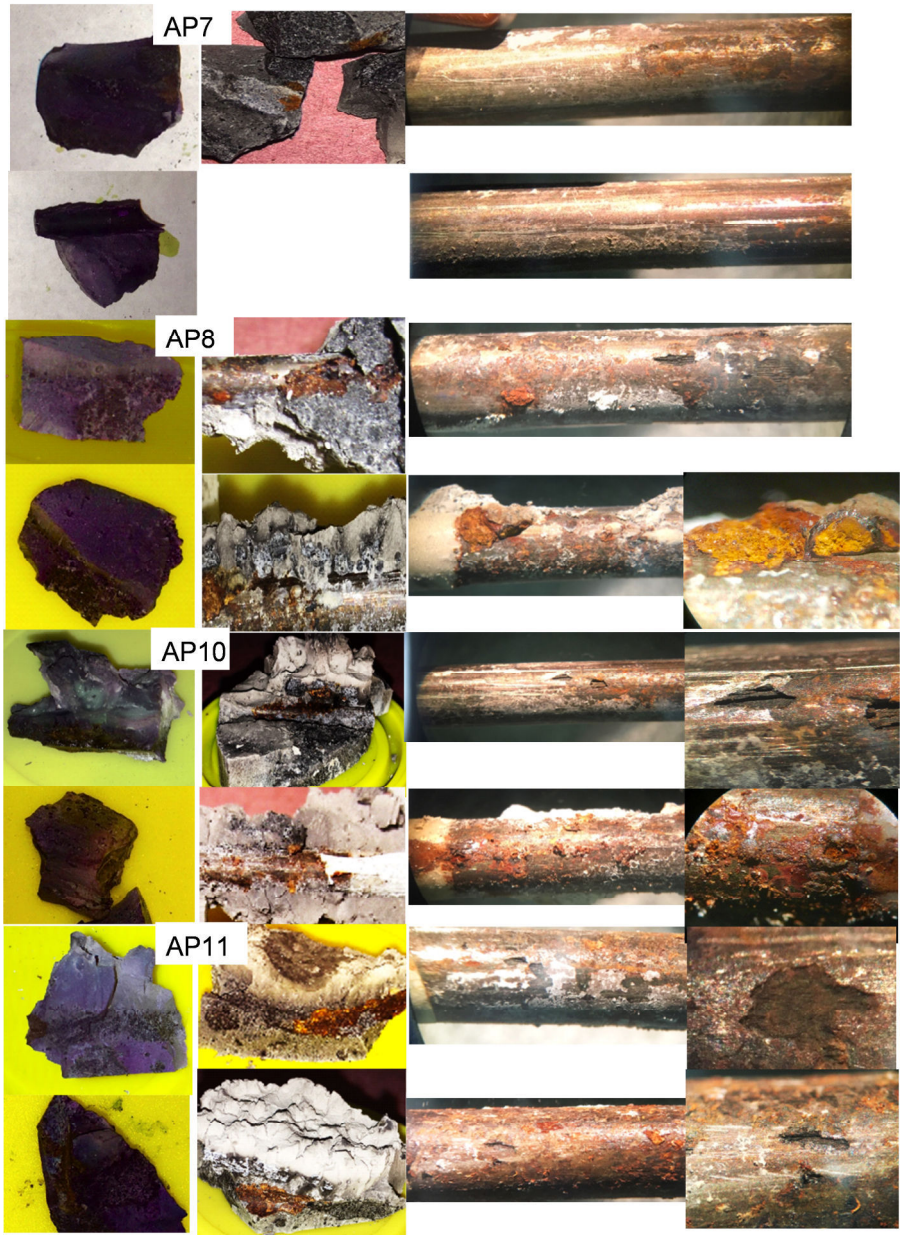

Figure 8.10. Close-up photos of corroded wire in segregated part of INT test samples (Case AP7-8,10-11).

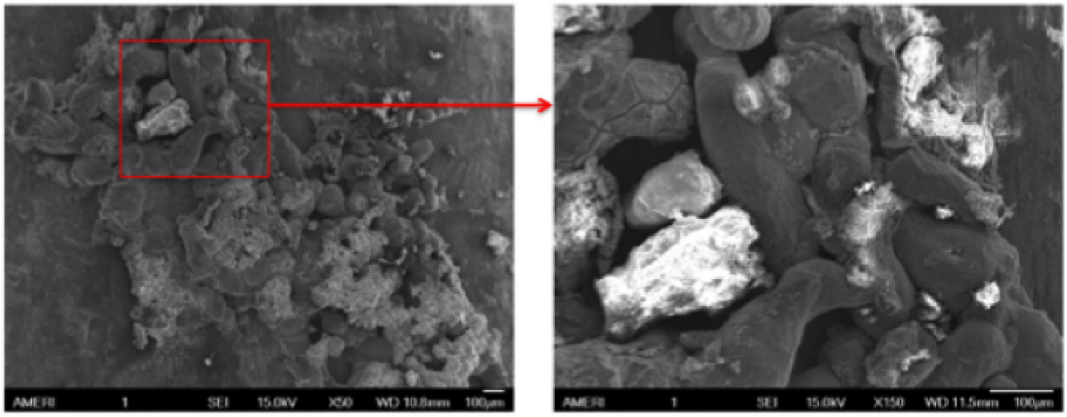

Figure 8.11. SEM micrograph for case AP3

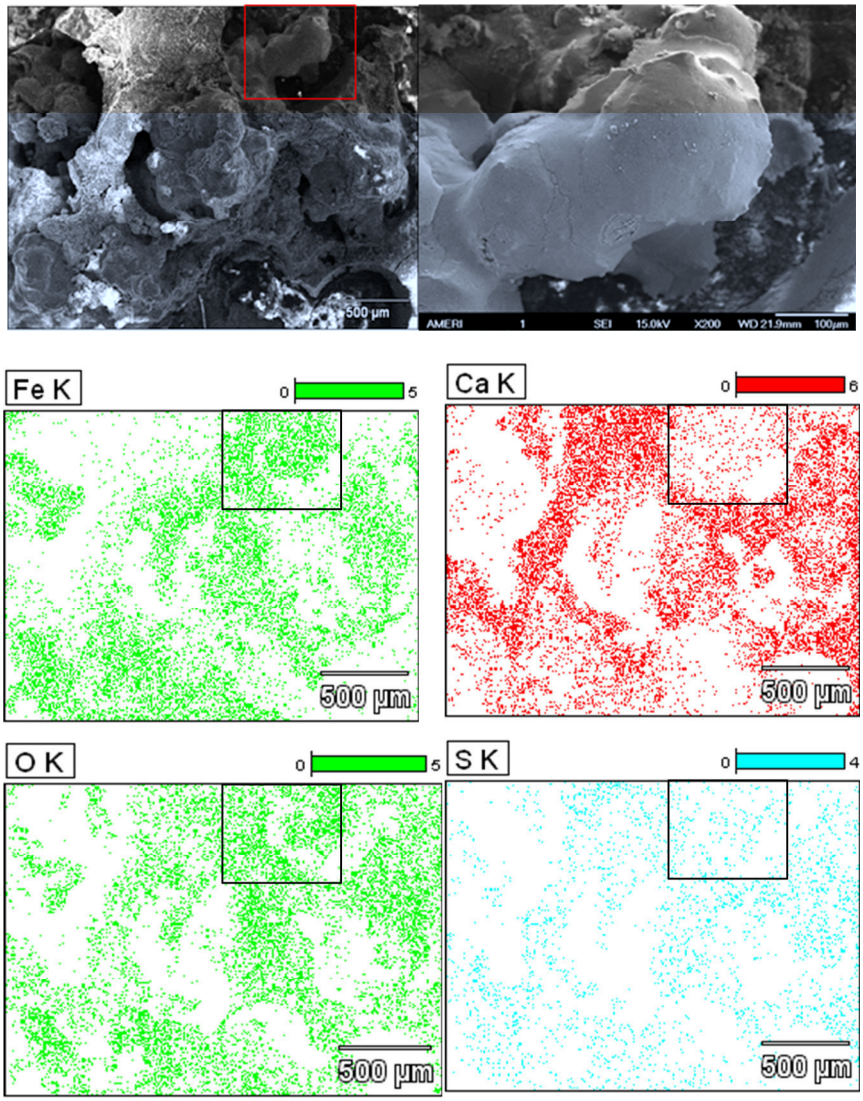

Figure 8.12. SEM micrograph and EDS elemental maps of corrosion product (Case AP11).

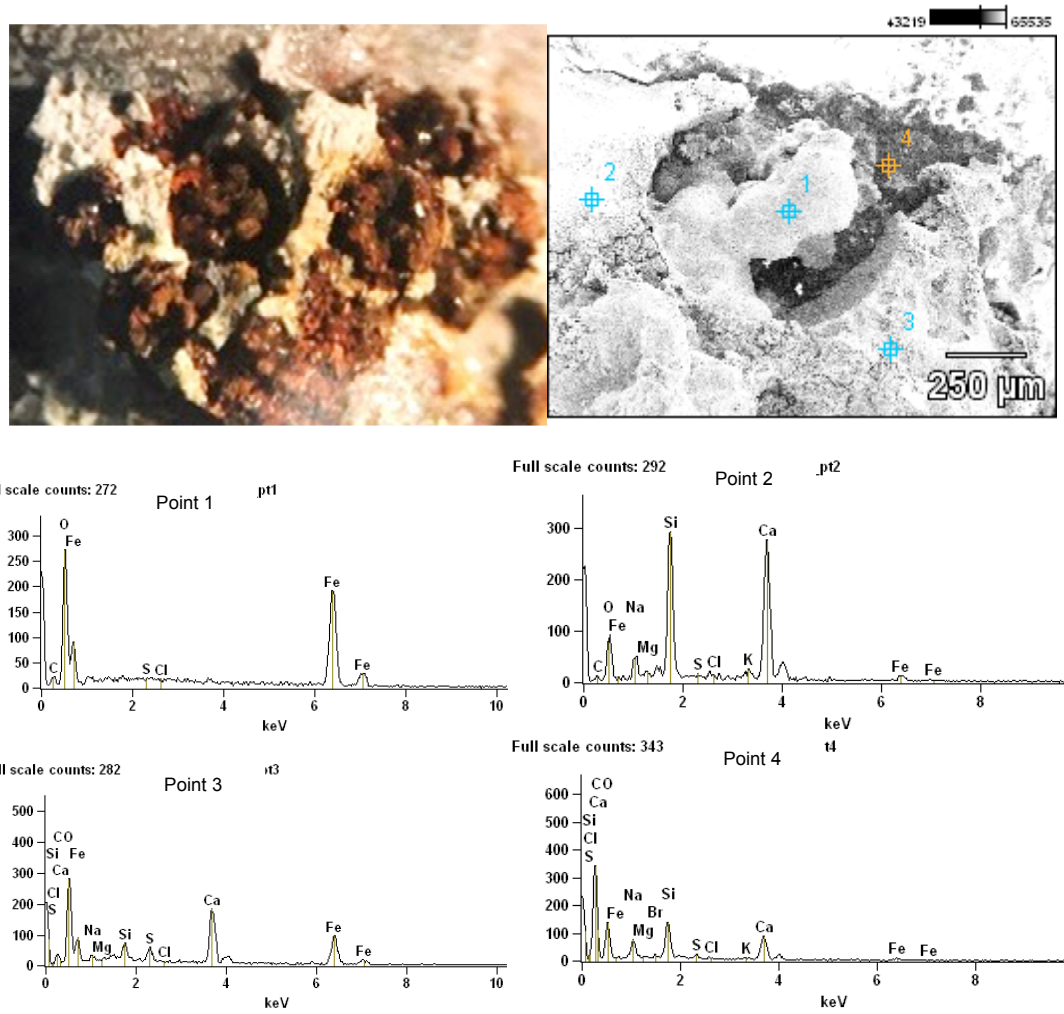

Atom%	Fe-K	O-K	C-K	S-K	Cl-K	Ca-K	Na-K	K-K	Mg-K	Si-K	Br-L
Point 1	27.84	45.88	26.28								
Point 2	1.59	44.65	18.67	0.32	0.12	17.76	3.87	0.62	0.62	11.79	
Point 3	9.43	52.84	26.00	1.36	0.02	7.78	1.22		0.01	1.34	
Point 4	0.32	18.08	79.92	0.15	0.08	1.67	1.20	0.07	0.02	1.39	0.08

Weight%	Fe-K	O-K	C-K	S-K	Cl-K	Ca-K	Na-K	K-K	Mg-K	Si-K	Br-L
Point 1	59.70	28.18	12.12								
Point 2	4.02	32.28	10.13	0.46	0.19	32.16	4.02	1.09	0.69	14.97	
Point 3	25.01	40.13	14.28	2.07	0.04	14.80	1.33		0.01	1.78	
Point 4	1.28	20.94	66.85	0.36	0.20	4.86	2.00	0.20	0.04	2.83	0.44

Figure 8.13. SEM micrograph and EDS elemental spot analysis of corrosion product (Case AP11).

Point 1: Corrosion, Point 2 and 3 Surface with Grout Residue, Point 4 Sample Surface.

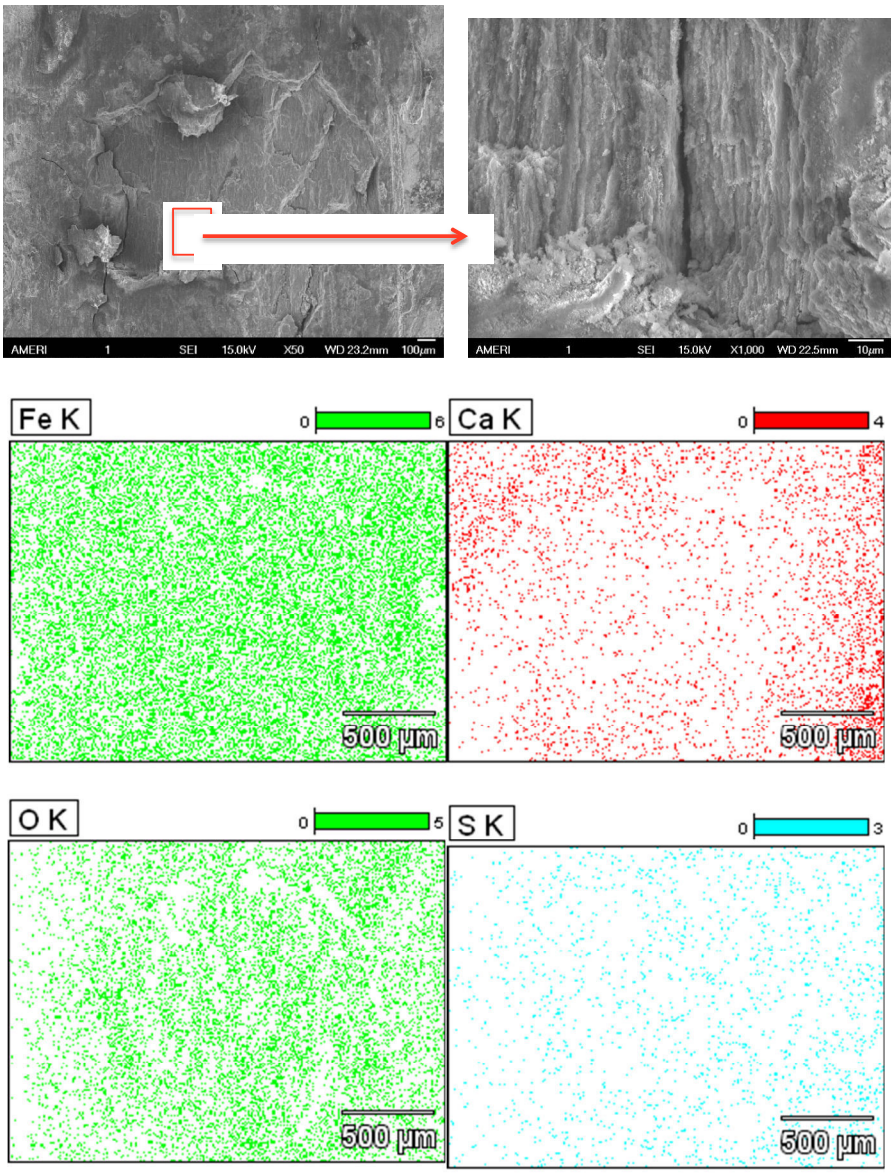

Figure 8.14. SEM micrograph and EDS elemental maps on corroded wire surface (Case AP11).

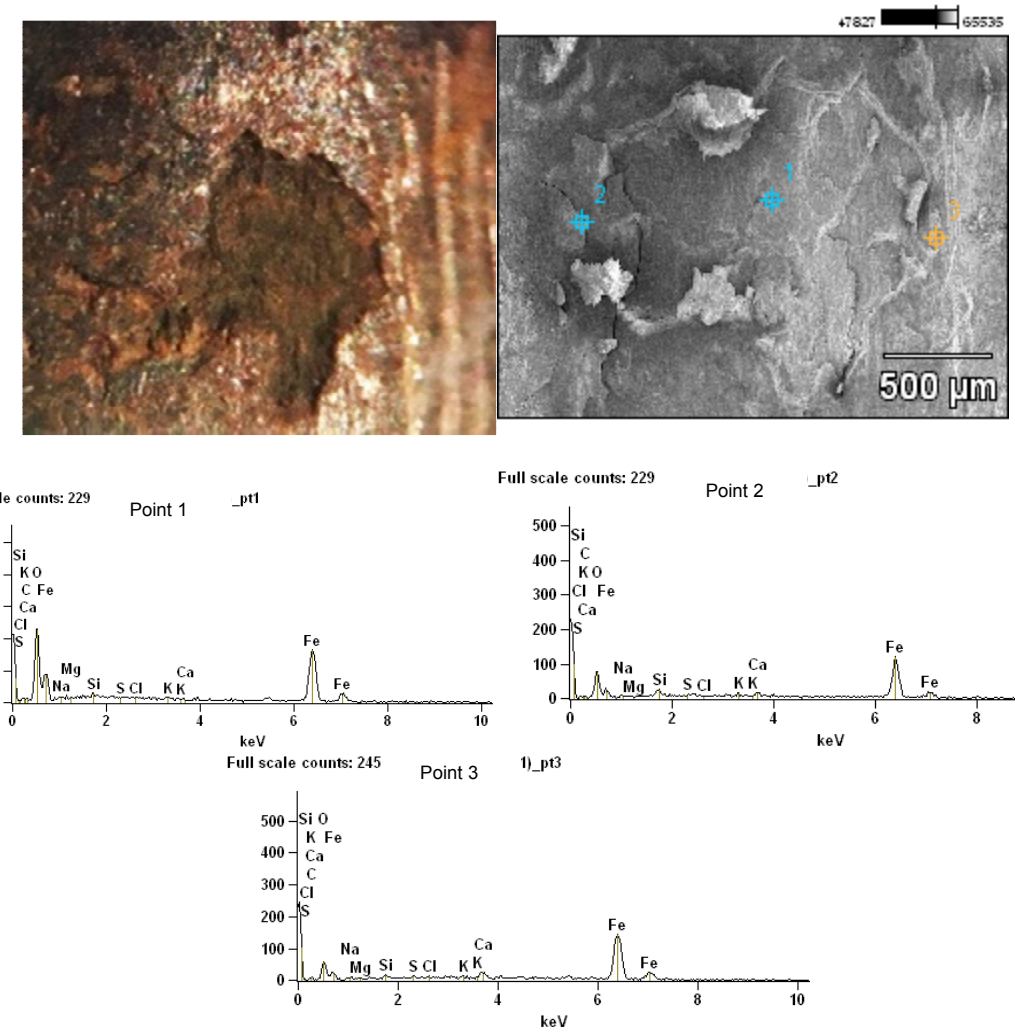

Atom%	Fe-K	O-K	C-K	S-K	Cl-K	Ca-K	Na-K	K-K	Mg-K	Si-K	Br-L
Point 1	32.24	49.14	16.62	0.12		0.12	0.92	0.24		0.61	
Point 2	40.21	35.23	18.33	0.41	0.03	1.26	2.26	0.35		1.92	
Point 3	49.43	22.82	22.29	0.16	0.31	2.34	1.39	0.32	0.08	0.87	

Weight%	Fe-K	O-K	C-K	S-K	Cl-K	Ca-K	Na-K	K-K	Mg-K	Si-K	Br-L
Point 1	63.35	27.66	7.02	0.13		0.16	0.74	0.33		0.60	
Point 2	69.88	17.54	6.85	0.40	0.04	1.57	1.62	0.43		1.68	
Point 3	77.24	10.21	7.49	0.14	0.31	2.63	0.89	0.35	0.05	0.68	

Figure 8.15. SEM micrograph and EDS elemental spot analysis of corroded surface (Case AP11).

Points 1-3: Corroded Surface

9. RISK ASSESSMENT CRITERIA

Changes in pore water chemistry can affect the initiation of steel corrosion in the presence of sulfate ions. Earlier electrochemical testing showed possibility for corrosion initiation of steel in sulfate solutions in pH 12.6 but could not initiate corrosion in pH 13.3 even with sodium sulfate concentrations as high as 65,000ppm. It was evident that propensity for corrosion initiation in solution can't be defined by sulfate content alone. Instead a ratio of $[SO_4^{2-}]/[OH^-]$ was adopted for analysis (Figure 9.1). The figure also shows for comparison the same data for samples cast in grout but with sulfate concentrations expressed as $g_{sulfate}/g_{powder}$.

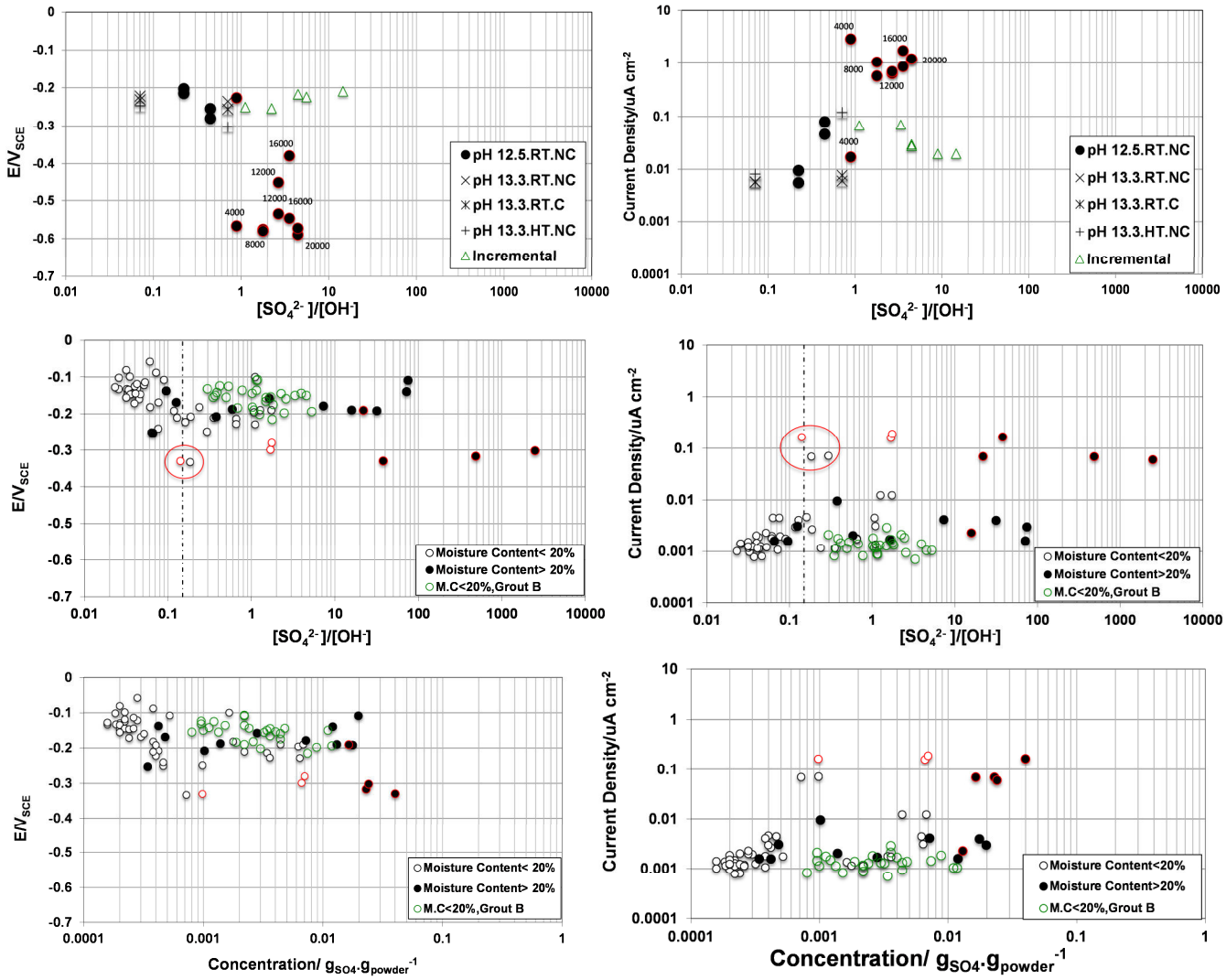

Figure 9.1. Sulfate threshold value based on corrosion potential and current density. Top: Sulfate Solution. Middle: Grout $[SO_4^{2-}]/[OH^-]$. Bottom: Grout $g_{sulfate}/g_{powder}$. (Red symbols indicate where corrosion developed).

The corrosion potential and corrosion current density of steel in the different grout test conditions in the research (MIT and INT) were compiled to evaluate sulfate content, the pore

water conditions and grout conditions where corrosion can occur. Two samples, with surface rust development, showed enhanced corrosion current density (i_{corr} ~0.3 μA/cm^2) with active corrosion potentials (OCP ~-0.3 mV_{sce}) at $[SO_4^{2-}]/[OH^-]$~1. At $[SO_4^{2-}]/[OH^-]$ ~0.15, two other samples had similar active corrosion electrochemical parameters, but the steel in this case did not develop significant surface rust during the time of the experiment. To characterize the extent of sulfate accumulation, three levels were proposed based on experimental observations. Low sulfate accumulation was assumed to have concentrations less than 0.00042 $g_{sulfate}/g_{Powder}$, which was the highest amount of sulfate measured in the as-received grout that did not have any grout degradation. A proposed high-end value was based on the sulfate level where corrosion developed in the testing. The intermediate sulfate range was proposed as characterizing moderate sulfate accumulation.

Figure 9.2 shows the corrosion potential and current density versus total chloride content from compiled tests results. Steel corrosion initiated in conditions where sulfate levels (~0.0007 $g_{sulfate}/g_{Powder}$) exceeded the low level of sulfate range. The value corresponded to the test sample conditions suggesting the $[SO_4^{2-}]/[OH^-]$ = 0.15 limit for typical grout pH environments. As shown in Figure 9.2, sulfate accumulation by segregation can cause corrosion initiation. Furthermore, addition of low amount of chloride in deficient grout can significantly increase the corrosion rate of steel. The samples with chloride level from 0.0002-0.002 ($g_{Chloride}/g_{Powder}$) corroded when the deficient grout contained sulfates exceeding the low range of sulfate accumulation. It was apparent that assessment of corrosion susceptibility by chloride values alone in deficient grout is insufficient as sulfate ion presence and grout characteristics are also important.

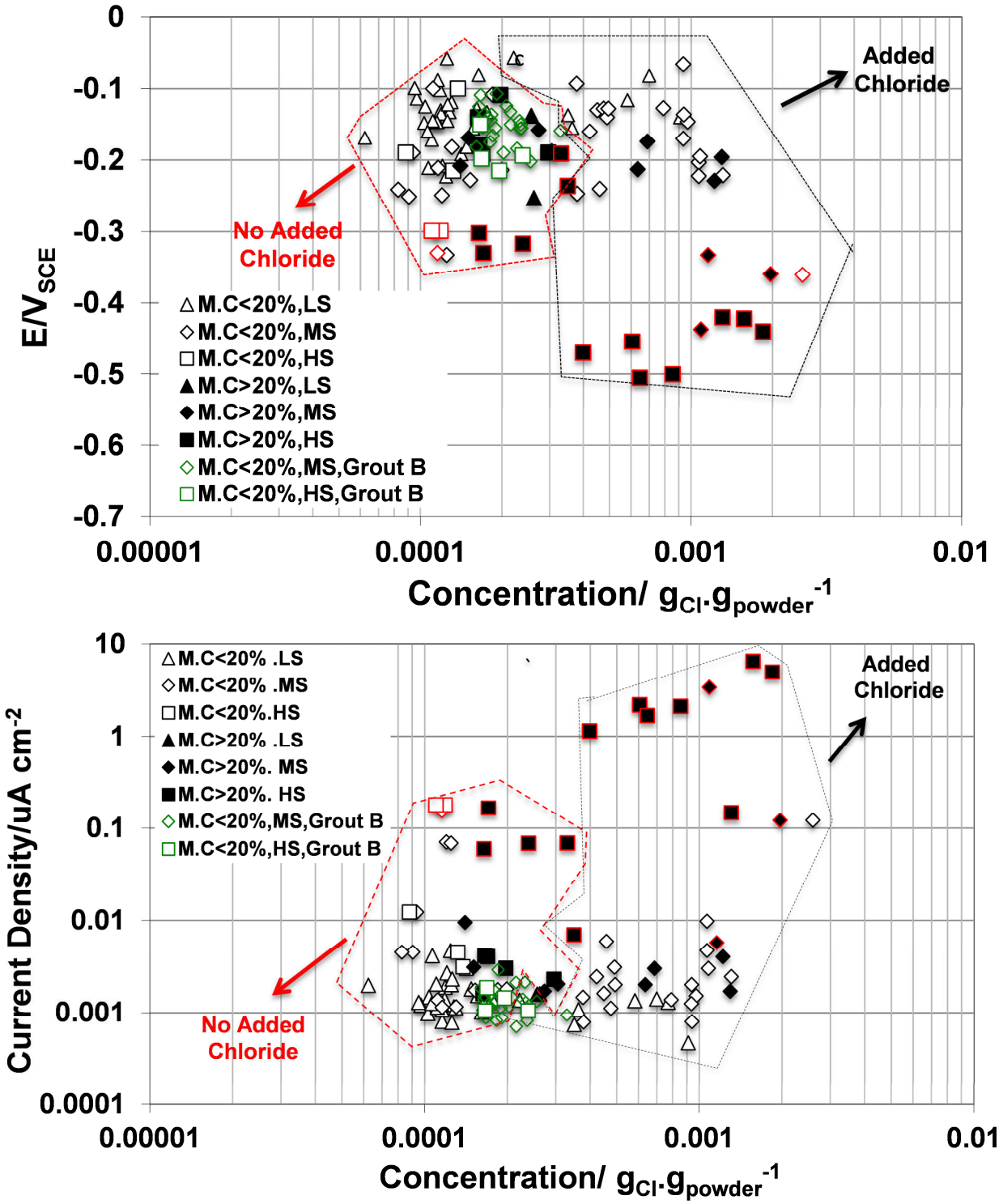

Figure 9.2. Corrosion potential and current density versus total chloride content.
(Red symbols indicate where corrosion developed)
Low Sulfate (LS) < 0.00042 $g_{sulfate}/g_{Powder}$
0.00042 < Med Sulfate (MS) < 0.006 $g_{sulfate}/g_{Powder}$,
High Sulfate(HS) > 0.006 $g_{sulfate}/g_{Powder}$

Compilation of pH and sulfate content in grout extracted from Florida bridges indicated that corrosion had occurred in deficient grouts where the sulfate to hydroxyl ratio exceeded 0.1 (Figures 9.3-9.4). In some of the most aggressive corrosion conditions the ratio was quite large. Corrosion testing in admixed sulfate solutions showed corrosion development at sulfate to hydroxyl ratio greater than 0.7 (Figure 9.3). No corrosion developed on steel immersed in solution with incremental sulfate additions to $[SO_4^{2-}]/[OH^-]$ as high as ~10. Corrosion occurred in mockup tendon samples when sulfate to hydroxyl ratio was more than 0.15. Nevertheless, $[SO_4^{2-}]/[OH^-]=0.15$ may be considered as a conservative limit. At this limit, the sulfate content in pH 12.6-13.3 pore solution corresponds to ~600-3000 ppm. (The corresponding samples showing the conservative values had sulfate concentration 0.0007 g/g.)

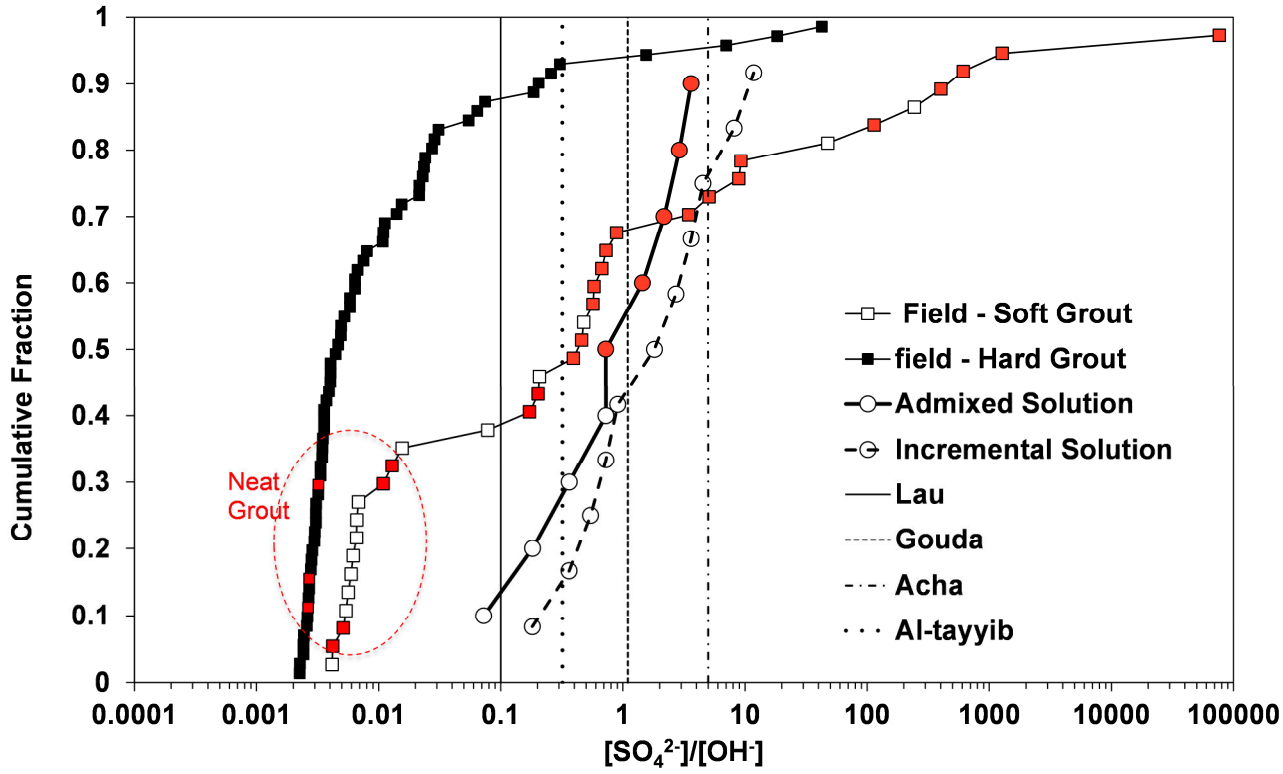

Figure 9.3. Sulfate levels for corrosion development in alkaline sulfate solution.
(Red symbols indicate where corrosion developed)

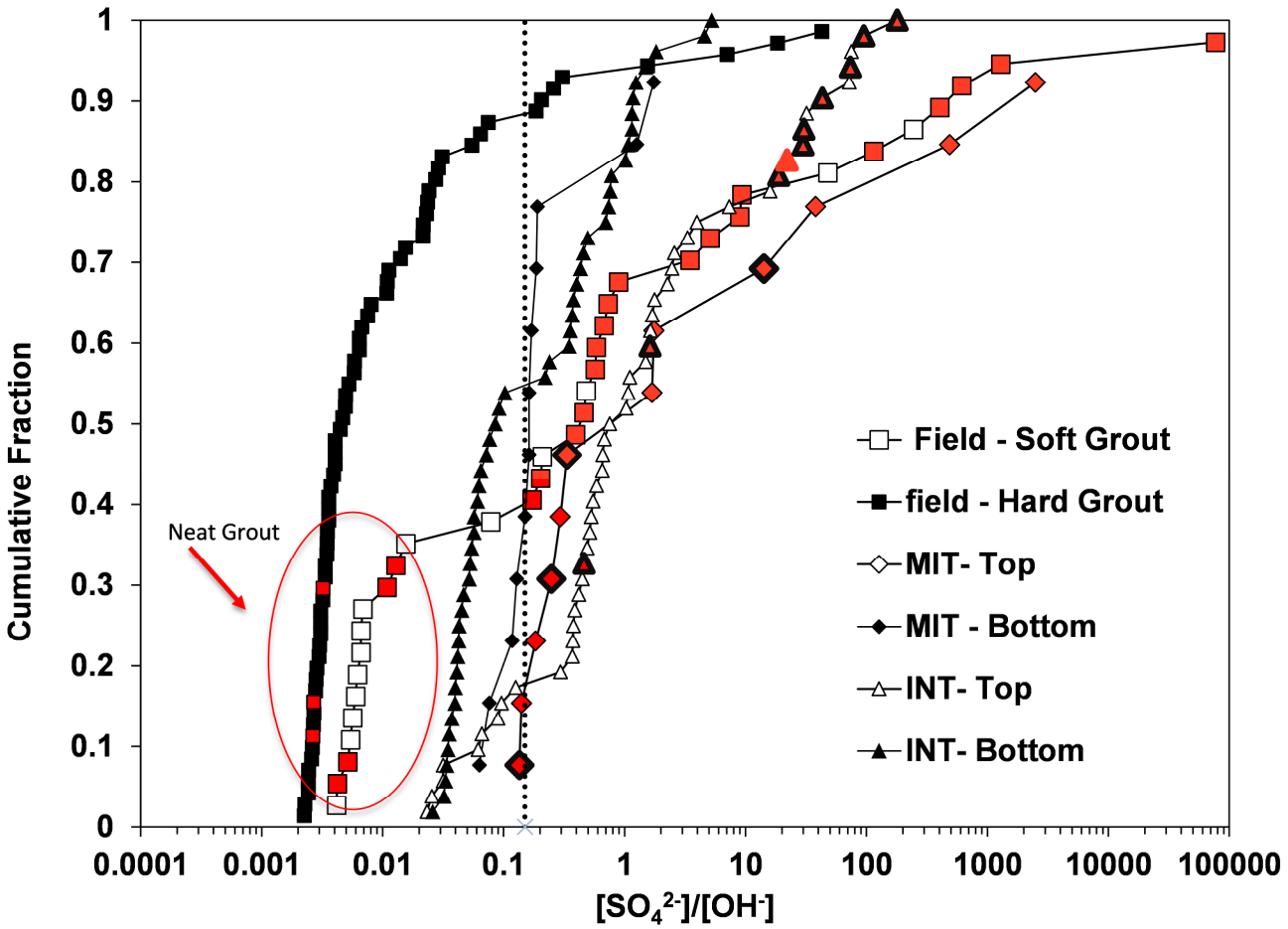

Figure 9.4. Sulfate levels for corrosion development in grout.
(Red symbols indicate where corrosion developed)

An important finding from field observations and laboratory cast grout samples is that the steel corrosion in presence of sulfate ions occurred primarily in deficient grout. It is posed that significant early sulfate accumulation and availability of sufficient levels is necessary to hinder stable steel passive film formation but depassivation of steel by sulfates is otherwise difficult. In the deficient grout, there is abundant moisture with available free sulfates from the initial grout injection. On the other hand, hardened grout sometimes had enhanced sulfate content, but the bulk moisture content in the macro pores was low possibly limiting free sulfate availability at the steel interface relatively to the high moisture conditions of deficient grouts. The possible role of sulfates in steel corrosion initiation were thought to be related to localized corrosion process by reaction such as $Fe^{2+} + 2H_2O + SO_4^{2-} \rightarrow Fe(OH)_2 + H_2SO_4$ (Jones, 1996). Even though the pH of the deficient grout was typically observed to be high, the hydrolysis reaction would promote lower pH conditions. Local areas of reduced pH may be possible within the interstitial spaces of the strand. The reduced presence of cement and the generally poor bulk quality of the deficient grout could further allow development of lower pH conditions by processes such as carbonation. Furthermore, the lower cement content would minimize any interaction of the free sulfates with the cement during hydration. The laboratory observations of

corrosion in testing in admixed sulfate solution with somewhat lower pH levels (pH~12.6) also reflects early disruption to passive film growth and corrosion development in of strand embedded in the deficient grout soon after injection where the grout pore water chemistry is still changing. The lack of corrosion with incremental additions of sulfates even up to high levels in both pH ~13 and 12.6 solutions furthermore would indicate that the mechanism of corrosion relates to the early instability of the steel passivity involving early sulfate presence.

The work sought to provide data to support recommendations relating sulfates in deficient grout and corrosion. Test results have shown positive indicators relating free sulfates to corrosion; however, the challenge of providing a complete mechanistic description on how sulfates disrupts passive film development at this time remains elusive and conflicting experiences is disseminated in the literature. Nevertheless, the serious consequence of observed corrosion in the field warrants addressing the issue. The other difficulty with specifications relating to possible limits on sulfate content in PT grouts lies in the fact that sulfur-containing species are regularly part of cementitious materials. The effect of limiting sulfates on the performance of the material should be considered. Finally, much of the findings in the work relate corrosion to the enhanced presence of sulfates in deficient grout. It was evident that enhancement of sulfate ions is in part due to transport of the ion to the areas of grout segregation. Definitions of sulfate limits should address that even low concentrations of sulfates in well hydrated grout may locally aggregate due to segregation. Limits of sulfates relating to recent corrosion observations should be related to grout robustness.

10. CONCLUSIONS

- Grout leachate from deficient grout contained enhanced sulfate concentrations. Deficient grout associated with steel corrosion found in a second bridge in Florida was similar to that found in deficient grout from the Ringling Bridge.

- High moisture content promotes grout deficiency. The effect from excess admixed water (15%-20% above manufacturer's recommended limit) was more significant than grout pre-hydration after up to 7 days of grout powder pre-exposure in 100% relative humidity.

- The level of grout deficiency caused by excess mix water and pre-exposure in 100% relative humidity can vary by grout product.

- High sulfate concentrations can be accumulated in deficient grouts without external sulfate sources. Even low concentrations of sulfates in well hydrated grout may locally aggregate due to segregation.

- Grout leaching methods for sulfates need to be developed. Consideration of practical sample size requirements; segregated grout drying during sample collection, leaching; and units of metrics should be made.

- MIT and INT test methods can promote grout segregation and differentiate grout robustness to adverse mix conditions and identify corrosion activity.

- Enhanced corrosion can occur in deficient grout created with expired grout and excessive mix water. In laboratory testing, enhanced corrosion occurred at elevated portions of test samples.

- The effect of crevice environments to aggravate corrosion conditions was not well differentiated in laboratory testing in solution or grout.

- In the open circuit potential condition for pH 13 solutions, additions of sodium sulfate with concentrations as high as 65,000 ppm after pre-conditioning in sulfate-free solution did not show ability to depassivate steel. Pre-mixed sodium sulfate concentrations as high as 20,000 ppm did not show indication to destabilize passive film growth.

- Results from anodic polarization tests of steel in pH 13 solution with up to pre-mixed 20,000 ppm sodium sulfate did do not indicate strong tendency of sulfates to disrupt passive film formation.

- In the open circuit potential condition for pH 12.6 solutions, additions of sodium sulfate with concentrations as high as 65,000 ppm after pre-conditioning in sulfate-free solution did not show ability to depassivate steel.

- In the open circuit potential condition for pH 12.6, destabilization of passive film growth resulting in severe corrosion occurred in pre-mixed >4,000 ppm sodium sulfate solution.

- Results from anodic polarization tests in pH 12.6 and pre-mixed >4,000 ppm sulfate solution indicated instability of passive film resulting in severe corrosion sometimes exhibiting pitting corrosion.

- Corrosion developed in deficient grout with 20,000-ppm addition of sodium sulfate to its mix water. Corrosion was also observed in deficient grout with as low as 2,000-ppm sodium sulfate when combined with chloride. In these cases, corrosion occurred when the sulfate ion concentration was >~0.01 $g_{Sulfate}/g_{Powder}$.

- Additions of 0.08 and 0.2% chloride by cement in itself did not initiate corrosion of steel in any of the segregated grout layers. Corrosion developed in deficient grout materials with similar low-level additions of chlorides (0.03 to 0.18% of total grout mass) when combined with as low as 2,000-ppm sodium sulfate in its mix water. The enhanced sulfate addition apparently had effect to initiate corrosion in presence of low-level chlorides.

- XRD and SEM-EDS results did not show strong indicators of sulfur-bearing iron corrosion products.

- The enhanced sulfate additions apparently had adverse effect in the corrosion development of steel in grouts with low level chlorides indicating adverse effects of combined low level chlorides and sulfate presence. The finding would suggest that assessment of corrosion susceptibility of deficient grout by chloride content alone would not be sufficient.

- Changes in pore water chemistry can affect the initiation of steel corrosion in the presence of sulfate ions and it was evident that propensity for corrosion initiation in solution can't be defined by sulfate content alone. However, practical limits accounting for expected grout pore water conditions may be proposed.

- Active corrosion conditions developed where sulfate levels exceeded sulfate range (~0.0007 $g_{sulfate}/g_{Powder}$). The value corresponded to the test sample conditions suggesting $[SO_4^{2-}]/[OH^-]$ =0.15 limit for typical grout pH environments.

- Propensity for chloride and sulfate accumulation in grout segregation should be considered as part of robustness testing of grout materials.

- It was posed that significant early sulfate accumulation and availability of sufficient levels is necessary to hinder stable steel passive film formation but depassivation of steel by sulfates is otherwise difficult. As initial assessment, the possible role of sulfates in steel corrosion initiation were thought to be related to localized corrosion process by reaction such as $Fe^{2+} + 2H_2O + SO_4 \rightarrow Fe(OH)_2 + H_2SO_4^2$.

- The disparate developed corrosion potential of steel in different grout conditions, apparent condition of maintained active corrosion, and apparent adverse electrical grout characteristics may lead to adverse macrocell development causing enhanced corrosion rates.

REFERENCES

Acha, M., Alonso, C., and Andrade, C., (1990). “Corrosión bajo tension de alambres de acero de pretensado en medios alcalinos, conteniendo sulfatos.“ Hormigón y Acero, 2 Trimestre, pp. 89-94.

Al-Amoudi, O. Baghabra, S., and Maslehuddin, M., (1993). "The effect of chloride and sulfate ions on reinforcement corrosion." Cement and Concrete Research, V.23.1. pp. 139-146.

Al-Amoudi, O., Baghabra, S., Maslehuddin, M. and Yaser, A., (1995). "Role of chloride ions on expansion and strength reduction in plain and blended cements in sulfate environments." Construction and Building Materials, V.9.1 pp. 25-33.

Al-Tayyib, A.J., and Khan, M.S., (1991). “Effect of Sulfate Ions on the Corrosion of Rebars Embedded in Concrete.” Cement and Concrete Composites, V.13. pp. 123-7.

Al-Tayyib, A.J., Somuah, S.K., Boah, J.K., Leblanc, P., and Al-Mana, A,I., (1982). Cement and Concrete Research, V. 18. pp. 774-782.

Angst, U., Elsener, B., Larsen, C., and Vennesland, O., (2009). “Critical Chloride Content in Reinforced Concrete- A Review.” Cement and Concrete Research, Vol. 39. pp. 1122-1138.

ASTM, C566-13, (2013).”Standard Test Method for Total Evaporable Moisture Content of Aggregate by Drying,” American Society for Testing and Materials, West Conshohocken, PA.

Bertolini, L., and Carsana, M., (2011). “High pH Corrosion of Prestressing Steel in Segregated Grout.” Modeling of Corroding Concrete Structures, RILEM Bookseries, V.5. RILEM.

Blactot, E., Brunet-Vogel, C., Farcas, F., Gailet, L., Mabille, I., Chaussadent, T., and Sutter, E., (2007). “Electrochemical behavior and corrosion sensitivity of prestressed steel in cement grout.” WIT Transactions on Engineering Sciences, Simulation of Electrochemical Processes II, Vol.54. pp. 267-76.

Broomfield, J., (2000). "Carbonation and its effects in reinforced concrete." Materials Performance,V.39.1.

Corven, J., (2001). “Mid Bay Bridge Post Tensioning Evaluation,” Final Report to FDOT, Tallahassee, FL.

Dehwah, H. A. F., Maslehuddin, M., and Austin, S.A., (2003). "Effect of sulfate ions and associated cation type on the pore solution chemistry in chloride-contaminated plain and blended cements." Cement and Concrete Composites, V.25.4 pp. 513-525.

Dehwah, H.A.F., Maslehuddin, M., and Austin, S.A., (2002) “Long-term effect of sulfate ions and associated cation type on chloride-induced reinforcement corrosion in Portland cement concrete.” Cement and Concrete Composites, V. 24. pp. 17-225.

FDOT (Florida Department of Transportaton), “Sunshine Skyway Bridge Post-Tensioned Tendons Investigation,” Tallahassee, 2002.

FDOT Standard Specifications, (2010). Section 938, Florida Department of Transportation. Tallahassee, FL.

FM 5-516, (2013) “Florida Method of Test For Determining Low-Levels of Chloride in Concrete and Raw Materials“ Florida Department of Transportation. Tallahassee, FL.

FHWA, (2012). “Literature Review of Chloride Threshold Values for Grouted Post-Tensioned Tendons.” Publication No. FHWA-HRT-12-067. November 2012. Federal Highway Administration. Washington, DC.

Gavele, J.R., (1976). “Transport process and the mechanism of pitting of metals.”J. Electrochemical Society, Vol.122. pp.464.

Gouda, V.K., (1970). “Corrosion and corrosion inhibition of reinforcing steel: I. Immersed in alkaline solution.” British Corrosion Journal, V.5. pp. 198-203.

Gouda, V.K. and Halaka, W.Y., (1970). “Corrosion and corrosion inhibition of reinforcing steel: II. Embedded in concrete.” British Corrosion Journal, V.5. pp. 204-8.

Hansen, B., (2007). “Forensic Engineering: Tendon Failure Raises Questions about Grout in Post-Tensioned Bridges,” Civil Engineering News, V.77.11. pp. 17-18.

Holden, W. R., Page,C., and Short, N., (1983). "Corrosion of reinforcement in concrete construction." Chichester: Ellis Horwood Ltd. pp. 143-50

Hartt, W. and Venugopalan, S. “Corrosion Evaluation of Post-Tensioned Tendons on the Mid Bay Bridge in Destin, Florida.” FDOT, Tallahassee, FL, 2002.

Jones, D., (1996). *Principles and Prevention of Corrosion,* 2nd edition. Upper Saddle River, NJ: Prentice Hall.

Krishna Vigneshwaran, K.K , Permeh,S, Lasa,I and Lau, K., (2015). “Anodic Behavior of Steel in Deficient Grout with Enhanced Sulfate Ion Concentrations.” Concrete Service Life Extension 2015, Paper no. CCC15-6942. Philadelphia, PA. NACE Int.. Houston, TX.

Lau, K., Lasa, I., and Paredes, M., (2013a). “Corrosion Failure of Post-Tensioned Tendons in Presence of Deficient Grout.” NACE Corrosion 2013, Paper No. 2600. NACE Int. Houston, TX.

Lau, K., Rafols, J., Lasa, I., and Paredes, M., (2013b) “Laboratory Corrosion Assessment of Post-Tensioned Tendons Repaired with Dissimilar Grout.” NACE Corrosion 2013, Paper No. 2602. NACE Int. Houston, TX.

Lau, K, Powers, R., and Paredes, M., (2013c). “Corrosion Evaluation of Repair-Grouted Tendons is Presence of Bleed Water.” NACE Corrosion 2013, Paper No. 2604. NACE Int. Houston, TX.

Lau, K., Lasa, I., and Paredes M., (2013d) “Corrosion of Post-Tensioned Tendons in Presence of Bleed Water.” Presentation at NACE Risk Management of Corrodible Systems. June 19-20, 2013. NACE Int. Houston, TX.

Lau, K., Lasa, I., and Paredes, M., (2014). ”Update on Corrosion of Post-Tensioned Tendons with Deficient Grout in Florida.” NACE Corrosion 2014. NACE Int. Houston, TX.

Lee, S.K and Zielske ,J., (2014). “An FHWA Special Study: Post-tensioning Tendon Grout Chloride Thresholds.” No. FHWA-HRT-14-039.

Li, L and Sagüés, A., (2001). “Chloride Corrosion Threshold of Reinforcing Steel in Alkaline Solutions-open-Circuit Immersion Tests”, Corrosion, V. 57. pp. 19.

Maslehuddin, M and Paget, C.L., (1997). "Temperature effect on the pore solution chemistry in contaminated cements." Magazine of Concrete Research, V.49.178 pp. 5-14.

Merrill, B., (2010). Memo. Grout Testing and Analysis. Texas Department of Transportation. September 14, 2010.

Mindess, S,, Young, J.S., and Darwin, D., (2003). *Concrete*. Upper Saddle River, NJ: Prentice Hall.

Pradhan, B., (2014). "Corrosion behavior of steel reinforcement in concrete exposed to composite chloride–sulfate environment." Construction and Building Materials, V.72. pp. 398-410.

O’Reilly, M., Darwin, D., and Browning, J., (2012). “Corrosion Performance of Prestressing Strands in Contact with Dissimilar Grouts.” Report to Kansas Department of Transportation. SL Report 12-1. April 2012.

Page, C.L., and Vennesland O., (1983). “Pore solution composition and chloride binding capacity of silica-fume cement paste.” Matériaux et Constructions, V.16.1. pp. 19-25.

Permeh,S, Krishna Vigneshwaran, K.K. ,Lau,K, Lasa, I and Paredes ,M., (2015).“Material and Corrosion Evaluation of Deficient PT Grout with Enhanced Sulfate Concentrations.” NACE Corrosion 2015, Paper no. 5828. NACE Int. Houston, TX.

Powers, R.G., (1999). “Corrosion Evaluation of Post-Tensioned Tendons on the Niles Channel Bridge,” FDOT, Gainesville, FL.

Pradhan, B., (2014). "Corrosion behavior of steel reinforcement in concrete exposed to composite chloride–sulfate environment." Construction and Building Materials, V.72. pp. 398-410.

PTI M55.1-12, (2012). “Specification for Grouting of Post-Tensioned Structures.” Post Tensioning Institute. Farmington Hills, MI.

Sagues, A., (2015). “Corrosion of Post-Tensioning Strands,” FDOT, Tallahassee, FL.

Saleem, M., (1996). "Effect of moisture, chloride and sulphate contamination on the electrical resistivity of Portland cement concrete." Construction and Building Materials, V.10.3 pp. 209-214.

Sprinkel, M., (2010). “Varina Enon Tendon Failure.” Transportation Research Board 89th Annual Meeting, Paper No. 10-2382. The National Academies. Washington D.C.

Sprinkel, M., and Napier, C., (2008). Presentation at Virginia Concrete Conference. “VDOT experience with grouted tendons in Varina-Enon precast segmental post-tensioned bridge” VTRC. March 2008.

Tex-620-J, (2005). “Determining chloride and sulfate contents in soil “, Construction Division, August 2005

Trejo, D., Hueste, M.B., Gardoni, P., Pillai, R., Reinschmidt, K., Im, S.B., Kataria, S., Hurlebaus, S., Gamble, M., an Ngo, T.T., (2009). “Effect of Voids in Grouted, Post-Tensioned Concrete Bridge Construction: Vol.1-Electrochemical Testing and Reliability Assessment,” Report No. 0-4588-1.TTI. College Station, TX.

Yonezawa T, Ashworth V. Procter R. (1989). “The mechanism of fixing Cl by cement hydrates resulting in the transformation of NaCl to NaOH. Proceedings of the 8th International Conference on Alkali-Aggregate Reaction. Kyoto. pp. 153–160.

Zuquan, Jin, et al. (2007). "Interaction between sulfate and chloride solution attack of concretes with and without fly ash." Cement and Concrete Research, V.37.8. pp. 1223-1232.

APPENDIX: PETROGRAPHY

Table A1. Petrography Sample Legend

Samples ID In Petrographic Report	Test Cases
Field Samples (Ringling)	
R1	Segregated Grout from 403-6 Tendon (12:00)
R2	Hard Grout from 403-6 Tendon
MIT Test samples	
AL1	A (~0.3 ft. from top)
AL2	A (~7 ft. from top)
INT Test Samples	
SA	AA1
SE1	AP1 (Tee Header)
SE2	AP1 (Tee Body)
EA	BA1
EE1	BP1 (Tee Header)
EE2	BP1 (Tee Body)
C1	AP8 (Tee Header)
C2	AP8 (Tee Body)

American Petrographic Services, Inc.

REPORT OF CONCRETE TESTING

PROJECT:

CORROSION OF POST-TENSIONED TENDONS WITH EFFICIENT GROUT

REPORTED TO:

FLORIDA INT'L UNIVERSITY
CIVIL & ENVIRONMENTAL ENGINEERING
10555 WEST FLAGLER STREET
MIAMI, FL 33174

ATTN: SAMANBAR PERMEH

APS PROJECT NO: 10-08795

DATE: APRIL 21, 2016

INTRODUCTION

This report presents the results of laboratory work performed by our firm on eight cementitious section samples (labeled EE1, EE2, C1, C2, SE1, SE2, EA and SA) submitted to us by Ms. Samanbar Permeh of Florida International University, Department of Civil Environmental Engineering on March 28, 2016. We understand the cementitious samples are being examined to determine their composition. The scope of our work was limited to performing thin section analysis on all eight samples to determine the composition of the cementitious material.

CONCLUSIONS

Based on our observations, test results, and past experience, our conclusions are as follows:

1. Sample #EE1 was composed of portland cement, fly ash, silica fume, and hydrated lime. The grout contained abundant spherical, mostly entrained-sized air voids; with a higher concentration or coalescence of void spaces along what appeared to be a formed edge of the sample. The total air content was estimated to be greater than 10%. No carbonate filler was present in the sample and the w/cm was estimated to be between 0.43 and 0.48.

   A percentage estimate of the components of the material was not able to be determined with reasonable certainty. However, we do believe the relative amounts of the constituents from most to least, were as follows:

   Portland cement
   Fly ash (> 30%)
   Silica fume
   Hydrated lime

2. Sample #EE2 was composed of portland cement, fly ash, silica fume, and hydrated lime. The sample contained some spherical entrained-sized voids with the total air content estimated at less than 3%. No carbonate filler was present in the sample and the w/cm was estimated to be between 0.40 and 0.45.

A percentage estimate of the components of the material was not able to be determined with reasonable certainty. However, we do believe the relative amounts of the constituents from most to least, were as follows:

Portland cement
Fly ash (> 30%)
Silica fume/Hydrated lime (sub-equal amounts)

3. Sample #C1 was extremely soft (less than 1 on Mohs scale) and porous, and likely represented a severely segregated portion of grout. The sample appeared to be composed of very fine portlandite with a few grains of very fine carbonate filler, all bound together with calcium silicate hydrate. No visual evidence of any residual cement was observed in the sample. Abundant shrinkage microcracks were present in the sample and the w/cm was estimated to be in excess of 0.70.

4. Sample #C2 was composed of portland cement, coarse carbonate flour, and silica fume. The sample contained a very small amount (< 1%) of spherical, very fine entrained-sized air voids. Tabular portlandite was present within a few of the void spaces. An abundance of carbonate filler was present proximal to a fractured edge of the sample (segregated). The portland cement in the sample was tightly-packed and the w/cm of the grout was estimated to be between 0.35 and 0.40.

   A percentage estimate of the components of the material was not able to be determined with reasonable certainty. However, we do believe the relative amounts of the constituents from most to least, were as follows:

   Portland cement
   Carbonate flour
   Silica Fume

5. Sample #SE1 was composed of portland cement, silica fume, and carbonate flour. At least one cold joint was present in the grout fragment. The grout on one side of the joint was mostly composed of silica fume agglomerations which were up to 1 mm in diameter. The interstitial material on this side of the joint was mostly composed of portland cement. The other side of the cold joint was chiefly composed of portland cement with some carbonate flour and a small amount of silica fume. This side of the cold joint contained 'graded' laminations of alternating paste coloration (darker gray to lighter gray), likely representing segregation of the mixture. The w/cm of the sample was highly variable due to the presence of the cold joint and observed segregation and was estimated to range between 0.40 and 0.60.

   A percentage estimate of the components of the material was not able to be determined with reasonable certainty. However, we do believe the relative amounts of the constituents from most to least, were as follows:

   Portland cement
   Silica fume
   Carbonate flour

6. Sample #SE2 was composed of portland cement, carbonate flour, and silica fume. A few very fine plastic void spaces and channels were present in the sample which were less than 1 mm in length. The carbonate flour in the sample was segregated, with an abundance on one side of the sample and absence on the other. Much coarse portlandite was present within the paste and the w/cm was estimated to be between 0.40 and 0.45.

   A percentage estimate of the components of the material was not able to be determined with reasonable certainty. However, we do believe the relative amounts of the constituents from most to least, were as follows:

   Portland cement
   Carbonate flour
   Silica Fume

7. Sample #EA was composed of portland cement, fly ash, silica fume, and hydrated lime. The grout contained many fine, entrained-sized spherical voids with an estimated air content of 4 – 5%. A very small amount of acicular ettringite was observed sprouting in an air void on a fractured edge of the sample. No carbonate flour was present in the material and the w/cm of the sample was estimated at 0.40 to 0.45.

   A percentage estimate of the components of the material was not able to be determined with reasonable certainty. However, we do believe the relative amounts of the constituents from most to least, were as follows:

   Portland cement
   Fly ash (> 30%)
   Silica Fume/Hydrated lime (sub-equal amounts)

8. Sample #SA was composed of portland cement, carbonate flour, and silica fume. The sample contained a small amount of air (estimated 1 – 2%). The w/cm of the sample was relatively low and estimated to be between 0.35 and 0.40.

   A percentage estimate of the components of the material was not able to be determined with reasonable certainty. However, we do believe the relative amounts of the constituents from most to least, were as follows:

   Portland cement
   Carbonate flour
   Silica Fume

SAMPLE IDENTIFICATION

Sample Number:	EE1	EE2	C1	C2
Sample Type:	Hardened Cementitious Sections			
Original Sample Dimensions:	32 mm (1-1/4") x 25mm (1") x 13mm (1/2")	32 mm (1-1/4") x 25 mm (1") x 19 mm (3/4")	13 mm (1/2") x 13mm (1/2") x 13mm (1/2")	38 mm (1-1/2") x 32mm (1-1/4") x 6mm (1/4")

Sample Number:	SE1	SE2	EA	SA
Sample Type:	Hardened Cementitious Sections			
Original Sample Dimensions:	32 mm (1-1/4") x 25 mm (1") x 25 mm(1")	38 mm (1-1/2") x 32 mm (1-1/4") x 6 mm(1/4")	38 mm (1-1/2") x 32 mm (1-1/4") x 13 mm(1/2")	32 mm (1-1/4") x 32 mm (1-1/4") x 13 mm (1/2")

TEST PROCEDURES

Laboratory testing was performed on March 28, 2016 and subsequent dates. Our procedures were as follows:

Petrographic Analysis

A petrographic analysis was performed in accordance with APS Standard Operating Procedure 24-LAB-001, "Petrographic Examination of Hardened Concrete," ASTM C856-latest revision. The petrographic analysis consisted of reviewing cement paste and aggregate qualities on a whole basis as well as on a cut/polished section. The water/cement ratio of the concrete was estimated by viewing a thin section of the concrete under a Nikon E600 polarizing microscope at magnification up to 600x. Thin section analysis was performed in accordance with APS Standard Operating Procedure 24-LAB-009, "Determining the Water/Cement of Portland Cement Concrete, APS Method." The sample is first highly polished then epoxied to a glass slide. The excess sample is cut from the glass and the slide is polished until the concrete reaches 25 microns or less in thickness.

REMARKS

The test samples will be retained for a period of at least thirty days from the date of this report. Unless further instructions are received by that time, the samples may be discarded. Test results relate only to the items tested. No warranty, express or implied, is made.

Report Prepared By:
American Engineering Testing, Inc.

Blake M. Lemcke, PG
Geologist/Petrographer
MN License #50337
blemcke@amengtest.com

Report Reviewed By:
American Petrographic Services, Inc.

Scott F. Wolter, PG
President
MN License No. 30024
Phone: 651-659-1345
swolter@amengtest.com

APS PROJECT NO: 10-08795 **DATE:** APRIL 21, 2016

PROJECT: CORROSION OF POST-TENSIONED TENDONS WITH EFFICIENT GROUT

PHOTO: 1

SAMPLE ID: C1 **DESCRIPTION:** View of grout fragment as received. Several finer fragments and some powder were also received in the sample cup.

PHOTO: 2

SAMPLE ID: C2 **DESCRIPTION:** View of grout fragment as received.

APS PROJECT NO: 10-08795 **DATE:** APRIL 21, 2016

PROJECT: CORROSION OF POST-TENSIONED TENDONS WITH EFFICIENT GROUT

PHOTO: 3

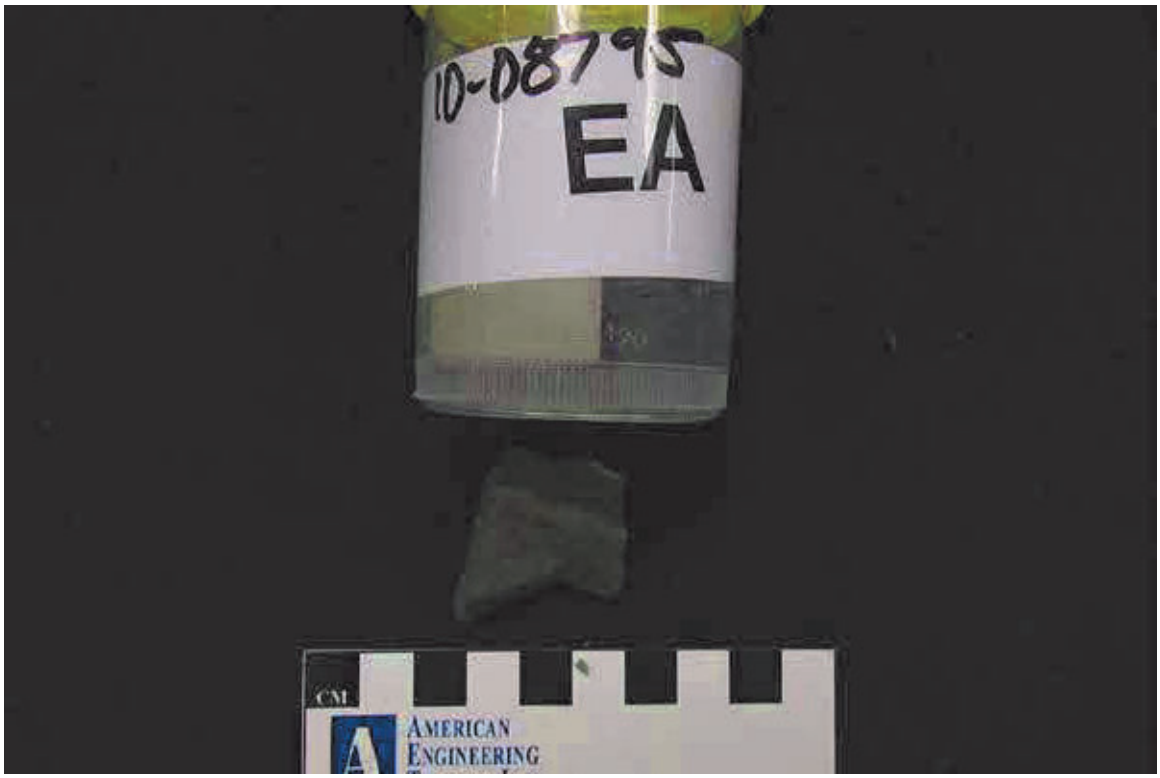

SAMPLE ID: EA **DESCRIPTION:** View of grout fragment as received.

PHOTO: 4

SAMPLE ID: EE1 **DESCRIPTION:** View of grout fragment as received.

APS PROJECT NO: 10-08795 **DATE:** APRIL 21, 2016

PROJECT: CORROSION OF POST-TENSIONED TENDONS
WITH EFFICIENT GROUT

PHOTO: 5

SAMPLE ID: EE2 **DESCRIPTION:** View of grout fragment as received.

PHOTO: 6

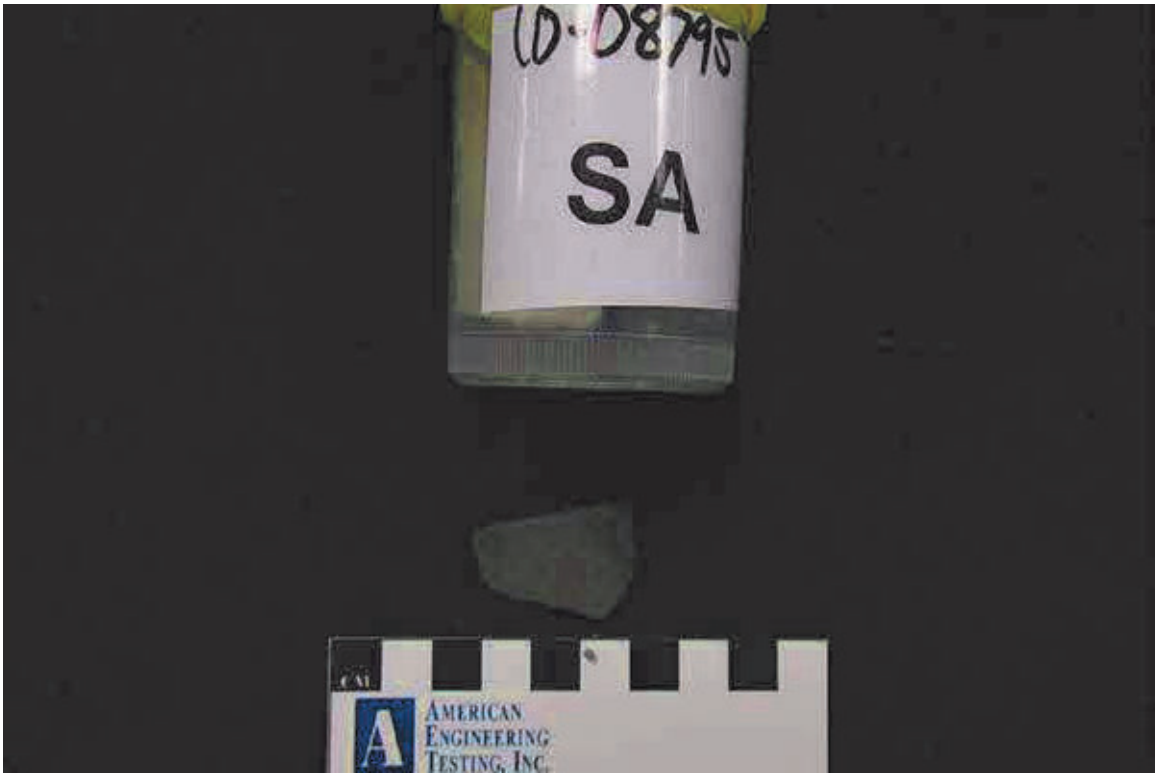

SAMPLE ID: SA **DESCRIPTION:** View of grout fragment as received.

APS PROJECT NO: 10-08795 **DATE:** APRIL 21, 2016

PROJECT: CORROSION OF POST-TENSIONED TENDONS WITH EFFICIENT GROUT

PHOTO: 7

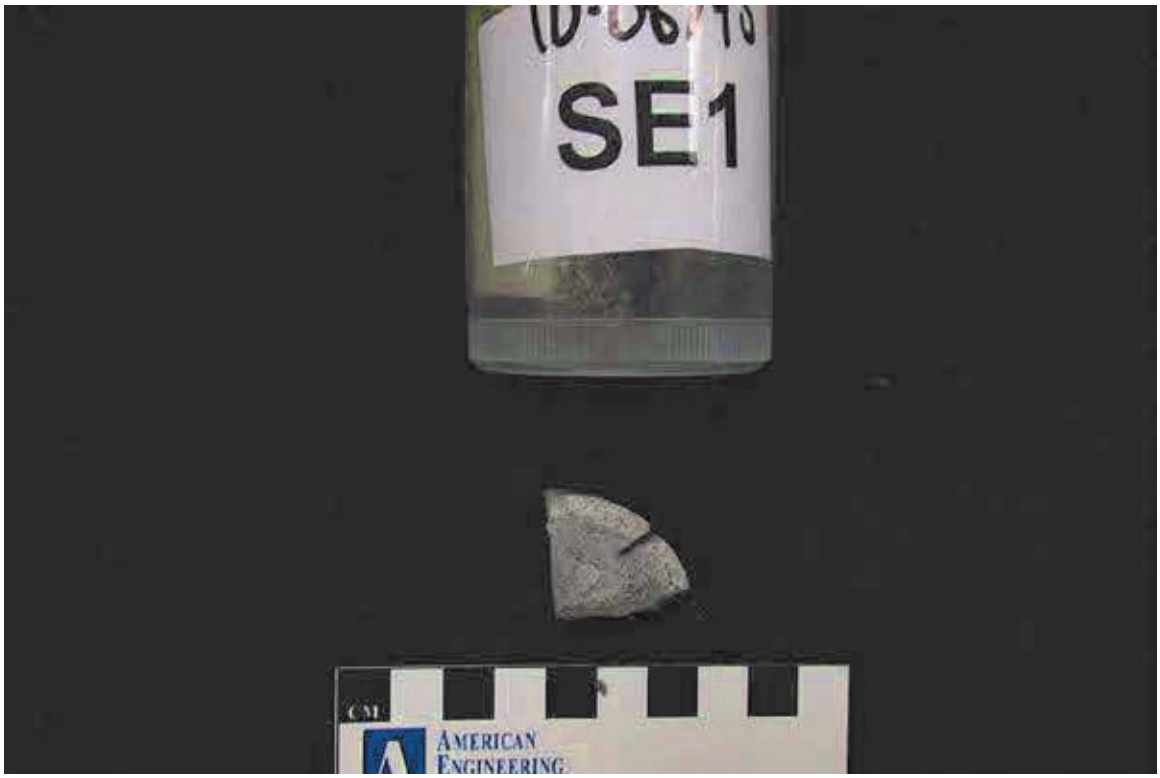

SAMPLE ID: SE1 **DESCRIPTION:** View of grout fragment as received. Several finer fragments and some powder were also received in the sample cup.

PHOTO: 8

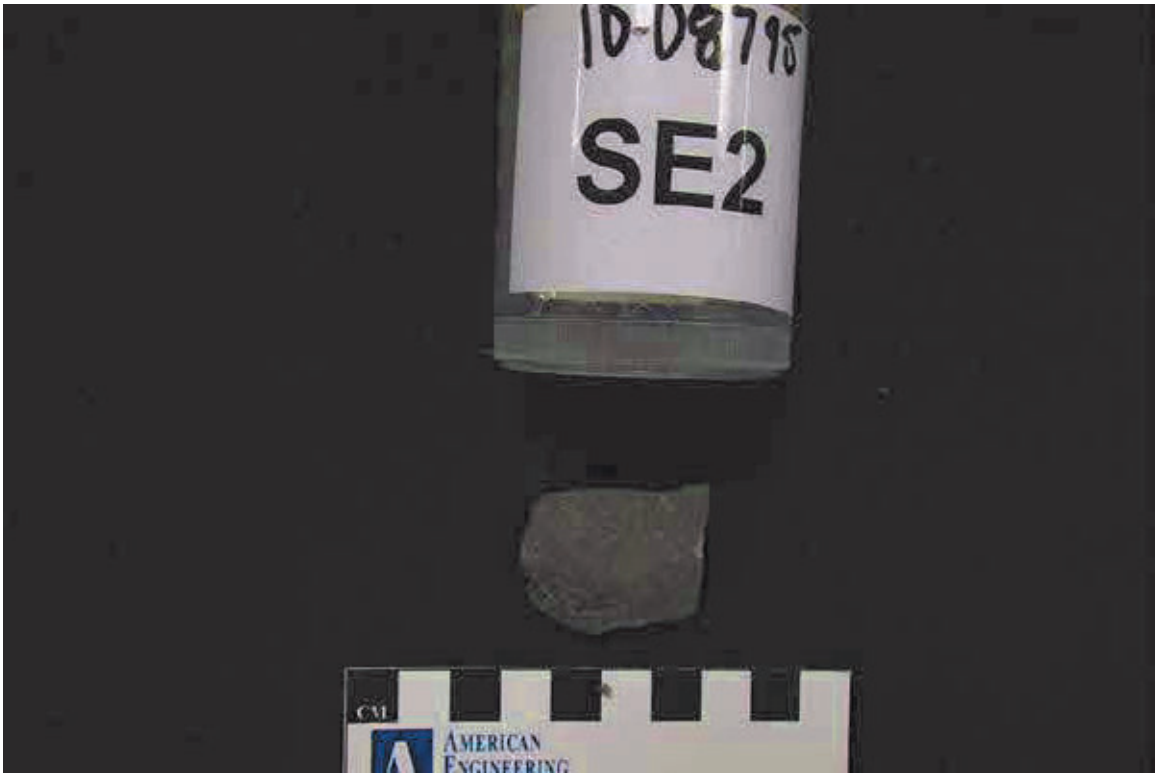

SAMPLE ID: SE2 **DESCRIPTION:** View of grout fragment as received.

APS PROJECT NO: 10-08795 **DATE:** APRIL 21, 2016
PROJECT: CORROSION OF POST-TENSIONED TENDONS WITH EFFICIENT GROUT

PHOTO: 9

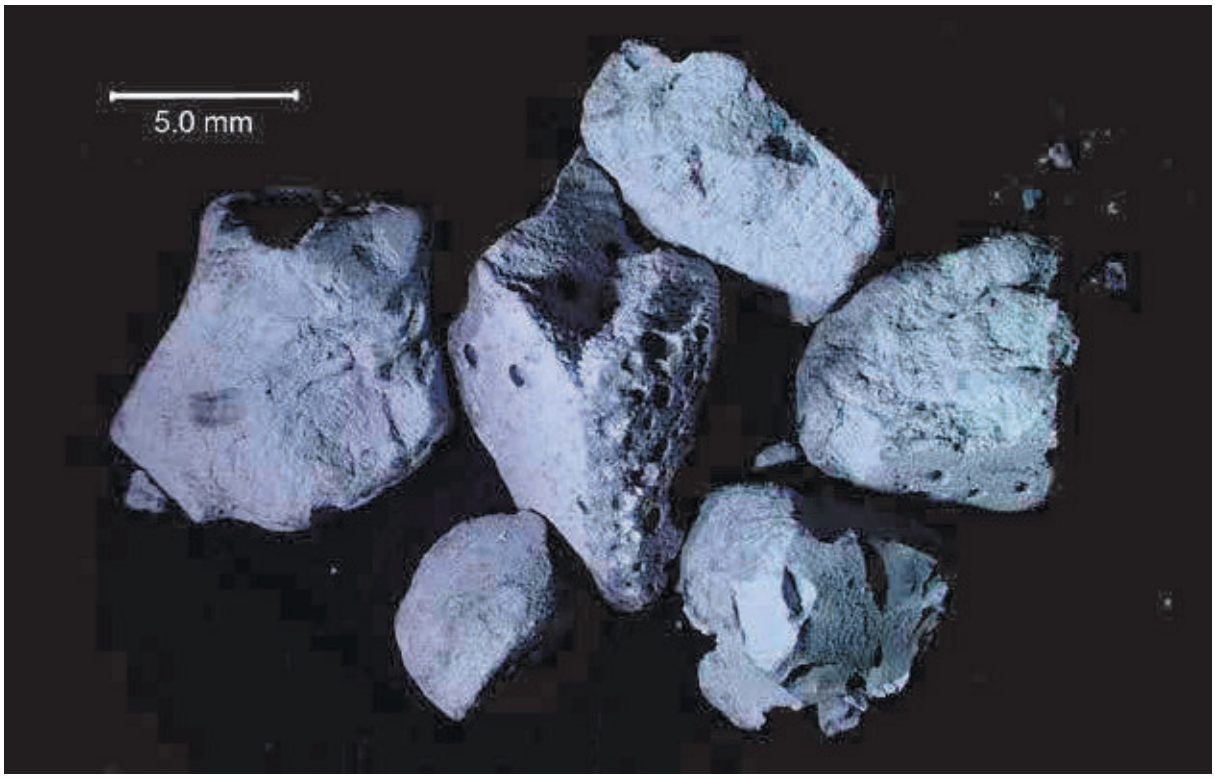

SAMPLE ID: C1 **DESCRIPTION:** Magnified view of finer grout fragments. The material was very soft and porous, with fractured surfaces often exhibiting rounded edges/contours.
MAG: 5x

PHOTO: 10

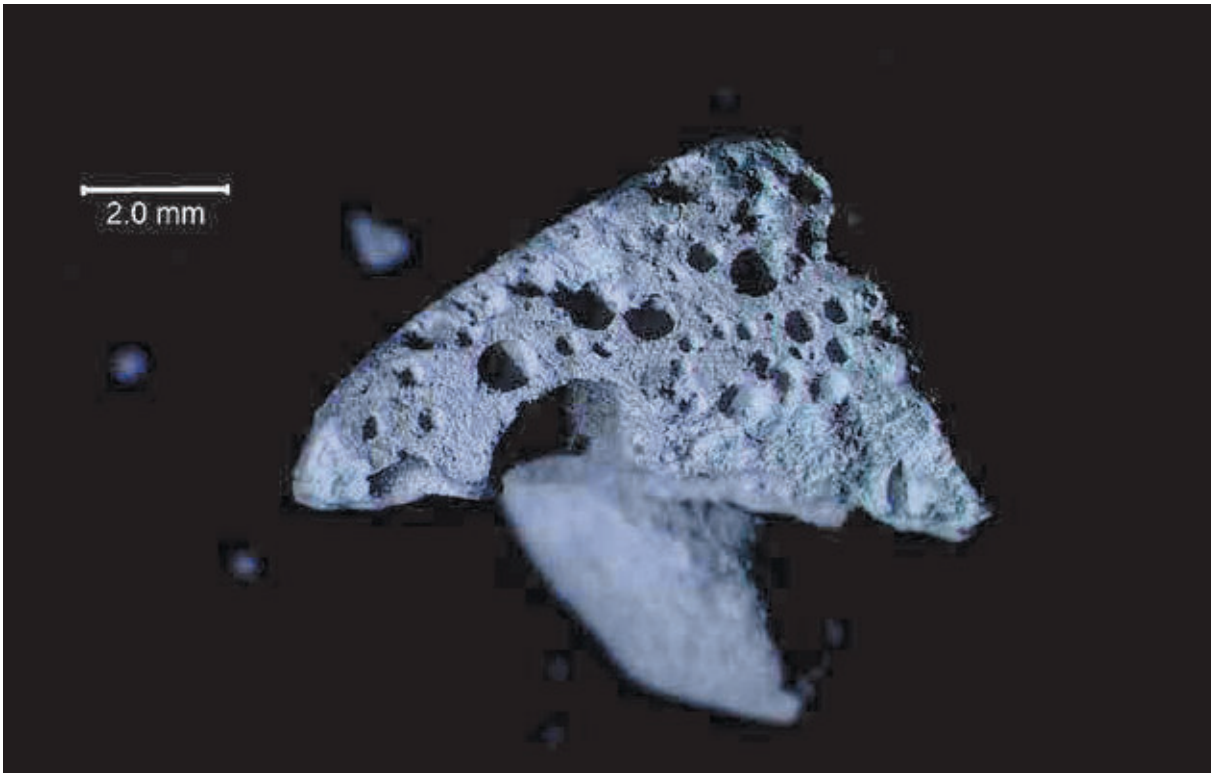

SAMPLE ID: C1 **DESCRIPTION:** Formed surface on one of the grout fragments which exhibits several 'bug holes'.
MAG: 10x

APS PROJECT NO: 10-08795 **DATE:** APRIL 21, 2016

PROJECT: CORROSION OF POST-TENSIONED TENDONS WITH EFFICIENT GROUT

PHOTO: 11

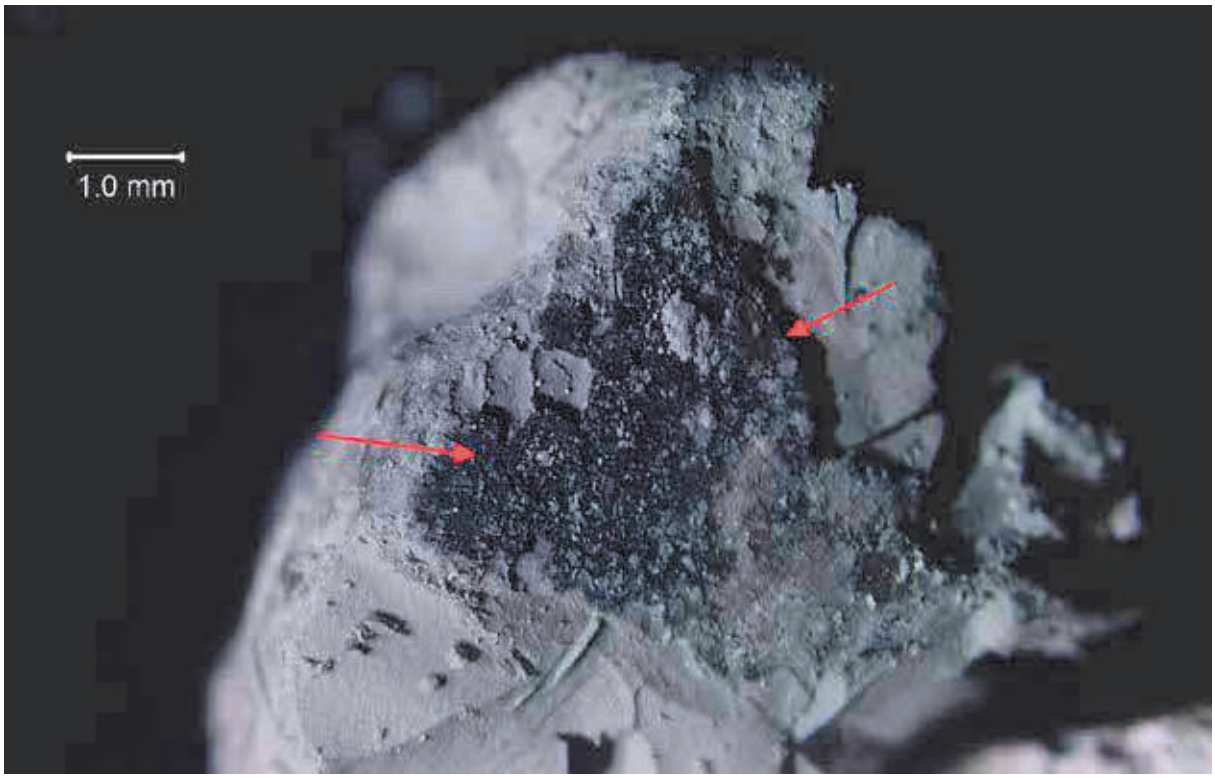

SAMPLE ID: C1 **DESCRIPTION:** Unidentified black material (red arrows) on the surface of one of the grout fragments.

MAG: 15x

PHOTO: 12

SAMPLE ID: C2 **DESCRIPTION:** Tendon impression on the surface of grout fragment which exhibits several 'bug holes'.

MAG: 15x

APS PROJECT NO: 10-08795 **DATE:** APRIL 21, 2016

PROJECT: CORROSION OF POST-TENSIONED TENDONS WITH EFFICIENT GROUT

PHOTO: 13

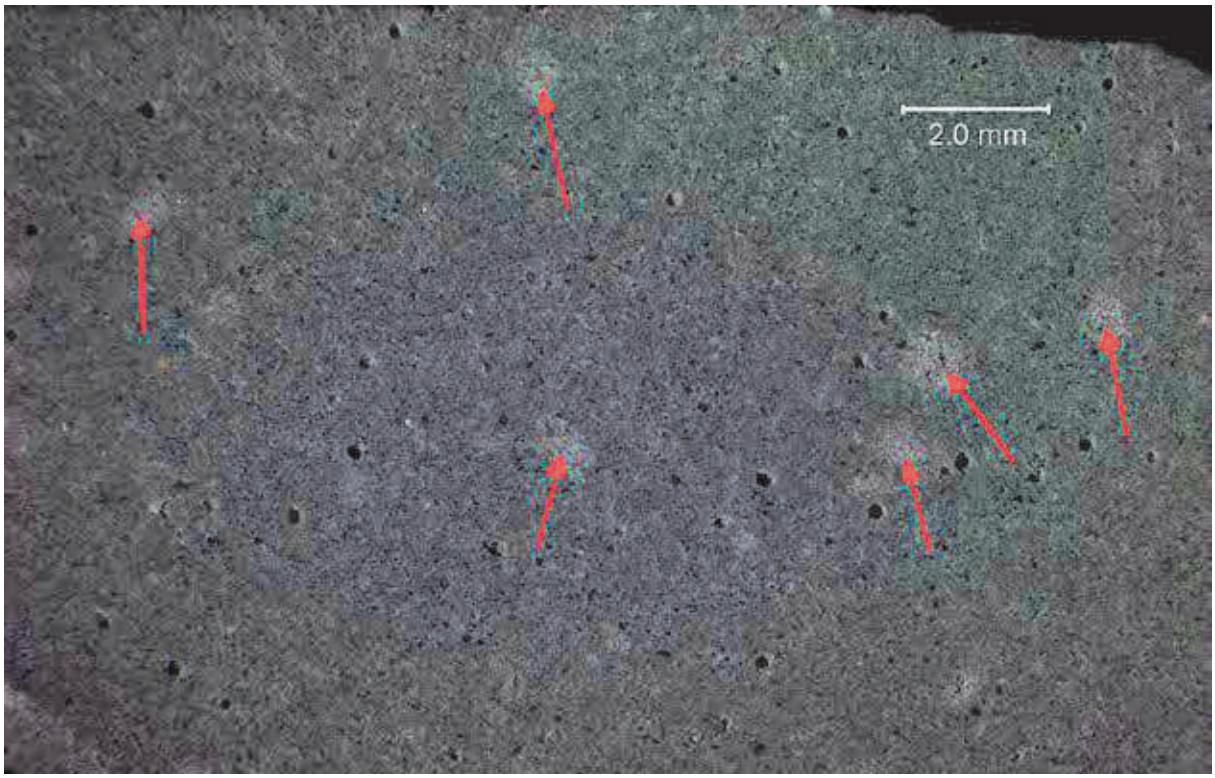

SAMPLE ID: C2 **DESCRIPTION:** Saw cut and lapped section of grout showing several round 'spots' of lighter-colored and softer paste (red arrows). The origin of these features was not clear from the analysis.

MAG: 10x

PHOTO: 14

SAMPLE ID: C2 **DESCRIPTION:** More magnified view of the round spots of lighter-colored and softer paste (red outlines) in lapped section of grout.

MAG: 50x

APS PROJECT NO: 10-08795 **DATE:** APRIL 21, 2016
PROJECT: CORROSION OF POST-TENSIONED TENDONS WITH EFFICIENT GROUT

PHOTO: 15

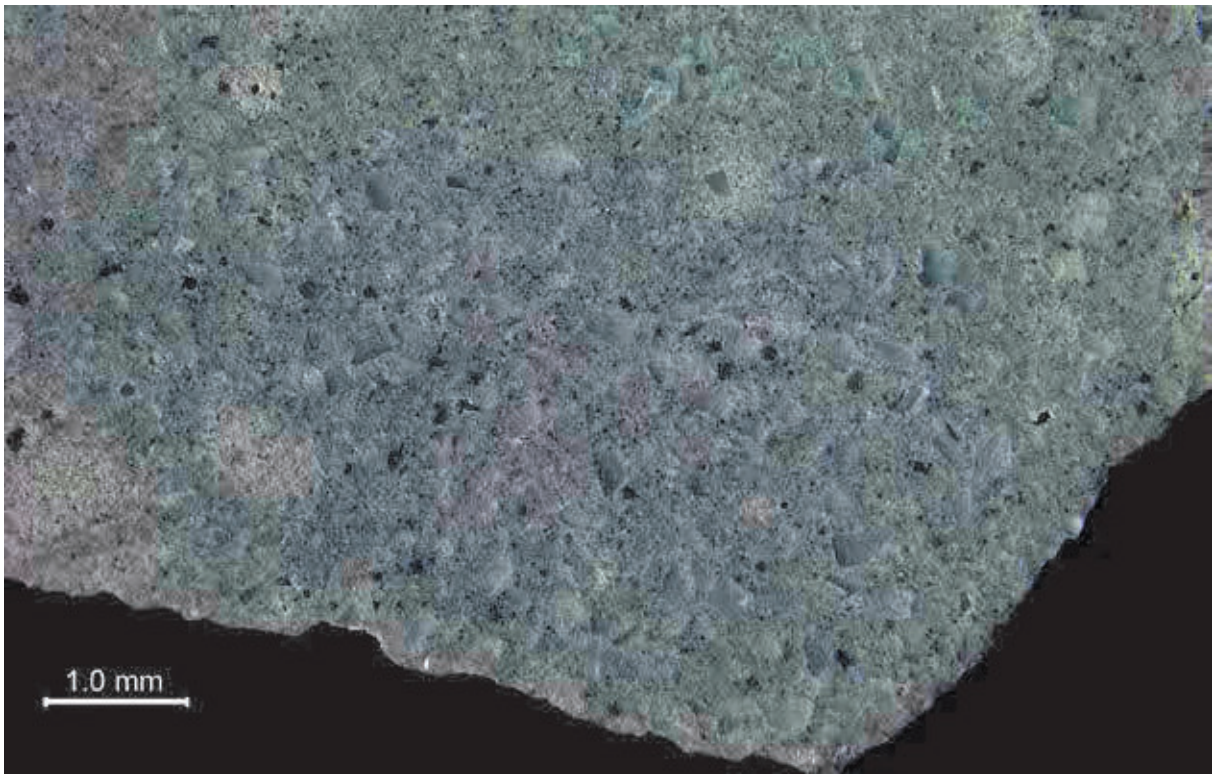

SAMPLE ID: C2 **DESCRIPTION:** An abundance of coarse carbonate flour particles (colorless and angular) near one edge of the sample in lapped profile.
MAG: 15x

PHOTO: 16

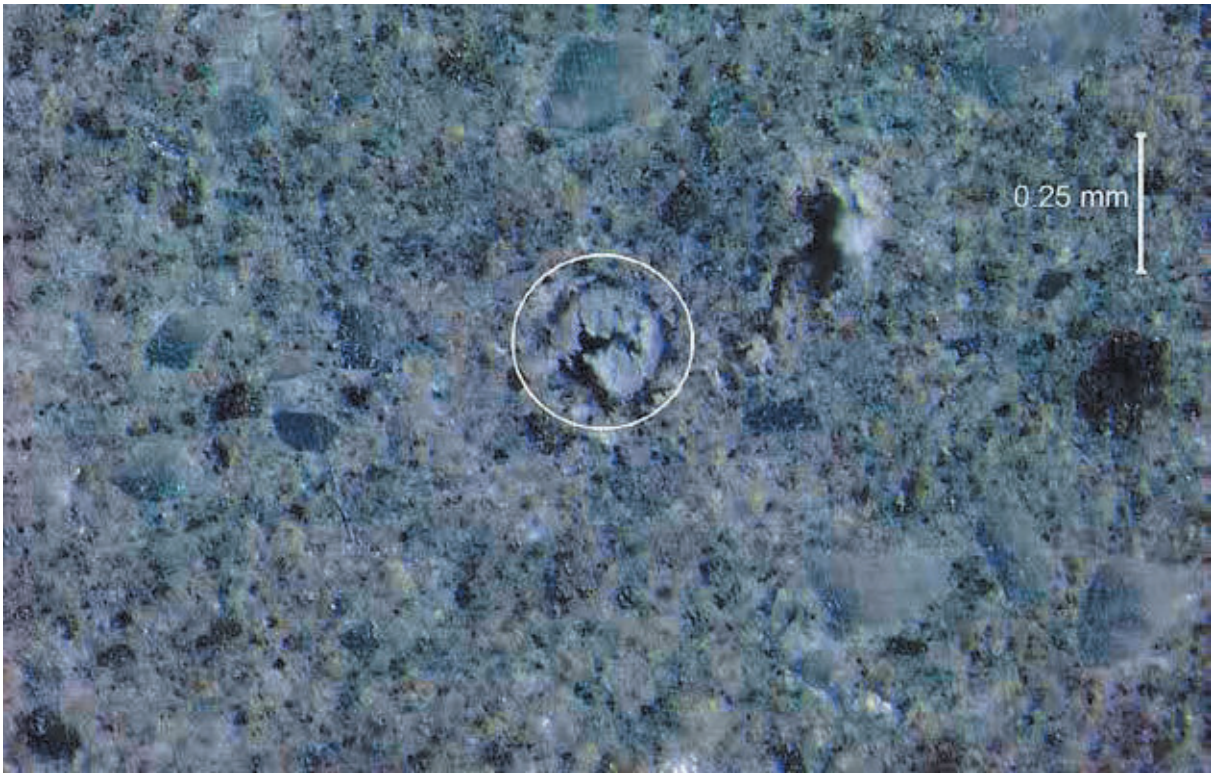

SAMPLE ID: C2 **DESCRIPTION:** Fine silica fume agglomeration (white circle) in lapped section of grout.
MAG: 75x

APS PROJECT NO: 10-08795 **DATE:** APRIL 21, 2016
PROJECT: CORROSION OF POST-TENSIONED TENDONS WITH EFFICIENT GROUT

PHOTO: 17

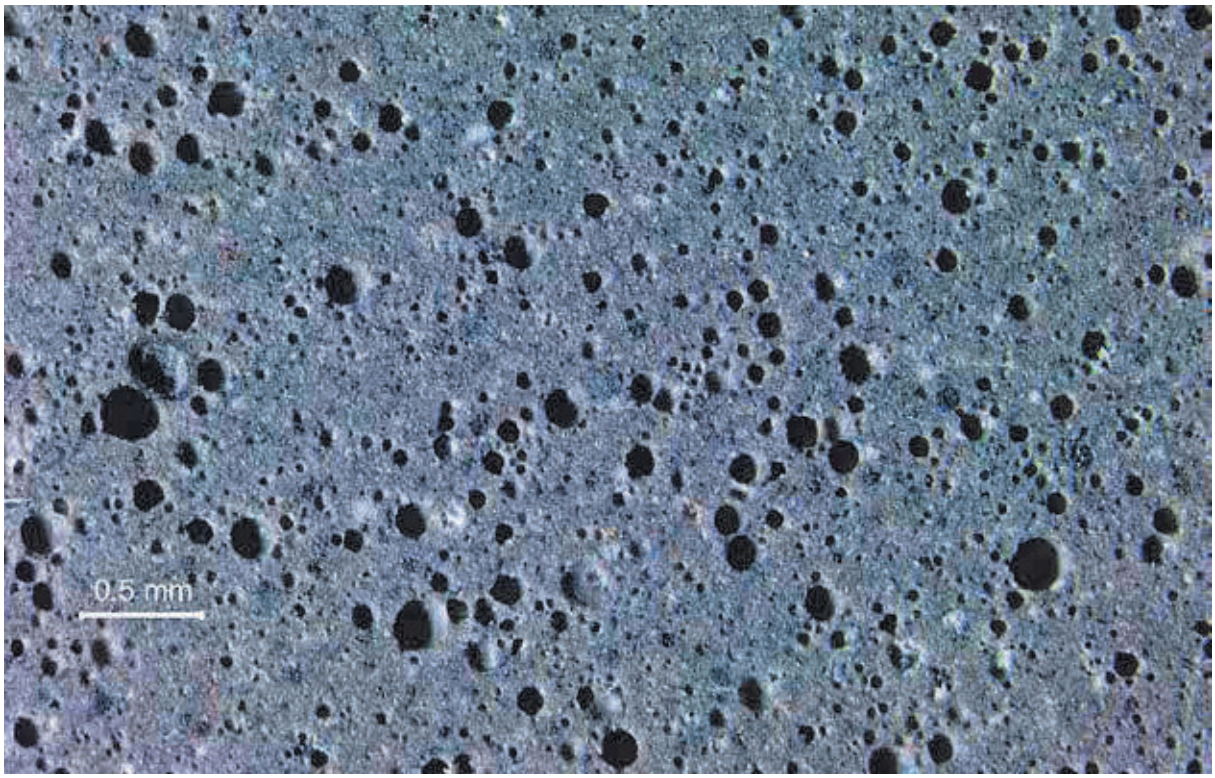

SAMPLE ID: EA **DESCRIPTION:** Lapped section of grout showing several spherical and entrained-sized air voids.
MAG: 30x

PHOTO: 18

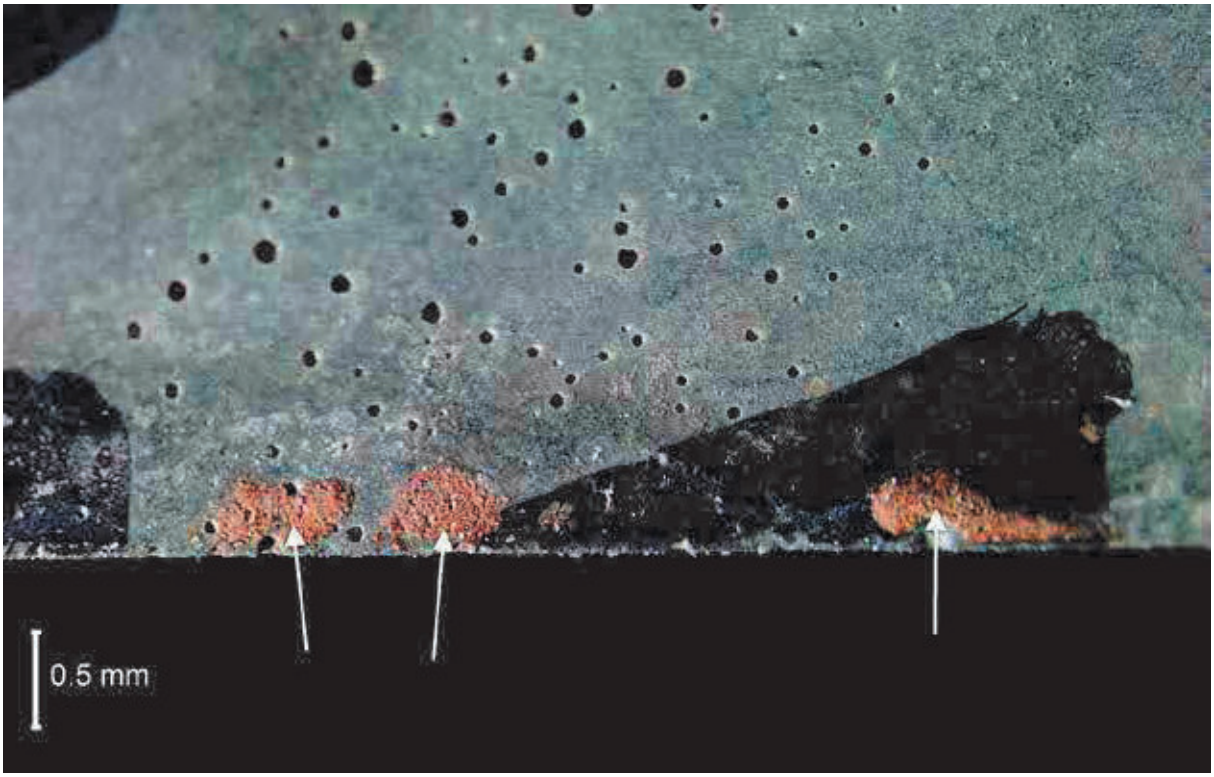

SAMPLE ID: EA **DESCRIPTION:** Brownish-colored corrosion product (white arrows) on the formed edge of the sample.
MAG: 25x

APS PROJECT NO: 10-08795 **DATE:** APRIL 21, 2016
PROJECT: CORROSION OF POST-TENSIONED TENDONS WITH EFFICIENT GROUT

PHOTO: 19

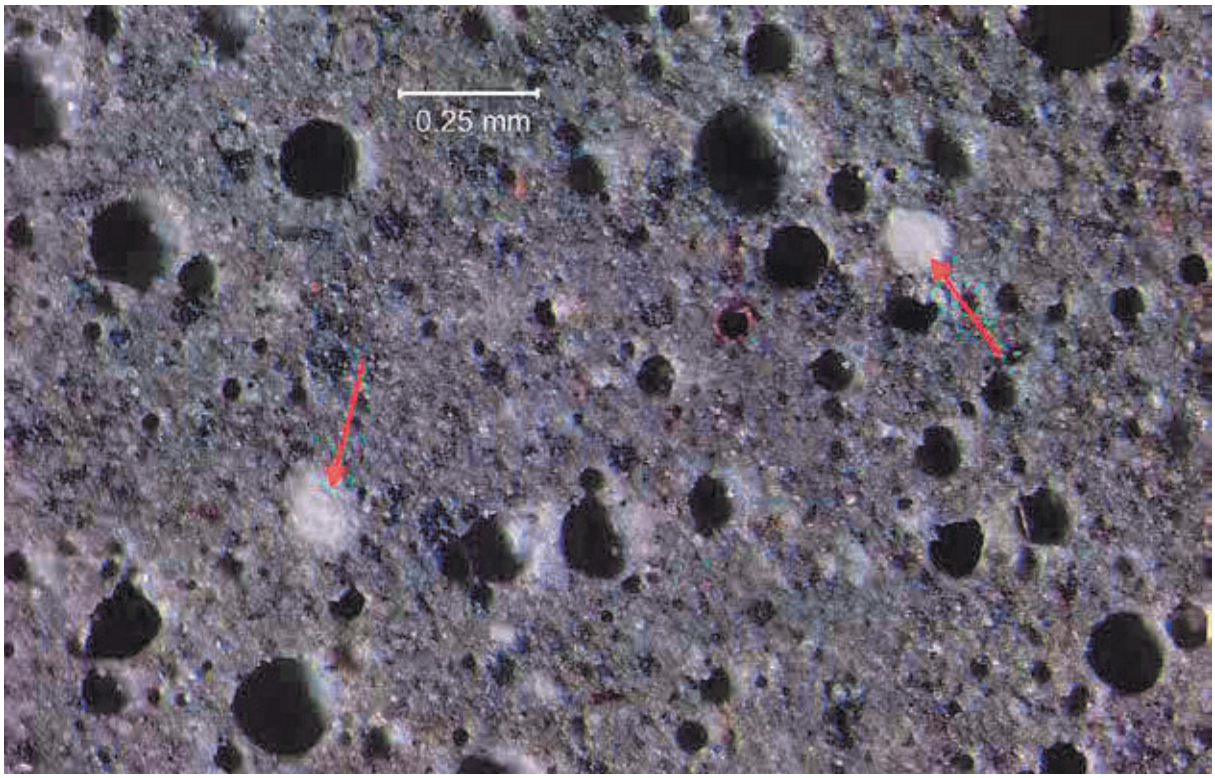

SAMPLE ID: EA **DESCRIPTION:** White-colored lime nodules (red arrows) in lapped section of grout.
MAG: 75x

PHOTO: 20

SAMPLE ID: EA **DESCRIPTION:** Overall view of lapped section of grout under low magnification.
MAG: 10x

APS PROJECT NO: 10-08795 **DATE:** APRIL 21, 2016

PROJECT: CORROSION OF POST-TENSIONED TENDONS WITH EFFICIENT GROUT

PHOTO: 21

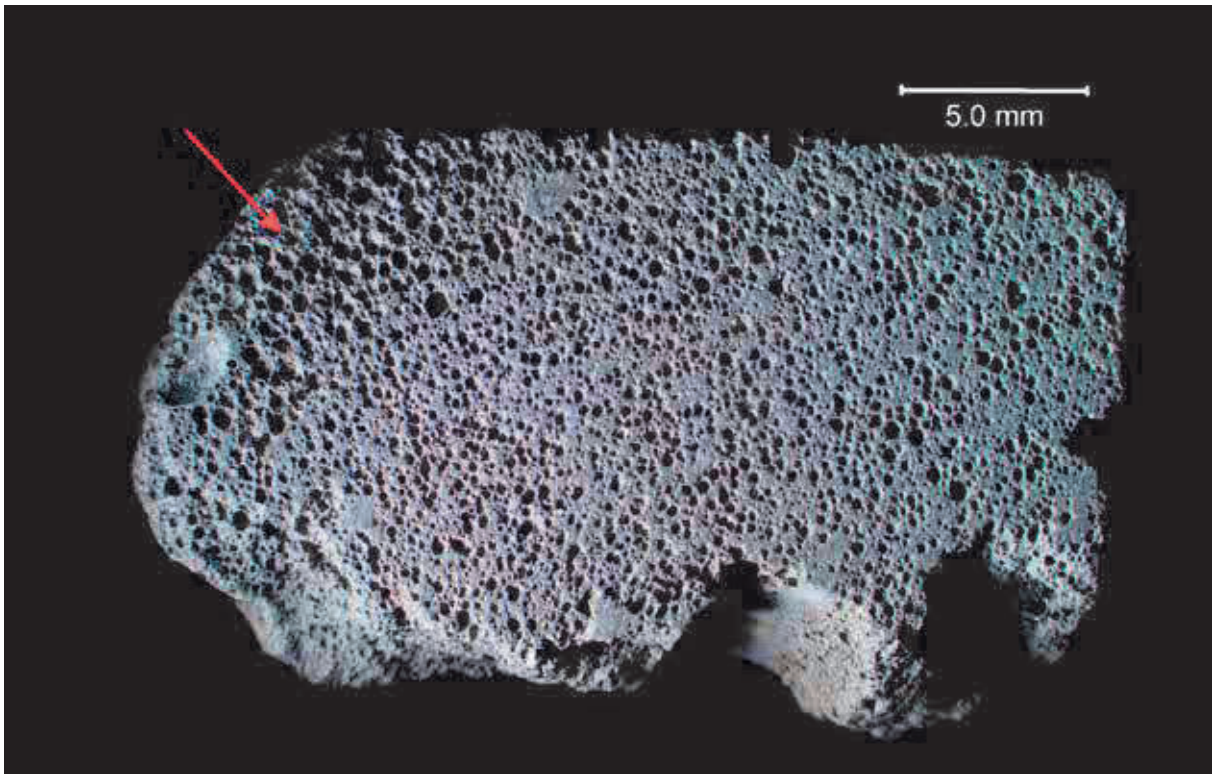

SAMPLE ID: EE1 **DESCRIPTION:** Overall view of lapped grout section showing abundant spherical and entrained-sized voids. A concentration of coarser voids was present near one edge of the sample (red arrow).

MAG: 5x

PHOTO: 22

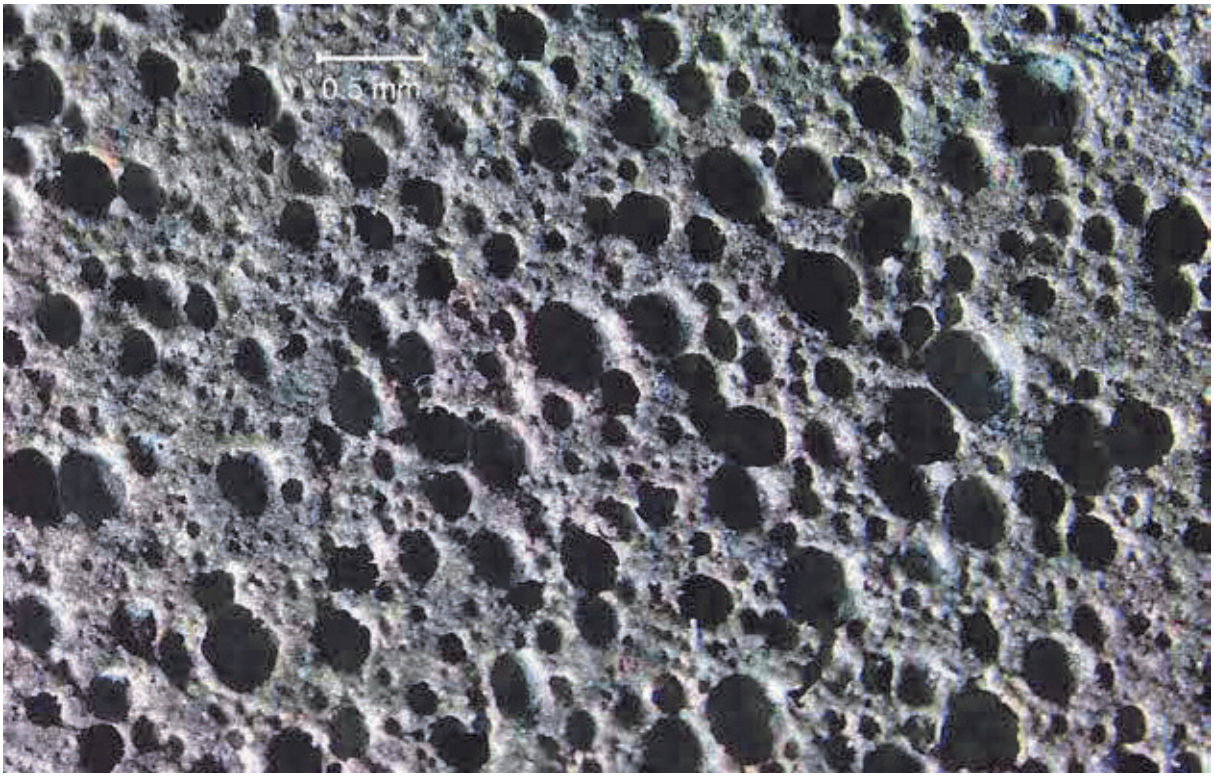

SAMPLE ID: EE1 **DESCRIPTION:** More magnified view of lapped section showing abundant entrained-sized air voids.

MAG: 30x

APS PROJECT NO: 10-08795 **DATE:** APRIL 21, 2016

PROJECT: CORROSION OF POST-TENSIONED TENDONS WITH EFFICIENT GROUT

PHOTO: 23

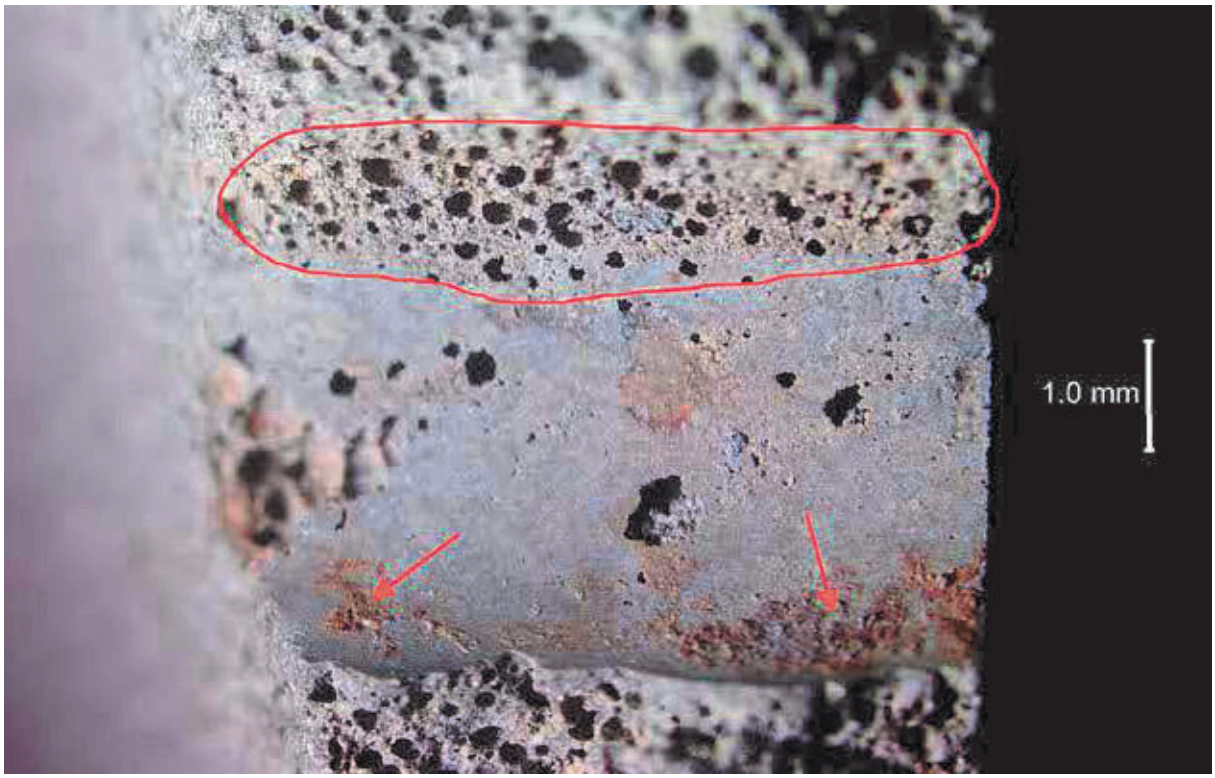

SAMPLE ID: EE1 **DESCRIPTION:** Formed tendon impression on a grout surface with several 'bug holes' (red outline) and some brownish-colored corrosion product (red arrows).

MAG: 15x

PHOTO: 24

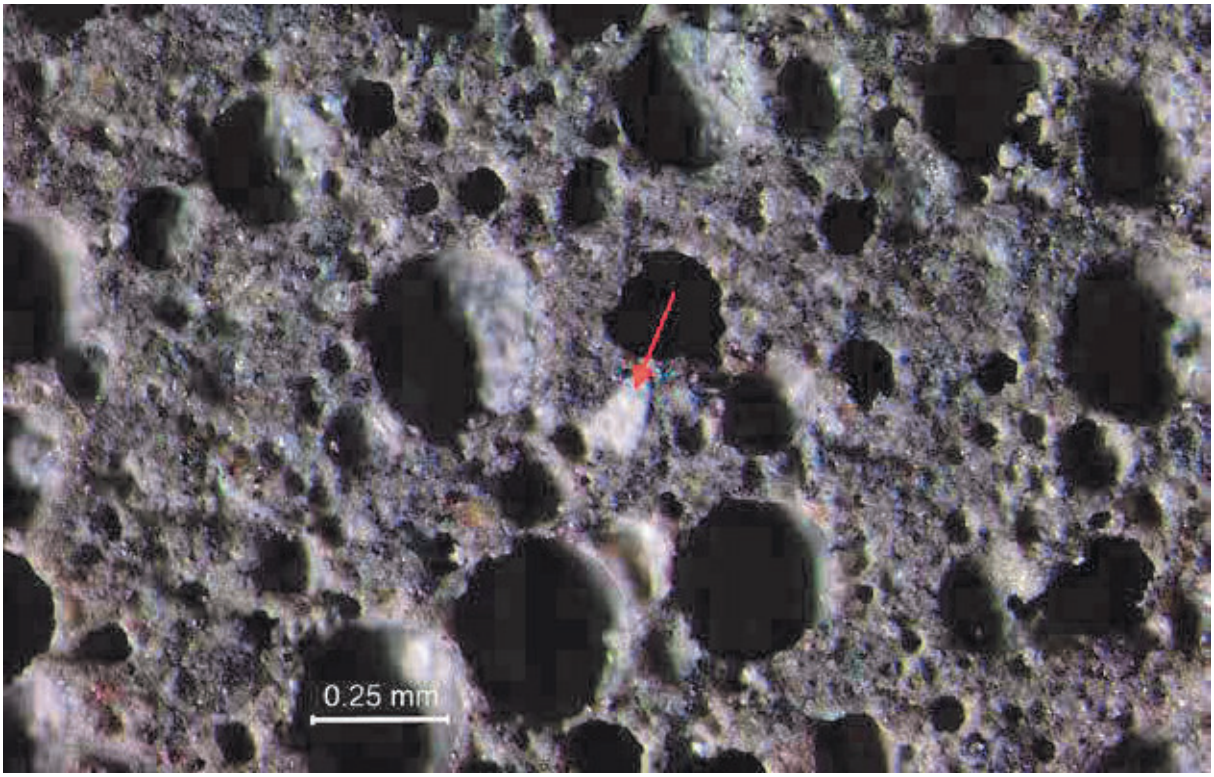

SAMPLE ID: EE1 **DESCRIPTION:** White-colored lime nodule (red arrow) in lapped section of grout.

MAG: 75x

APS PROJECT NO: 10-08795 **DATE:** APRIL 21, 2016
PROJECT: CORROSION OF POST-TENSIONED TENDONS WITH EFFICIENT GROUT

PHOTO: 25

SAMPLE ID: EE2 **DESCRIPTION:** Overall view of lapped section of grout.
MAG: 10x

PHOTO: 26

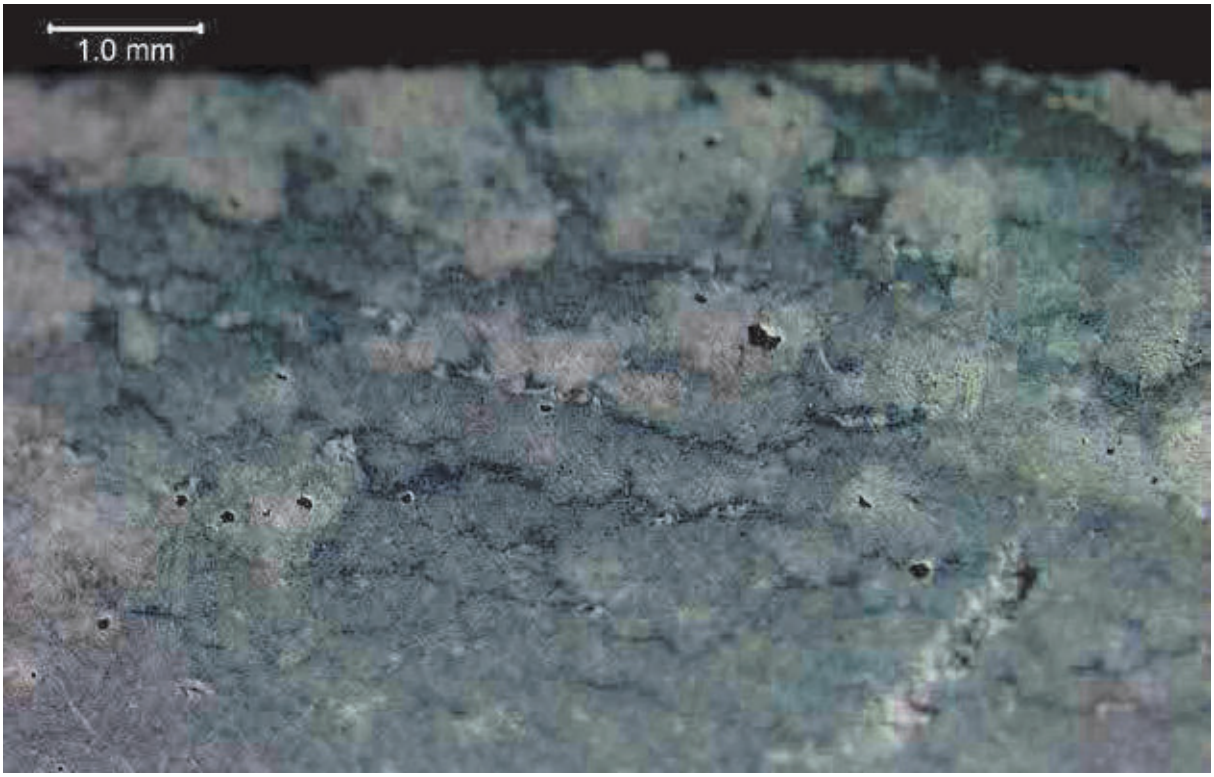

SAMPLE ID: EE2 **DESCRIPTION:** Variegated texture of paste on the formed surface of grout sample.
MAG: 20x

APS PROJECT NO: 10-08795 **DATE:** APRIL 21, 2016
PROJECT: CORROSION OF POST-TENSIONED TENDONS WITH EFFICIENT GROUT

PHOTO: 27

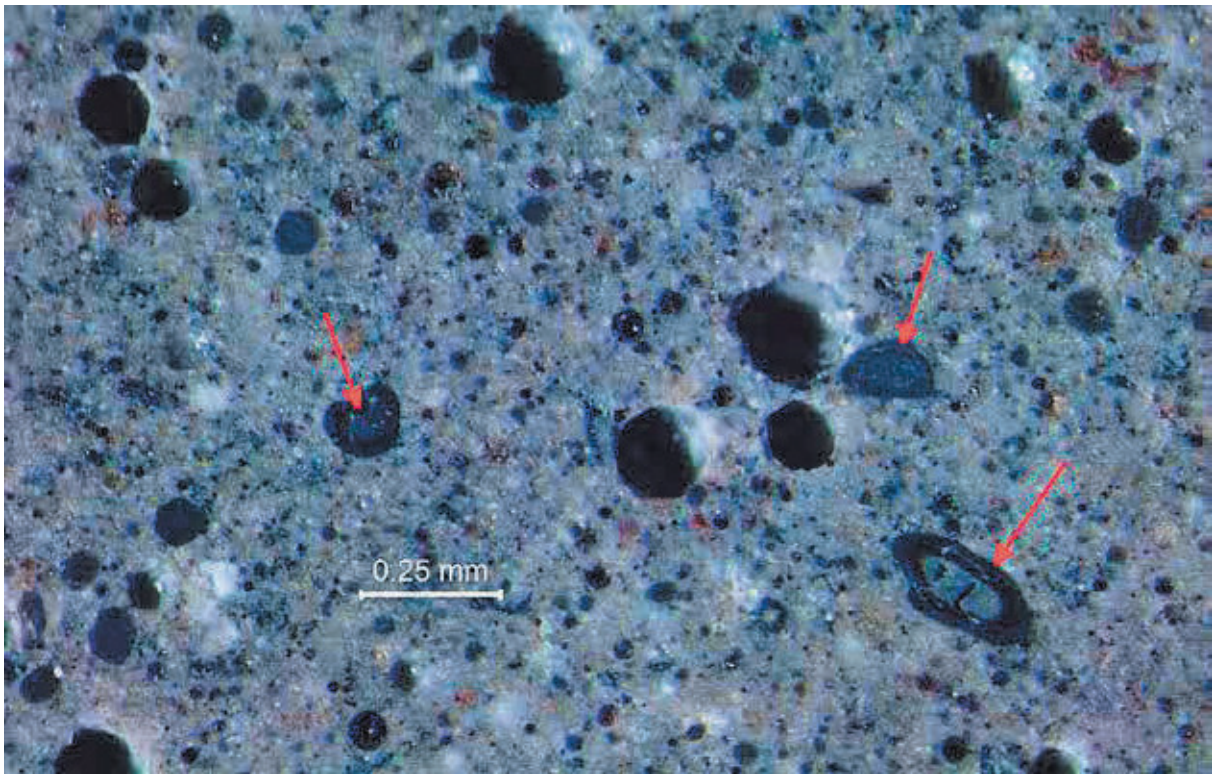

SAMPLE ID: EE2 **DESCRIPTION:** Silica fume agglomerations (red arrows) in lapped section of grout.
MAG: 75x

PHOTO: 28

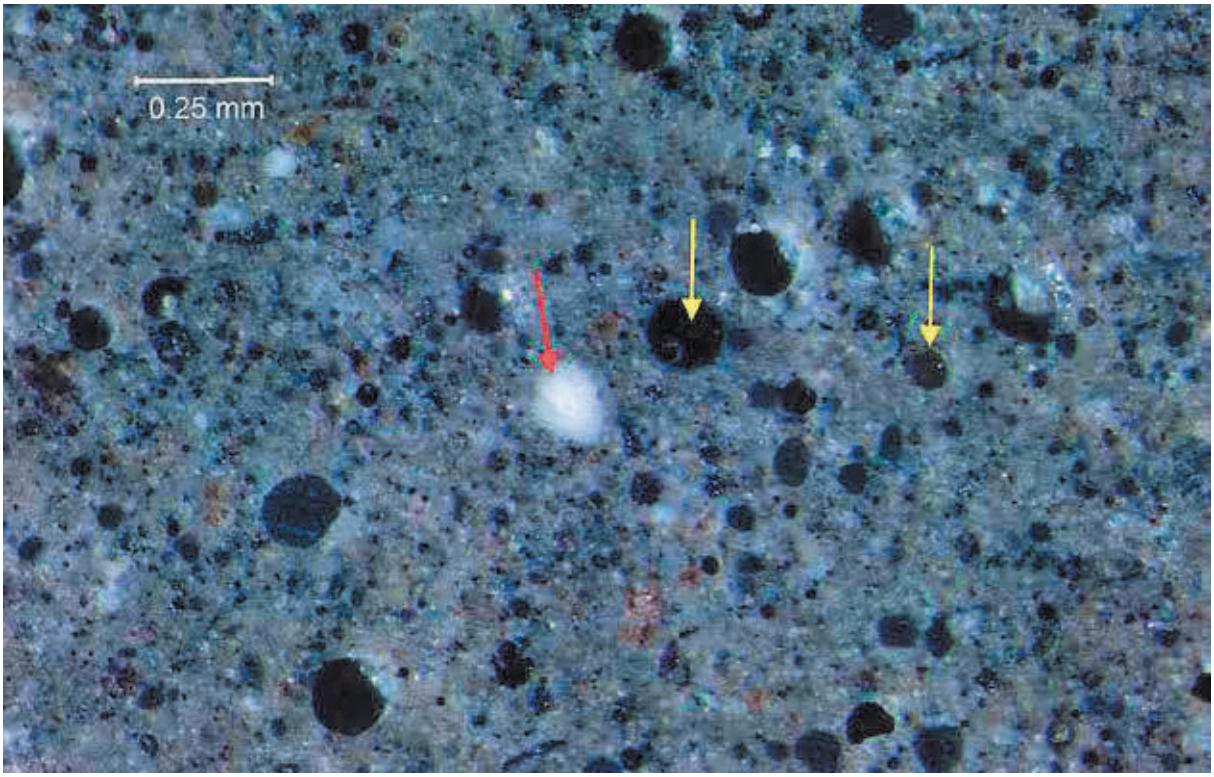

SAMPLE ID: EE2 **DESCRIPTION:** White lime nodule (red arrow) and dark and spherical fly ash particles (yellow arrows)
MAG: 75x in lapped section of grout.

APS PROJECT NO: 10-08795 **DATE:** APRIL 21, 2016
PROJECT: CORROSION OF POST-TENSIONED TENDONS WITH EFFICIENT GROUT

PHOTO: 29

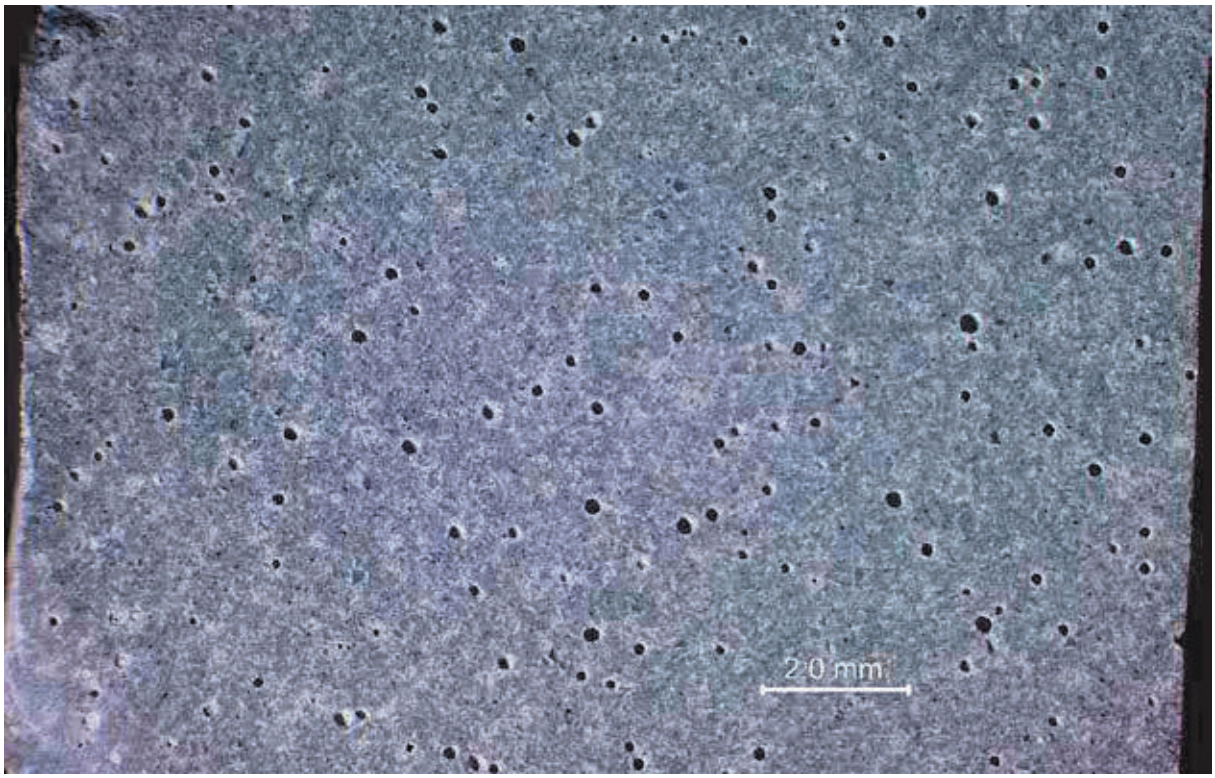

SAMPLE ID: SA **DESCRIPTION:** View of lapped section of grout showing a few fine, spherical, entrained-sized air voids.
MAG: 10x

PHOTO: 30

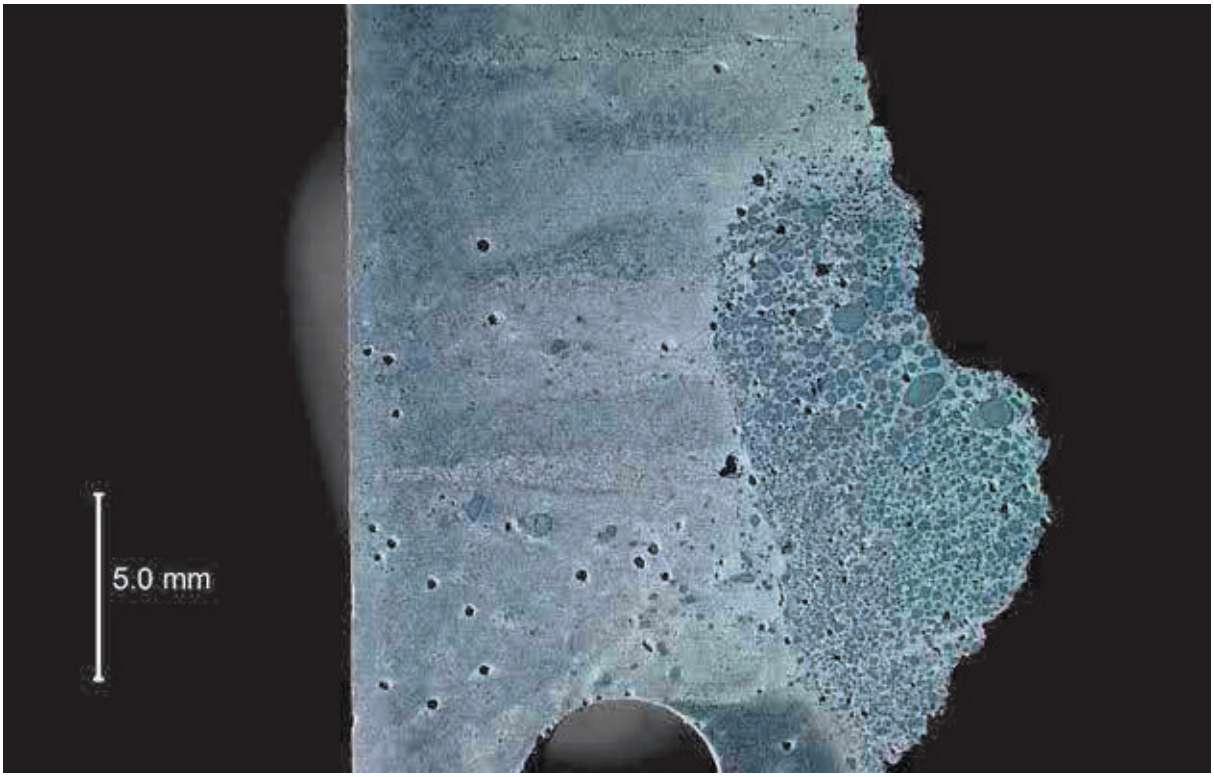

SAMPLE ID: SE1 **DESCRIPTION:** Lapped section of grout showing a cold joint which separates a silica fume-rich paste from a segregated grout of varying paste colors. A tendon impression is also present near the bottom of the photo.
MAG: 5x

APS PROJECT NO: 10-08795 **DATE:** APRIL 21, 2016
PROJECT: CORROSION OF POST-TENSIONED TENDONS WITH EFFICIENT GROUT

PHOTO: 31

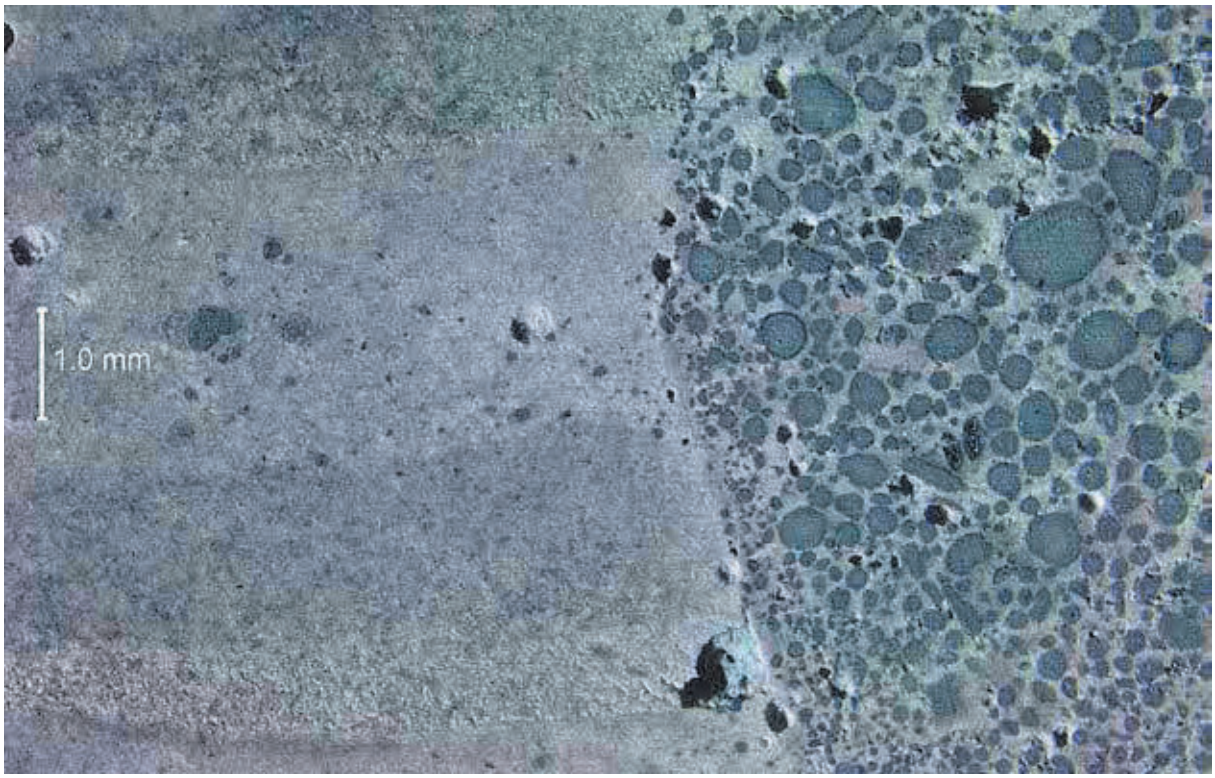

SAMPLE ID: SE1 **DESCRIPTION:** More magnified view of the cold joint and different-textured grout materials. The
MAG: 15x layering or segregation is apparent in the material on the left of the joint.

PHOTO: 32

SAMPLE ID: SE1 **DESCRIPTION:** Several 'bug holes' on the tendon impression surface of the sample.
MAG: 10x

APS PROJECT NO: 10-08795 **DATE:** APRIL 21, 2016

PROJECT: CORROSION OF POST-TENSIONED TENDONS WITH EFFICIENT GROUT

PHOTO: 33

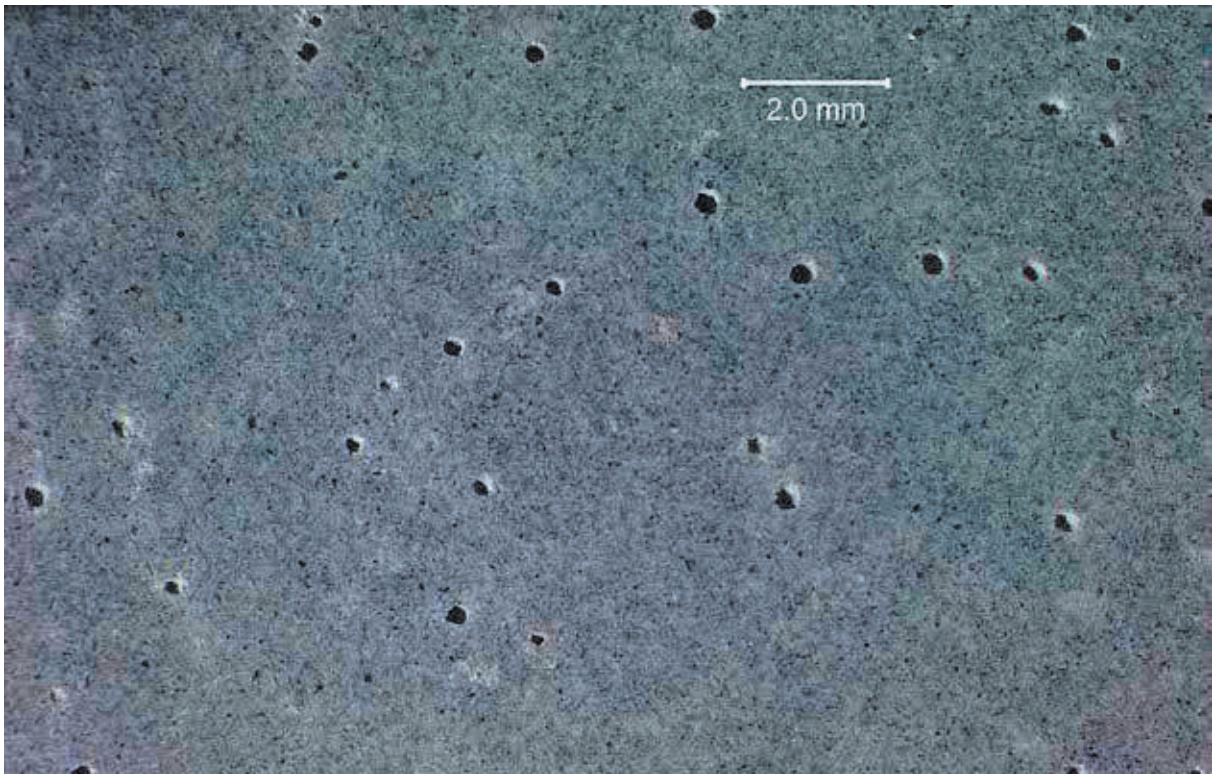

SAMPLE ID: SE2 **DESCRIPTION:** View of lapped grout section showing very few, very fine, spherical and entrained-sized air voids.
MAG: 10x

PHOTO: 34

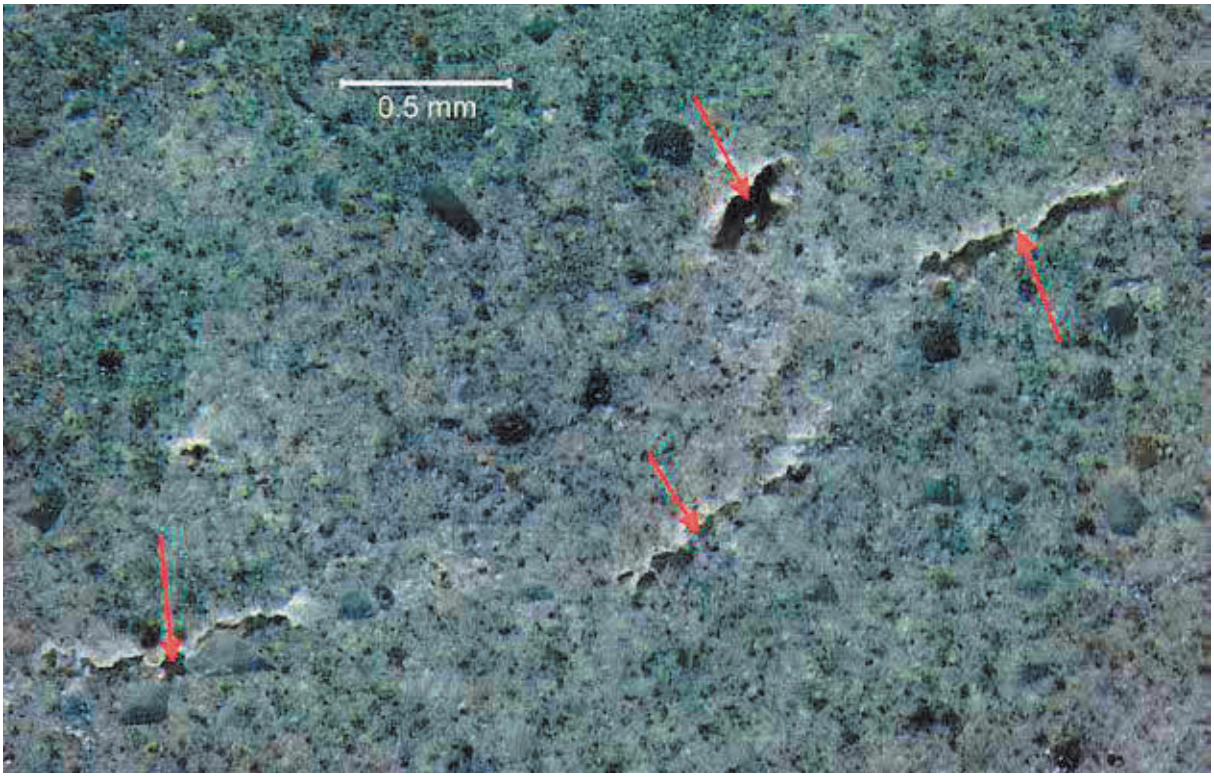

SAMPLE ID: SE2 **DESCRIPTION:** A few fine channel-shaped voids (red arrows) in lapped section of grout.
MAG: 50x

APS PROJECT NO: 10-08795 **DATE:** APRIL 21, 2016

PROJECT: CORROSION OF POST-TENSIONED TENDONS WITH EFFICIENT GROUT

PHOTO: 35

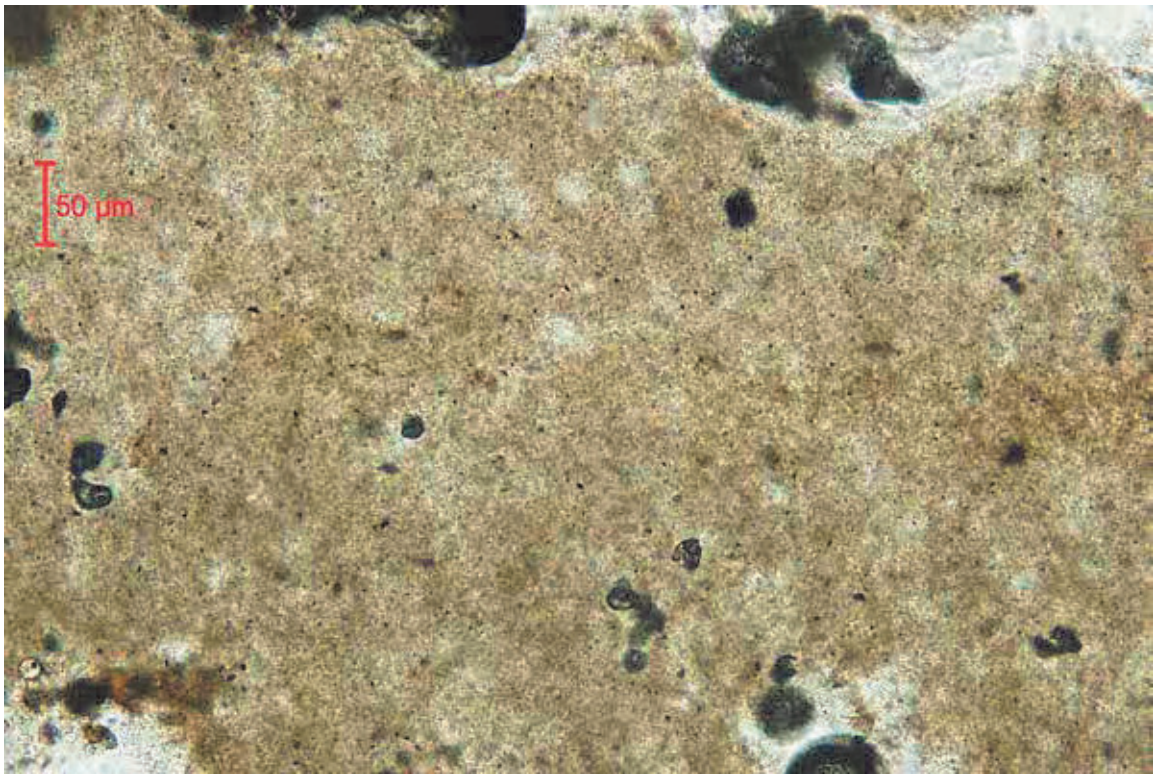

SAMPLE ID: C1 **DESCRIPTION:** View of grout in thin section under transmitted plane polarized light. Note the material is almost entirely composed of portlandite and apparent calcium silicate hydrate.

MAG: 200x

PHOTO: 36

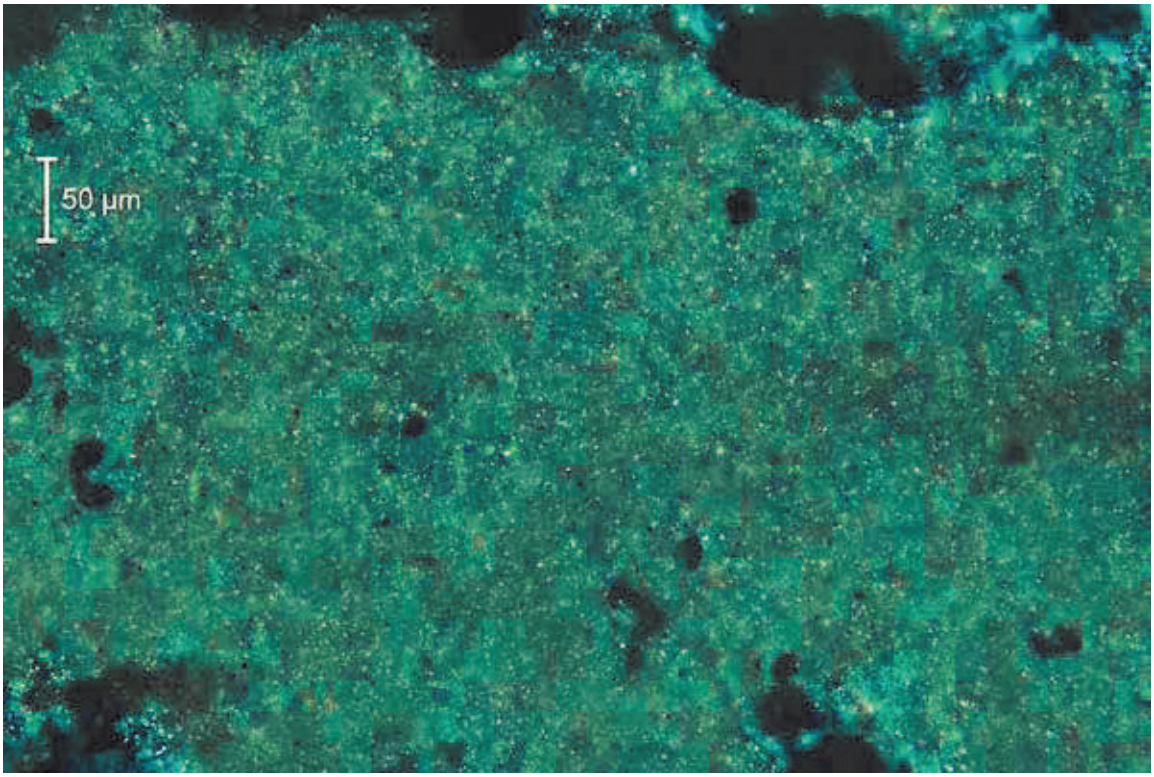

SAMPLE ID: C1 **DESCRIPTION:** Same view as above under transmitted cross polarized light.

MAG: 200x

APS PROJECT NO: 10-08795 **DATE:** APRIL 21, 2016
PROJECT: CORROSION OF POST-TENSIONED TENDONS WITH EFFICIENT GROUT

PHOTO: 37

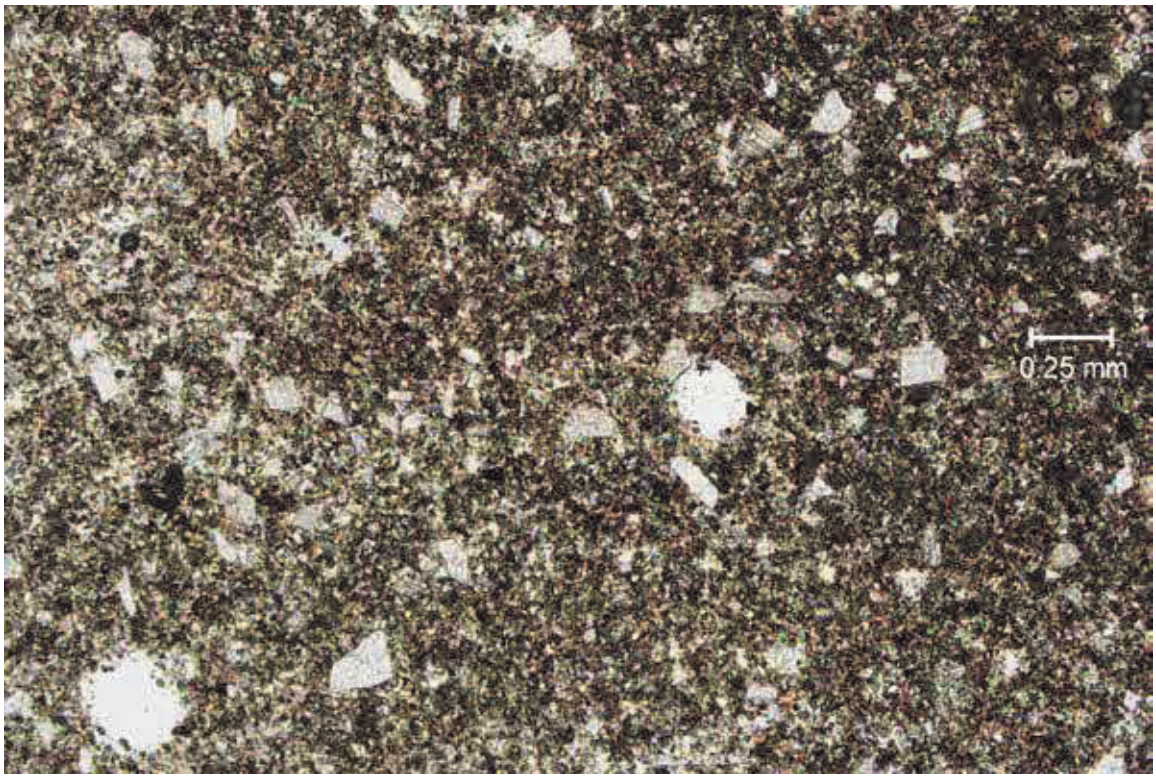

SAMPLE ID: C2 **DESCRIPTION:** Overall view of grout in thin section under transmitted plane polarized light.
MAG: 40x

PHOTO: 38

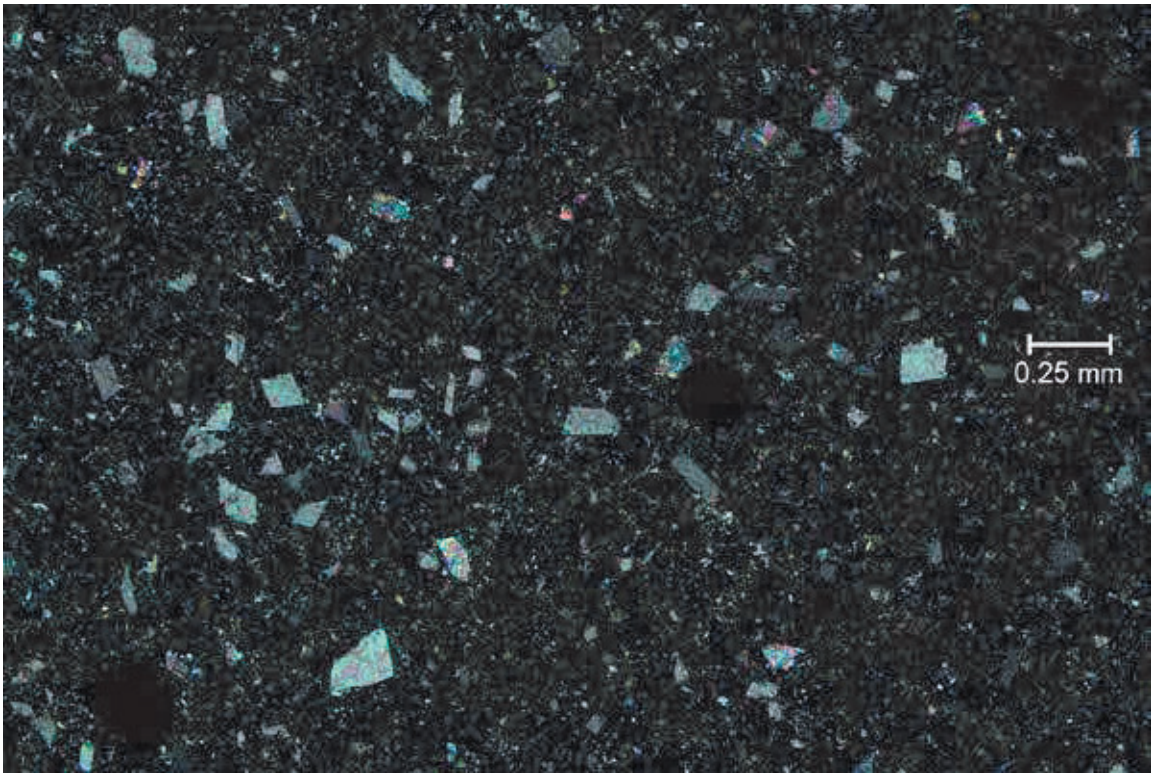

SAMPLE ID: C2 **DESCRIPTION:** Same view as above under transmitted cross polarized light. Note the brightly-colored
MAG: 40x carbonate flour particles and mostly isotropic (black) paste.

APS PROJECT NO: 10-08795 **DATE:** APRIL 21, 2016
PROJECT: CORROSION OF POST-TENSIONED TENDONS WITH EFFICIENT GROUT

PHOTO: 39

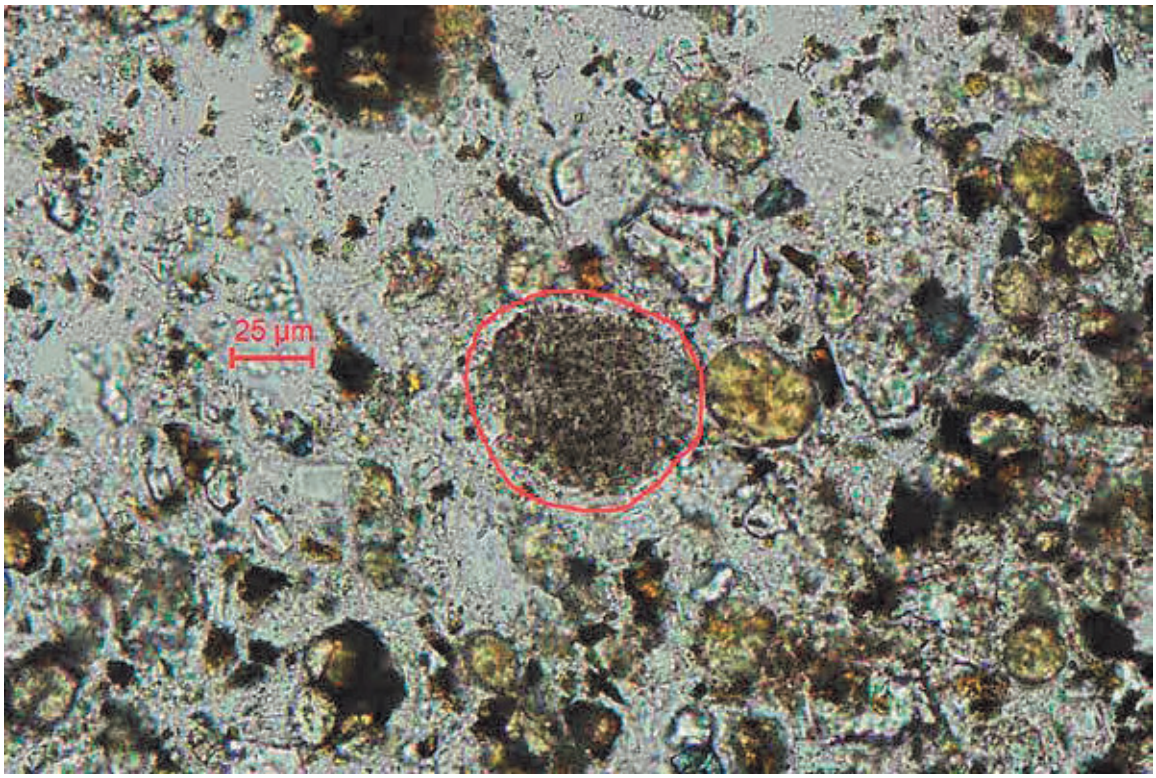

SAMPLE ID: C2
MAG: 400x
DESCRIPTION: Agglomeration of silica fume (red outline) in thin section of grout under transmitted plane polarized light.

PHOTO: 40

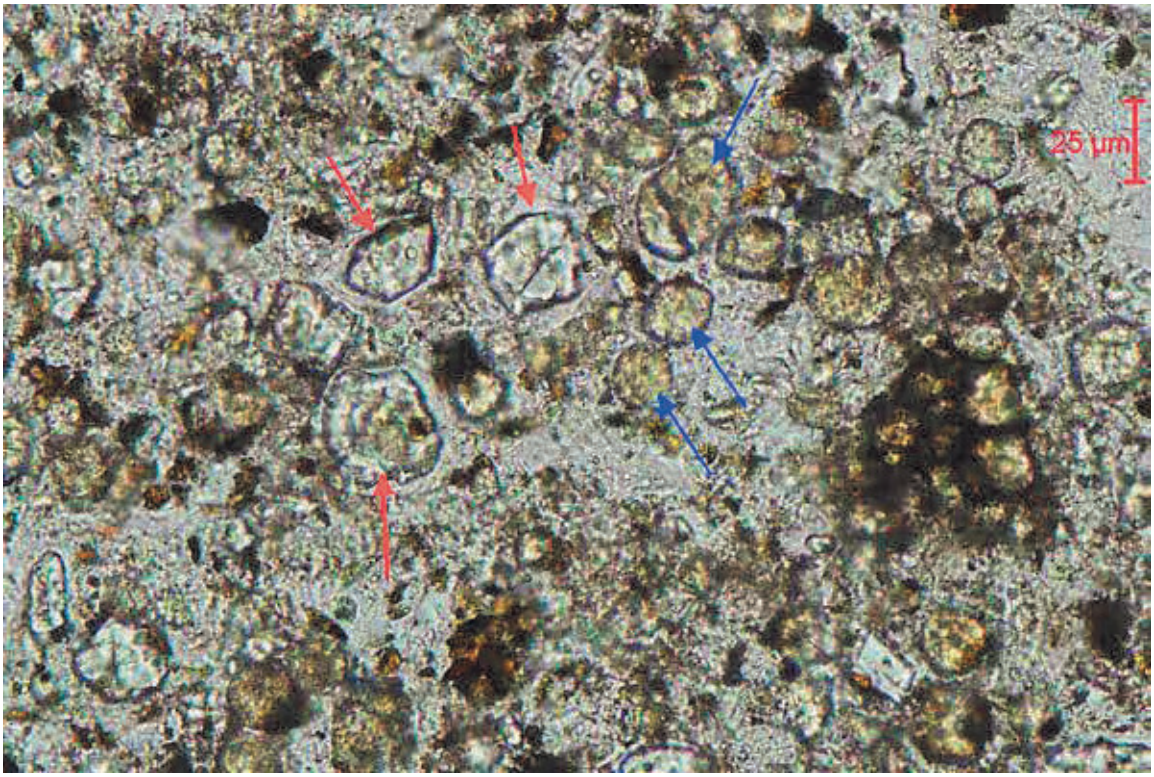

SAMPLE ID: C2
MAG: 400x
DESCRIPTION: Well hydrated alite portland cement clinker particles (red arrows) and low to moderately hydrated belite portland cement clinker particles (blue arrows) in thin section of grout under transmitted plane polarized light. Note the tight-packing of cement grains.

APS PROJECT NO: 10-08795 **DATE:** APRIL 21, 2016
PROJECT: CORROSION OF POST-TENSIONED TENDONS WITH EFFICIENT GROUT

PHOTO: 41

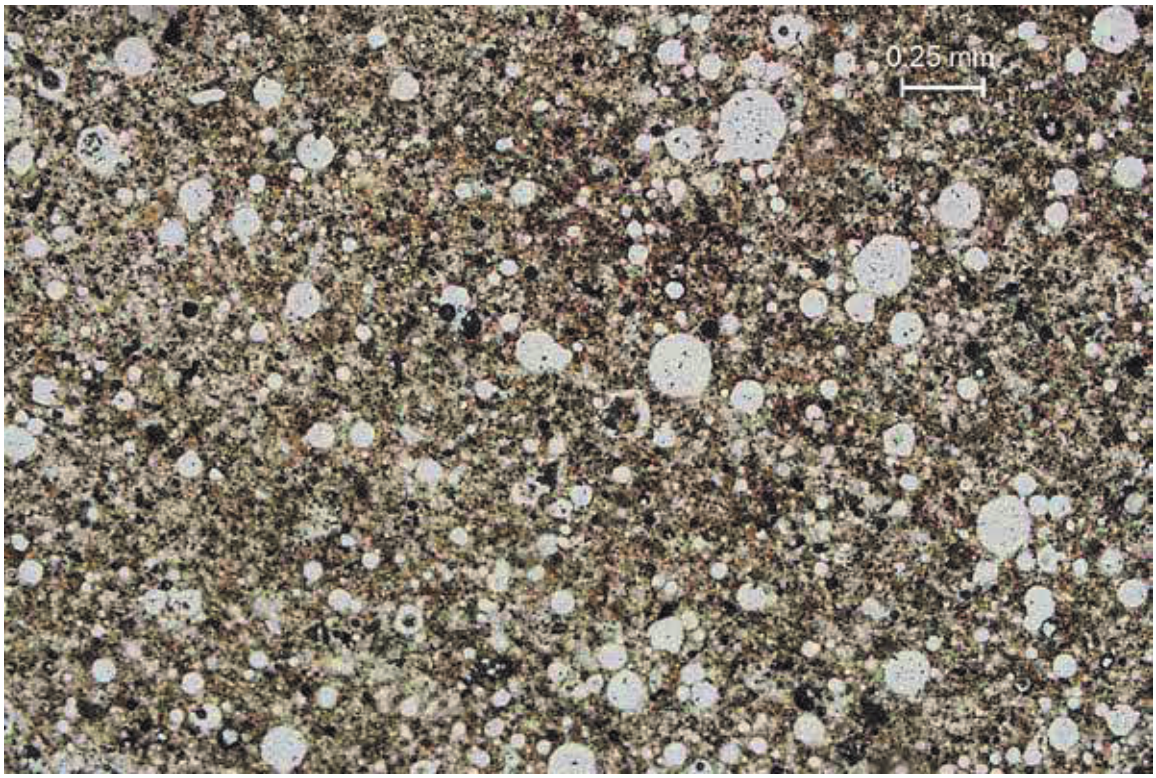

SAMPLE ID: EA **DESCRIPTION:** Overall view of grout in thin section under transmitted plane polarized light.
MAG: 40x

PHOTO: 42

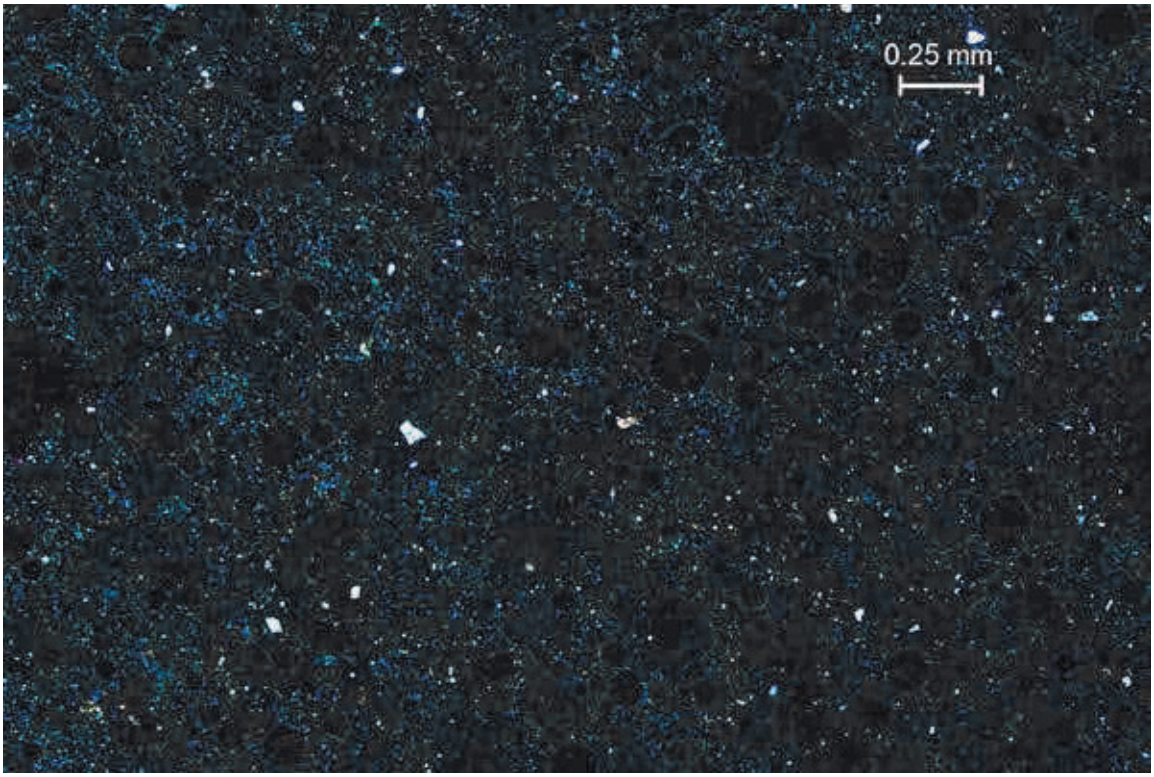

SAMPLE ID: EA **DESCRIPTION:** Same view as above under transmitted cross polarized light. Note the absence of carbonate flour.
MAG: 40x

APS PROJECT NO: 10-08795 **DATE:** APRIL 21, 2016
PROJECT: CORROSION OF POST-TENSIONED TENDONS WITH EFFICIENT GROUT

PHOTO: 43

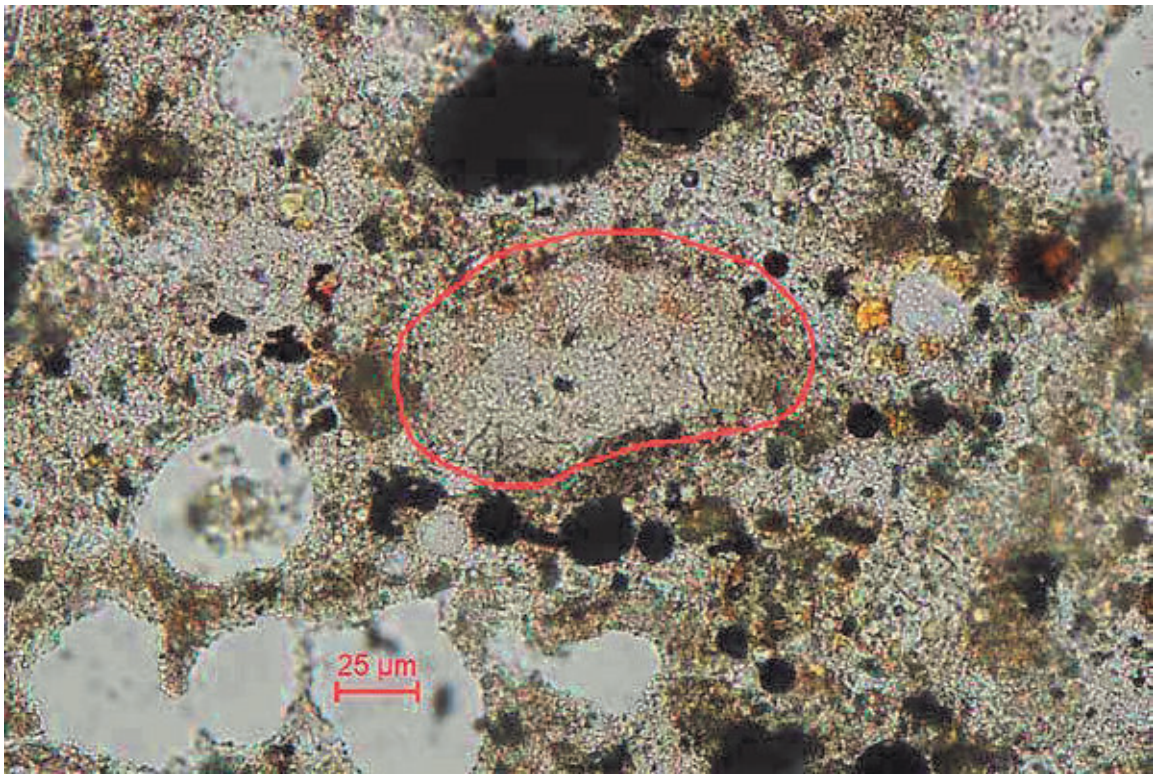

SAMPLE ID: EA **DESCRIPTION:** Hydrated lime nodule (red outline) in thin section of grout under transmitted plane polarized light.
MAG: 400x

PHOTO: 44

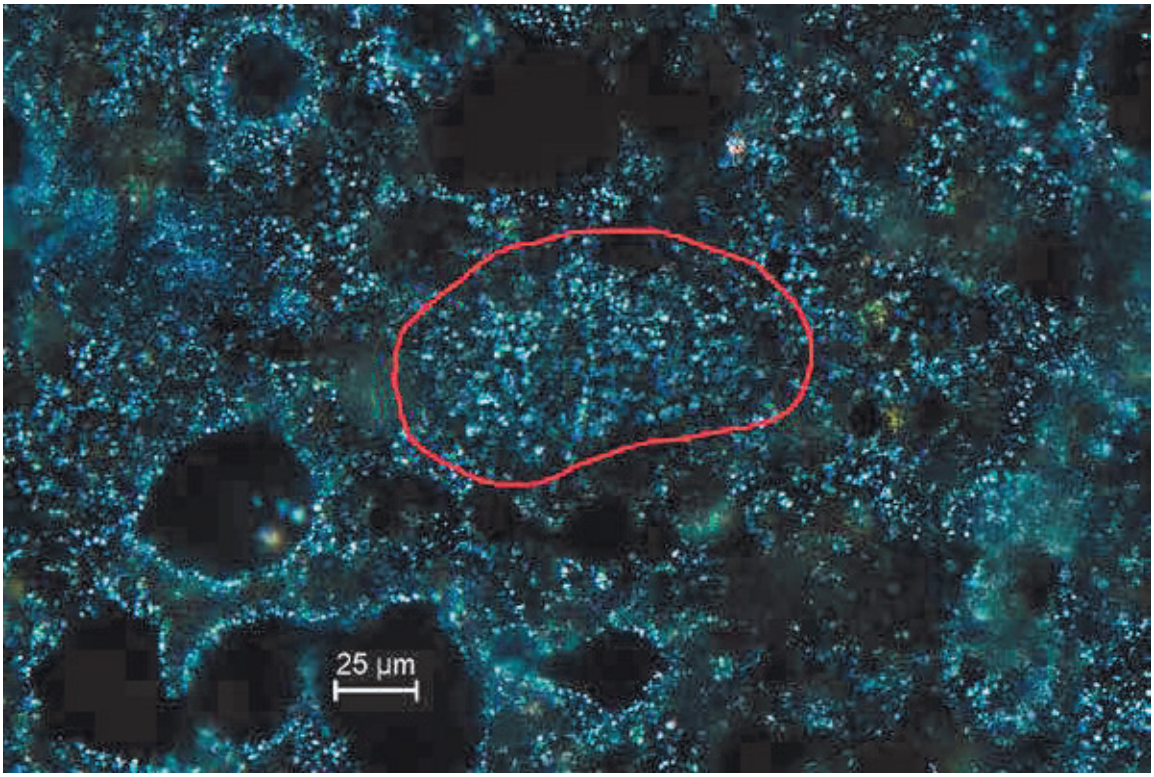

SAMPLE ID: EA **DESCRIPTION:** Same view as above under transmitted cross polarized light. Note the white to gray birefringence of the hydrated lime.
MAG: 400x

APS PROJECT NO: 10-08795 **DATE:** APRIL 21, 2016
PROJECT: CORROSION OF POST-TENSIONED TENDONS WITH EFFICIENT GROUT

PHOTO: 45

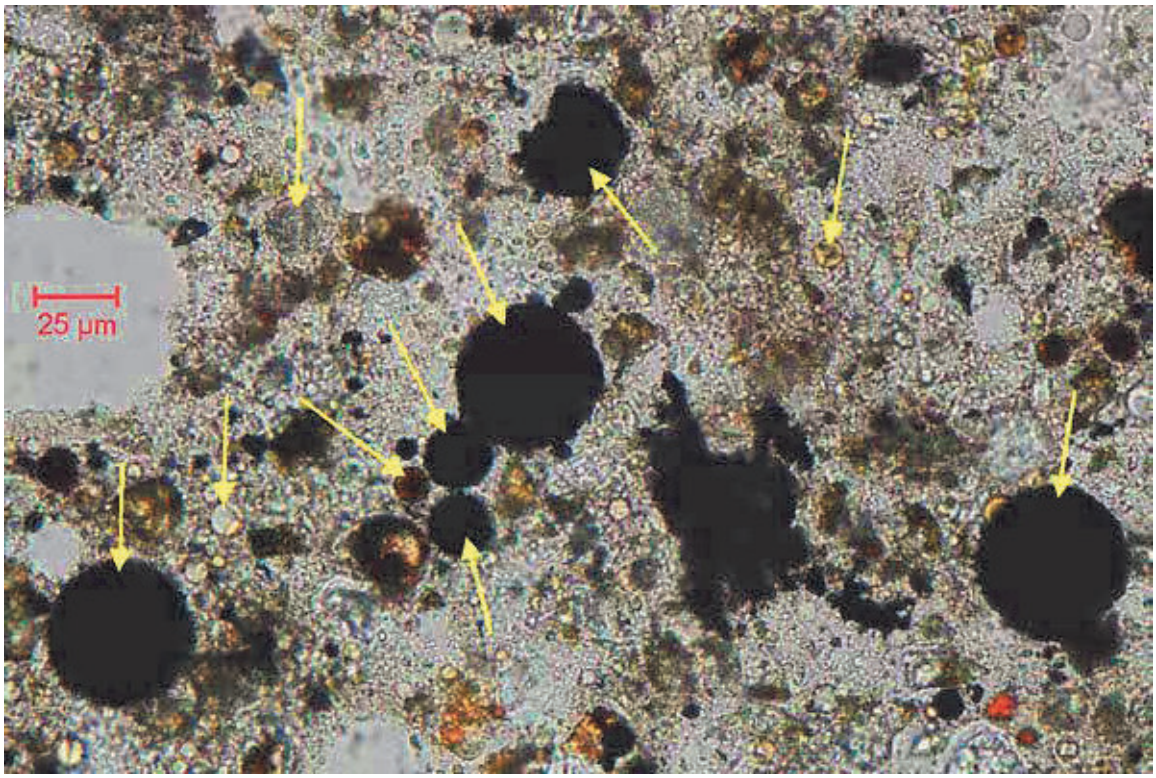

SAMPLE ID: EA **DESCRIPTION:** Abundant spherical and often dark-colored fly ash pozzolan particles (yellow arrows) in thin section of grout under transmitted plane polarized light.
MAG: 400x

PHOTO: 46

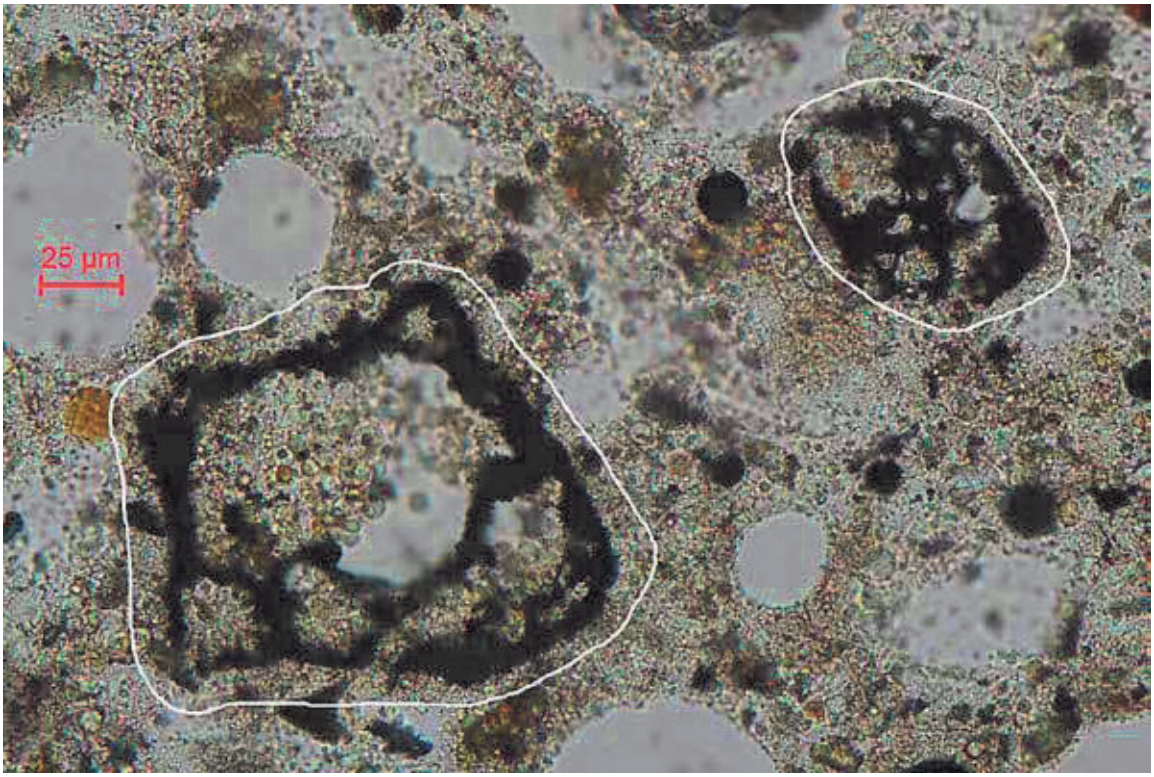

SAMPLE ID: EA **DESCRIPTION:** Opaque/black particles of carbon (white outlines) in thin section of grout under transmitted plane polarized light. The carbon was likely present in the fly ash.
MAG: 400x

APS PROJECT NO: 10-08795 **DATE:** APRIL 21, 2016
PROJECT: CORROSION OF POST-TENSIONED TENDONS WITH EFFICIENT GROUT

PHOTO: 47

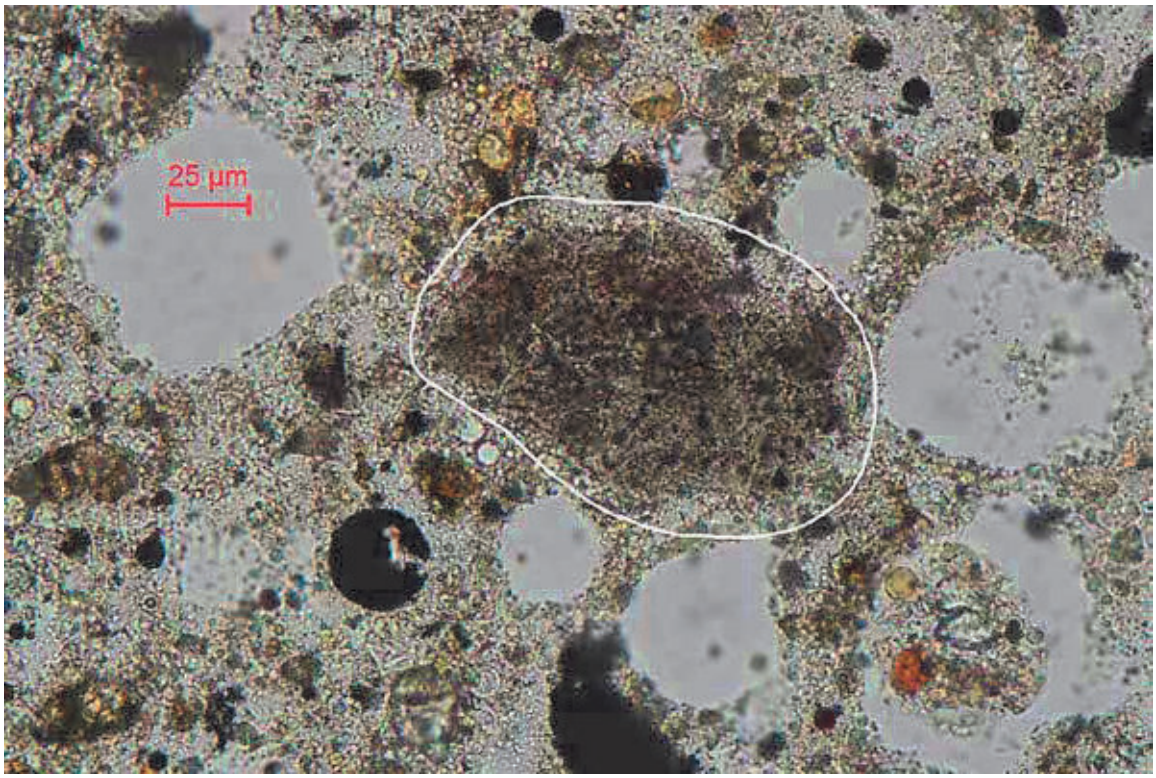

SAMPLE ID: EA **DESCRIPTION:** Silica fume agglomeration (white outline) in thin section of grout under transmitted plane polarized light.
MAG: 400x

PHOTO: 48

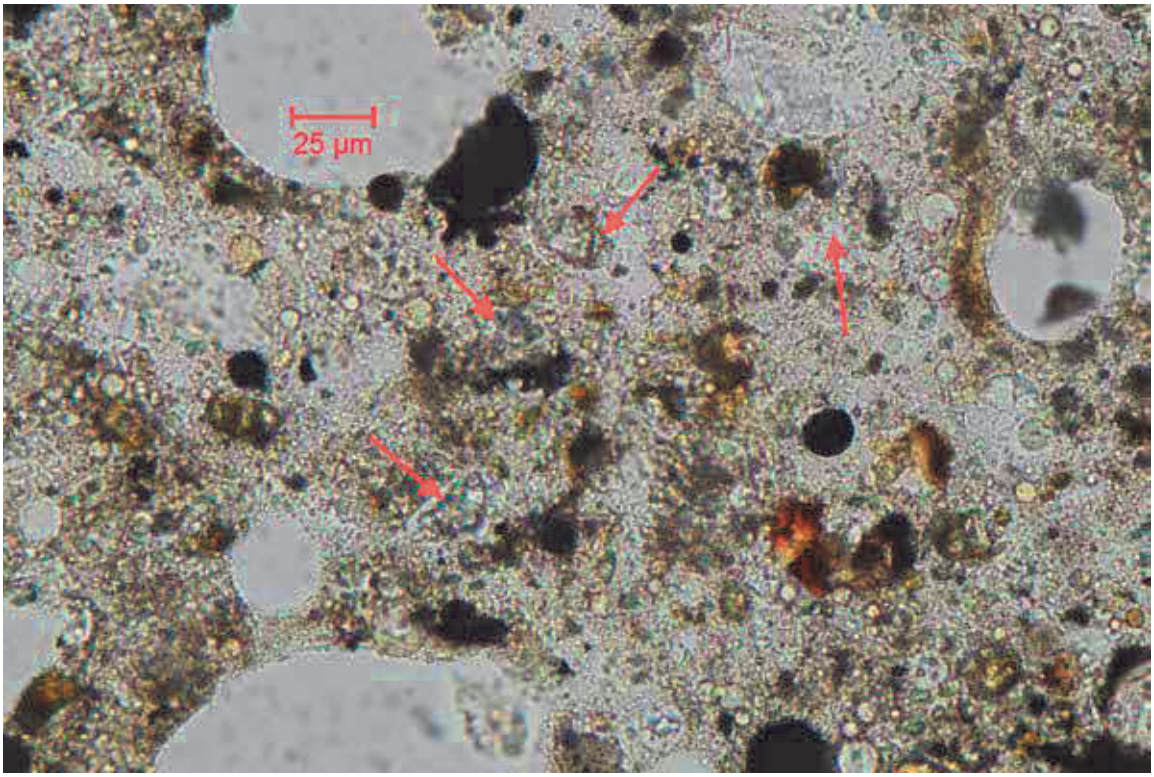

SAMPLE ID: EA **DESCRIPTION:** Well to fully hydrated alite portland cement clinker particles (red arrows) in thin section of grout under transmitted plane polarized light.
MAG: 400x

APS PROJECT NO: 10-08795 **DATE:** APRIL 21, 2016
PROJECT: CORROSION OF POST-TENSIONED TENDONS WITH EFFICIENT GROUT

PHOTO: 49

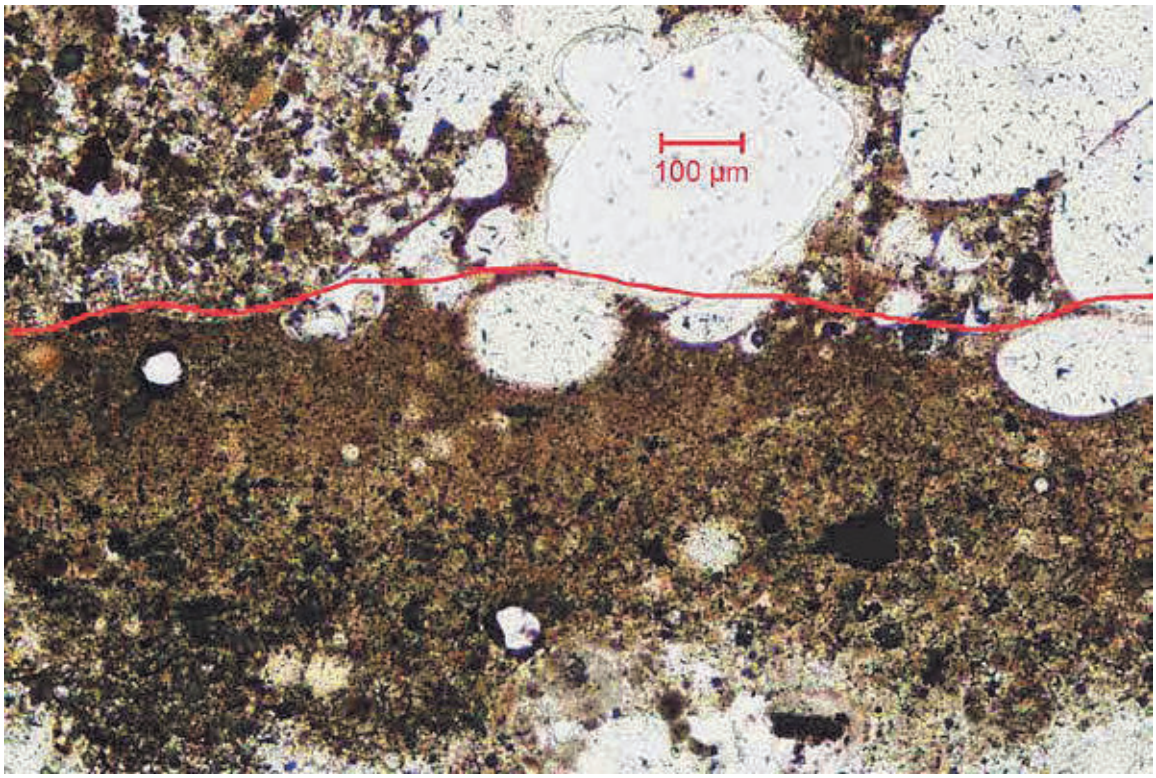

SAMPLE ID: EE1 **DESCRIPTION:** Apparent cold joint (red line) within grout in thin section under transmitted plane polarized light.
MAG: 100x

PHOTO: 50

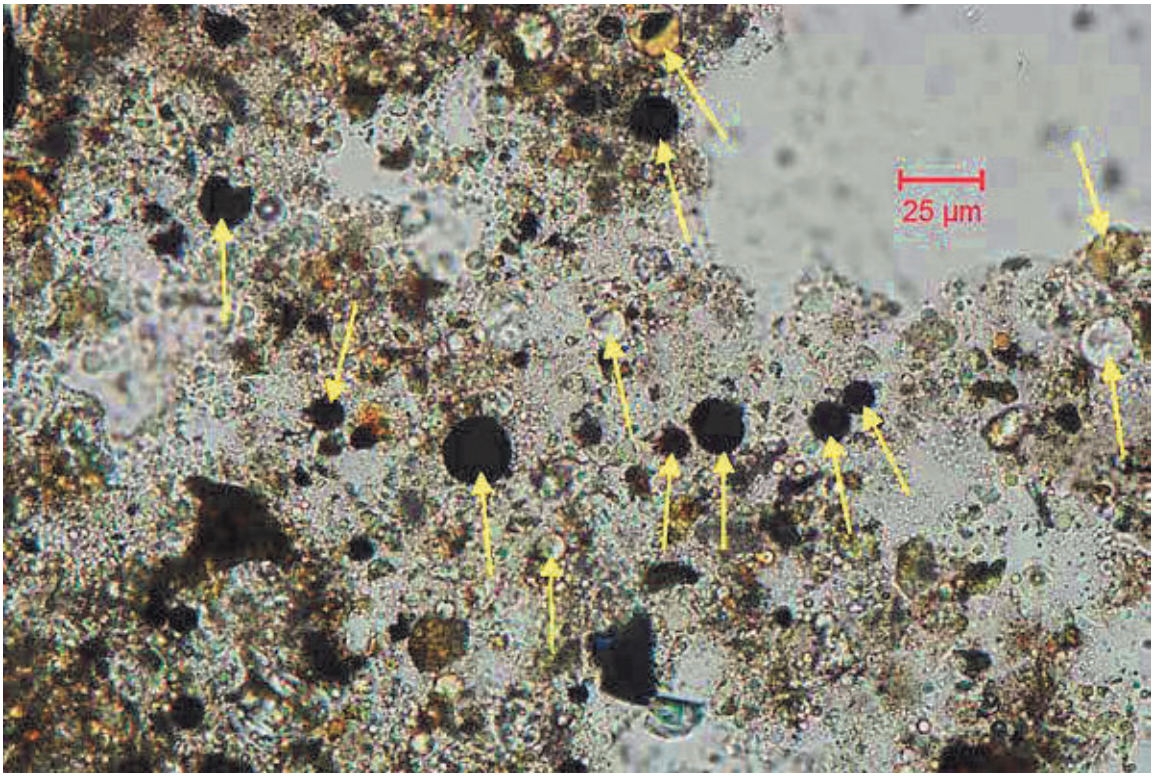

SAMPLE ID: EE1 **DESCRIPTION:** Abundant spherical fly ash pozzolan particles (yellow arrows) in thin section of grout under transmitted plane polarized light.
MAG: 400x

APS PROJECT NO: 10-08795 **DATE:** APRIL 21, 2016

PROJECT: CORROSION OF POST-TENSIONED TENDONS WITH EFFICIENT GROUT

PHOTO: 51

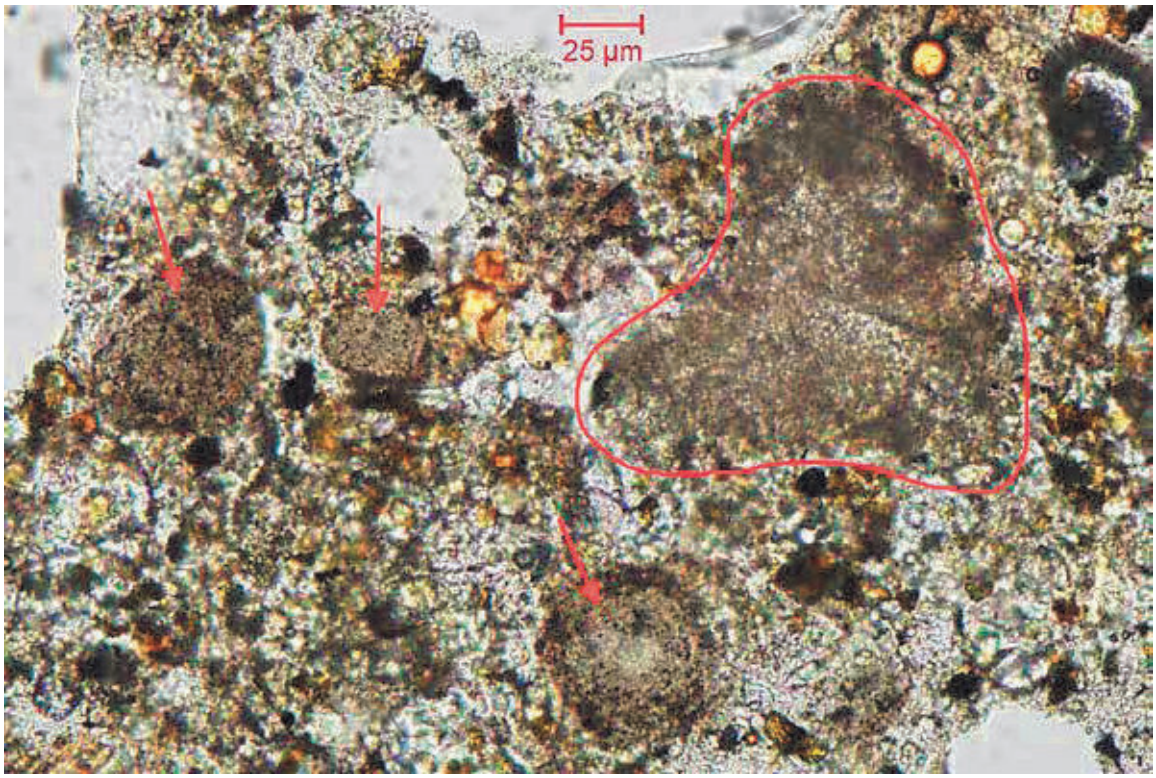

SAMPLE ID: EE1 **DESCRIPTION:** Silica fume nodules/agglomerations (red arrows) and hydrated lime nodule (red outline) in thin section of grout under transmitted plane polarized light.

MAG: 400x

PHOTO: 52

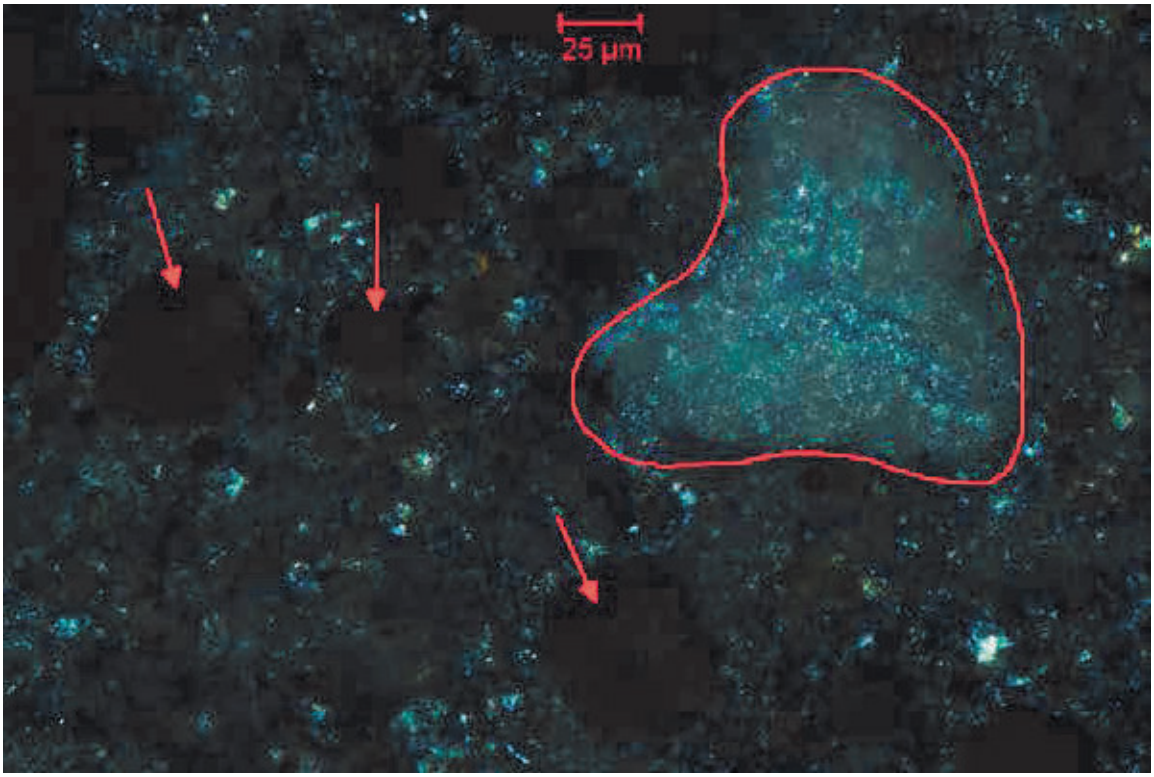

SAMPLE ID: EE1 **DESCRIPTION:** Same view as above under transmitted cross polarized light. Note the silica fume is isotropic or black and the hydrated lime shows white to gray-colored birefringence.

MAG: 400x

APS PROJECT NO: 10-08795 **DATE:** APRIL 21, 2016
PROJECT: CORROSION OF POST-TENSIONED TENDONS WITH EFFICIENT GROUT

PHOTO: 53

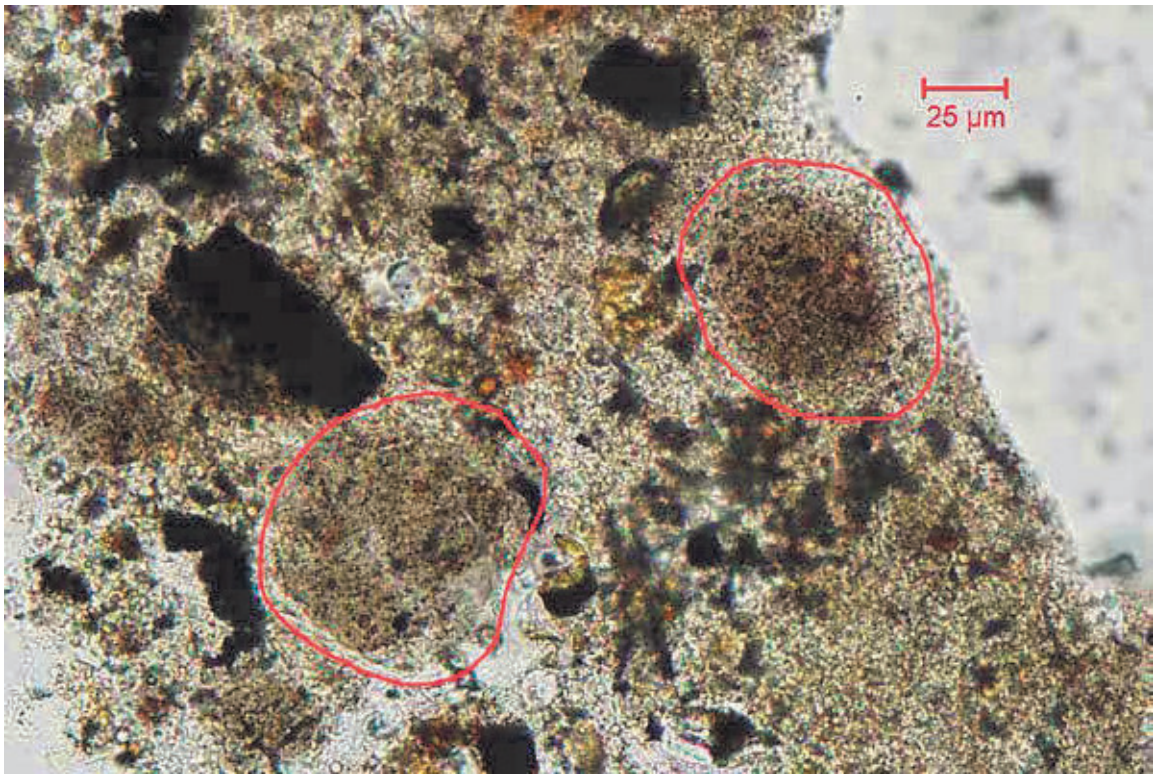

SAMPLE ID: EE1 **DESCRIPTION:** Silica fume agglomerations (red outlines) in thin section of grout under transmitted plane polarized light.
MAG: 400x

PHOTO: 54

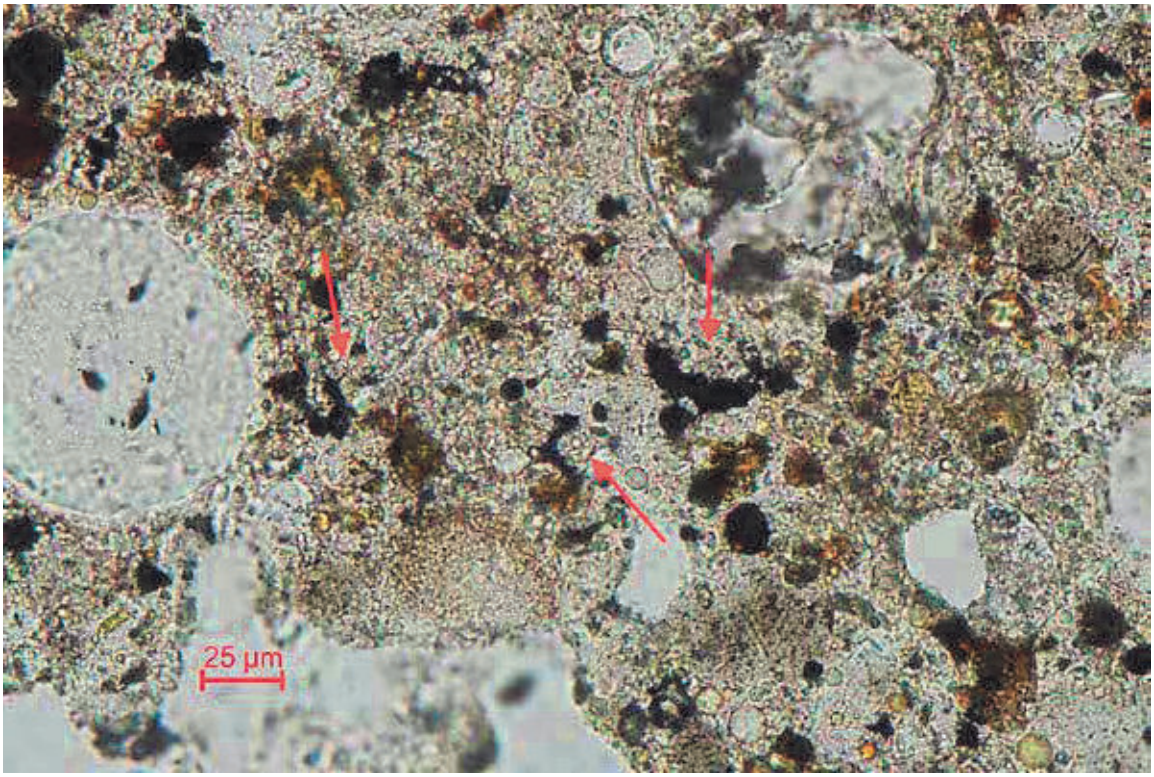

SAMPLE ID: EE1 **DESCRIPTION:** Well to fully hydrated alite portland cement clinker particles/relics (red arrows) in thin section of grout under transmitted plane polarized light.
MAG: 400x

APS PROJECT NO: 10-08795 **DATE:** APRIL 21, 2016
PROJECT: CORROSION OF POST-TENSIONED TENDONS WITH EFFICIENT GROUT

PHOTO: 55

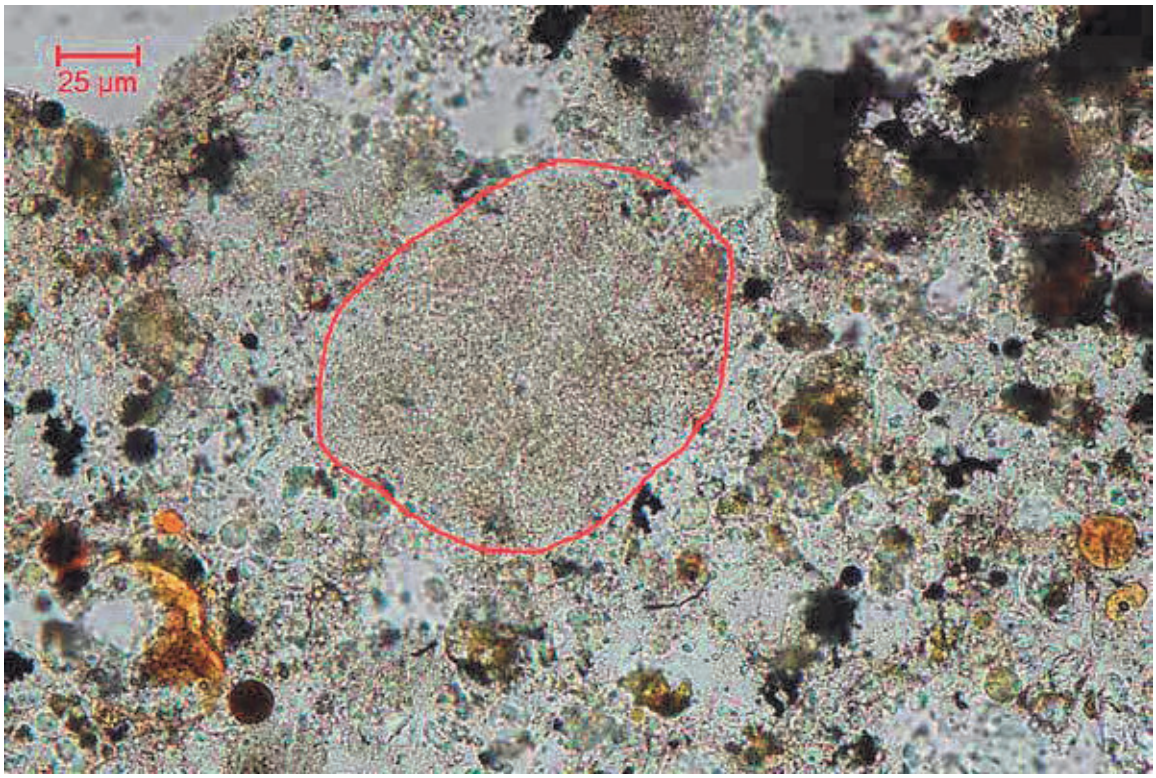

SAMPLE ID: EE2 **DESCRIPTION:** Hydrated lime nodule (red outline) in thin section of grout under transmitted plane polarized light.
MAG: 400x

PHOTO: 56

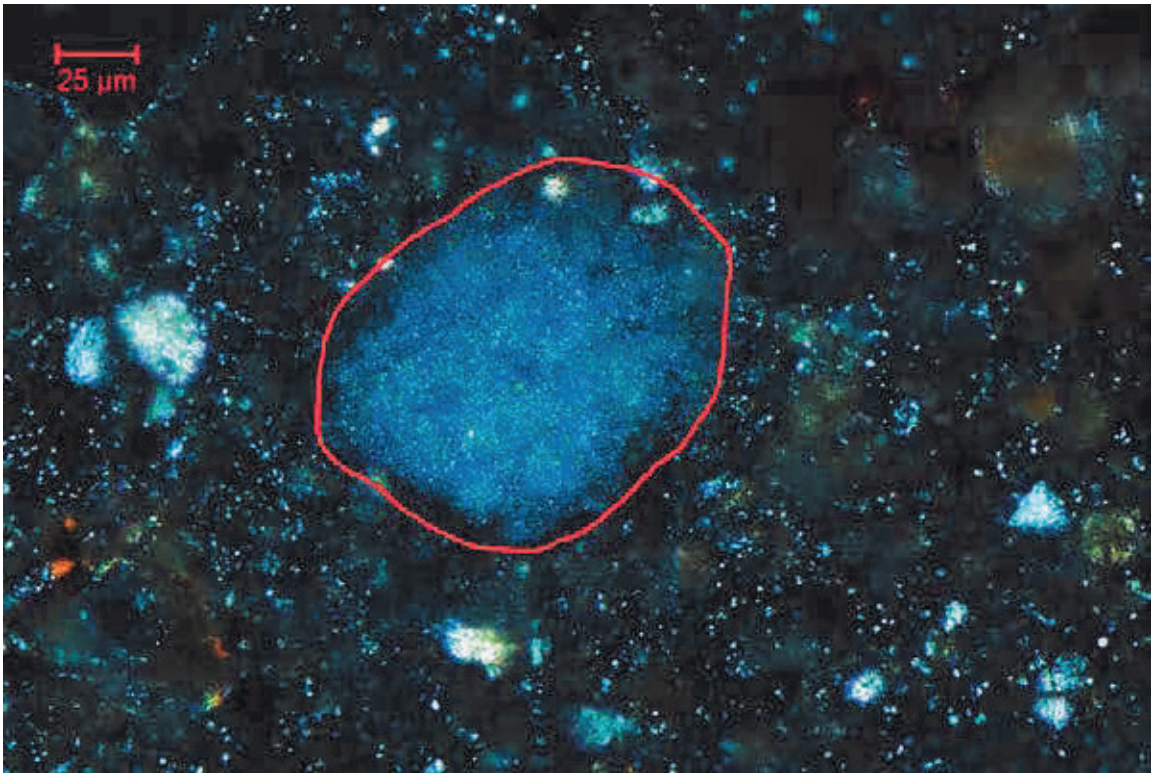

SAMPLE ID: EE2 **DESCRIPTION:** Same view as above under transmitted cross polarized light. Note the white to gray-colored birefringence of the lime.
MAG: 400x

APS PROJECT NO: 10-08795 **DATE:** APRIL 21, 2016
PROJECT: CORROSION OF POST-TENSIONED TENDONS WITH EFFICIENT GROUT

PHOTO: 57

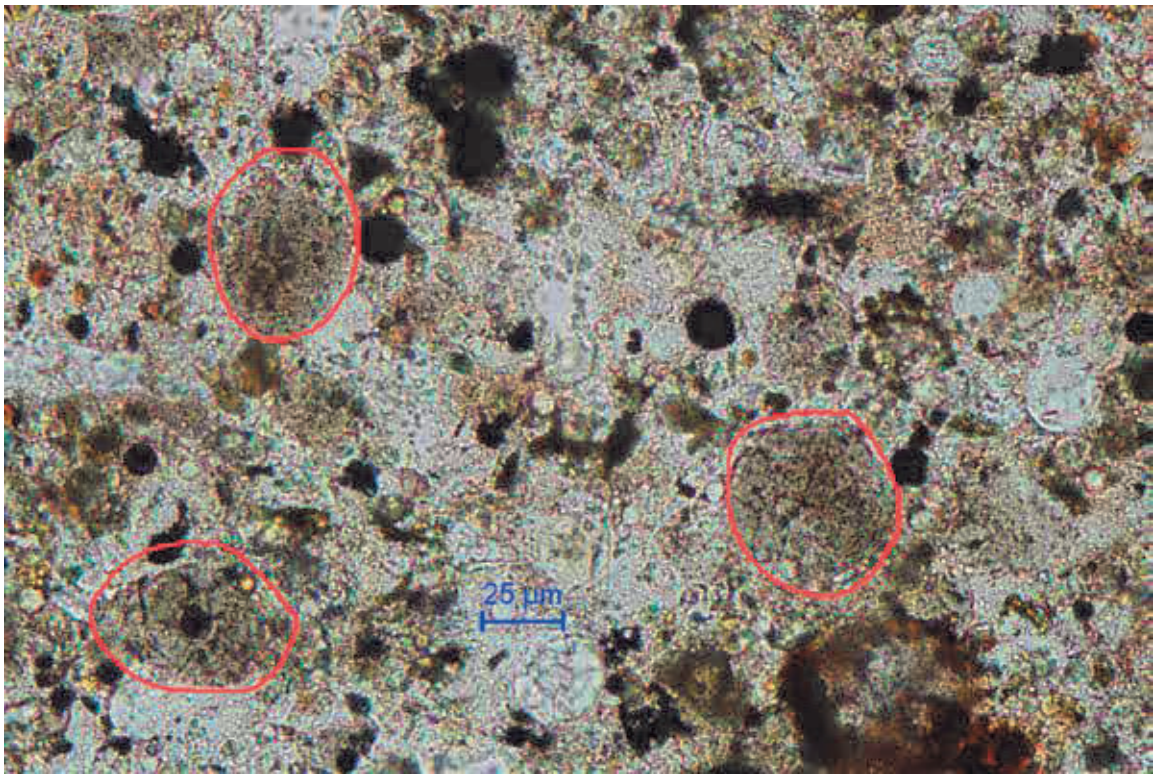

SAMPLE ID: EE2 **DESCRIPTION:** Silica fume agglomerations (red outlines) in thin section of grout under transmitted plane polarized light.
MAG: 400x

PHOTO: 58

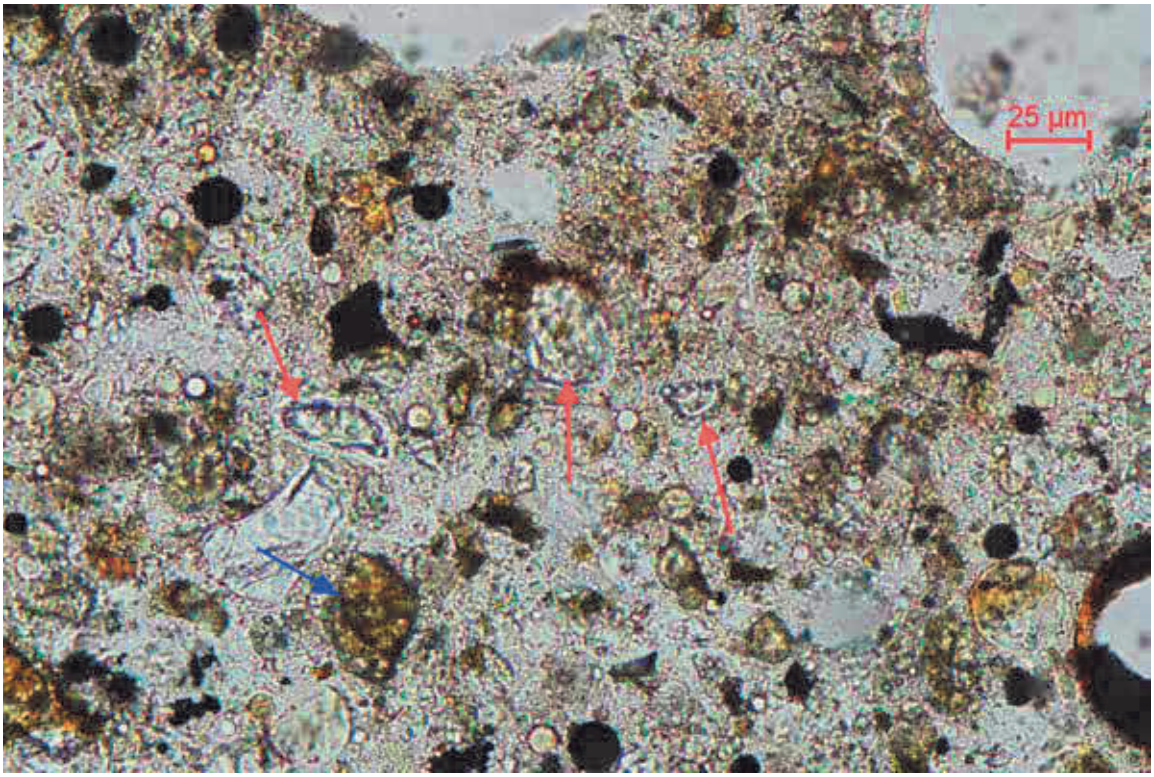

SAMPLE ID: EE2 **DESCRIPTION:** Well hydrated alite portland cement clinker particles (red arrows) and low to negligibly hydrated belite portland cement clinker particle (blue arrow) in thin section of grout under transmitted plane polarized light. Also note spherical fly ash pozzolan particles.
MAG: 400x

APS PROJECT NO: 10-08795 **DATE:** APRIL 21, 2016
PROJECT: CORROSION OF POST-TENSIONED TENDONS WITH EFFICIENT GROUT

PHOTO: 59

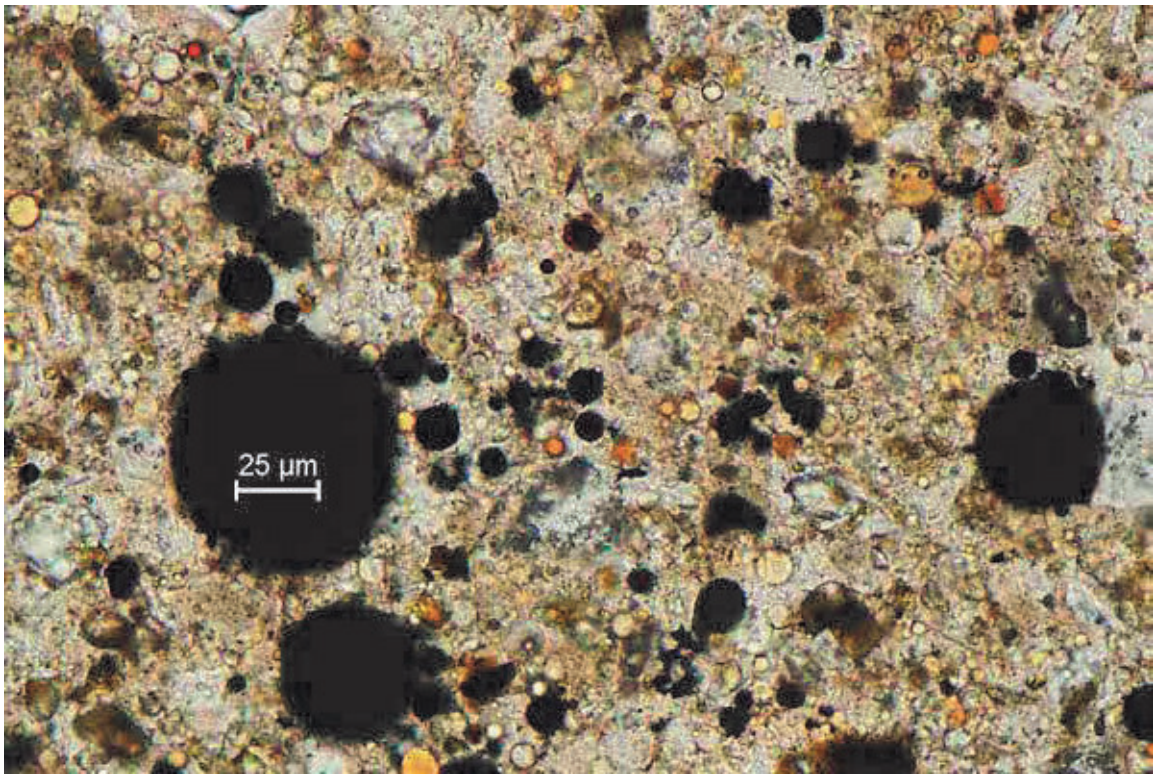

SAMPLE ID: EE2 **DESCRIPTION:** Abundant spherical fly ash pozzolan particles in thin section of grout under transmitted
MAG: 400x plane polarized light. Many particles are black to brown and amber in coloration.

PHOTO: 60

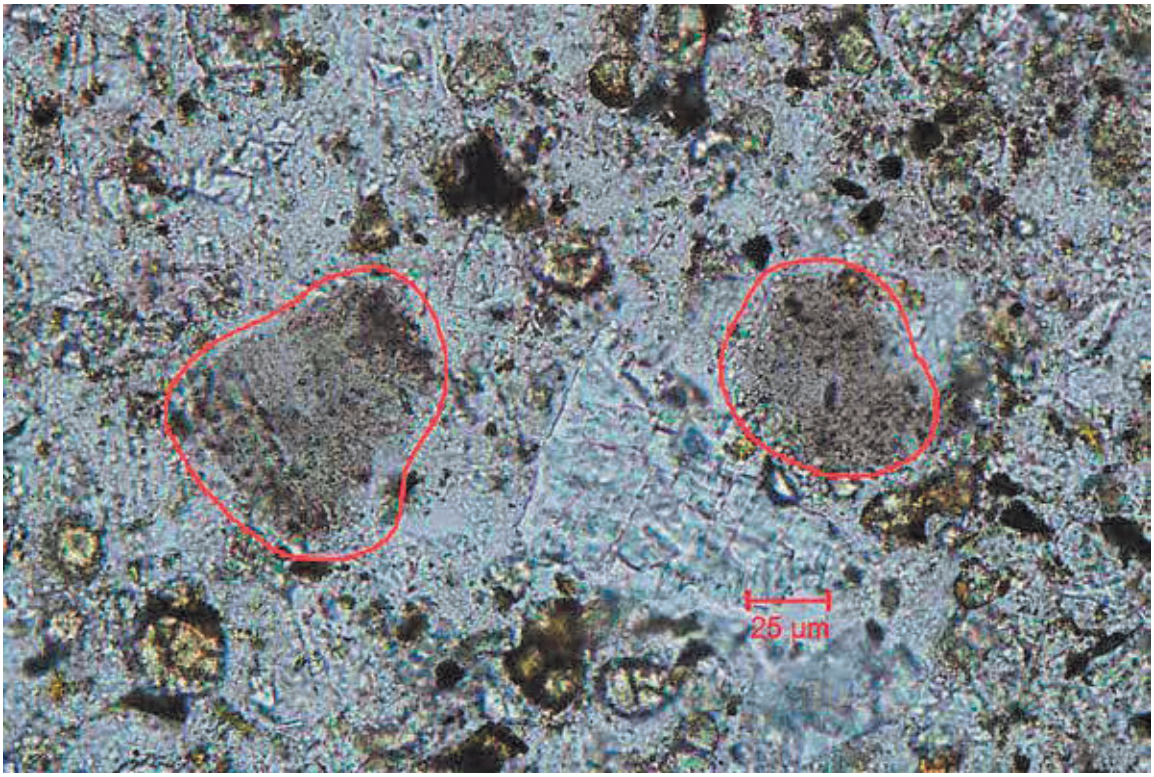

SAMPLE ID: SA **DESCRIPTION:** Silica fume agglomerations (red outlines) in thin section of grout under transmitted
MAG: 400x plane polarized light.

APS PROJECT NO: 10-08795 **DATE:** APRIL 21, 2016
PROJECT: CORROSION OF POST-TENSIONED TENDONS WITH EFFICIENT GROUT

PHOTO: 61

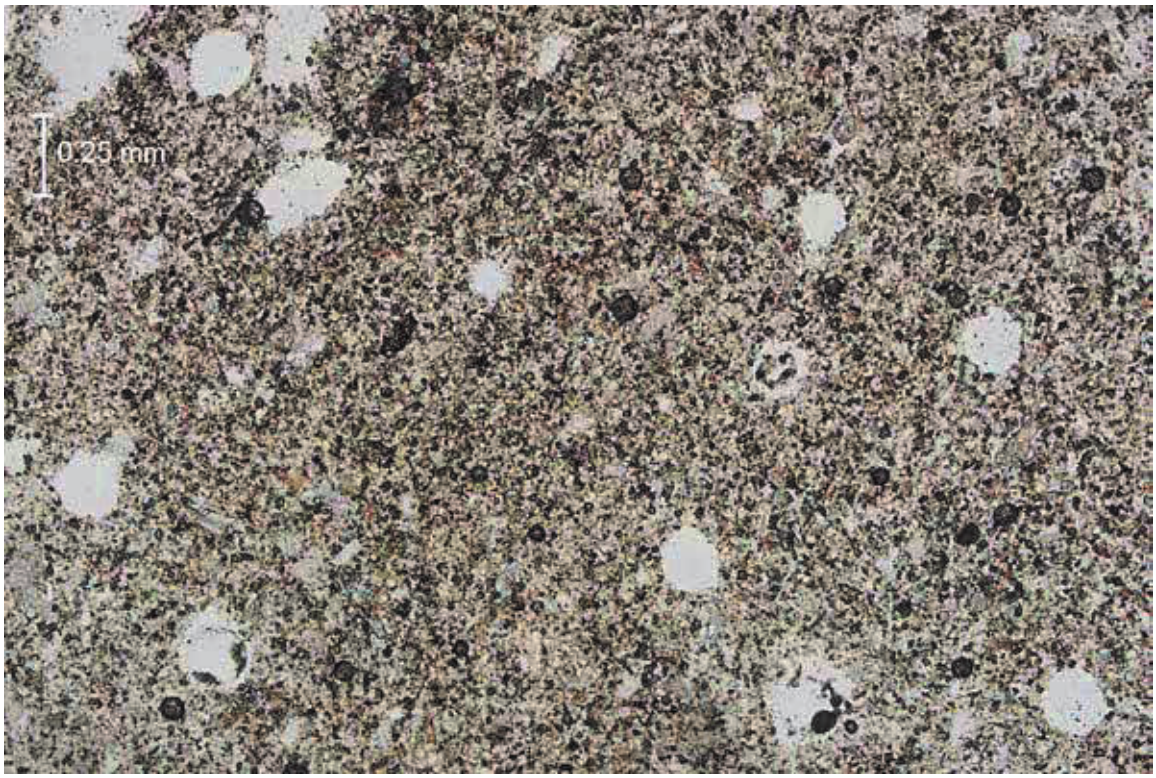

SAMPLE ID: SA **DESCRIPTION:** Overall view of grout in thin section under transmitted plane polarized light.
MAG: 40x

PHOTO: 62

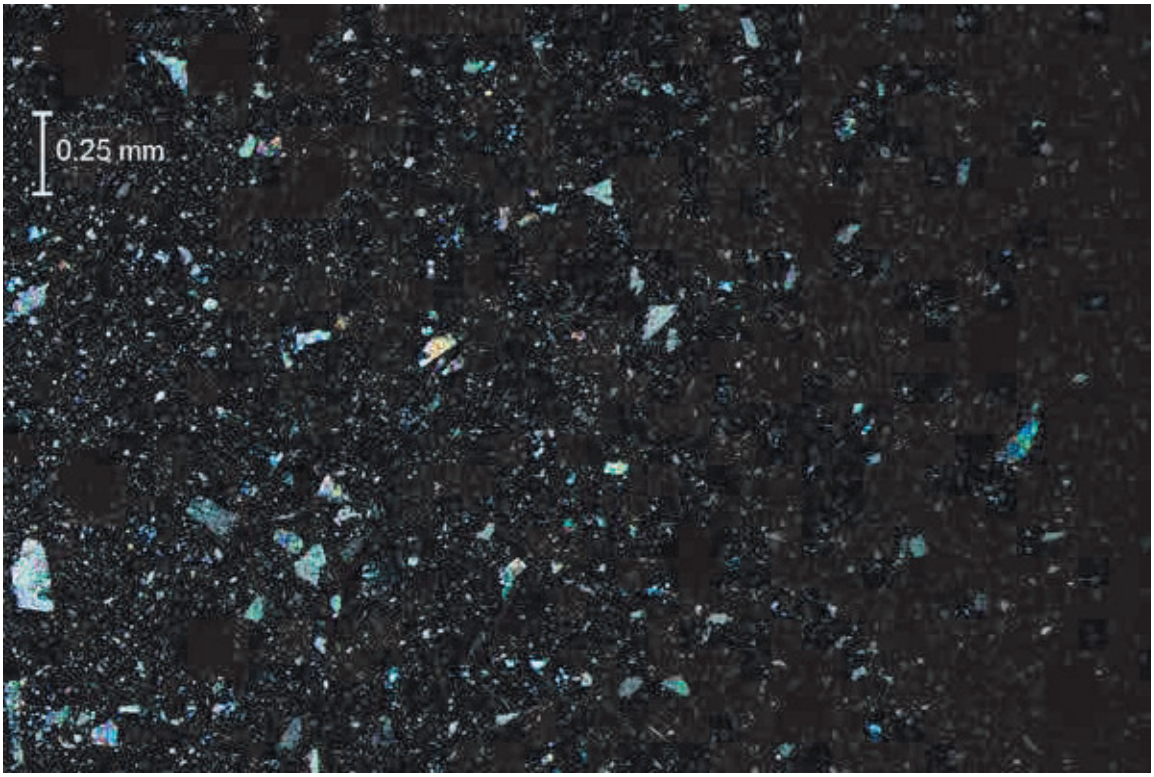

SAMPLE ID: SA **DESCRIPTION:** Same view as above under transmitted cross polarized light. Note the few brightly-colored carbonate particles.
MAG: 40x

APS PROJECT NO: 10-08795 **DATE:** APRIL 21, 2016

PROJECT: CORROSION OF POST-TENSIONED TENDONS WITH EFFICIENT GROUT

PHOTO: 63

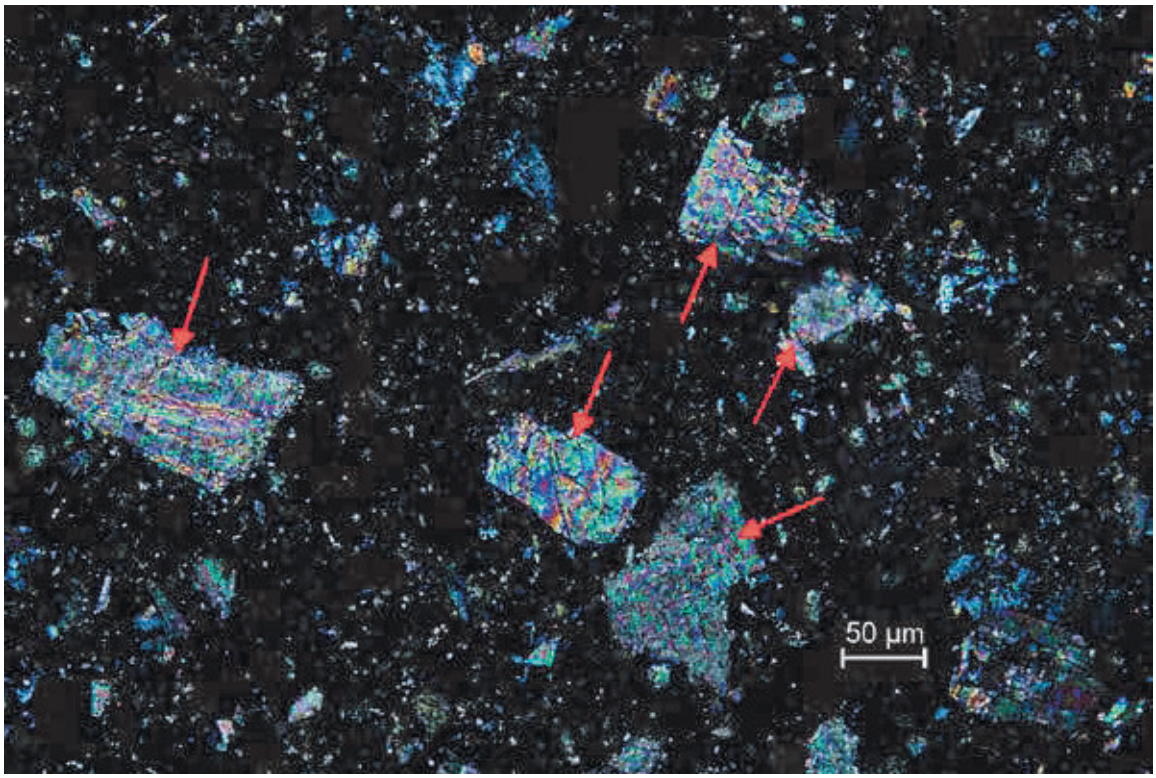

SAMPLE ID: SA
MAG: 200x

DESCRIPTION: Brightly-colored carbonate particles (red arrows) in thin section of grout under transmitted cross polarized light.

PHOTO: 64

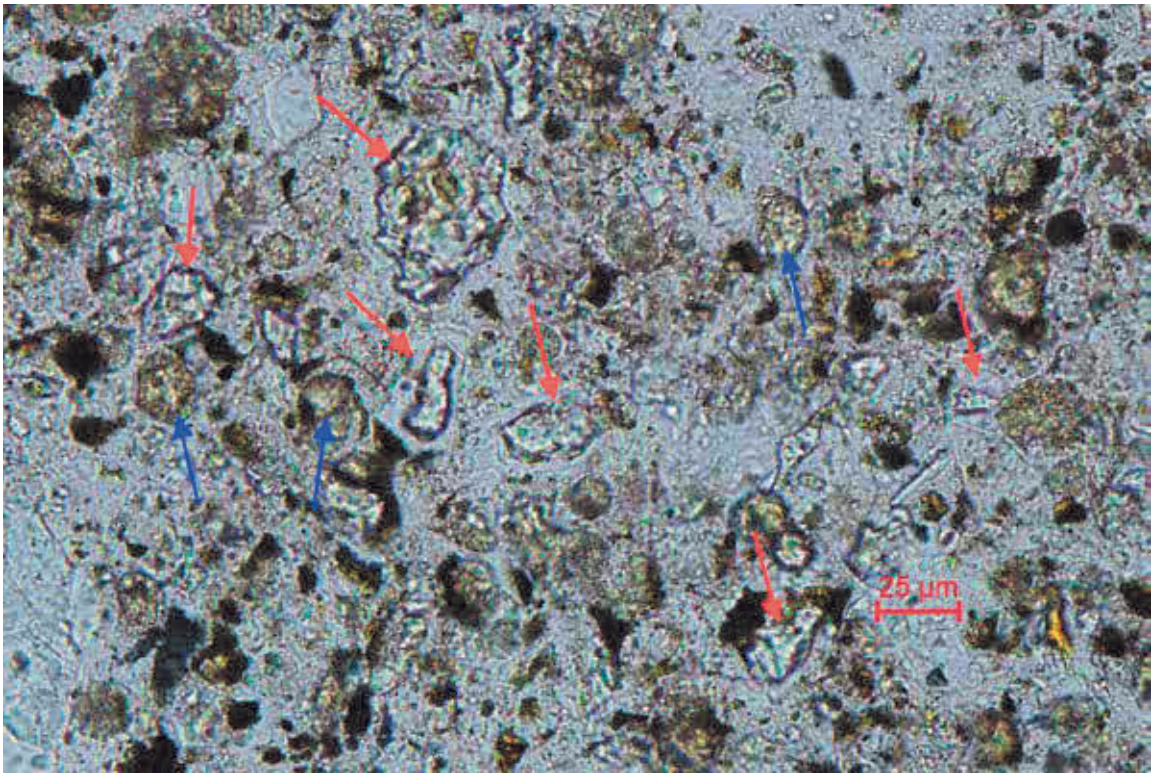

SAMPLE ID: SA
MAG: 400x

DESCRIPTION: Well hydrated alite portland cement clinker particles (red arrows) and low to moderately hydrated belite portland cement clinker particles (blue arrows) in thin section of grout under transmitted plane polarized light.

APS PROJECT NO: 10-08795 **DATE:** APRIL 21, 2016
PROJECT: CORROSION OF POST-TENSIONED TENDONS WITH EFFICIENT GROUT

PHOTO: 65

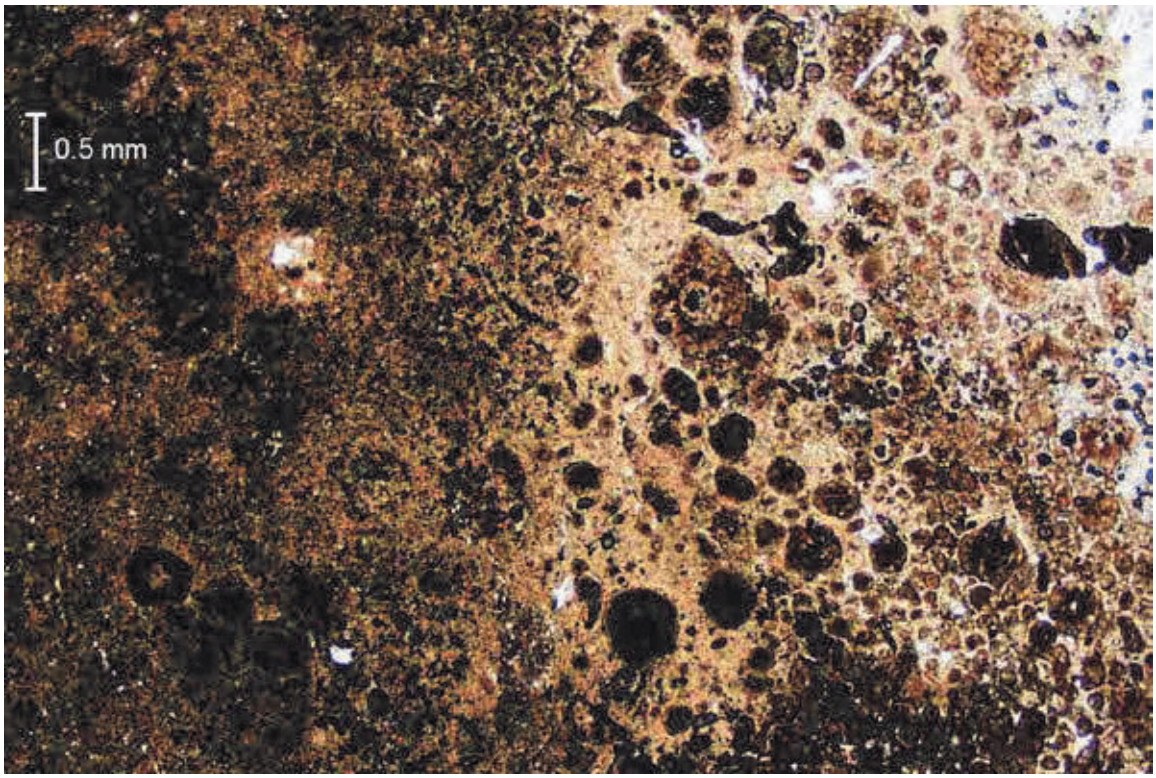

SAMPLE ID: SE1 **DESCRIPTION:** Overall view of grout in thin section under transmitted plane polarized light showing cold joint separating silica fume-rich paste from adjacent paste.
MAG: 20x

PHOTO: 66

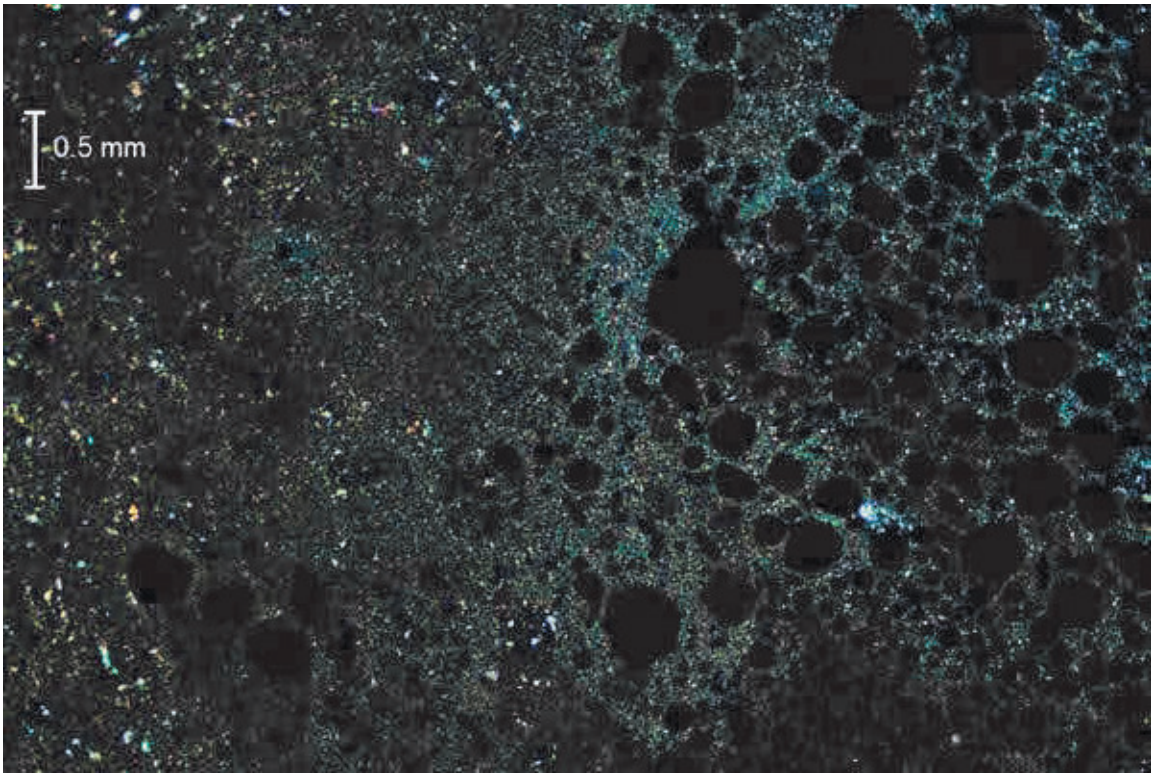

SAMPLE ID: SE1 **DESCRIPTION:** Same view as above under transmitted cross polarized light.
MAG: 20x

APS PROJECT NO: 10-08795 **DATE:** APRIL 21, 2016
PROJECT: CORROSION OF POST-TENSIONED TENDONS WITH EFFICIENT GROUT

PHOTO: 67

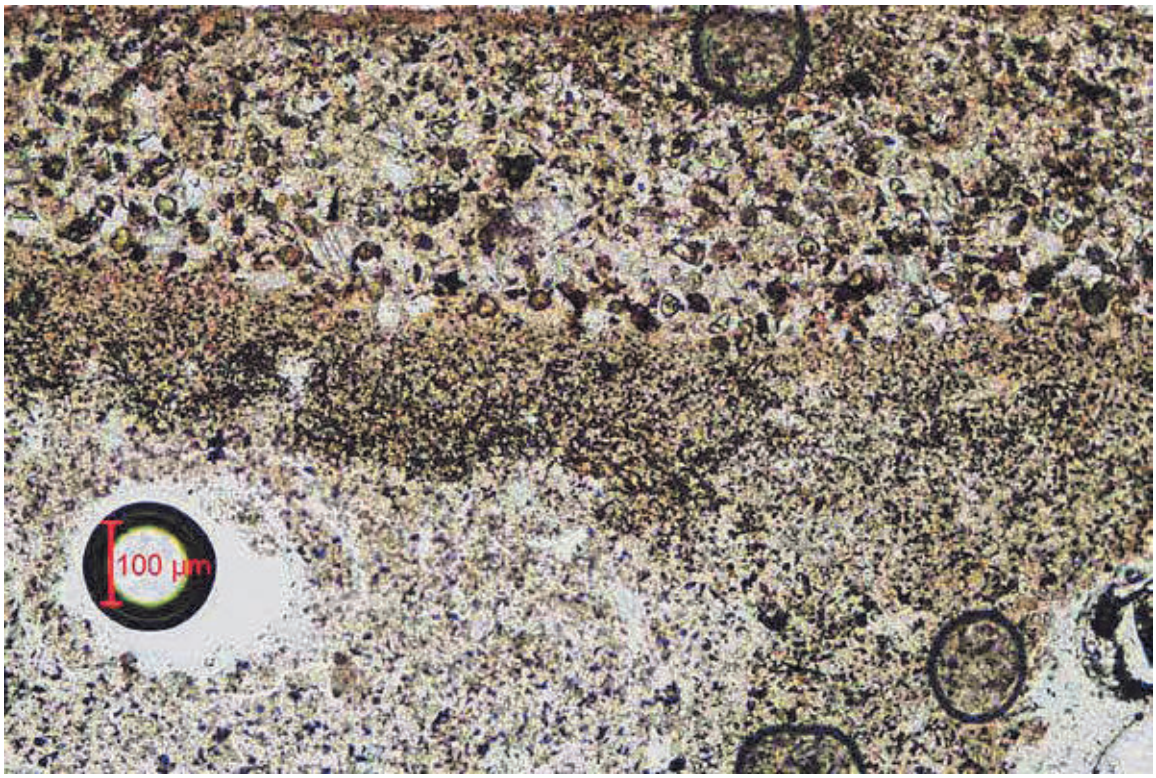

SAMPLE ID: SE1 **DESCRIPTION:** Segregated paste on one side of the cold joint in thin section of grout under transmitted
MAG: 100x plane polarized light.

PHOTO: 68

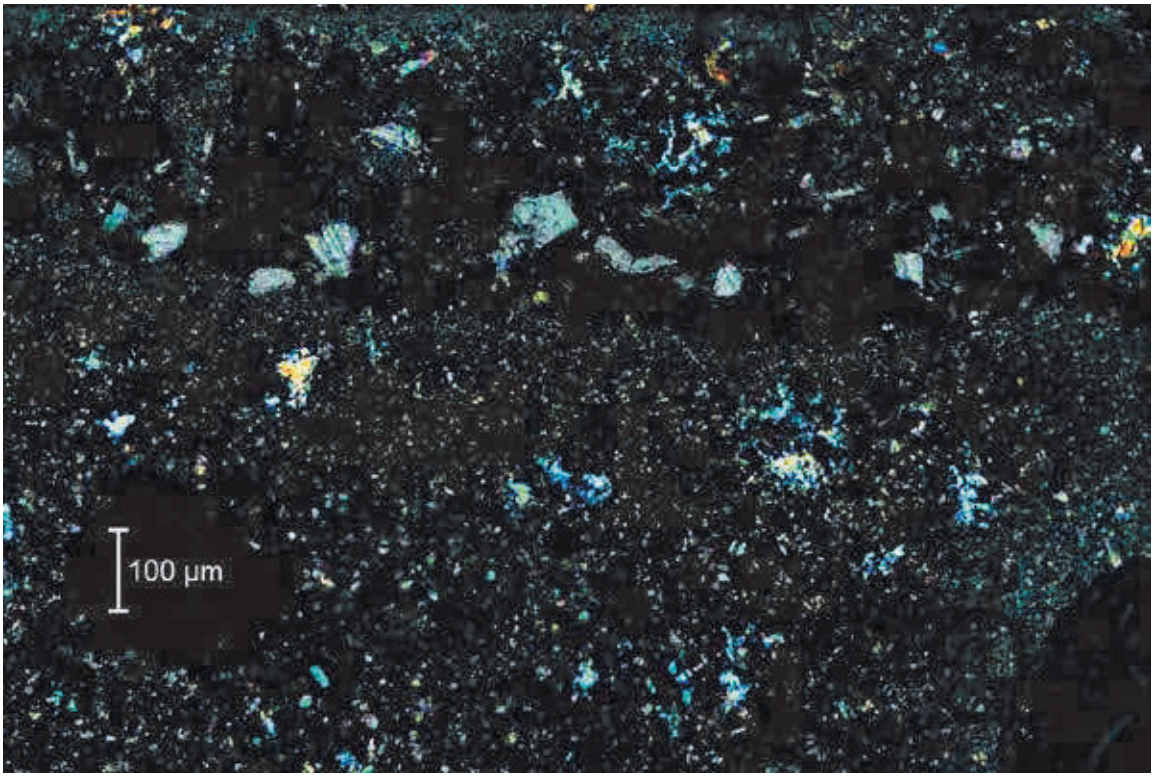

SAMPLE ID: SE1 **DESCRIPTION:** Same view as above under transmitted cross polarized light. Note a few coarse
MAG: 100x carbonate flour particles near the top of the photo and several coarse portlandite crystals throughout the photo.

APS PROJECT NO: 10-08795 **DATE:** APRIL 21, 2016
PROJECT: CORROSION OF POST-TENSIONED TENDONS WITH EFFICIENT GROUT

PHOTO: 69

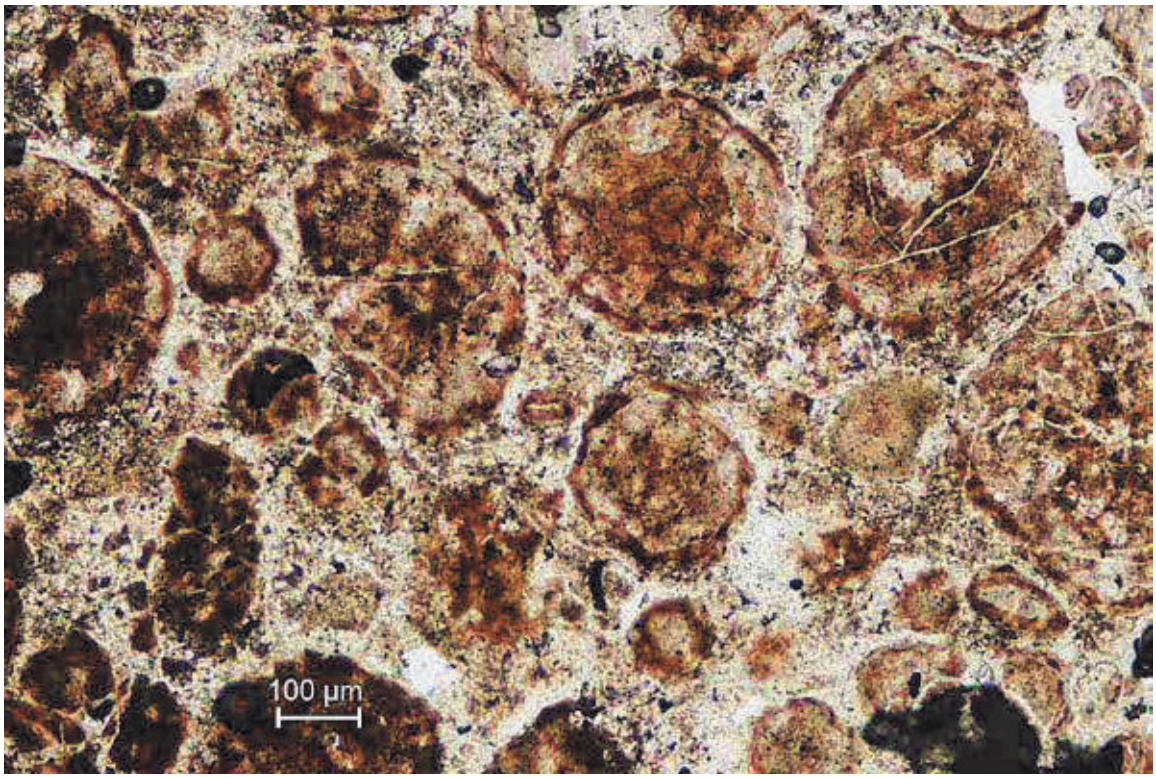

SAMPLE ID: SE1 **DESCRIPTION:** Abundant silica fume nodules on one side of cold joint in thin section of grout under
MAG: 100x transmitted plane polarized light.

PHOTO: 70

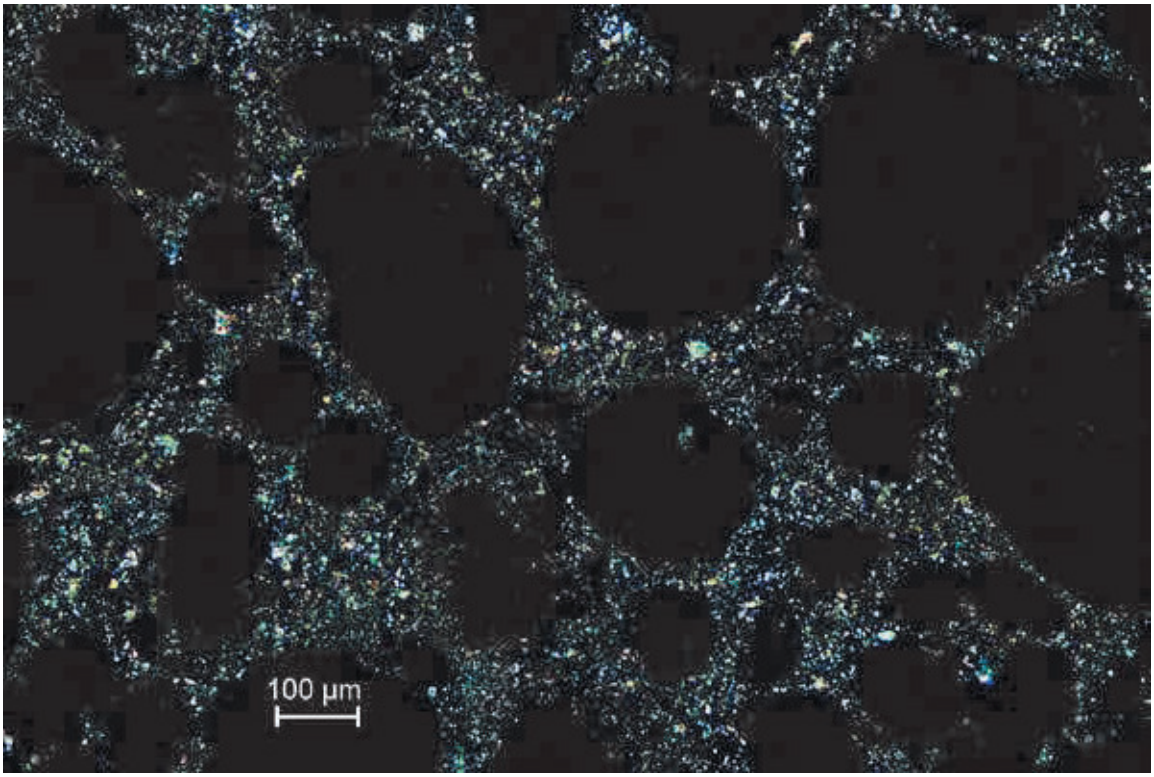

SAMPLE ID: SE1 **DESCRIPTION:** Same view as above under transmitted cross polarized light. Note the isotropic/black
MAG: 100x silica fume nodules and the interstitial, brightly-colored carbonate flour and portlandite.

APS PROJECT NO: 10-08795 **DATE:** APRIL 21, 2016

PROJECT: CORROSION OF POST-TENSIONED TENDONS WITH EFFICIENT GROUT

PHOTO: 71

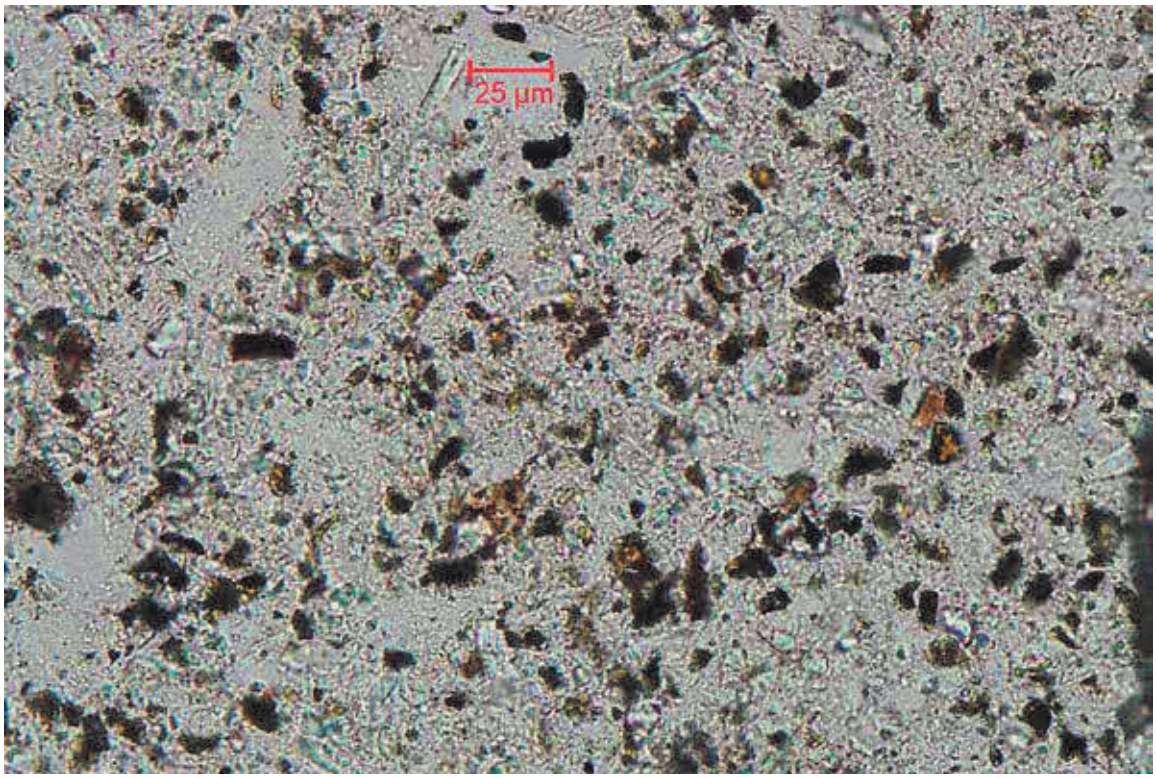

SAMPLE ID: SE1
MAG: 400x

DESCRIPTION: Fully hydrated paste with abundant dark-colored residual ferrite phase in lighter-colored paste in thin section of grout under transmitted plane polarized light.

PHOTO: 72

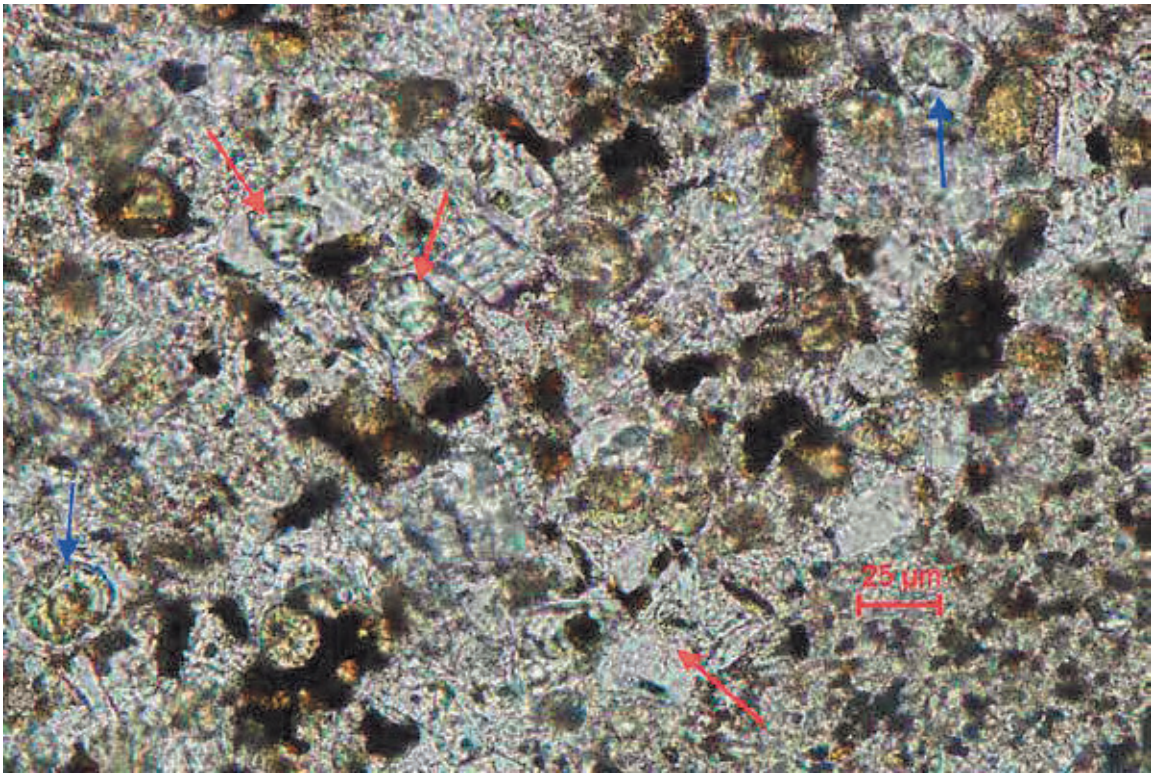

SAMPLE ID: SE1
MAG: 400x

DESCRIPTION: Well to fully hydrated alite portland cement clinker particles/relics (red arrows) and moderate to well hydrated belite portland cement clinker particles (blue arrows) in darker-colored paste in thin section of grout under transmitted plane polarized light.

APS PROJECT NO: 10-08795 **DATE:** APRIL 21, 2016
PROJECT: CORROSION OF POST-TENSIONED TENDONS WITH EFFICIENT GROUT

PHOTO: 73

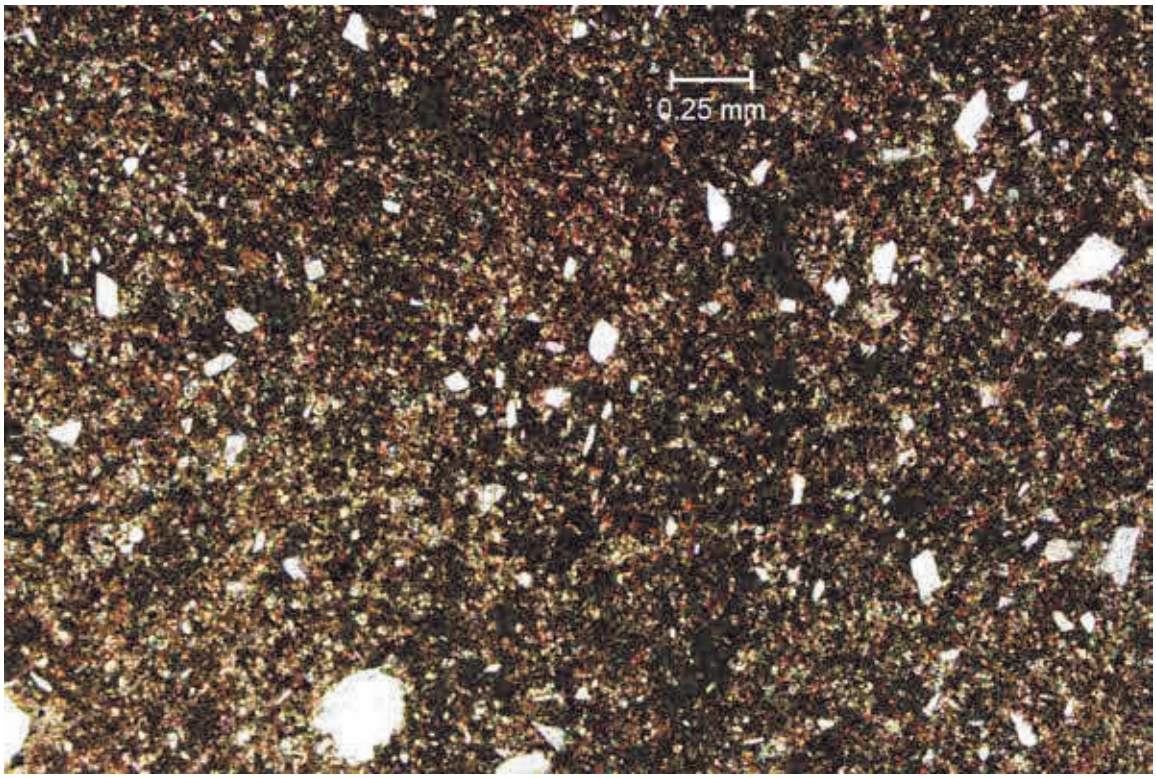

SAMPLE ID: SE2 **DESCRIPTION:** Overall view of grout with very few particles of carbonate flour in thin section under
MAG: 40x transmitted plane polarized light.

PHOTO: 74

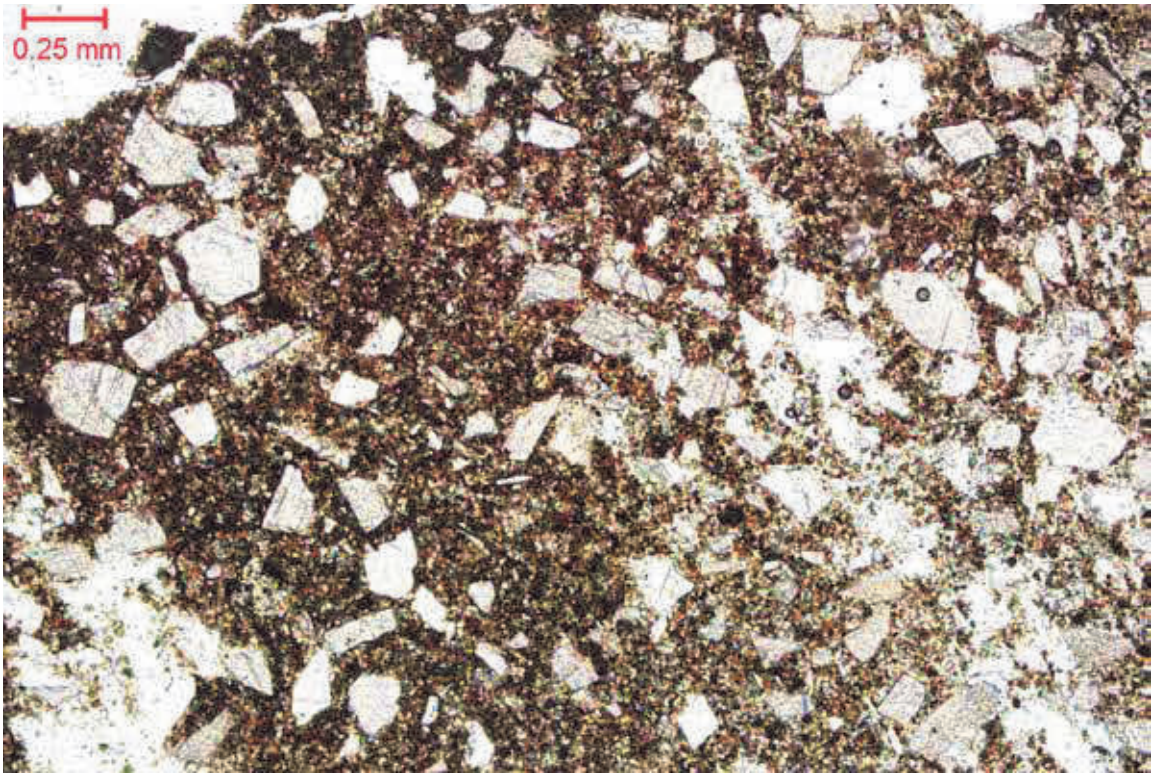

SAMPLE ID: SE2 **DESCRIPTION:** Overall view of grout with abundant particles of carbonate flour in thin section under
MAG: 40x transmitted plane polarized light.

APS PROJECT NO: 10-08795 **DATE:** APRIL 21, 2016
PROJECT: CORROSION OF POST-TENSIONED TENDONS WITH EFFICIENT GROUT

PHOTO: 75

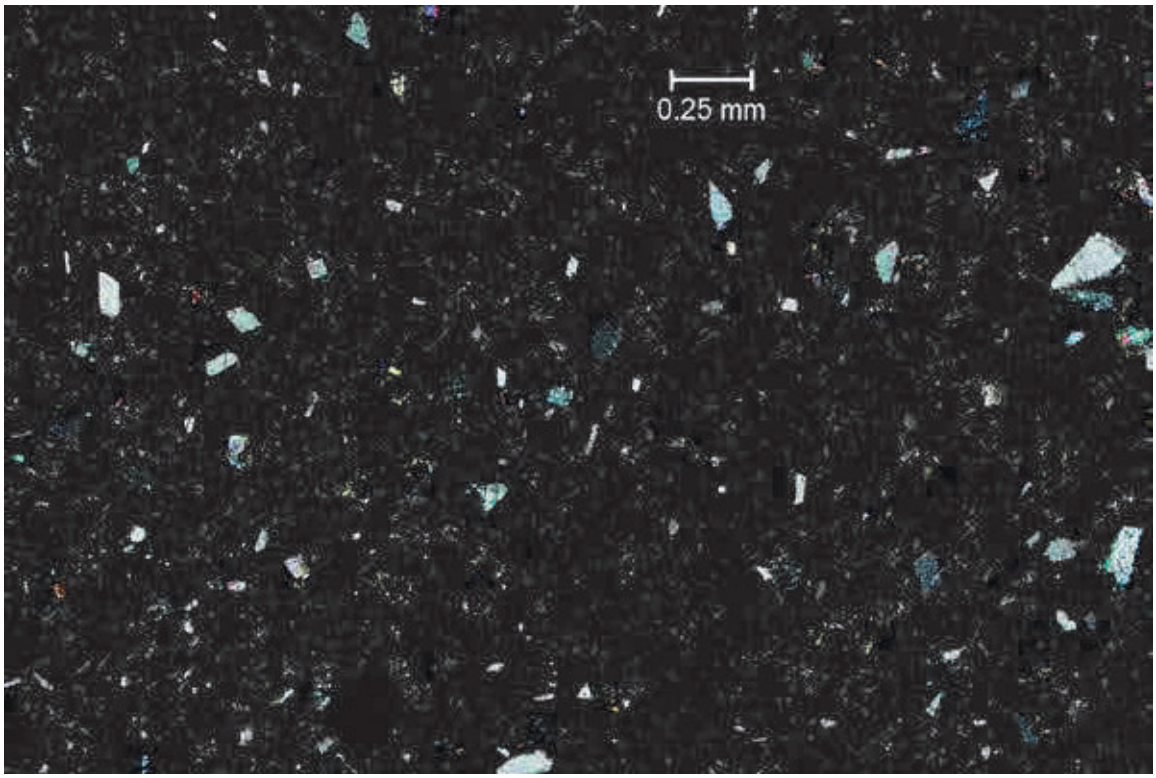

SAMPLE ID: SE2 **DESCRIPTION:** Overall view of grout with very few particles of carbonate flour in thin section under
MAG: 40x transmitted cross polarized light.

PHOTO: 76

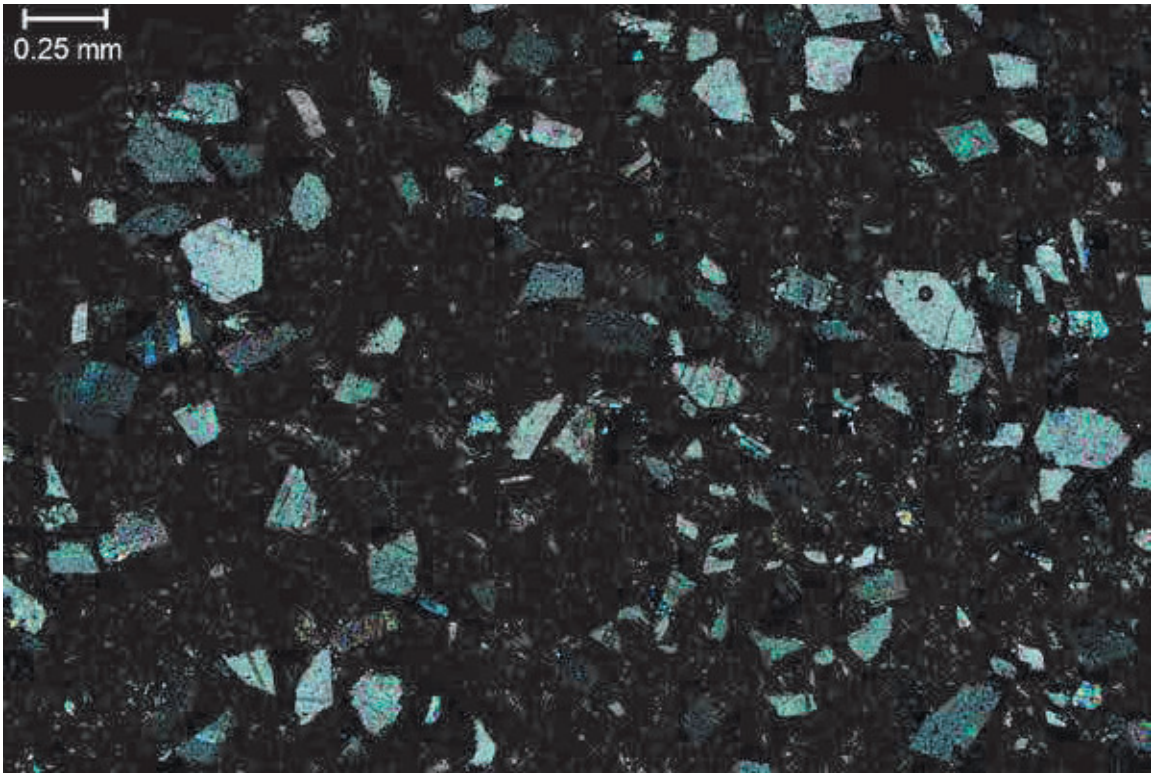

SAMPLE ID: SE2 **DESCRIPTION:** Overall view of grout with abundant particles of carbonate flour (brightly-colored) in
MAG: 40x thin section under transmitted cross polarized light.

APS PROJECT NO: 10-08795 **DATE:** APRIL 21, 2016
PROJECT: CORROSION OF POST-TENSIONED TENDONS WITH EFFICIENT GROUT

PHOTO: 77

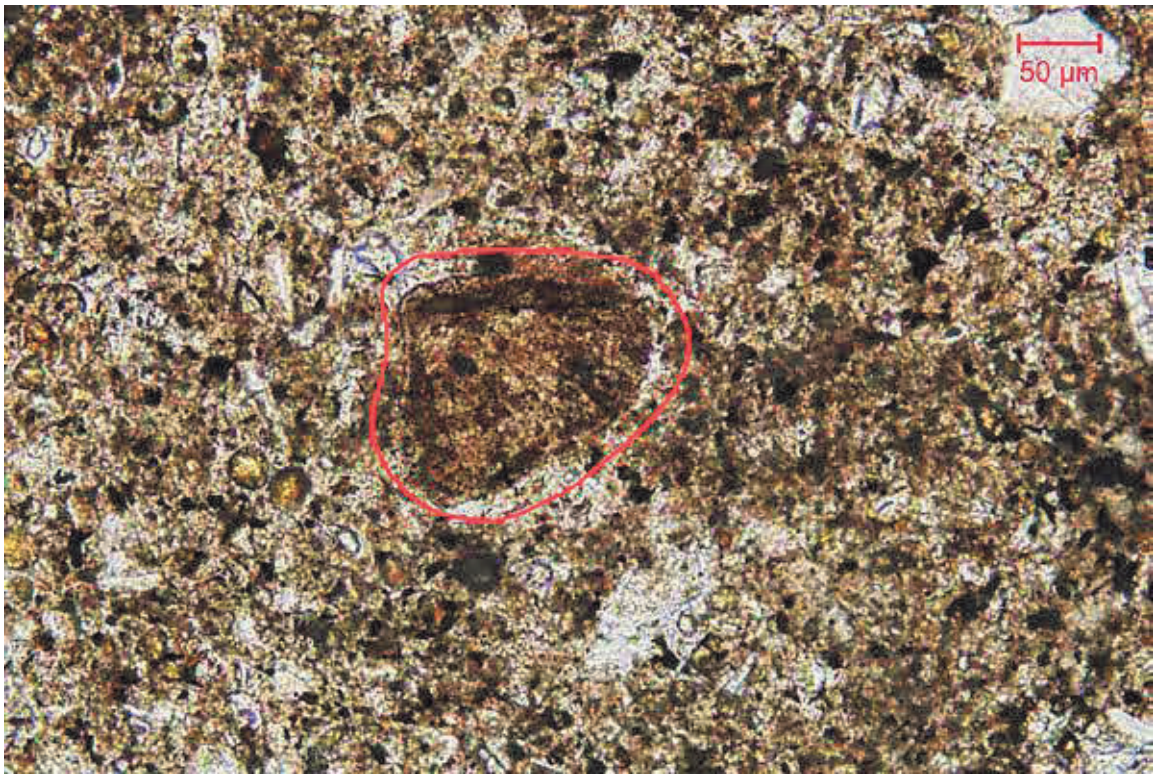

SAMPLE ID: SE2 **DESCRIPTION:** Silica fume agglomeration (red outline) in thin section of grout under transmitted plane
MAG: 200x polarized light.

PHOTO: 78

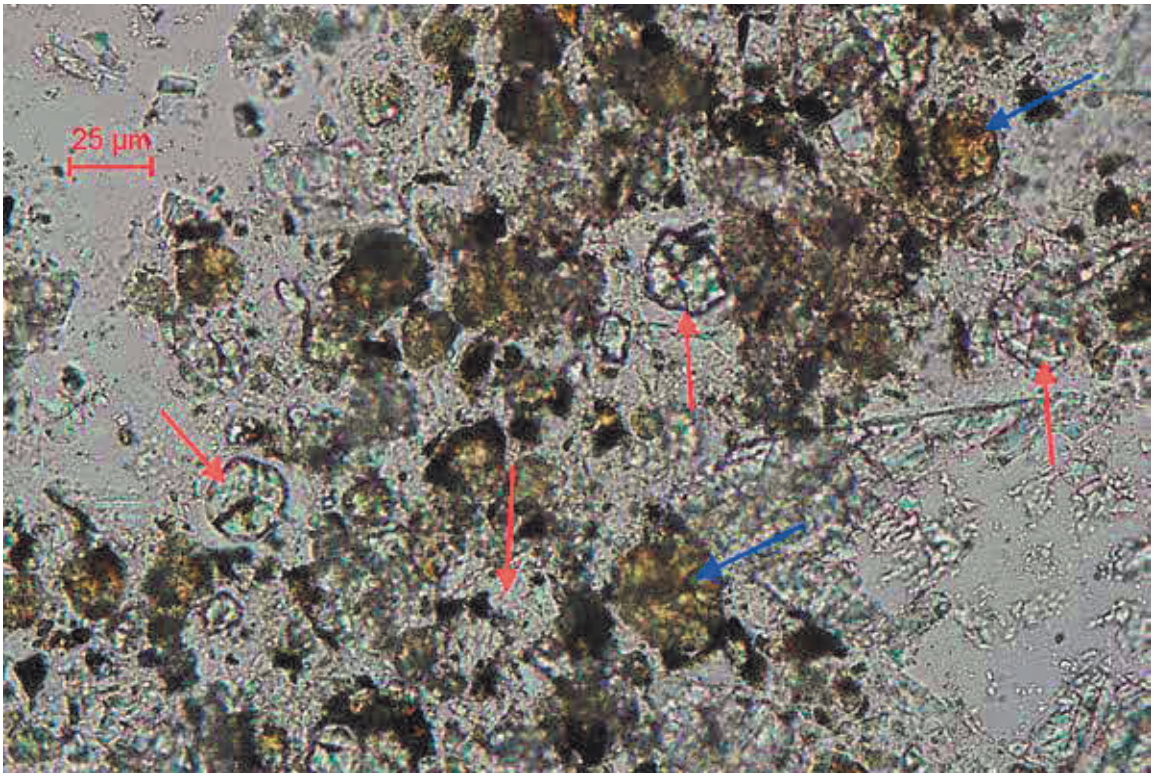

SAMPLE ID: SE2 **DESCRIPTION:** Well to fully hydrated alite portland cement clinker particles/relics (red arrows) and
MAG: 400x low to moderately hydrated belite portland cement clinker particles (blue arrows) in thin section of grout under transmitted plane polarized light.